CANADIAN THESES ON MICROFICHE

THÈSES CANADIENNES SUR MICROFICHE

National Library of Canada
Collections Development Branch

Canadian Theses on
Microfiche Service

Ottawa, Canada
K1A 0N4

Bibliothèque nationale du Canada
Direction du développement des collections

Service des thèses canadiennes
sur microfiche

NOTICE

The quality of this microfiche is heavily dependent upon the quality of the original thesis submitted for microfilming. Every effort has been made to ensure the highest quality of reproduction possible.

If pages are missing, contact the university which granted the degree.

Some pages may have indistinct print especially if the original pages were typed with a poor typewriter ribbon or if the university sent us an inferior photocopy.

Previously copyrighted materials (journal articles, published tests, etc.) are not filmed.

Reproduction in full or in part of this film is governed by the Canadian Copyright Act, R.S.C. 1970, c. C-30. Please read the authorization forms which accompany this thesis.

AVIS

La qualité de cette microfiche dépend grandement de la qualité de la thèse soumise au microfilmage. Nous avons tout fait pour assurer une qualité supérieure de reproduction.

S'il manque des pages, veuillez communiquer avec l'université qui a conféré le grade.

La qualité d'impression de certaines pages peut laisser à désirer, surtout si les pages originales ont été dactylographiées à l'aide d'un ruban usé ou si l'université nous a fait parvenir une photocopie de qualité inférieure.

Les documents qui font déjà l'objet d'un droit d'auteur (articles de revue, examens publiés, etc.) ne sont pas microfilmés.

La reproduction, même partielle, de ce microfilm est soumise à la Loi canadienne sur le droit d'auteur, SRC 1970, c. C-30. Veuillez prendre connaissance des formules d'autorisation qui accompagnent cette thèse.

THIS DISSERTATION
HAS BEEN MICROFILMED
EXACTLY AS RECEIVED

LA THÈSE A ÉTÉ
MICROFILMÉE TELLE QUE
NOUS L'AVONS REÇUE

Canada

NL 339 (r. 86/09)

26c

National Library of Canada
Bibliothèque nationale du Canada

Ottawa, Canada
K1A 0N4

TC – 67509

ISBN 0-315-19601-7

CANADIAN THESES ON MICROFICHE SERVICE – SERVICE DES THÈSES CANADIENNES SUR MICROFICHE

PERMISION TO MICROFILM – AUTORISATION DE MICROFILMER

- Please print or type – Écrire en lettres moulées ou dactylographier

AUTHOR – AUTEUR

Full Name of Author – Nom complet de l'auteur

JOSE ROBERTO THEDIM BRANDT

Date of Birth – Date de naissance

MAY, 1ST, 1953

Canadian Citizen – Citoyen canadien

☐ Yes / Oui ☒ No / Non

Country of Birth – Lieu de naissance

BRAZIL

Permanent Address – Résidence fixe

AV. ADILSON SEROA DA MOTA, 231
22600 RIO DE JANEIRO, RJ.
BRASIL.

THESIS – THÈSE

Title of Thesis – Titre de la thèse

BEHAVIOUR OF SOIL CONCRETE INTERFACES

Degree for which thesis was presented
Grade pour lequel cette thèse fut présentée

Ph. D

Year this degree conferred
Année d'obtention de ce grade

1985

University – Université

UNIVERSITY OF ALBERTA

Name of Supervisor – Nom du directeur de thèse

Z. EISENSTEIN

AUTHORIZATION – AUTORISATION

Permission is hereby granted to the NATIONAL LIBRARY OF CANADA to **microfilm** this thesis and to **lend** or **sell copies of the film.**

The author reserves other publication rights, and neither the thesis nor extensive extracts from it may be printed or otherwise reproduced without the author's written permission.

L'autorisation est, par la présente, accordée à la BIBLIOTHÈQUE NATIONALE DU CANADA de **microfilmer** cette thèse et de **prêter** ou de **vendre des exemplaires du film.**

L'auteur se réserve les autres droits de publication; ni la thèse ni de longs extraits de celle-ci ne doivent être imprimés ou autrement reproduits sans l'autorisation écrite de l'auteur.

ATTACH FORM TO THESIS – VEUILLEZ JOINDRE CE FORMULAIRE À LA THÈSE

Signature

Date

April 24, 1985

NL-91 (r. 84/03)

Canada

THE UNIVERSITY OF ALBERTA

BEHAVIOUR OF SOIL-CONCRETE INTERFACES

by

©

JOSE ROBERTO THEDIM BRANDT

A THESIS

SUBMITTED TO THE FACULTY OF GRADUATE STUDIES AND RESEARCH
IN PARTIAL FULFILMENT OF THE REQUIREMENTS FOR THE DEGREE
OF DOCTOR OF PHILOSOPHY

CIVIL ENGINEERING

EDMONTON, ALBERTA
SPRING 1985

THE UNIVERSITY OF ALBERTA

RELEASE FORM

NAME OF AUTHOR JOSE ROBERTO THEDIM BRANDT

TITLE OF THESIS BEHAVIOUR OF SOIL-CONCRETE INTERFACES

DEGREE FOR WHICH THESIS WAS PRESENTED DOCTOR OF PHILOSOPHY

YEAR THIS DEGREE GRANTED SPRING 1985

Permission is hereby granted to THE UNIVERSITY OF ALBERTA LIBRARY to reproduce single copies of this thesis and to lend or sell such copies for private, scholarly or scientific research purposes only.

The author reserves other publication rights, and neither the thesis nor extensive extracts from it may be printed or otherwise reproduced without the author's written permission.

(SIGNED) ....

PERMANENT ADDRESS:

Av. Adilson Seroa da Mota, 231
22600 Rio de Janeiro, R.J.
Brasil

DATED: April, 19th 1985

THE UNIVERSITY OF ALBERTA

FACULTY OF GRADUATE STUDIES AND RESEARCH

The undersigned certify that they have read, and recommend to the Faculty of Graduate Studies and Research, for acceptance, a thesis entitled BEHAVIOUR OF SOIL-CONCRETE INTERFACES submitted by JOSE ROBERTO THEDIM BRANDT in partial fulfilment of the requirements for the degree of DOCTOR OF PHILOSOPHY.

Dr. Z. Eisenstein ....
Supervisor

Dr. A. Craggs ....A. Craggs....

Dr. N.R. Morgenstern ....

Dr. S. Thomson ....S Thomson....

Dr. D.W. Murray ....D W Murray....

Dr. D.H. Shields ....
External Examiner

Date : April 19th, 1985

DEDICATION

This degree is dedicated to the three most important persons of my life: my wife Claudia and my daughters Fernanda and Sabrina. This work has only been possible because of their love, understanding and patient support.

Claudia gave up her professional career during this almost five years to follow me to Canada so I could pursue my objectives. Apart from her moral support and love I also counted on her time, typing endless versions and corrections of this thesis. During some difficult moments I also enjoyed her technical opinions. She suggested the use of silk to reduce friction in the laboratory test equipment, ending an almost dramatic moment. To her all my thanks from the bottom of my heart would not be enough to express my love and gratitude.

During these "thesis years" our two daugthers Fernanda and Sabrina were born, adding happiness to our life. Their love contributed to make our time in Canada a real pleasure. The time I spend with them recovers my energy for the next working day.

Additionaly, my parents Lusmila and Rudolf, my brother Luiz and his wife Virginia and my dear sister Cristina have supported me throughout my life and in particular during the last five years. Their encouragement and support was of utmost importance. To them, my love.

To my parents-in-law, Margaret and Delphim who have always been very important in our life as a family, I would like to express my gratitude for their love and support.

ABSTRACT

Interfaces are artificially made types of joints. They occur in most civil engineering projects.

Several authors have called attention to the importance of interfaces in the behaviour of these projects and to the potential risk that these areas represent.

During the last two decades, the study of soil-concrete interfaces has received the constant attention of researchers. However, the great majority of the studies were concentrated in the area of analytical modelling.

A standard procedure was frequently used in connection with the finite element method to model interfaces. However, no discussions of the validity of the procedures adopted could be found. This thesis, therefore, concentrates on the physical interpretation of soil-concrete interface behaviour.

Due to the large number of cases involved in this area of study, only planar concrete structures in contact with a compacted silty clay soil are considered.

The "macro" behaviour was modelled in an experimental embankment constructed in the area of Dickson Dam. The results of this field test led to a series of laboratory tests, including a reduced scale model. Based upon some observed features of the large test, a phenomenological model was proposed and used to analyse the conventional techniques of analytical modelling.

It was concluded that these standard procedures lack representation of the physical phenomena involved in the behaviour of soil-concrete interfaces.

ACKNOWLEDGEMENTS

This research was undertaken under the guidance and encouragement of Prof. Z. Eisenstein. The opportunity to work with him was most rewarding and I am deeply grateful to him.

The comments and suggestions offered by Professors D.W. Murray, A. Craggs, N.M. Morgenstern, D.H. Shields, D.S. Sego and S. Thomson were very much appreciated.

The work presented in this thesis includes the contribution of several friends and colleagues. I would like to thank some of them individually.

The technical staff of the Department of Civil Engineering provided invaluable help during the field and laboratory work. Among them D. Gagnon and C. Hurley are acknowledged. Special thanks are extended to G. Cyre and S. Gamble for their dedication. It was a great pleasure for me work with them.

To F. Heinz, coordinator of the Department of Civil Engineering machine shop I owe my gratitude for his effort in building the laboratory test facilities. On several occasions immediate modifications were required and he replied in his friendly way: "We do it right away". Heinz, thank you very much.

I also would like to extend my thanks to J. Kennedy for her very friendly way to hand the students.

The field work also counted on the help of C. McKay and H. Heinz. I also wish to thank Mrs. D. Phelps, G. Walker and

R. Dagg from Underwood McLellan for their help. In particular Mr. Phelps had to stand my pressure during the period of negotiation to have the field instrumentation approved.

To three dear friends I owe my deepest gratitude. They are Paulo Branco, Arsenio Negro and Dave Chan.

Paulo, who became part of my family during these thesis years, spent endless hours with me in the most fruitful discussions, during several stages of this thesis. In particular Chapter 5 is totally owed to him. His criticism in editing my manuscript transformed my mixed ideas into a series of logical chapters. To him and his wife Lucila, I also owe the best moments in Canada, over several Saturday night dinners at their place. Paulo and Lu also helped us to settle in Edmonton during the difficult first days in a foreign country. They made our stay in Canada unforgetable and our friedship indestructable.

Although in spasmodic encounters, the contribution of my dear friend Arsenio in day-long discussions were of fundamental importance. His encouragement in down moments and his energy to work twenty-six hours a day helped me in several circumstances.

To Dave Chan I owe most of Chapter 6. Dave almost held my hand when I was writing the finite element program described in that chapter. His ability to handle "unskilled" students has proved to me that the Department of Civil Engineering made a wise choice inviting him to joint the academic staff. Several of his plotting programs were used throughout this thesis. Dave, thank you very much and good luck in your new position.

I am also grateful to the academic staff of the Civil Engineering Department, in special to Profs. S. Thomsom, D. Murray and N. Morgenstern for their always friendly discussions and suggestions. Prof. Thomsom spent his valuable time editing this thesis.

Financial support to built the test embankment was provided by the Alberta Environment. My thanks are specially to Dr. R. McManus, Dickson Dam Project Manager for his support. Further support was provided by the Natural Science and Engineering Research Council of Canada.

I am indebted to Conselho Nacional de Desenvolvimento Cientifico e Tecnologico - CNPq of Brasil for the personal support provided for my studies in Canada. Without their financial aid this thesis would not have been possible.

Finally I would like to thank again Dr. Z. Eisentein and his family and Dr. D.W. Murray and his family. They all welcomed me to Edmonton and helped me in the initial difficult days. Their families served as example for me in several ways and their help and friendship during my residence in Canada will never be forgotten.

Table of Contents

Chapter Page

1. INTRODUCTION 1

1.1 GENERAL 1

1.2 BRIEF HISTORY OF THE TREATMENT OF SOIL-CONCRETE INTERFACES 1

1.3 MECHANISTIC VIEWPOINT 4

1.4 OBJECTIVES AND SCOPE OF THIS RESEARCH 6

1.5 CONTENTS OF THIS THESIS 7

2. ANALYTICAL VERSUS EXPERIMENTAL MODELLING 9

2.1 INTRODUCTION 9

2.2 LITERATURE REVIEW 9

2.2.1 The Concept of Joint Element 9

2.2.2 Review of Analytical Formulations 12

2.2.3 Review of Soil Mechanics Experience 23

2.3 CONCLUSIONS 32

3. TEST EMBANKMENT 33

3.1 GENERAL 33

3.2 DESCRIPTION OF THE TEST EMBANKMENT 33

3.3 INSTRUMENTATION 45

3.3.1 Fill Instrumentation 46

3.3.1.1 Multipoint Extensometers 46

3.3.1.2 Earth Pressure Cells 50

3.3.2 Wall Instrumentation 63

3.3.2.1 Contact Pressure Cells 64

3.3.2.2 Shear Displacement Device (S.D.D.) 67

3.3.2.3 Shear Stress Device (S.S.D.) 72

3.3.3 Additional Supporting Instruments 79
3.3.3.1 Slope Indicator Casing 79
3.3.3.2 Settlement Points 81
3.3.3.3 Bench Marks 81
3.3.3.4 Piezometers 82
3.4 PRESENTATION AND DISCUSSION OF RESULTS 82
3.4.1 Fill Instrumentation 82
3.4.1.1 Settlement Measurement 82
3.4.1.2 Earth Pressure Cells. 90
3.4.2 Wall Instrumentation 95
3.4.2.1 Contact Pressure Cells 95
3.4.2.2 Shear Displacement Devices 97
3.4.2.3 Shear Stress Device 99
3.5 CONCLUSIONS 103
4. LABORATORY TESTS 108
4.1 INTRODUCTION 108
4.2 CONVENTIONAL DIRECT SHEAR BOX TESTS 109
4.2.1 Equipment and Procedures 109
4.2.2 Presentation and Discussion of Results ...111
4.3 LARGE SHEAR BOX TEST 121
4.3.1 General 121
4.3.2 Design of the Laboratory Apparatus 122
4.3.2.1 Concrete Base and Sample Container 122
4.3.2.2 Horizontal Loading System 128
4.3.2.3 Vertical Loading System 128
4.3.3 Instrumentation 133

4.3.4 Sample Preparation 135
4.3.5 Testing Procedure and Tests Performed 140
4.3.6 Presentation of Results 142
4.4 PERFORMANCE OF APPARATUS AND DISCUSSION OF RESULTS 151
4.4.1 Difficulties in Designing the Apparatus ..151
4.4.2 Normal Stress Distribution 156
4.4.3 Shear Stress Distribution 159
4.5 CONSTITUTIVE LAW - DISCUSSION 166
4.6 CONCLUSIONS 179
5. PHENOMENOLOGICAL MODEL 181
5.1 INTRODUCTION 181
5.2 PRESENTATION OF THE MODEL 182
5.2.1 Required Properties 182
5.2.2 Proposed Model and Its Elements 185
5.2.3 Mathematical Solution 189
5.2.4 Details of the Mathematical Solution 193
5.3 IDEALIZED INPUT PARAMETERS 194
5.3.1 Even Springs and Frictional Blocks 194
5.3.2 Odd Springs 197
5.4 APPLICATIONS OF THE MODEL 200
5.4.1 Analyses of Large Shear Test 200
5.4.2 Behaviour of Frictional Piles 204
5.4.3 Behaviour of the Test Embankment 208
5.5 THE USE OF DIRECT SHEAR BOX TEST AS INPUT FOR JOINT ELEMENTS 215
5.6 CONCLUSIONS 227
6. FINITE ELEMENT ANALYSES OF TEST EMBANKMENT 229

6.1 INTRODUCTION 229

6.2 FINITE ELEMENT PROGRAM 231

6.2.1 General 231

6.2.2 Capabilities of the Program 231

6.2.3 Additional Features 234

6.2.3.1 The Skyline Method 235

6.2.3.2 Equation Solver 239

6.3 JOINT ELEMENT 239

6.3.1 General 239

6.3.2 Goodman's Joint Element 240

6.3.3 Zero Thickness Assumption 240

6.3.4 Constitutive Matrix 242

6.4 TESTS FOR INTERDAM PROGRAM 243

6.4.1 General 243

6.4.2 Test for Implementation of Joint Elements 243

6.4.3 Test for INTERDAM Code 244

6.4.4 Efficiency of INTERDAM program 247

6.5 REVIEW OF THE MECHANICAL BEHAVIOUR OF WALL INSTRUMENTS 250

6.6 ANALYSES OF TEST EMBANKMENT 253

6.6.1 General 253

6.6.2 Finite Element Mesh 254

6.6.3 Method of Simulation 256

6.6.4 Boundary Conditions 257

6.6.5 Back Analyses of Interface Behaviour 259

6.6.5.1 General 259

6.6.5.2 Linear versus Nonlinear Analysis .262

6.6.5.3 Effect of Variations in the Elastic Parameters 267

6.6.5.4 Effect of Method of Sample Preparation 272

6.6.5.5 Full Slip and No Slip Conditions .274

6.6.6 Back Analyses of Soil Behaviour 279

6.7 CONCLUSIONS 286

7. CONCLUSIONS AND SUGGESTIONS FOR FURTHER RESEARCH ...289

7.1 GENERAL 289

7.2 SUMMARY OF CONCLUSIONS 289

7.3 SUGGESTIONS FOR FURTHER RESEARCH 292

REFERENCES 294

APPENDIX A - NUCLEAR DENSOMETERS 308

APPENDIX B - MULTIPOINT EXTENSOMETER CURVES 315

APPENDIX C - TRIAXIAL TESTS FOR FINITE ELEMENT ANALYSES .327

APPENDIX D - DETAILS OF THE LARGE SHEAR TEST APPARATUS ..332

APPENDIX E - VERTICAL DISPLACEMENT DURING SHEAR 340

APPENDIX F - FORTRAN PROGRAM FOR PHENOMENOLOGICAL MODEL .344

APPENDIX G - GOODMAN'S JOINT ELEMENT FORMULATION 359

APPENDIX H - CONSTITUTIVE MODELS IMPLEMENTED IN INTERDAM 366

List of Tables

Table Page

2.1 Summary of Joint Elements..........................22

3.1 Properties of Test Embankment Soil..................41

3.2 Types and Quantities of Instruments 47

4.1 Summary of Direct Shear Box Tests..................112

4.2 Summary of Tests - Large Shear Box Test............141

4.3 Ratio Between External and Internal Forces.........162

6.1 Summary of Parametric Study of Test Embankment.....260

C.1 Summary of Triaxial Compression Tests..............329

List of Figures

Figure Page

1.1 The Concept of Two Elastic Bodies in Contact.........5

2.1 Details of Some Joint Element Formulations..........13

2.2 Details of Some Joint Element Formulations - cont...............................19

2.3 Derivation of Hyperbolic Model.....................25

2.4 Derivation of Bilinear Model.......................29

3.1 Location of Dickson Dam Site.......................35

3.2 Sequence of Excavation.............................37

3.3 Rate of Construction - Test Embankment.............42

3.4 Grain Size - Test Embankment Material..............43

3.5 Compaction Control - Test Embankment...............44

3.6 General View of Instrumentation....................48

3.7 Modified Multipoint Extensometers..................49

3.8 Position of Multipoint Extensometers...............51

3.9 Pressure Cell Calibration Chamber..................53

3.10 Pressure Cell Calibration - Sand K=1...............56

3.11 Pressure Cell Calibration - Sand K=1/2.............57

3.12 Pressure Cell Calibration - Sand K=4/3.............58

3.13 Pressure Cell Calibration - Till K=1...............59

3.14 Pressure Cell Calibration - Simulating Installation.60

3.15 Location of Earth Pressure Cells...................62

3.16 Location of Wall Instruments.......................65

3.17 Details of Shear Displacement Device...............68

3.18 Details of Shear Stress Devices....................73

3.19 Set Up for Shear Stress Devices Calibration........75

Figure Page

3.20 Calibration Results - Shear Stress Devices..........77

3.21 Results of Slope Indicator Casing Inside Wall.......80

3.22 Total Settlement Versus Time - ME-3.................84

3.23 Total Settlement Versus Distance from Wall - MP-4...................................85

3.24 Fill Settlement versus Distance From Wall - MP-4......................................88

3.25 Stress Path - Earth Pressure Cells..................91

3.26 Overburden Pressure versus Vertical Stress..........93

3.27 Sketch for Proposed Load Transfer Mechanism.........94

3.28 Normal Stress versus Height of Wall.................96

3.29 Shear Displacement versus Increasing Height of Fill.....................................98

3.30 Shear Displacement versus Height of Wall...........100

3.31 Shear Stress vesus Increasing Height of Fill.......101

3.32 Shear Stress versus Height of Wall.................102

3.33 Normalized Stress-Displacement Curve...............104

3.34 Stress-Path Observed at the Concrete Wall..........107

4.1 Results of Direct Shear Test - Series 100..........113

4.2 Results of Direct Shear Test - Series 200..........114

4.3 Expected Contact Surface Soil-Concrete.............117

4.4 Envelope for Direct Shear Tests....................118

4.5 Suggested Displacement Path for Grain of Soil......120

4.6 Evaluation of Method of Friction Reduction.........125

4.7 Sketch of Large Shear Box Apparatus................126

4.8 Loading Head for Vertical Load.....................131

Figure Page

4.9 Device to Measure Vertical Displacement during Shear..136

4.10 Position of Instruments in a Typical Sample........137

4.11 Results of Large Shear Test - Test#9 143

4.12 Results of Large Shear Test - Test#3 144

4.13 Results of Large Shear Test - Test#6 145

4.14 Results of Large Shear Test - Test#8 146

4.15 Detail of Stress Displacement Curve - Test#3.......148

4.16 Vertical Displacement During Shear - Test#8 149

4.17 Strength Envelope for Large Shear Tests............150

4.18 Study of Rate Effect - Large Shear Test............152

4.19 Comparison Between Two Loading Systems............158

4.20 Idealized Shear Stress Distribution................160

4.21 Stress Displacement Curves - Large Shear Test (Internal)....................................168

4.22 Normalized Shear Stress-Displacement Curves........172

4.23 Normalized Stress-Displacement Curves - Series 100..174

4.24 Normalized Stress-Displacement Curves - Series 200..175

4.25 Normalized Stress-Displacement Curves - Internal...176

4.26 Normalized Stress-Displacement Curves - External...177

4.27 Proposed Constitutive Relationship for Interfaces..178

5.1 Shear Displacement versus Time - Test # 11.........183

5.2 Units Composing the Phenomenological Model.........186

5.3 Final Configuration of the Proposed Model..........188

5.4 Simplified Phenomenological Model.................190

Figure Page

5.5 Definition of Equivalent and Individual Stiffnesses192

5.6 Idealized Input Data for Model....................196

5.7 Large Shear Test Simulation - Stress-Displacement Curve.............................202

5.8 Shear Stress Distribution Along Interface..........203

5.9 Shear Displacement Distribution Along Interface....205

5.10 Results of Axial Loading Test in Frictional Piles.................................207

5.11 Shear Stress Distribution Along Pile...............209

5.12 Field Measurements Simulation - Linear Function I..212

5.13 Field Measurement Simulation - Linear Function II.......................................213

5.14 Field Measurements Simulation - Hypebolic Function.214

5.15 Comparison Between Two Sizes of Shear Box Tests....218

5.16 Comparison Between Three Sizes of Shear Box Tests.......................................219

6.1 Example of Banded Matrix...........................237

6.2 Example of Matrix with Skyline.....................238

6.3 Input and Results of Shear Box Test Simulation.....245

6.4 Mesh and Input Parameters - Tets for INTERDAM......246

6.5 Results of Retaining Wall Simulation...............248

6.6 Mesh for Comparison Between INTERDAM and FENA-2D...249

6.7 Comparison Between INTERDAM and FENA-2D...........251

6.8 Finite Element Mesh - Test Embankment Backanalyses.255

6.9 Back Analysed Normal Stresses Acting at the Wall..263

6.10 Back Analysed Shear Displacements.................265

Figure Page

6.11 Back Analysed Shear Stresses........................266

6.12 Effect of Variation of Elastic Parameter - Normal Stress....................................269

6.13 Effect of Variations of Elastic Parameters - Shear Displacements...................270

6.14 Effect of Variations of Elastic Parameters -Shear Stresses.........................271

6.15 Effect of Sample Preparation - Shear Displacements.273

6.16 Shear Displacements - Extreme Conditions...........276

6.17 Shear Stresses for No Slip Condition...............277

6.18 Results of Settlements of Fill - Back Analyses.....282

6.19 Load Transfer Ratio versus Height of Wall..........284

6.20 Extension of Region Subjected to Load Transfer.....285

A.1 Comparison Between Laboratory Nuclear Densometer 312

A.2 Laboratory vs Nuclear Densometer - Average Results...................................314

B.1 Total Settlements vs Distance from Wall - MP-1.....316

B.2 Total Settlements vs Distance from Wall - MP-2.....317

B.3 Fill Settlements vs Distance from Wall - MP-2......318

B.4 Total Settlements vs Distance from Wall - MP-3.....319

B.5 Fill Settlements vs Distance from Wall - MP-3......320

B.6 Total Settlements vs Distance from Wall - MP-5.....321

B.7 Fill Settlements vs Distance from Wall - MP-5......322

B.8 Total Settlements vs Distance from Wall - MP-6.....323

B.9 Fill Settlements vs Distance from Wall - MP-6......324

B.10 Total Settlements vs Distance from Wall - MP-7.....325

B.11 Fill Settlements vs Distance from Wall - MP-7......326

Figure Page

C.1 Stress-Strain Curves for Triaxial Tests............331

D.1 Detailed View of Large Shear Box Test..............333

D.2 Detail of Recess for Shear Stress Device...........334

D.3 View of Modified Version of Shear Stress Device....335

D.4 Detail of Outer Box for SHera Stress Device........336

D.5 Detail of Inner Box for Shear Stress Device........337

D.6 Detail of Removable Angle to Reduce Sample Size....................................338

E.1 Vertical Displacements During Shear - Test#9.......341

E.2 Vertical Displacements During Shear - Test#3.......342

E.3 Vertical Displacements During Shear - Test#5.1.....343

G.1 Representation of Goodman's Joint Element 360

H.1 Comparison for Constitutive Models.................376

List of Plates

Plate Page

3.1 Excavation Stages.................................38

3.2 View of Wall Instruments............................66

3.3 Sequence of Installation - Shear Displacement Devices..........................71

3.4 Shear Stress Device after Instalation................78

4.1 General View of Large Shear Apparatus..............127

4.2 Loading Head for Vertical Stresses.................132

4.3 Device to Measure Vertical Displacement during Shear....................................138

D.1 Detail of Connection U-Frame - Concrete Base.......339

1. INTRODUCTION

1.1 GENERAL

The objective of this thesis is to study the behaviour of soil-structure interfaces. Despite the frequency of their occurrence in most large civil engineering projects, scant attention has been given to the subject, in particular to the fundamental physical phenomena and their interpretation as well as to the influence on the behaviour of the soil mass.

For the purposes of this research the structure is represented by a planar concrete wall and the soil mass by a compacted soil. Therefore, most of the discussions presented during this thesis are related to problems such as joints between earth and concrete dams, retaining walls or wing walls of bridges. When applicable, reference will be made to other examples.

1.2 BRIEF HISTORY OF THE TREATMENT OF SOIL-CONCRETE INTERFACES

The stability of soil-concrete interfaces was of great concern before the beginning of the last century. In 1776, Coulomb developed a method of determining the limiting earth pressure acting on retaining structures, considering the effect of the friction between soil and structure. Later, in 1857, Rankine presented a similar theory not considering the effect of the friction. These two independent works comprise the Classical Theory of Limit Equilibrium and their applicability is widespread and suitable for most practical problems.

However, in some cases, not only the **factor of safety against collapse** is desired, but also the development of stresses and strains both at the interface and in the adjacent soil mass is of interest. Analyses using limit equilibrium fail to furnish this information.

With the advent of numerical techniques, such as the finite difference method, the boundary element method and the finite element method, the calculation of stresses and strains in soil masses became possible, even in circumstances where exact solutions (closed form solutions based on the theory of elasticity) were not available.

Among the methods mentioned, the finite element method is of particular interest for its flexibility in modelling complex problems, including anisotropy, nonhomogeneity, complex geometry and discontinuities. The last point is a very common feature of rock masses (joints or fractures) and efforts have been devoted during the last two decades to improve the methods of modelling. As a result of this line of analytical research, a special type of element has been derived, termed **joint element.**

Due to the similarities between the representation of discontinuities in rock masses and soil-concrete interfaces, using the finite element method, the joint element became widespread in simulations involving interfaces. Hence, since the 1970's, the study of this type of interface has been reinitiated, with special attention to the area of numerical modelling (the first reported joint element is dated 1968). However, irrespective of the differences inherent in these two classes of problems (jointed rocks and soil-concrete interfaces) advances in finite element techniques for interfaces, based primarily on jointed rock concepts, have been developed in an uneven proportion to the understanding of the physical processes involved in the soil-concrete interface. Furthermore, the emphasis in numerical modelling seems to have overshadowed fundamental physical concepts, as well as the urge for field observations of the interface behaviour. The former is of utmost importance in avoiding misinterpretation of the basic mechanical processes influencing the interface behaviour. The latter is the only possible method of ensuring that the advances in analytical modelling lead to a more realistic representation of the problem, since exact solutions based on the theory of elasticity (closed form solutions), are not readly available.

Therefore, a brief review of some mechanical concepts of elastic bodies in contact will be presented in the following section, aiming to revive the fundamental theory.

1.3 MECHANISTIC VIEWPOINT

An important mechanical concept governing the behaviour of interfaces between elastic bodies can be found, not in advanced engineering books, but in classical physics and statics books. As will be shown during the presentation of this research, this basic concept seems to have been neglected and replaced by more complex theories, not always more appropriate, to represent the physical process involved.

For the sake of this introductory presentation, a simple example will be discussed, as shown in Figure 1.1.

This figure depicts an elastic body "A" resting on a inclined plane. This plane has variable angle of inclination, θ. First, let the angle θ assume a null value. In this configuration equilibrium of the system is ensured by a vertical reaction equal and opposite to the body force that is, only the vertical component exists.

If the angle θ is increased, a component of the body forces, acting parallel to the inclination θ of the plane will be generated. To satisfy equilibrium in this new configuration a reaction (equal and in opposite direction) appears, acting at the interface. As long as the value of this reaction, τ, is not overcome, the system satisfies equilibrium and no movement can be observed.

For continuous increases in the angle of inclination there will exist an angle θ for which the value of the reaction τ will assume its maximum value. This angle is

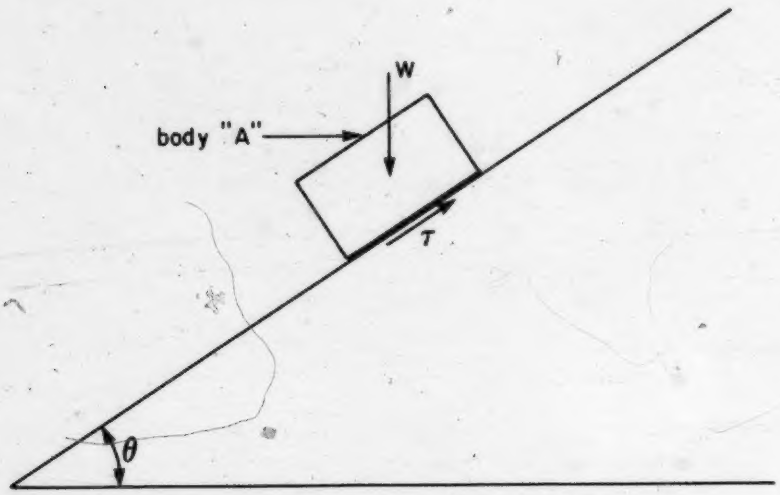

W - weight of elastic body
τ - shear stress

Figure 1.1 The Concept of Two Elastic Bodies in Contact

called the "crictical angle". Any further increase in θ will cause block "A" to slide on the inclined plane. At this moment, equilibrium is no longer satisfied, the value of τ is constant and is equal to its maximum possible value. It is said that, for this angle θ_{crit}, block "A" has overcome the "static friction" and the tangent of θ_{crit} is called the coefficient of static friction (μ). The value of μ is a property of the interface and, as such, is unique. It will change only if one of the elastic bodies involved in the experiment described above is replaced.

The value defined in the above discussion is of fundamental importance because it seems to be the only existing **fundamental quantity** that can be measured for an interface. As a fundamental quantity, this concept holds for any type of interface under any circumstance. This concept, however, does not consider strains and displacements.

Furthermore, the recognition that tangential stresses (reaction τ) are developed to maintain equilibrium is also of great interest for the discussion that follows.

All these points will be further explored in later chapters.

1.4 OBJECTIVES AND SCOPE OF THIS RESEARCH

This research aims to discuss three major issues related to the behaviour of interfaces soil-concrete.

First, the analysis of the interface in terms of stresses and displacement will be considered.

In this part it is intended to create an overall understanding of the behaviour of interfaces and their influence on the behaviour of the soil mass placed adjacent to the structure. For this purpose, a program of field instrumentation was planned and carried out in an experimental embankment. This part can be regarded as a view of the **macro** behaviour of the interface.

The analysis of this first part led to a tentative description of the physical behaviour of this type of interface, in order to explain certain observed features.

Finally, the use of the finite element method as a **tool** for analysis of interfaces is addressed. As will be seen in subsequent chapters, several methods of analyses have been proposed in the past. However, in most cases, only one type of test is generally used to determine the parameters for the analyses, namely the direct shear box test. The suitability of this test to represent the behaviour of interfaces is discussed based on the physical interpretation of the interface behaviour.

1.5 CONTENTS OF THIS THESIS

The first step of this research included a detailed study of the available literature on soil-concrete interfaces. This is reviewed in Chapter 2, and demonstrates the necessity for field observations of interface behaviour. This subject is covered in Chapter 3 which describes a program of field instrumentation carried out in a test fill, built in the area of Dickson Dam. During the design of the field instrumentation, the need to develop new field instruments was faced. Therefore, two new devices have been created and are described.

Aiming to reproduce part of the field instrumentation, Chapter 4 describes a reduced scale prototype built in the laboratory. Under these more controlled conditions several features could be observed and as a result a **"phenomenological model"** was derived. This model is described in Chapter 5. Apart from its presentation, examples are described to prove its reliability and appropriateness in describing the interface behaviour.

Finally in Chapter 6, a Finite Element analyses of the test embankment is presented. The features of the program used are described and examples provided to assess the reliability of the program.

In Chapter 7, the main conclusions are summarized and recommendations for further reseach are presented.

2. ANALYTICAL VERSUS EXPERIMENTAL MODELLING

2.1 INTRODUCTION

In this chapter a literature review is presented, emphasizing the most pertinent articles for this research. The review is subdivided into two parts. In the first part some of the joint elements used in connection with the finite element method are described. The objective is to familiarize the reader with some of the most used techniques.

In the second part some applications of these methods in problems involving soil-concrete interfaces are described with special attention given to the reports presenting constitutive models. This is followed by a summary of some practical experiences related to actual engineering projects. This second part intended to draw attention to the lack of experimental observations of interface behaviour.

2.2 LITERATURE REVIEW

2.2.1 The Concept of Joint Element

The finite element method is a very powerful numerical method able, at least in theory, to solve the most complex problems encountered in civil engineering. Its ability to incorporate complexities has made the method one of the most used numerical techniques now available.

Among the available formulations used in the method, the most important of which, widely used in the solution of practical problems, is the displacement-based finite element formulation. The major reason for its wide use is its simplicity, generality and good numerical properties (Bathe and Wilson, 1976). Other formulations, not used as often are the equilibrium formulation, hybrid and mixed methods.

Whenever the finite element method is referred to in this thesis it is the displacement-based formulation, unless stated otherwise.

In the displacement formulation, the solution of a particular problem can be summarized as the solution of a set of linear equations of the type:

$$KU = R$$

where:

R - load vector including all the forces acting in the body.

U - displacement vector and the unknowns of the problem.

K - stiffness of the body.

The matrix K can be determined as follow (Zienkiewicz, 1971):

$$K = \Sigma \int [B]_i^T [C]_i [B]_i \, dV_i$$

where:

$[B]_i$ - geometric matrix for the element

$[C]_i$ - constitutive matrix of the element

dV_i - integral over the volume

The integral over the volume applies for three dimensional problems. For most civil engineering applications, plane analyses can be performed (plane stress or plane strain) and then the integral is evaluated over the area of the element.

Under certain circumstances the formulation of the stiffness matrix, as presented above, becomes meaningless since neither geometry (area) nor elastic properties can be assigned to a particular region of the continuum; such are the cases involving fractures in rock masses, or soil-concrete interfaces. For these particular applications special formulations have been derived, based on techniques such as Lagrange multipliers or the constraint methods (Zienkiewicz, 1971; among others)

On the other hand, if the joint can be assumed to have some thickness, such as when rock joints are filled with soil, the definition of the stiffness matrix, as presented above, holds and the representation can follow the conventional derivation.

In the following section some of these formulations are briefly reviewed.

It is worth mentioning that models derived to represent fluid flow through discontinuities (such as Noorishad (1971) or Gale et al (1974)) are not included in this review.

2.2.2 Review of Analytical Formulations

In this section 15 different joint elements are presented, including a brief description of each. In Figures 2.1 and 2.2 their geometry is shown and the notation used in the text is explained in these figures.

It is of interest to notice that most of the joint elements found in the literature follow either the Goodman et al (1968) proposition for zero thickness elements or Zienkiewicz et al (1970) for finite thickness elements.

The element proposed by Goodman et al (op.cit.) has been improved twice by the same author (1972 and 1976) to account for dilatance and rotation respectively.

The element has four nodes and eight degrees-of-freedom. The "strain vector" $\{\epsilon_j\}$ for the joint element is defined by the relative displacements and rotations of the two sides (top and bottom) measured at the centre of the element, as shown in Figure 2.1, or:

$$\{\epsilon_j\}^T = [\Delta u_o \; \Delta v_o \; \Delta w_o]$$

where,

u_o, v_o and w_o are shear, normal and rotational "strains" respectivelly.

This "joint strain" is related to the nodal displacement using the relationship:

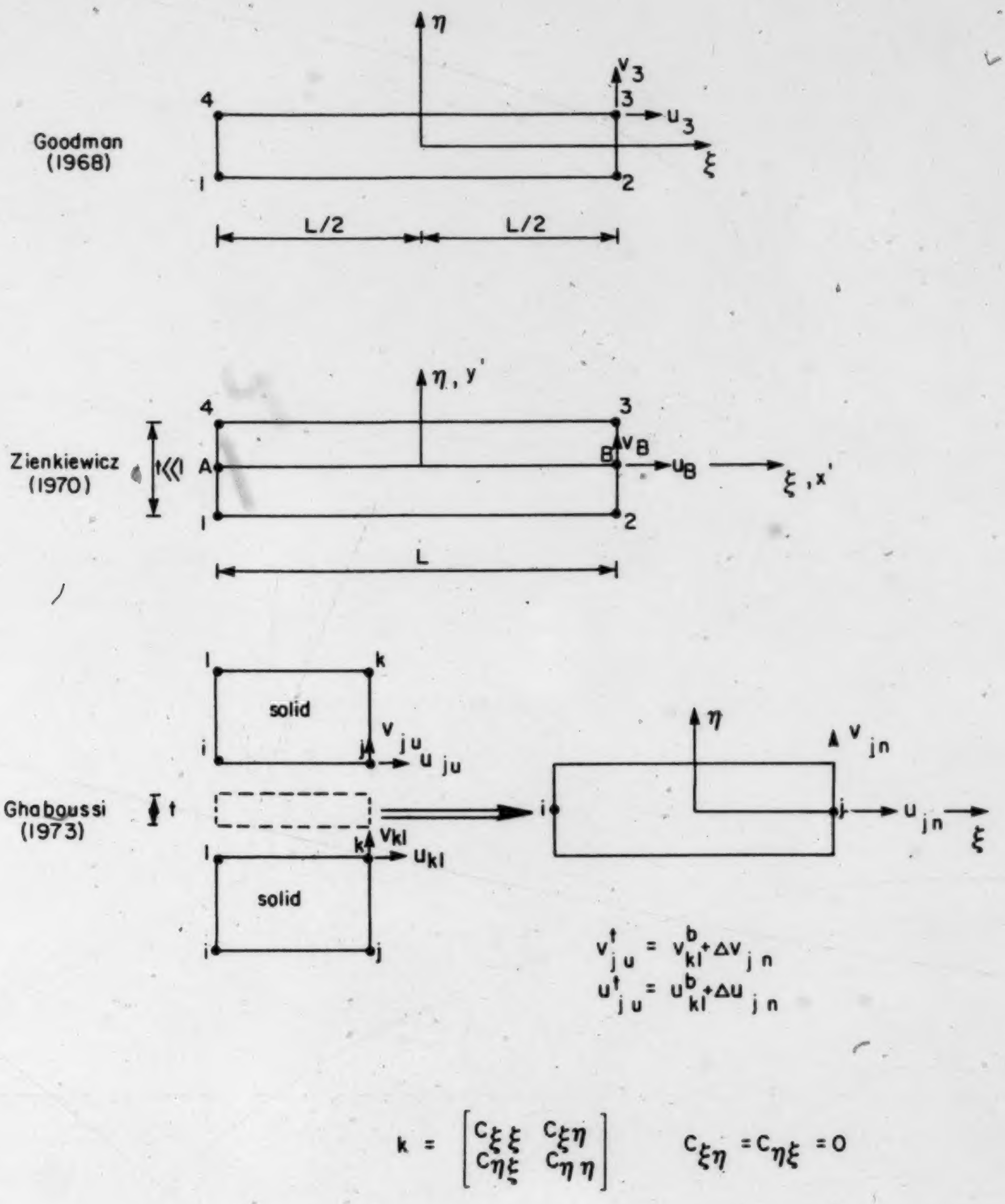
Goodman
(1968)
η
ξ
v3
u3
1
2
3
4
L/2
L/2
Zienkiewicz
(1970)
t≪l
η, y'
ξ, x'
A
B
vB
uB
1
2
3
4
L
Ghaboussi
(1973)
t
solid
solid
i
j
k
l
v ju
u ju
vkl
ukl
η
ξ
v jn
u jn
$v^t_{ju} = v^b_{kl} + \Delta v_{jn}$
$u^t_{ju} = u^b_{kl} + \Delta u_{jn}$
$k = \begin{bmatrix} c_{\xi\xi} & c_{\xi\eta} \\ c_{\eta\xi} & c_{\eta\eta} \end{bmatrix} \qquad c_{\xi\eta} = c_{\eta\xi} = 0$

Figure 2.1 Details of Some Joint Element Formulations

$$\{\epsilon_j\} = [T]\{\underline{u}\}$$

and the stresses can be found using the constitutive matrix as:

$$\{\sigma\} = [C_i]\{\epsilon_j\}$$

where,

$$C_i = \begin{bmatrix} K_s & 0 & 0 \\ 0 & K_n & 0 \\ 0 & 0 & K_w \end{bmatrix}$$

in which,

K_s - shear stiffness (similar to K_t)

K_n - normal stiffness

K_w - rotational stiffness

The last term can be expressed as a function of the normal stiffness and equals:

$$K_w = (K_n \times l^3)/4$$

where,

l - length of joint element.

It should be noticed that the constitutive matrix $[C_i]$ has six zero terms, suggesting that dilatancy is not considered.

This element has been used extensively in the past and several modifications have been proposed to accomplish specific needs. In 1972, Rouvray and Goodman presented a modified formulation aiming to account for initial stress dependency on the joint parameters, dilatancy and a criteria for crack initiation in rock blocks.

Although the basic formulation remained unaltered, the constitutive matrix was reformulated using the "Perturbational Method" (Heuze, 1971) to derive the stiffness parameters. Dilatancy was considered using a similar approach (Perturbational Method - Goodman and Dubois, 1972) since the evaluation of off-diagonal terms K_{sn} and K_{ns} in the matrix:

$$C = \begin{bmatrix} K_{ss} & K_{sn} \\ K_{ns} & K_{nn} \end{bmatrix}$$

is rather difficult.

These two terms represent the effect of the shear stress on the normal displacement and vice-versa, or:

$$K_{sn} = [\delta\tau/\delta v]_u$$

and

$$K_{ns} = [\delta\sigma/\delta u]_v$$

where:

τ - shear stress

σ - normal stress

u, v - shear and normal displacements.

The element proposed by Zienkiewicz et al (1970) has been modified by Sharma et al (1976) and applied in several different practical cases.

Zienkiewicz drew attention to the difficulties arising in the use of solid elements to represent interface behaviour, primarily caused by the elongated geometry (narrow and thin) of this region. Therefore, Zienkiewicz derived a new joint element capable of assuming such a configuration.

Although thickness is considered when computing the element properties, the nodes represent physically the same point (same coordinate). In other words, in the general description of the problem the element will be represented by the two mid side points A and B in Figure 2.1.

The displacements are described using linear shape functions of the type:

$$\xi = 2x'/L$$

and

$$\eta = 2y'/t$$

where

ξ and η - local normalized coordinates
x' and y' - local coordinates
L - length of joint element
t - thickness of joint element.

Thereafter, the element is derived as a conventional isoparameteric solid element.

Sharma (1976) used a similar formulation to derive a new model to study the behaviour of a 260.5 m high rockfill dam with vertical and inclined cores (Tehri dam). This formulation assumes a nondilatant joint with zero off-diagonal terms in the constitututitive matrix.

Another two types of elements were presented by Ghaboussi et al(1976) and Desai et al (1984). Both assume that the element has a finite thickness. The former defines the relative displacement between the two continuous masses as independent degrees-of-freedom for the element. Ghaboussi's joint element has only two nodes as shown in Figure 2.1.

The displacements degree-of-freedom of one side of the slipping surface is transformed into relative displacement of the element as follows:

$$U_i^t = U_i^b + \Delta u_i$$

where superscrips b and t refer to "bottom" and "top" solid elements respectively. Similar expressions can be obtained for the second direction and for the other nodes (see Figure 2.1)

Since the element has thickness, joint strain can be defined as:

$$\{\epsilon\} = 1/t \ \{\Delta \underline{u}\}$$

where:

ϵ - shear and normal strains

t - thickness

Δu - incremental shear and normal displacements, in local coordinates

The general formulation for the stiffness matrix in local coordinates is:

$$[k] = \int [B]^T [C] [B] \, dA$$

where:

[B] - strain-displacement relationship matrix

[C] - constitutive matrix

This element was used as the basis for the derivation proposed by Saha (1982) for a new element.

The element described by Desai et al (1984) is a conventional isoparametric element applicable to a large range of aspect ratios (ratio between sides of the elements), but it differs from the Zienkiewicz et al(1970) element in its definition of the constitutive matrix $[C_{ij}]$.

Experiences reported by Desai et al (1984) suggested that aspect ratios up to 0.01 can be applied with no risk of numerical problems. Furthermore, such a ratio should be satisfactory for simulating most interface behaviour. Details of this element are also presented in Figure 2.2.

Finally, a similar approach was used on a separate occasion to derive the last two joint elements presented.

Herrmann
(1978)

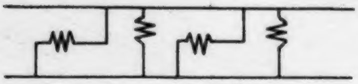

Desai
(1984)

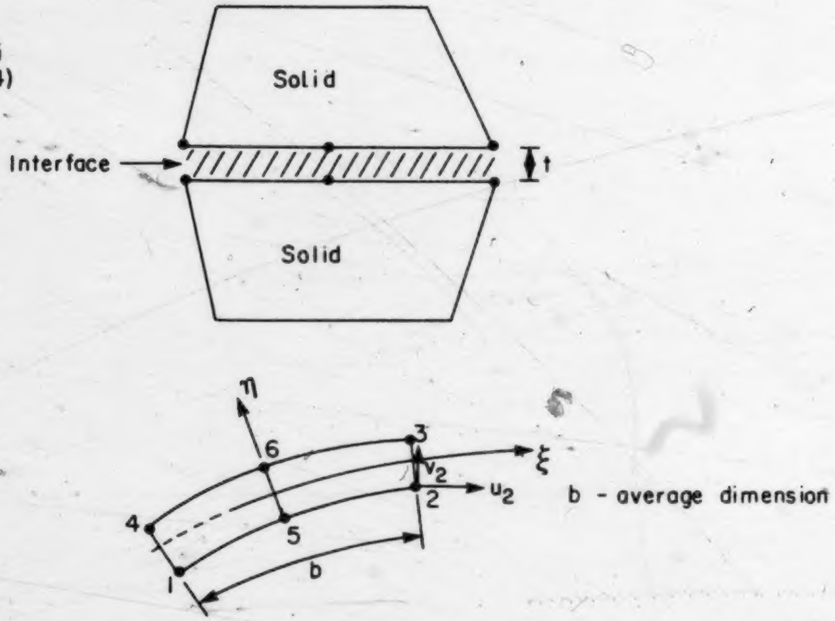
Solid
Interface
t
Solid
η
ξ
1
2
3
4
5
6
v_2
u_2
b
b - average dimension

$$[k] = \int_v [B]^T [C][B]\, dv$$

$$[C] = \begin{bmatrix} C_1 & C_2 & 0 \\ C_2 & C_1 & 0 \\ 0 & 0 & G_i \end{bmatrix}$$

$$C_1 = \frac{E\,(1-\nu)}{(1+\nu)(1-2\nu)}$$

$$C = \frac{E\nu}{(1+\nu)(1-2\nu)}$$

$$G_i \approx K_t$$

Figure 2.2 Details of Some Joint Element Formulations - cont.

Herrmann (1978) and Katona (1981) proposed joint elements using the "**constraint method**". The first element uses springs (Lagrange multipliers) to represent a particular constraint applied to a pair of nodes, initially in contact (same coordinates). The springs can be nonlinear and the bond that they represent can sustain a maximum load equivalent to a maximum shear stress determined by Coulomb's equation. Only after the attainable stress is fully mobilized, relative displacement (δ) occurs as slippage (if in the tangential direction) or separation (if in the normal direction). The method is both incremental and iterative in order to allow nonlinearity to be included and to permit the desired mode of deformation to be assumed (e.g. linkage, separation or slippage).

On the other hand, Katona (op.cit) used both the **constraint method** and the **directional stiffness** formulation (the later is the conventional method used, for example, by Goodman) to derive his element. However, instead of using Lagrangian multipliers to represent a particular constraint, the author applied a constraint equation directly in the basic equation of the **Principle of Virtual Work**. Thus, a constraint equation of the type:

$$C\underline{u} - a = 0$$

where,

C - constraint coefficient matrix

a - specified constant (e.g. displacement gaps)

$\underline{u}$ - incremental displacement vector.

and the consequent virtual work done by the force causing this particular constraint, that assumes the form:

$$\text{constraint virtual work} = \delta \underline{u}^T C^T \lambda$$

where,

$\delta \underline{u}$ - variation in the displacement vector

λ - constraint force

can be inserted in the general equation of the principle of virtual work, to get the final general equation including a constraint.

In this formulation, three modes of deformation can be imposed in the tangential direction (fix, free or slip) by selecting appropriate constraint matrix and load vectors.

Using this method the author simulated an idealized buried pipe and compared the normal stresses and shear tractions with exact closed form solution for extreme cases of friction (bonded and frictionless conditions). The results show very close agreement and a third example, using an intermediate condition (frictional slip) falls between the two extreme cases, as expected.

A summary of the elements discussed in this section is listed in Table 2.1. In this table the most important characteristics of each element are presented.

It is worth mentioning that, although the formulations described in this section are not identical, a commom

#	Reference	Geometry		No Thick	Rotat.	Dilat	Str. Soft.	Notes
		Plane	Axis					
1	Goodman 1968	•		•				Relative displacement between top and bottom of the element. Constant Strain. No cross stiffnesses terms.
2	Zienkiewicz 1970	•				•	•	Formulation for midside nodes. Pair of nodes approx. same coordinates. Can be curved or variable thickness.
3	Heuze 1971	•		•			•	Bassically element #1 with possibility to apply initial state of stress or change parameters. Iterative.
4	Rouvray 1972	•		•		•	•	Same as element #1 with special formulation. Derived new parameters. Stress tranfer method.
5	Goodman 1976	•		•		•	•	Same as element #1 with special formulation to determine stiffnesses. "Perturbational Method". Include cross terms.
6	Ghaboussi 1976	•						Element has thickness and uses "relative displacement as independent degree-of-freedom". Only four per element.
7	Goodman 1976	•		•	•	•	•	Same as element #1 with formulation to include rotation. Uses an special term in the stiffness matrix.
8	Sharma 1976	•						Similar to element #2. Uses "Hyperbolic Model". Assumes always contractant joint with increasing normal stiffness.
9	Herrmann 1978	•		•				Uses springsin both directions to simulate the joint behaviour. Formulation in terms of relative displacement.
10	Heuze 1979	•		•	•	•		Same as element #1 with special formulation to consider dilatance.
11	Xiurum 1981	•		•		•	•	Another new model applied to element #1 to consider dilatance.
12	Van Dillen 1981	• 3-D				•		Allows for 3-D simulation. Includes plasticity with associated flow rule.
13	Katona 1981			•		•		Uses "directional stiffness" together with " constraint method" into the Pricipal of Virtual Work.
14	Heuze 1982	•	•	•	•	•		Claims to be the only axissymetric element in working condition. Includes two new stiffness terms.
15	Desai 1984	• 3-D			•	•	•	Ordinary solid element with particular stiffness matrix to allow joint simulation. Allows elastic-plastic model.

Table 2.1 Summary of Joint Elements

feature can be observed in the majority of the joint elements, viz, the parameters for the analyses are obtained from conventional direct shear box tests. The only exception found in the literature was the publication by Desai and his co-authors (1984), where the parameters for the element are derived from a special apparatus called the "Cyclic Multi Degree-of-Freedom Device" (Desai, 1980).

Some of these elements have been implemented into finite element programs such as, "*F*inite element *I*soparametric, *N*onlinear with *I*nterface interaction and *N*on-tension (FINLIN)" developed at Purdue University, or "*C*ulvert *AN*alyses and *DE*sign program (CANDE)" developed at the U.S. Navy Civil Engineering Laboratory. Another two programs have been developed at the University of California at Berkeley by Duncan and his co-workers. A very comprehensive discussion of some of these programs is reported by Wu,(1980).

In the next section, a review of some reported experiences where these numerical models were used is presented. This review was carried out to demonstrate that the available literature is insufficient to supply the necessary information for more detailed research work in the subject.

2.2.3 Review of Soil Mechanics Experience

The first joint element was reported in the literature in 1968. In the early 1970's the first model that could account for partial slip (or partial bond) between the structure and the adjacent soil was proposed (Clough and Duncan, 1970). Following a similar approach used by Duncan and Chang (1969) for nonlinear stress-strain relationships for soils, Clough and Duncan (op.cit.) fit a hyberbola to a series of standard shear box test results. The sample was composed of concrete in the lower half of the box and sand in the upper half. The gap between the two halves was kept as small as possible and the relative movement between the two halves of the box was assumed to be entirely due to interface movement. In other words, it was assumed that failure occured at the interface.

An empirical equation was derived based on a normalized plot according Figure 2.3. With this approach the value of the **"tangential stiffness"** (K_t), could be obtained. This value varies with normal stress and the relative displacement. According to this study, the value of the **normal stiffness** (K_n) should be kept very high to avoid the elements representing the soil overlapping with those elements simulating the concrete.

These two values (tangential stiffness - K_t or C_{ss}, and normal stiffness -K_n or C_{nn}) were assigned to **"joint elements"** (Goodman's type).

Using the proposed formulation, an analysis of a retaining wall was simulated and the results of the passive and active earth pressures show good agreement, for conditions not near the limit equilibrium, for both rotating

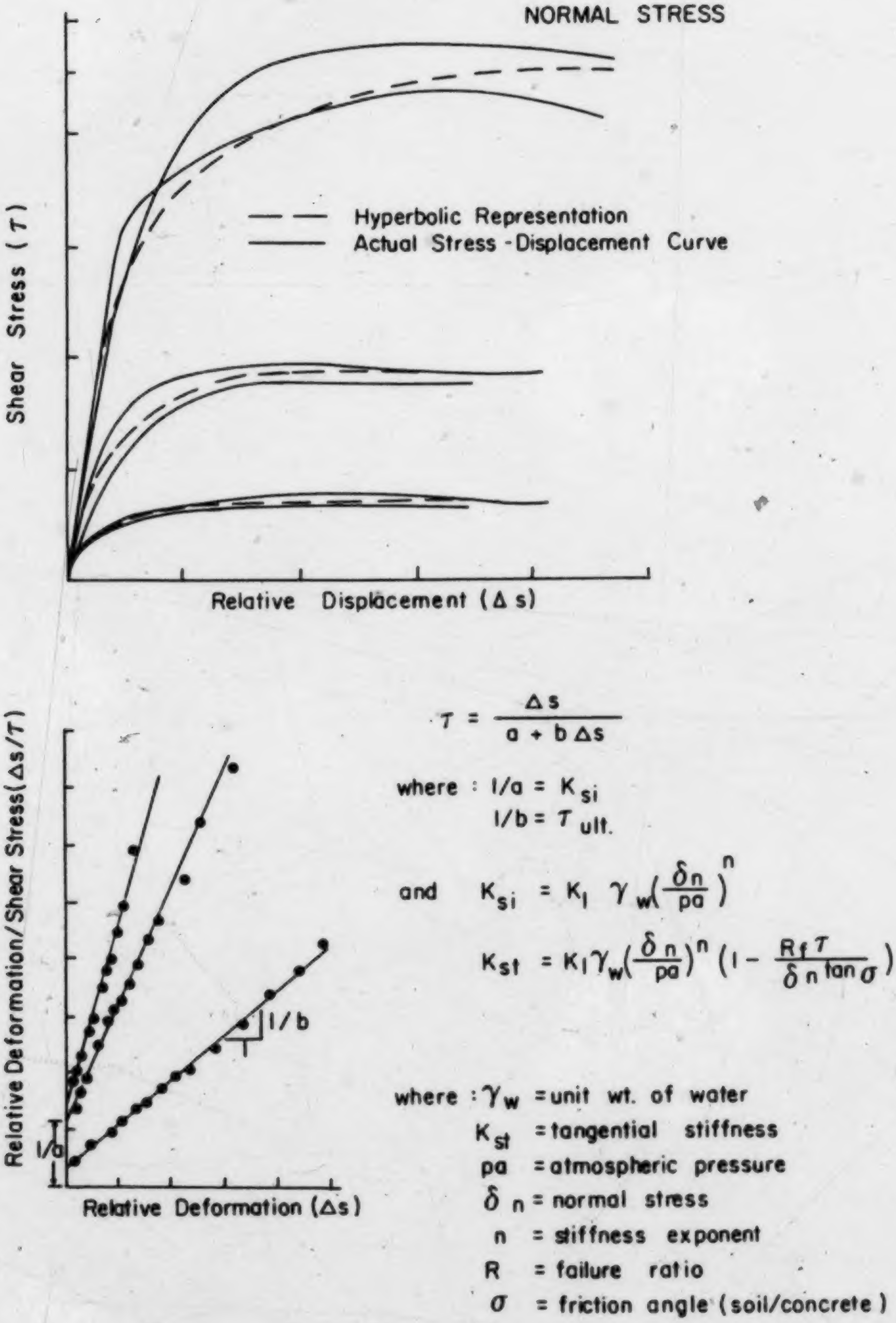

$$\tau = \frac{\Delta s}{a + b\,\Delta s}$$

where : $1/a = K_{si}$
$1/b = \tau_{ult.}$

and $K_{si} = K_1 \; \gamma_w \left(\frac{\delta_n}{pa}\right)^n$

$K_{st} = K_1 \gamma_w \left(\frac{\delta_n}{pa}\right)^n \left(1 - \frac{R_f \tau}{\delta_n \tan \sigma}\right)$

where : γ_w = unit wt. of water
K_{st} = tangential stiffness
pa = atmospheric pressure
δ_n = normal stress
n = stiffness exponent
R = failure ratio
σ = friction angle (soil/concrete)

Figure 2.3 Derivation of Hyperbolic Model

and translating walls.

The formulation was also used to analyse the earth pressure caused by a sand backfill during the construction stages of the Port Allen Lock (Duncan and Clough, 1970) with some degree of success.

The interest in the subject increased during the 1970's, specially in the area of earth dams. It seems that this sudden motivation was primarily promoted by the recognition of the **"potential zone of cracking and consequent hydraulic fracturing"** (during first impounding) that such type of interface can represent.

This risk was first recognized by Vaughan and Kennard (1972). For the case of Cow Green Dam, instrumented with contact pressure cells at the interface between the concrete and the earth dam, no risk of hydraulic fracturing was detected. Measurements showed that the normal stress in the concrete wall was consistently equal to 70% of the overburden pressure for four instrumented elevations. However, it is important to notice that the measurement of normal stress by itself does not provide sufficient information to define the **"state of stress"** at the wall. Therefore it is inconclusive whether or not the observed values were a consequence of overburden pressures solely or due to some load transfer mechanism that could have happened. This point is further discussed in Chapter 3.

A similar point of view was discussed by de Mello (1977) in the 17th Rankine Lecture, under the heading

"Design Considerations at the Critical Wrap-Around Details". According to de Mello, discontinuities are the **most critical points of design in embankment dams.** He quotes the contact core-concrete as a **problem of great responsibility with respect to cracking and piping.**

Probably spurred by these two very important papers, the International Commission on Large Dams devoted an entire session, during the 13th International Congress on Large Dams (New Delhi, 1979), to debate the subject. Due to the practical nature of this Congress, no major advances towards the physical or mechanical understanding of the behaviour of interfaces were reached, but it was a valuable opportunity to evaluate and call attention to several "**unexpected**" behaviours of this type of junction.

Empiricism and engineering judgement are the criteria most used in designing this important zone of a dam. Often past experience degenerated into a **"rule of thumb"**. The placement of clayey material, wetter than the optimum moisture content, compacted against a sloped concrete structure (this angle can vary from 70°-85° almost at random) is today assumed as a **design criterion.**

Subsequently, in the International Conference of Soil Mechanics and Foundation Engineering held in Stockholm in 1981, another session was dedicated to the subject. During this conference an important contribution was delivered (Roa, 1981). Roa used a linear-elastic-perfectly-plastic best-fitting approach to represent the behaviour of shear box tests in jointed rocks, as depicted in Figure 2.4. The convenience of his proposition is its simplicity and the ability to include loss of strength with increasing displacement (equivalent to strain softening, not represented in Figure 2.4).

Again, during the Fourteenth International Congress on Large Dams, held in Rio de Janeiro, another important case history was presented. It reports the behaviour of Roxo Dam (Guedes de Mello and Teixeira Direito, 1982).

The dam was built in Portugal between 1964 and 1968. Shortly after completion, signs of a defective behaviour in the earth dam, near the interface with the concrete structure, was detected in the form of excessive settlements.

The local geology comprised schist and porphyry. In the left abutment the quality of the foundation did not raise important problems. In the right abutment, on the other hand, the quality of the rock (mainly porphyry) became clearly worse and the formation showed faults and veins of schist and wide veins of heavily fractured quartz.

The defective behaviour was monitored with no major concerns regarding the causes of the problem until 1973. Since increasing settlement persisted it was decided to act in order to normalize the situation. At that time two kinds of action were suggested and discussed. One advocated very drastic measures such as the removal of the whole affected fill and its substitution by another one or two concrete

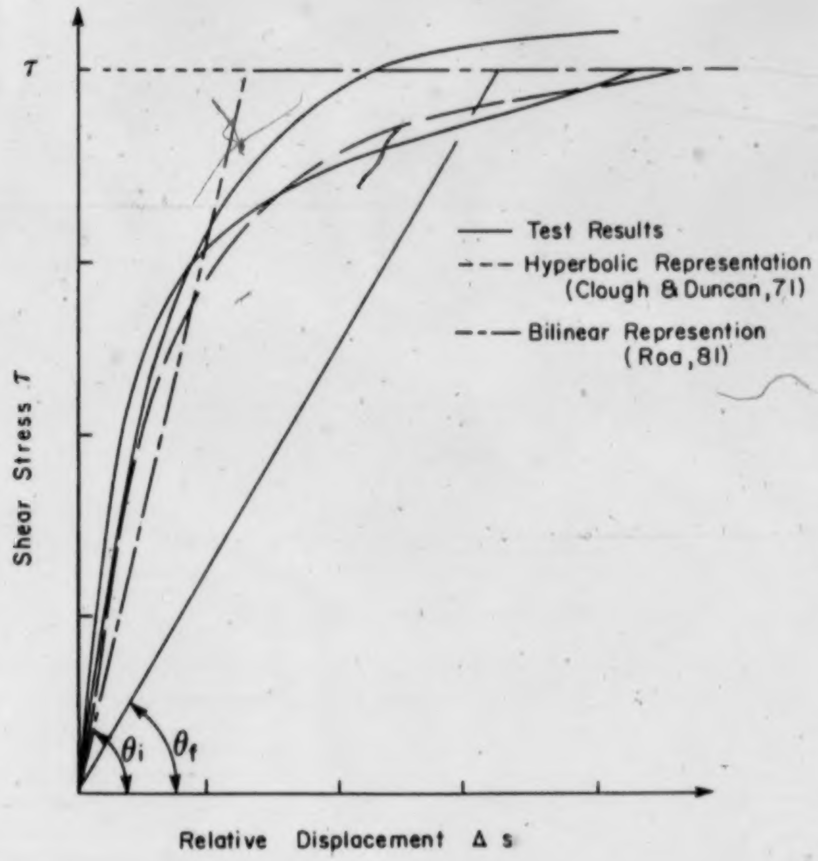

$\tau_f = \sigma_n \cdot \tan\delta$ where σ_n - normal stress
- friction angle

$Ks = \tan\theta_i = Ki\,\gamma_w\left(\frac{\sigma_n}{pa}\right)$ for $\tau < \tau_f$

$Ks = \tan\theta_f = \frac{\sigma_n \tan}{\Delta s}$ for $\tau = \tau_f$

where Ki , n - nondimensional parameters
Pa - atmospheric pressure

Figure 2.4 Derivation of Bilinear Model

sections. Such a solution was strongly contested due to the costs involved. Instead, a series of consecutive measures were adopted, hoping that some relatively simple and inexpensive remedial work would be the solution. Hence, between 1973 and 1976, more than one hundred boreholes were drilled for cement injection, instrumentation of high accuracy, sampling and so on.

Since no success was obtained after all these measures were tried, the solution of removing the earthfill affected by the excessive settlement and its replacement by another four blocks of concrete was undertaken.

In their conclusion, the authors' comment:

> "Unfortunately, the matter is not completely cleared up, although certain facts can be pointed out, each of them, though, insufficient to justify the behaviour of the dam."

In the writer's opinion, this case history justifies by itself the need for a more detailed study of interfaces, although it is not even completely clear whether or not the interface was the primary cause of the defective behaviour observed. Even with today's level of knowledge it was not possible to physically understand the reasons for the excessive settlement close to the soil-concrete interface.

It is true that the number of dams successfully constructed using today's state-of-the-art of interface design is much larger than the number of dams that showed defective behaviour.

However, as mentioned by De Mello (1977), despite the importance of this region of the design of dams, only scant attention has been given in the past to an understanding of soil-concrete interfaces behaviour. Surprisingly, as was mentioned before, numerical modelling, using the finite element approach, is far ahead of the development of the physical understanding of soil-concrete interface behaviour. (e.g. Desai et al, 1980; Desai et al,1984). In the writer's opinion, this seems inappropriate, since modelling should follow a complete understanding of the **"physical behaviour"** and not vice-versa.

Furthermore, none of the reports found in the literature and described in this section, have attempted to measure shear stresses and shear displacements at the interface. At most, measurements of normal stresses have been reported. However, to understand the behaviour of interfaces and the influence of the structure in the behaviour of the adjacent soil it seems of utmost importance to observe the shear stresses acting at the concrete wall, since these are the governing stresses for the behaviour of the adjacent soil, as will be discussed in later chapters.

Therefore, the study presented in the following chapters will focus on the shear stresses developed at the interface rather than normal stresses.

2.3 CONCLUSIONS

The literature review presented in this chapter showed a lack of information on the measured behaviour of soil concrete interfaces. Furthermore, most of the instrumentation programs discussed failed to determine some of the most important parameters for the analysis of such an interface, viz:

- measurements of shear stress, and shear displacement (relative displacement between the soil and the structure at the interface). These are the minimum requirements necessary to fully understand and model the behaviour of an interface.
- measurement of stress and displacements in the fill, including its trend towards the rigid boundary.

In order to accomplish these tasks, a test embankment was built in the area of Dickson Dam, at that time (1982) under construction in Alberta. This test fill is fully described in Chapter 3.

3. TEST EMBANKMENT

3.1 GENERAL

The major purpose of the Test Embankment was to cover the gap between "**analytical modelling**" and "**real behaviour**" of the prototype.

As in any field instrumentation project, the instruments have to provide the maximum possible information, with a minimum number of instruments. In the particular case of interfaces, the cost of the concrete structure governs the size of the test area (it represents approximately 20% of the total cost) and and the size dictates the number of instruments that can be installed in the test fill.

In this chapter a detailed description of the Test Embankment will be presented, including the geological features of the area, construction procedures, design details, quality control and instrumentation used.

It is worth mentioning that the state of the art of interface instrumentation in the early stages of this research induced the conception of two new instruments. They will be fully discussed in following sections.

3.2 DESCRIPTION OF THE TEST EMBANKMENT

The Test Embankment facilities included a 6 m high, 6 m wide reinforced concrete wall built prior to the fill placement. The area available for its construction lies within the reservoir of Dickson Dam, at that time (1982) under construction. The location of the dam site is presented in Figure 3.1. The nearest city is Innisfail, which is located approximately 250 km south of Edmonton, Alberta, and the dam site is about 25 km west of Innisfail.

The choice of locating the test area at Dickson Dam, and in particular inside the reservoir of the dam, was adopted for three main reasons:

- to avoid interference with the dam construction.
- proximity of material for backfilling.
- availability of contractors on the site.

At the same time this location imposed restrictions, the most important being the maximum elevation allowed at any point inside the reservoir. Since the site which was chosen was already at the maximum elevation permitted, the embankment had to be built inside an excavation which was opened up before the concrete wall was built.

The site lies in the Western Alberta Plains, just east of the Foothills of the Rocky Mountains. The area has a flat to gently undulating surface, except where glaciation and river erosion have formed broad, "U" shaped valleys. Thus, the stratigraphy generally consists of a thin cover of alluvially and glacially derived sediments overlying Tertiary sedimentary rocks of the Paskapoo Formation. The latter comprises layers of sandstone, siltstone, claystones and shales with minor layers of carbonaceous shales and argillaceous limestones. (Alberta Environment, 1980,

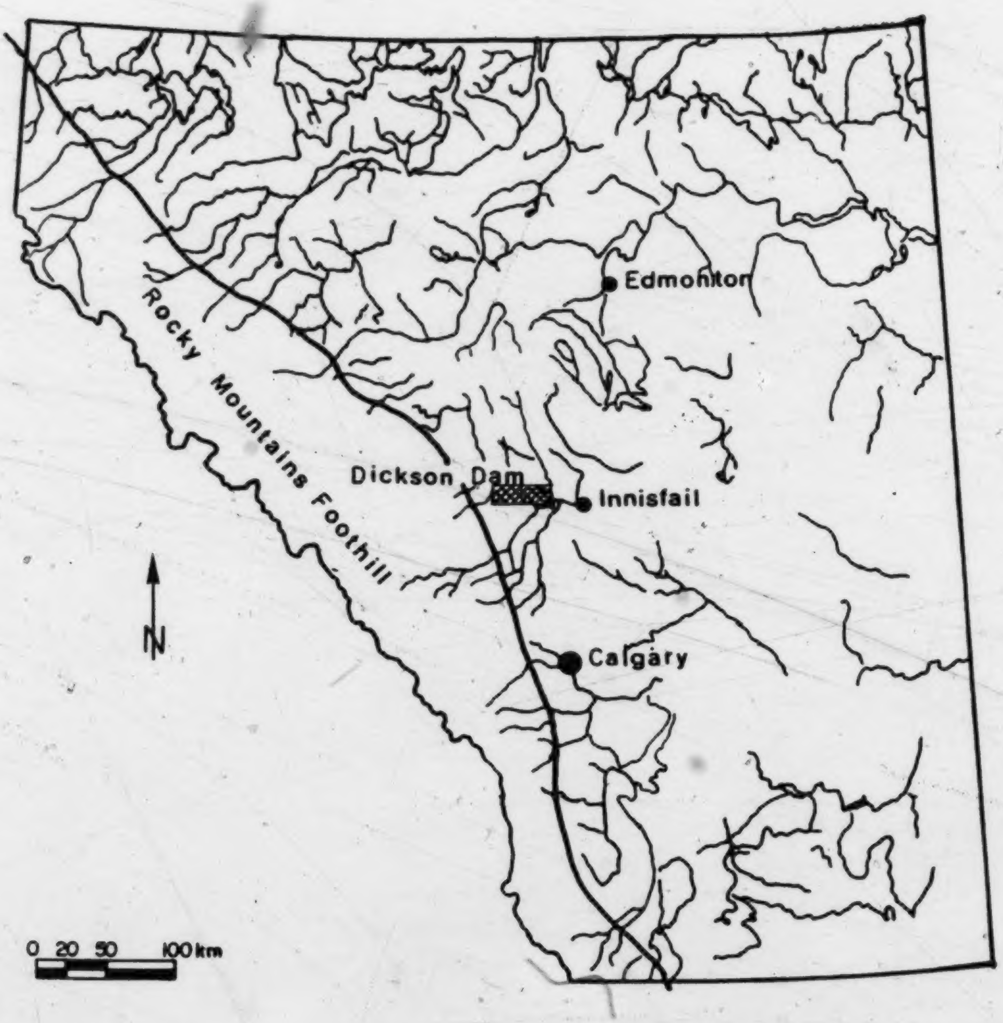
Edmonton
Rocky Mountains Foothill
Dickson Dam
Innisfail
Calgary
N
0 20 50 100km

Figure 3.1 Location of Dickson Dam Site

Report#8-31-0044). Several discontinuities can be identified in this material, most of them vertical and sub-horizontal.

Morgenstern and Eigenbrod (1974) tested several argillaceous materials including some samples of the Paskapoo Formation. They have shown that most of the clayey formations lose their strength rapidly, especially when immersed in water. According to their study, a loss of up to 90% of the original undrained shear strength can take place in few days.

In order to avoid the effect of the weathering process indicated above, the excavation for the test fill proceeded in two phases: During Phase I a small wedge of the material was removed, leaving an abutment inclined 1H:4V and enough space for the construction of the concrete wall which rests on that slope, as depicted in Figure 3.2.

As soon as the concrete wall was completed, Phase II of excavation proceeded, the final dimensions of the excavation being 100 m long (parallel to the wall) 25 m wide (perpendicular to the wall) and 5.5 m deep. Plate 3.1 provides a general view of the excavation stages.

It is important to notice that the excavation was made 100 m long to facilitate trafficability during excavation and backfilling. The "Test Embankment" was considered as only the center region, comprising the center 18 m with respect to the center of the wall (9 m each side). Quality control was carried out only in this area.

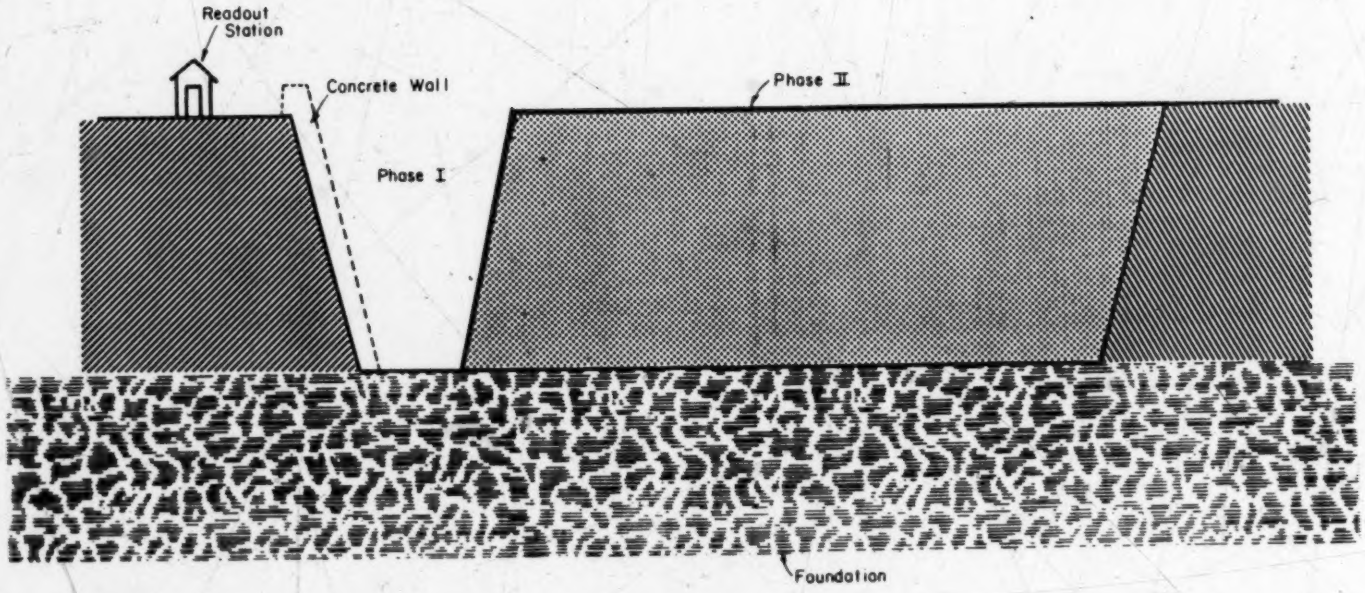
Readout Station
Concrete Wall
Phase I
Phase II
Foundation

Figure 3.2 Sequence of Excavation

a. Beginning of Phase I of Excavation

b. Final Excavation and Concrete Wall

Plate 3.1 Excavation Stages

Immediately after the excavation was completed the backfilling began. The fill was placed in 15 cm (6") thick layers after compaction.

The construction sequence used is described below:

- Approximately eight loads of loose material were placed on each side of the embankment area, using a scraper.
- A caterpillar D6 bulldozer spread the fill forming a uniform layer.
- When necessary a water truck was used to bring the material to the optimum moisture content.
- A sheepsfoot roller compacted the material. A tentative method showed that 8 passes would produce the desired degree of compaction.

It is generally known that compaction using a hand held compaction machines induces a rather different structure in compacted fills, as opposed to compaction using sheepsfoot roller. In order to reduce to a minimum the amount of fill manually compacted, the following sequence of compaction was used:

- 8 passes on each side of the fill with respect to the centre line (line containing the instrumentation as will be discussed in the next section), perpendicular to the wall;
- 8 passes on each side of the fill with respect to the center line, parallel to the wall and as close as possible to the wall. After this phase was

completed only a few centimeters of the fill had to be compacted using a hand held compactor.

- Finally, 8 passes between the instruments, where there was room for the sheepsfoot roller to travel. The remaining zone around the instruments was compacted using a hand held compaction machine.

With this procedure an average rate of construction of 0.33 m/day (aproximately two layers per day) was reached, as shown in Figure 3.3. The same figure shows the time when the initial reading for all the instruments was obtained.

The material used as back fill was obtained in part from the excavation and the remainder from a nearby borrow area. Similar material was used to build the dikes (aproximately 8 km) attached to the main dam of Dickson Dam.

A summary of the properties of this material is shown in Table 3.1, and Figure 3.4 presents the result of some 25 grain size analyses carried out during backfilling. Standard Proctor tests, performed prior to the fill placement, suggested that the average maximum dry density was 17.65 kN/m^3 (112 lb/ft^3) and the optimum moisture content was around 13.5%.

Compaction control was maintained using a Nuclear Densometer. In each layer, four tests located at randon, were performed, and after placement of every four layers a sample was collected to update the maximum dry density and optimum moisture content. The results of the compaction control is shown in Figure 3.5. Figure 3.5a presents the

Table 3.1 Properties of Test Embankment Soil

PARAMETER	UNITS	NUMBER OF TESTS	TYPE OF TEST	VALUE
Classification	-	25	Complete grain size	Sand Silt
Av	m^2/kN	5	Oedometric	2.5×10^{-4}
Mv	m^2/kN	5	Oedometric	2.2×10^{-4}
C	kPa	4	Triaxial	50.0
ϕ	degrees	4	Triaxial	33.7
γ	kN/m^3	25	Standard Proctor	17.65
Optimum Moisture Content	%	25	Standard Proctor	13.5
Atterberg Limits	%	5	Liquid Limit	28.9
	%	5	Plastic Limit	17.0
	%	5	Plastic Index	11.9

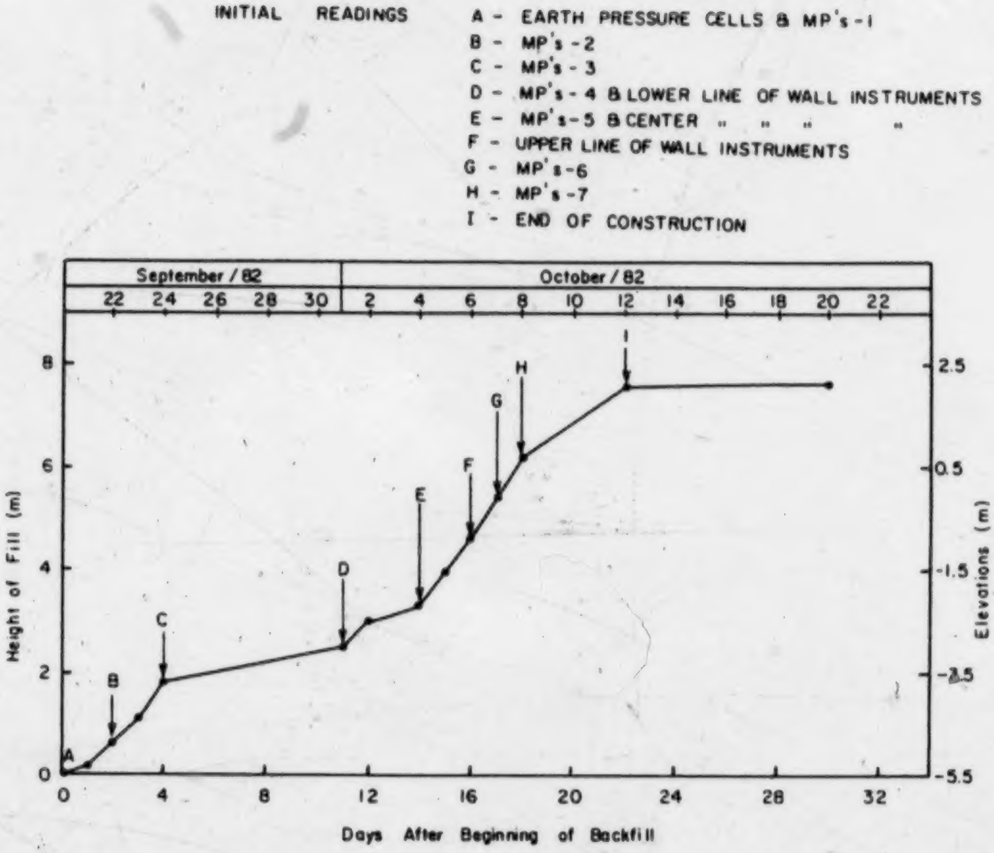

Figure 3.3 Rate of Construction - Test Embankment

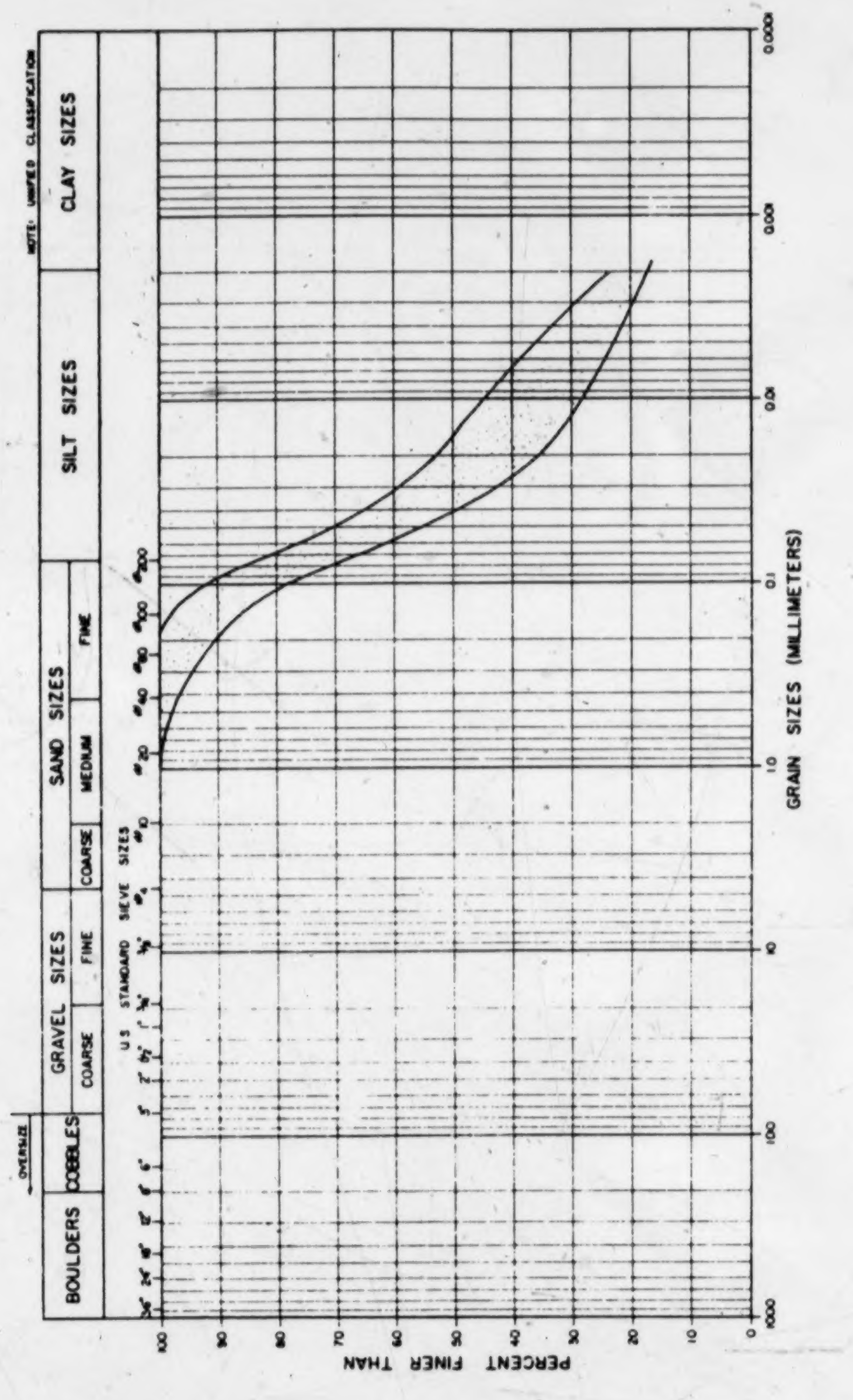

Figure 3.4 Grain Size - Test Embankment Material

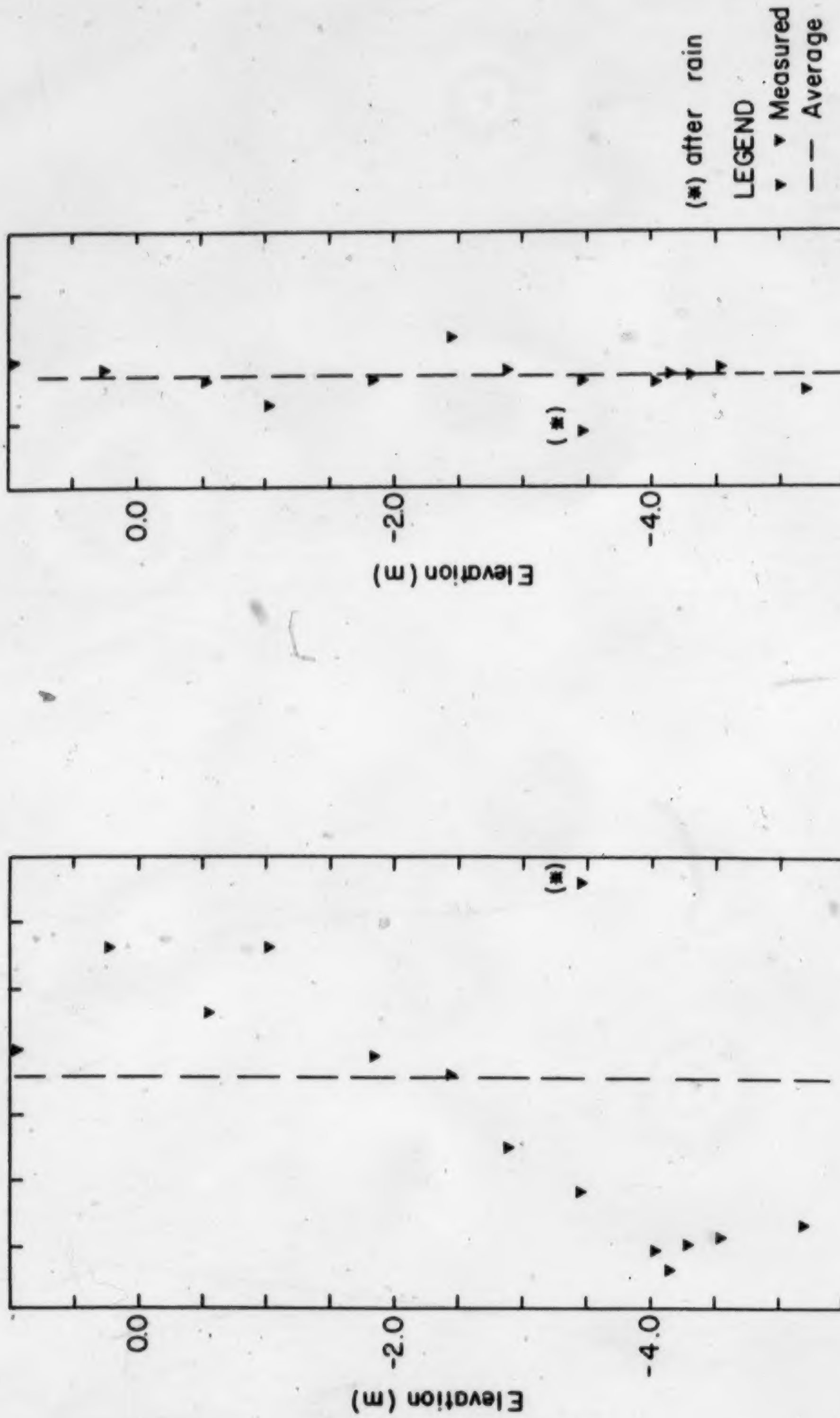

Figure 3.5 Compaction Control - Test Embankment

values of dry density and Figure 3.5b the optimum moisture content, as measured during construction.

It is worth mentioning that if in any circumstance the specifications of optimum moisture content (± 1%), and degree of compaction between 95% and 105% of the Standard Proctor were not met, a further two passes of the sheepsfoot roller would be necessary. If a low degree of compaction persisted, another two passes would be required.

If after this additional compaction the specifications were not satisfied, the layer would be removed and placement re-started with fresh material.

For the sake of completeness, Appendix "A" provides a brief description of Nuclear Gages with particular attention to the equipment used in the Test Embankment.

3.3 INSTRUMENTATION

Two different aspects were observed during the construction of the Test Embankment:

- the influence of the presence of the concrete wall on the behaviour of the soil mass.
- the behaviour of the interface.

In the first case, measurements of total stress and displacement fields, including its trend towards the wall, were performed.

In the latter, stresses and displacements were observed in order to determine a stress-displacement pattern for the interface. Whenever it was possible, the instruments were installed at the center line of the fill to avoid end effects and to permit plain-strain analyses to be performed.

A general view of all the instruments in their final location is shown in Figure 3.6. Table 3.2 presents a summary of quantities and different types instruments used.

In the next sections the instruments will be described in full.

3.3.1 Fill Instrumentation

In order to obtain the desired information, two different types of instruments were used in the fill:

- multipoint extensometers.
- earth pressure cells.

3.3.1.1 Multipoint Extensometers

To facilitate the installation procedure, a new shape was idealized for the multipoint extensometers. In this modified version a wooden plate, 30 cm X 30 cm X 2.5 cm thick (12" X 12" X 1"), replaced the original 30 cm (12") long PVC pipe containing four springs to hold the sensor in position inside a borehole (Burland et al, 1972). Figure 3.7 presents a detail of the plate used. The magnetic sensor is the same as in the original design. As a precaution, the wood was treated to avoid deterioration caused by the adverse environment.

TABLE 1

TYPE OF INSTRUMENT	LOCATIONS	TOTAL NUMBER OF INSTRUMENTS
Multipoint extensometer	7	45
Earth Pressure Cell	2	10
Settlement Hubs	3	3
Slope Indicator	1	1
Bench Mark	2	2
Shear Displac. Device	3	6
Shear Stress Device	3	3
Contact Pressure Cell	3	3
Piezometer	2	2

Table 3.2 Types and Quantities of Instruments

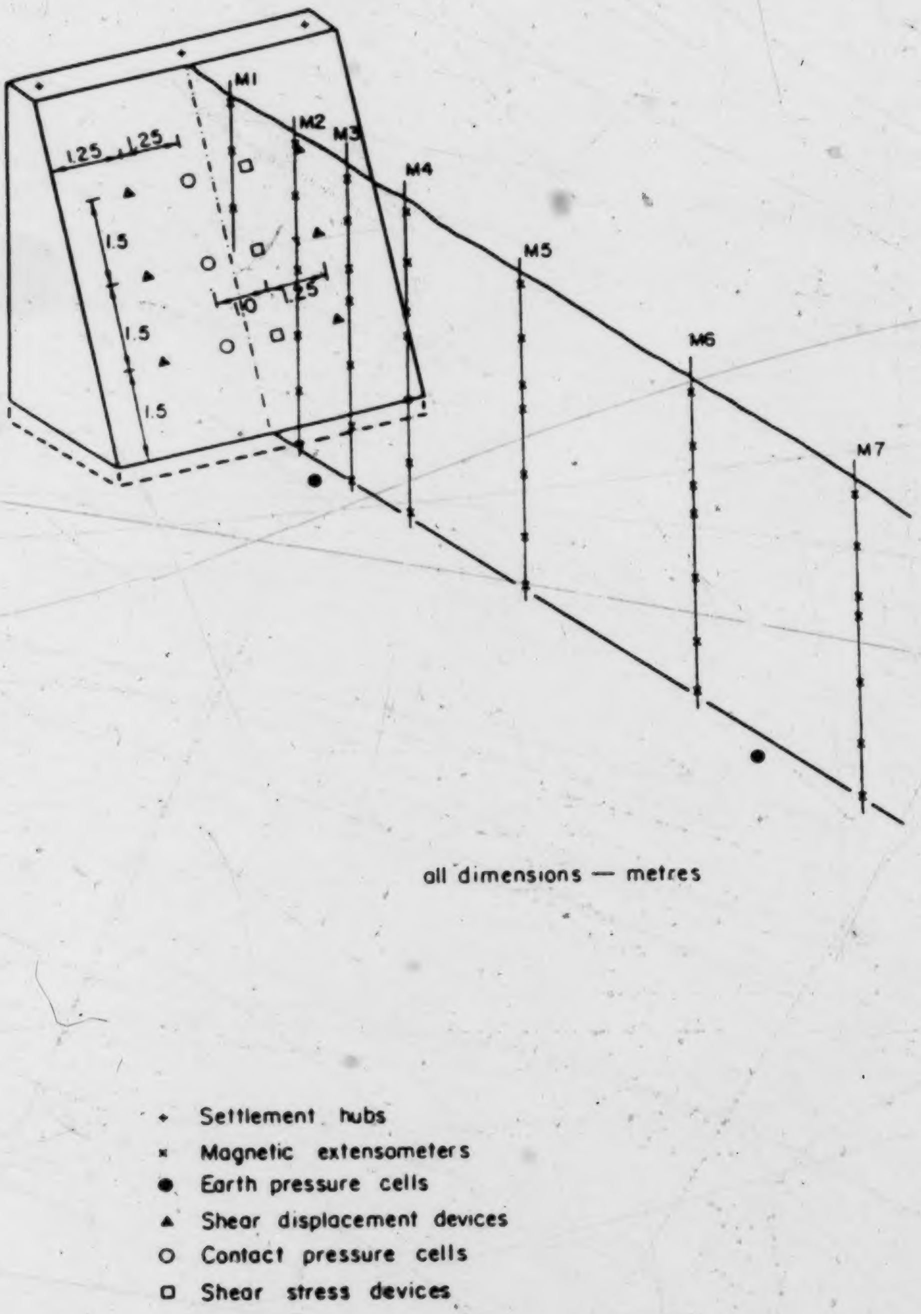
M1
M2
M3
M4
M5
M6
M7
1.25
1.25
1.5
1.5
1.5
1.0
1.25
all dimensions — metres
+ Settlement hubs
× Magnetic extensometers
● Earth pressure cells
▲ Shear displacement devices
○ Contact pressure cells
□ Shear stress devices

Figure 3.6 General View of Instrumentation

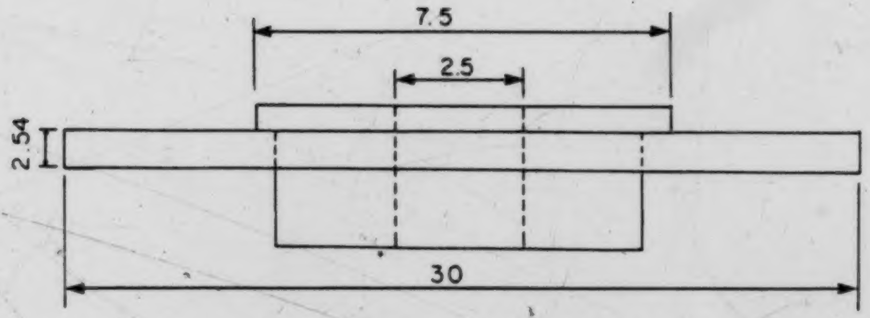
7.5
2.5
2.54
30
units: cm

Figure 3.7 Modified Multipoint Extensometers

Installation

The plates were installed at the center line of the fill, distributed in seven crossections. Their relative locations with respect to the top of the wall are presented in Figure 3.8. As can be seen in this figure, the verticals ME-2 through ME-7 had their first sensor at the fill-foundation interface, while the sensors installed at ME-1 began half way in the fill, having their access tube resting on the wall.

The plates were installed, at the desired elevation, by simply placing the plates around the access tube and pouring loose soil over it. To avoid damage to the plates, compaction around the access tube was permitted only after one full layer covered the plate.

3.3.1.2 Earth Pressure Cells

The earth pressure gauges were manufactured by Glöetzl and each cell consisted of a flat retangular steel chamber 20 cm X 30 cm X 1 cm thick filled with oil. The cell contains in its top a diaphragm which remains closed due to an in-built pressure left inside the chamber during manufacture. Earth pressure acting on the flat sides of the chamber increases the internal pressure.

Each cell is connected to a read-out station by means of two nylon tubes. The read-out consists of a small hand pump, a precise pressure gauge, an oil reservoir and a manifold with valves, so it can be

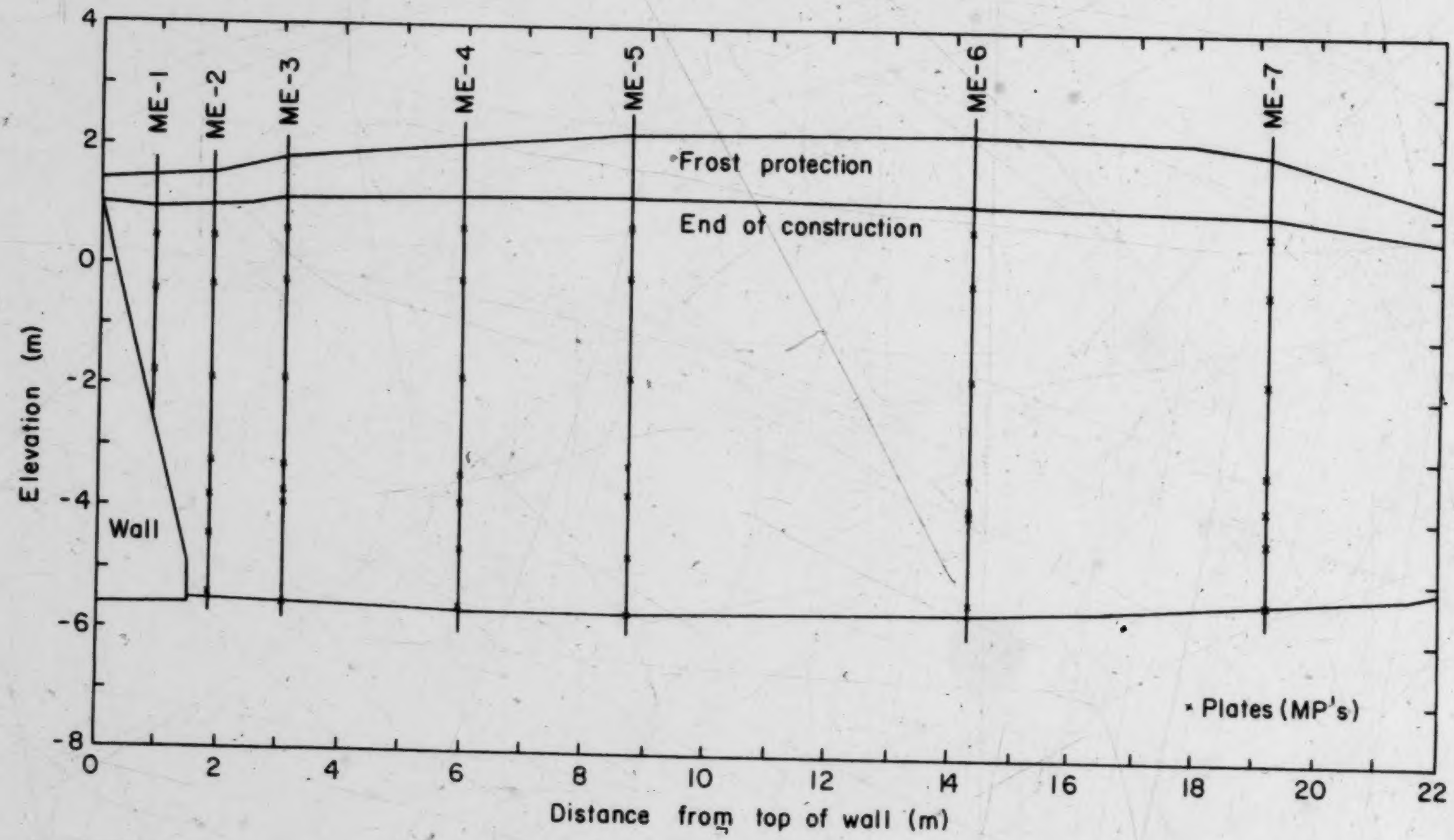

Figure 3.8 Position of Multipoint Extensometers

connected to several cells. Oil can be sent to the sensing unit through one of the nylon tubes. When the pressure on the diaphragm exceeds that of the oil chamber, the diaphragm opens, allowing oil to circulate through the chamber and return to the reservoir using the second tube. If pumping at constant rate is maintained, oil will flow from the reservoir to the cell and back, without further increase in the pressure readings. This procedure will permit the pressure in the chamber to be registered.

The accuracy of the readings is sensitive to the amount of air in the system. It is advisable to circulate oil in all sensing units before each reading.

It is important to notice that, due to reading procedures described above, the pressure registered is always slightly higher than the pressure acting in the chamber. It is, therefore, important to calibrate the cells against a known earth pressure.

Calibration

The calibration was run in an apparatus similar to that described by Plantemma (1953) and shown in Figure 3.9.

It consisted of a steel cylinder 70 cm (28") in diameter, 25 cm (10") high and 1/2" thick wall, containing a fixed bottom 1/2" thick, and a removable lid. The lid was some 20 cm (8") larger in diameter to allow six anchors 5/8" in diameter, to pass through the lid and hold it in

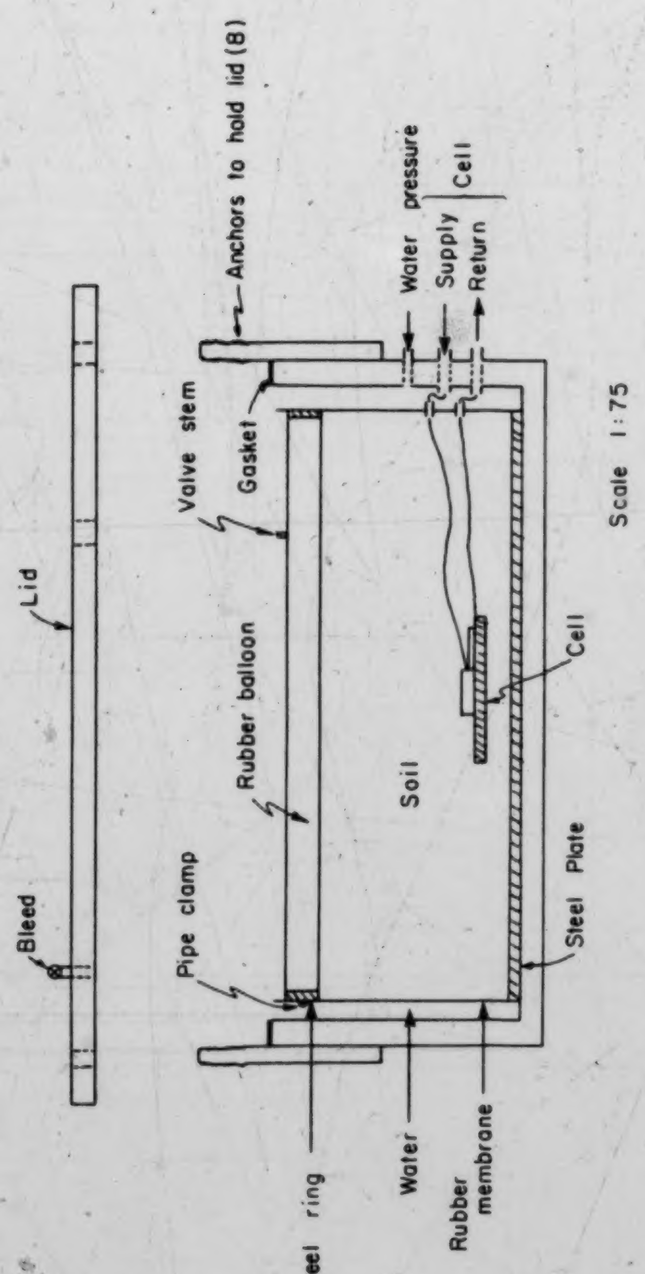
Lid
Bleed
Pipe clamp
Rubber balloon
Valve stem
Gasket
Anchors to hold lid (8)
Soil
Cell
Water pressure
Supply
Return
Cell
Steel ring
Water
Rubber membrane
Steel Plate
Scale 1:75

Figure 3.9 Pressure Cell Calibration Chamber

position.

The soil sample, in which the cell was embedded, was only 65 cm (26") in diameter, and was placed inside a rubber membrane. A collapsable metal shield shaped the membrane during the sample preparation.

After the sample was prepared, the gap between the rubber membrane and the cylindrical chamber was filled with water. With this set up the lateral friction was completely eliminated.

The vertical pressure was applied by a rubber balloon 63.75 cm (25.5") in diameter, that fitted inside the rubber membrane. A steel ring was left inside the balloon to permit the membrane to be sealed against the rubber balloon, using pipe clamps.

With the lid in position, the balloon was inflated to come into contact with the lid.

A steam valve connected to the side of the chamber allowed the vertical pressure to be applied. Almost simultaneously the lateral pressure was increased, and tests performed at different ratios, $K=\sigma_1/\sigma_3$. By calibrating the cells at several K ratios, a study of the cross sensitivity of the cells was procured, as defined by Brown and Pell (1967).

The total height of the sample was 17.5 cm (7") and tests were run with the sensor unit at several elevations to account for this effect. No influence was detected.

Some results of the calibration are shown in Figures 3.10 through 3.14.

In Figure 3.10 a dense sand was used and the ratio $K=\sigma_1/\sigma_3$ was kept equal to 1. The next two tests, shown in Figures 3.11 and 3.12, the ratio was 1/2 and 4/3 respectively. Based on these figures it was concluded that, for the range of pressure expected, the applied pressure was only slightly different from the measured pressure and no cross sensitivity was observed.

Subsequently, a test using a material similar to that used in the test embankment (labelled "Till" in the figure) was performed. The sample was compacted at about 20 kN/m^3, and moisture content of 12.5%. Since the ratio σ_1/σ_3 showed no effect in the cell response, this ratio was maintained equal to 1 for the subsequent calibration. The result is shown in Figure 3.13. Again, the results are similar to those of the previous calibration.

Finally, the installation procedure was tested. Thus, a sample was compacted inside the membrane and a trench cut, to embed the cell. The trench was then filled with sand and the remaining height of the chamber filled with compacted soil. The result is almost identical to the previous results, as can be seen in Figure 3.14.

Based upon these results, it was concluded that the cells manufactured by Glöetzl are of high quality for the range of stress for which they were tested.

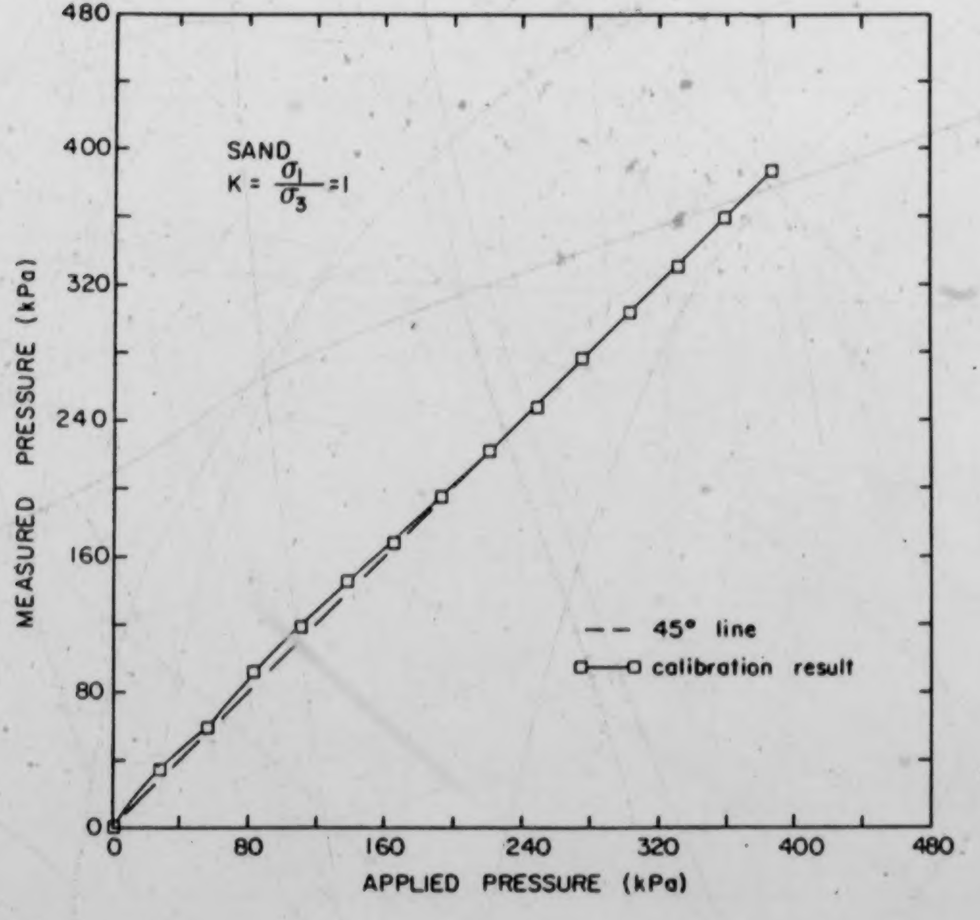

Figure 3.10 Pressure Cell Calibration - Sand K=1

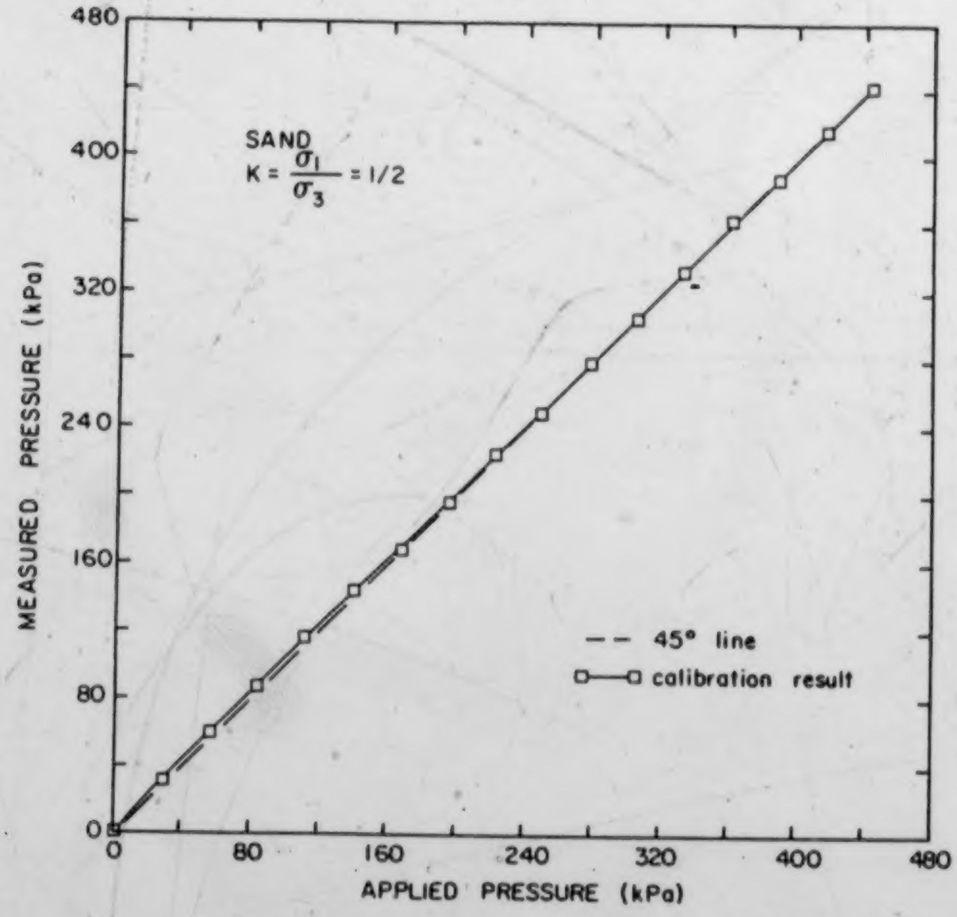

Figure 3.11 Pressure Cell Calibration - Sand K=1/2

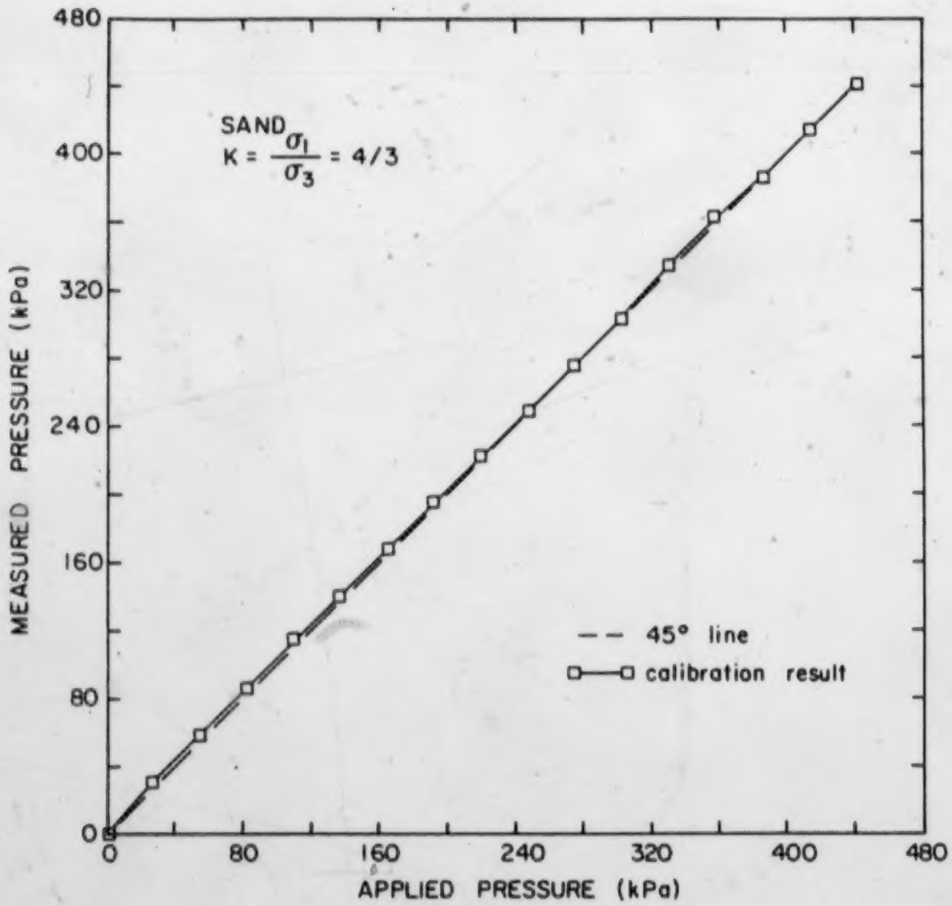

Figure 3.12 Pressure Cell Calibration - Sand K=4/3

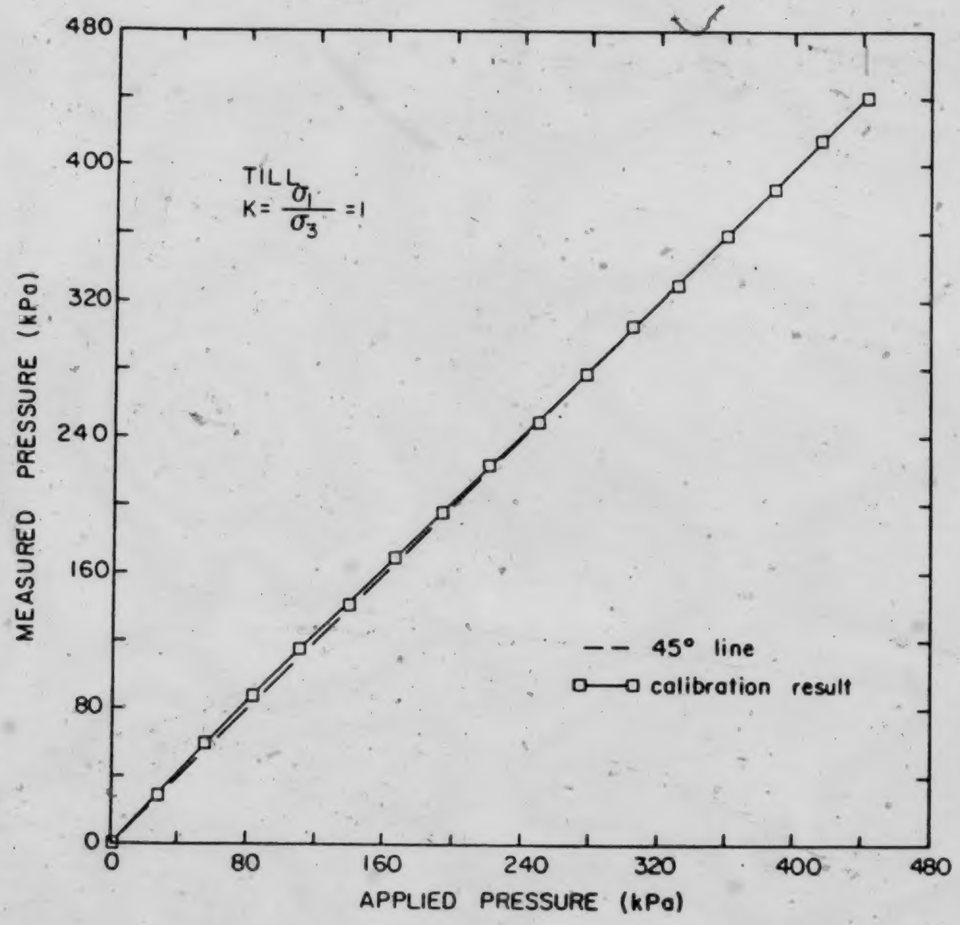

Figure 3.13 Pressure Cell Calibration - Till K=1

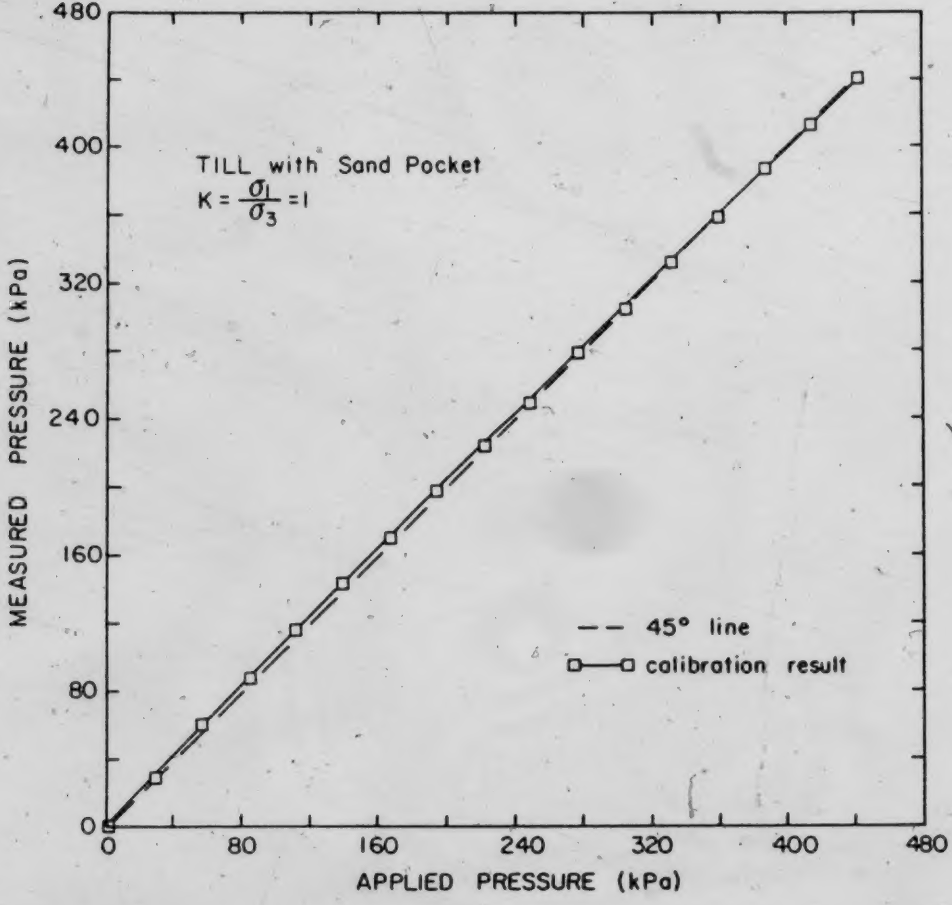

Figure 3.14 Pressure Cell Calibration - Simulating Installation

Calibration of similar cells are presented by Penman et al (1975), using a large oedometer. Those authors noticed a higher departure from the applied pressure, for higher pressure range.

It is important to mention that all the calibration tests in soil were run for one cell. Prior to installation all cells were tested against an all-round water pressure to check their response. All gave 100% response to the applied pressure.

Installation

The Glöetzl cells were installed in two clusters of five cells each. The first group was placed close to the concrete structure, and the second one as far as possible from the rigid boundary (limited by the opposite abutment).

The arrangement of the cells is shown in Figure 3.15 for both groups ("A"- close to wall, and "B" remote from the wall). In this figure their location with respect to the nearest access tube of a magnetic extensometer is given. The orientation of the cells were chosen in order to allow the principal stresses to be determined.

The installation procedure followed the routine used during the calibration, departing only in the size of the trench dug to embed the cells. To facilitate the installation one large trench was dug to accomodate all five cells of one cluster. To prevent mutual interference between the cells, they were placed as far as possible from each

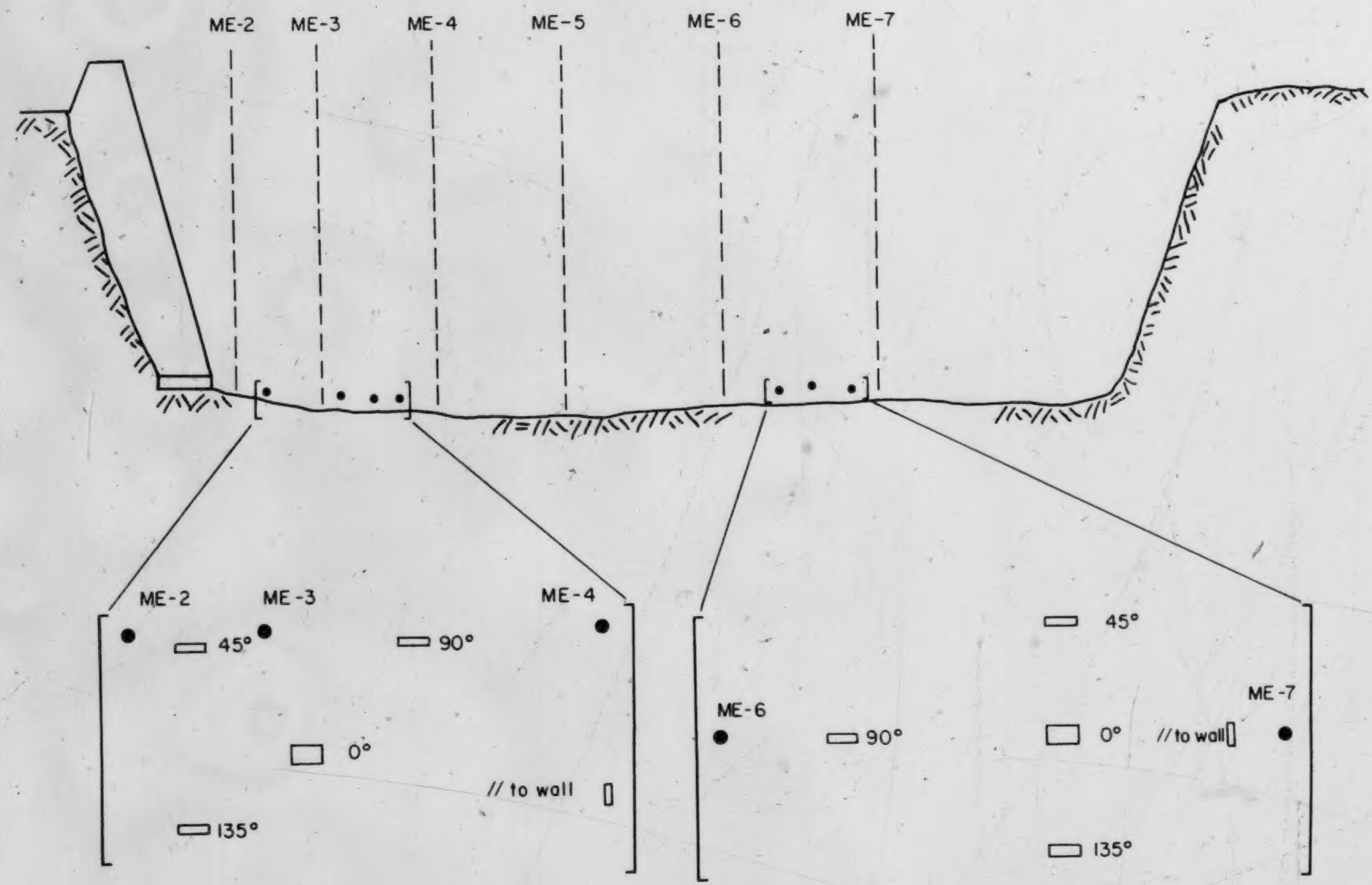
ME-2
ME-3
ME-4
ME-5
ME-6
ME-7
ME-2
ME-3
ME-4
45°
90°
0°
// to wall
135°
ME-6
ME-7
45°
90°
0°
// to wall
135°

Figure 3.15 Location of Earth Pressure Cells

other, as shown in Figure 3.15.

The nylon tubes were placed inside a second trench 0.5 m deep to avoid disrupting the traffic of heavy loads. The tubes were connected to the read-out station, placed behind the wall, through plastic pipes embedded in the concrete wall during construction. After positioning all the cells, oil was circulated to ensure full saturation of the system.

The cells were then covered with sand to inhibit large particles from applying an uneven pressure on the cell, followed by fine grained soil, lightly compacted.

At the end of the installation, initial readings were obtained.

3.3.2 Wall Instrumentation

In order to develop a constitutive relationship for the behaviour of the soil-concrete interface, simultaneous measurements of shear stress, normal stress and shear (contact) displacements are necessary.

Equipment suitable to measure shear stresses and normal stresses in laboratory, have been extensively reported (e.g. Arthur and Roscoe, 1961; Bauer et al, 1979; Doohan, 1975). However, the equipment referred in these publications do not seem suitable for field application, where sturdier instruments are required. Only recently the first cell to measure shear stress in the field has been presented in the literature (Askegaard, 1984). Furthermore, no account of the measurements of direct relative displacement between a concrete structure and a soil mass could be found.

Consequently, two new devices had to be designed to obtain the desired data. They are called Shear Stress Device (S.S.D.) and Shear Displacement Device (S.D.D.).

They were installed in three rows as shown in Figure 3.16 and Plate 3.2 together with contact pressure cells. Each of these rows contained one contact pressure cell, one shear stress device and two shear displacement devices. Rows were located at 1.5 m, 3.0 m and 4.5 m from the top of the wall.

Each of these instruments will be discussed in the following sections. Plastic pipes were also provided to conduct the wires and tubes of these instruments to the read-out station.

3.3.2.1 Contact Pressure Cells

Contact pressure cells were used to measure normal stresses acting on the wall. Several case histories involving the use of this instrument have been published (Kaufman and Sherman, 1964; Vaughan and Kennard, 1972; Jones and Sims, 1975; Carder et al, 1977).

For this test embankment Irad Gage pressure cells were chosen. It is a circular, oil filled cell, 22.9 cm (9") in diameter, containing a vibrating wire pressure transducer. A recess in both sides of the cell provide flexibility to the central diaphragm. This recess significantly improved the performance of the cell by increasing the sensitivity of the diaphragm and causing other, as shown in Figure 3.15.

The nylon tubes were placed inside a second trench 0.5 m deep to avoid disrupting the traffic of heavy loads. The tubes were connected to the read-out station, placed behind the wall, through plastic pipes embedded in the concrete wall during construction. After positioning all the cells, oil was circulated to ensure full saturation of the system.

The cells were then covered with sand to inhibit large particles from applying an uneven pressure on the cell, followed by fine grained soil, lightly compacted.

At the end of the installation, initial readings were obtained.

3.3.2 Wall Instrumentation

In order to develop a constitutive relationship for the behaviour of the soil-concrete interface, simultaneous measurements of shear stress, normal stress and shear (contact) displacements are necessary.

Equipment suitable to measure shear stresses and normal stresses in laboratory, have been extensively reported (e.g. Arthur and Roscoe, 1961; Bauer et al, 1979; Doohan, 1975). However, the equipment referred in these publications do not seem suitable for field application, where sturdier instruments are required. Only recently the first cell to measure shear stress in the field have been presented in the literature (Askegaard, 1984). Furthermore, no account of the measurements of direct relative displacement between a concrete structure and a soil mass could be found.

Consequently, two new devices had to be designed to obtain the desired data. They are called Shear Stress Device (S.S.D.) and Shear Displacement Device (S.D.D.).

They were installed in three rows as shown in Figure 3.16 and Plate 3.2 together with contact pressure cells. Each of these rows contained one contact pressure cell, one shear stress device and two shear displacement devices. Rows were located at 1.5 m, 3.0 m and 4.5 m from the top of the wall.

Each of these instruments will be discussed in the following sections. Plastic pipes were also provided to conduct the wires and tubes of these instruments to the read-out station.

3.3.2.1 Contact Pressure Cells

Contact pressure cells were used to measure normal stresses acting on the wall. Several case histories involving the use of this instrument have been published (Kaufman and Sherman, 1964; Vaughan and Kennard, 1972; Jones and Sims, 1975; Carder et al, 1977).

For this test embankment Irad Gage pressure cells were chosen. It is a circular, oil filled cell, 22.9 cm (9") in diameter, containing a vibrating wire pressure transducer. A recess in both sides of the cell provide flexibility to the central diaphragm. This recess significantly improved the performance of the cell by increasing the sensitivity of the diaphragm and causing

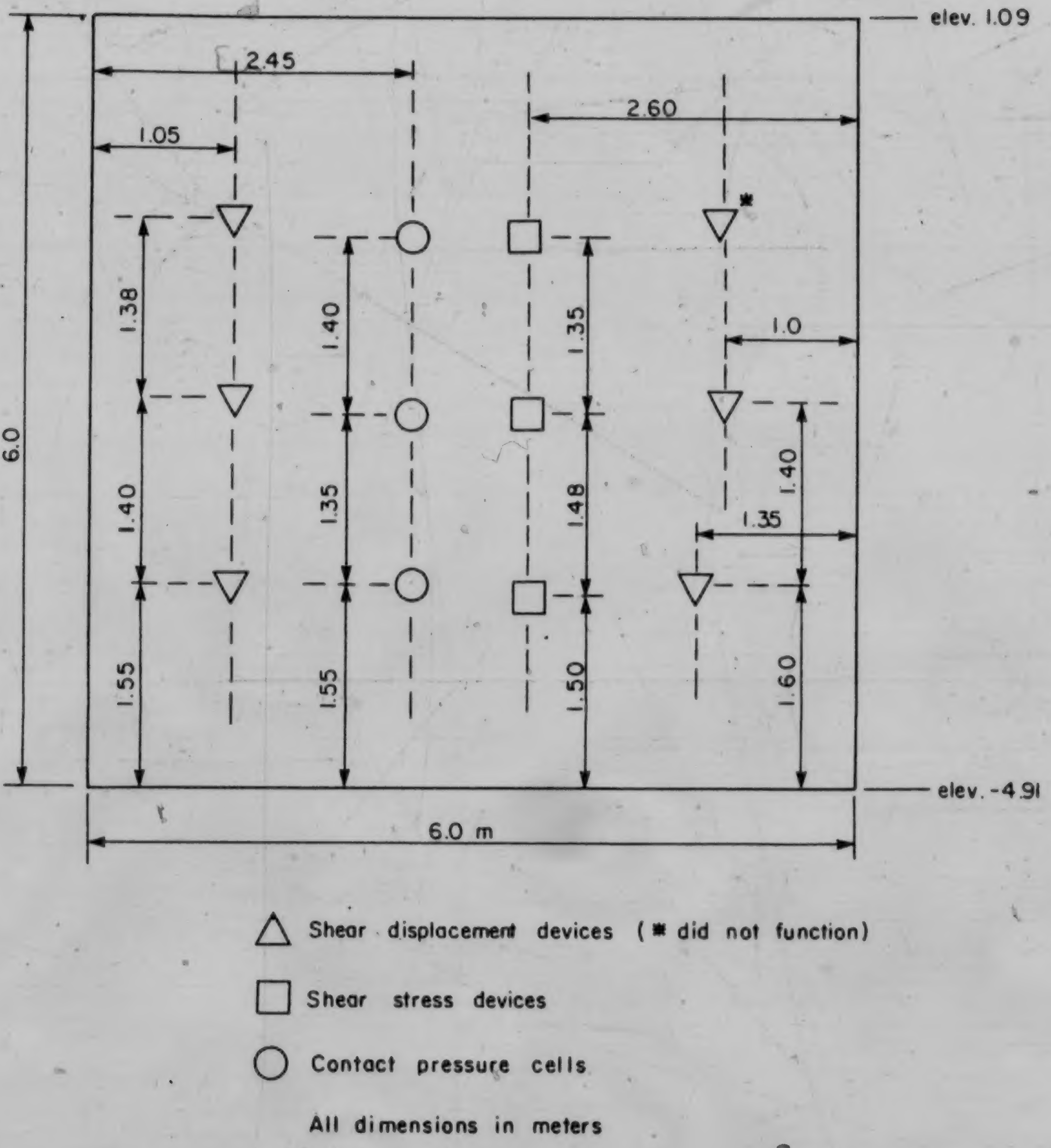
elev. 1.09
2.45
1.05
2.60
*
1.38
1.40
1.35
1.0
6.0
1.40
1.35
1.48
1.40
1.35
1.55
1.55
1.50
1.60
elev. -4.91
6.0 m
△ Shear displacement devices (* did not function)
□ Shear stress devices
○ Contact pressure cells
All dimensions in meters

Figure 3.16 Location of Wall Instruments

Plate 3.2 View of Wall Instruments

no disturbance to the overall stiffness.

Due to the large amount of past experience and available literature regarding contact and earth pressure cells (Peattie and Sparrow, 1954; Hamilton, 1960; Tory and Sparrow, 1967; Thomas and Ward, 1969; Felio, 1980) no further details of these instruments will be presented.

Installation

It is well known that the presence of a stiffer body within a soil mass, such as an instrument, can cause a concentration of stresses and hence misleading the measurements. To avoid this undesirable effect, the contact cells were installed flush against the wall. During the construction of the concrete structure an alluminum disc was placed in the form work with exactly the shape of the gauges. The cells were then glued inside this recess using quick dry grouting. A similar technique was reported by Coyle et al, (1974).

The initial readings were obtained after the grout had dried.

3.3.2.2 Shear Displacement Device (S.D.D.)

Design Detail

The basic components of this equipment, as shown schematically in Figure 3.17 are:

- a rectangular steel plate, 0.635 cm (1/4") thick (Plate "A")

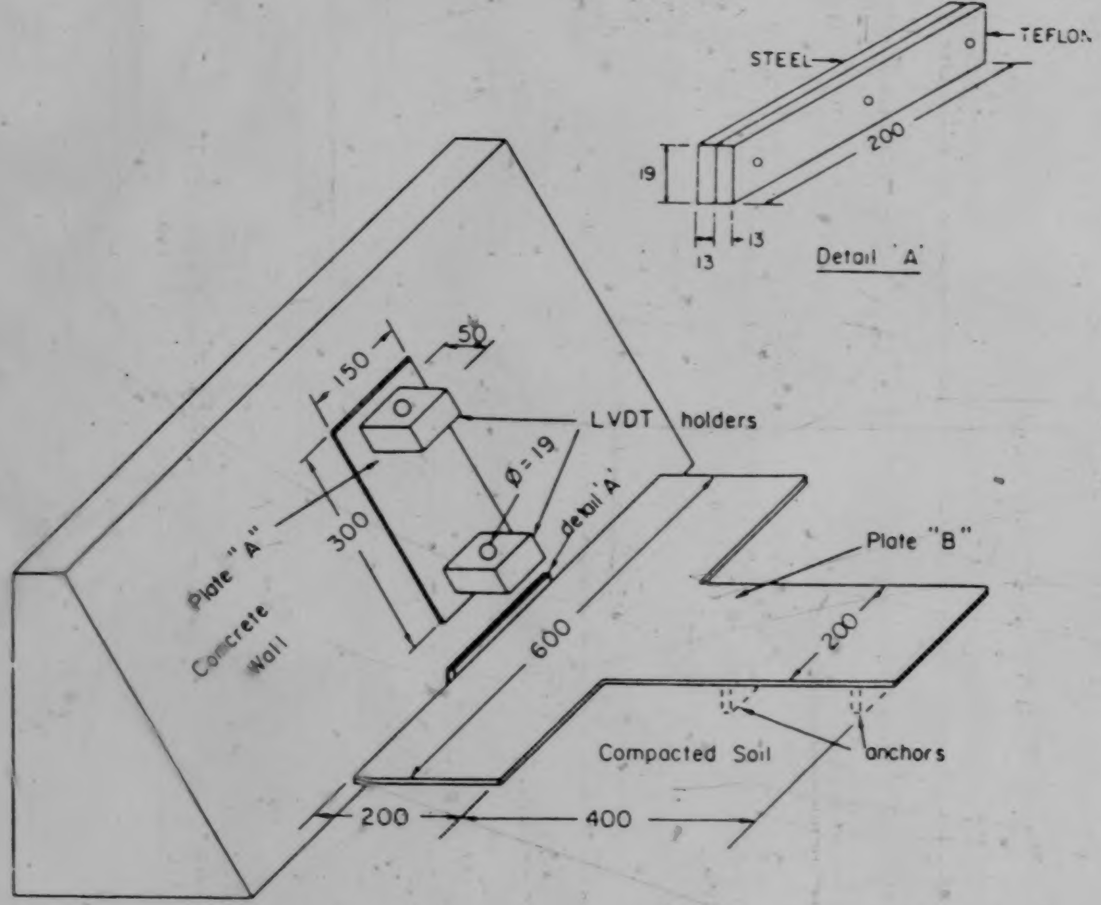
STEEL
TEFLON
200
19
13
13
Detail 'A'
150
50
LVDT holders
Ø=19
detail 'A'
300
Plate "A"
Concrete Wall
600
Plate "B"
200
Compacted Soil
anchors
200
400

all dimensions — mm

Figure 3.17 Details of Shear Displacement Device

- a T-shaped steel plate, 0.635 cm (1/4") thick (Plate "B")
- a Linear Variable Differential Transformer (LVDT) (not shown in Figure 3.17) '

The relative movement between the soil and the structure is obtained by recording the relative movement of the two plates.

In this sense, Plate "A" is firmly fixed to the concrete wall using four 1.27 cm (1/2") bolts, and has two steel blocks to hold the LVDT (Figure 3.17). The second plate is placed in the soil with the widest section of the "T" towards the wall. To minimize lateral movements of this plate two anchors were installed, as shown in Figure 3.17. The inner core of the LVDT is attached to this plate.

In order to reduce friction between the structure and plate "B" a teflon sheet 0.318 cm (1/8") thick is placed in the contact area and a teflon head provided to Plate "B", as shown in detail "A" of Figure 3.17. With this arrangement, the contact between the concrete and the steel is replaced by a contact between two layers of teflon.

The LVDT chosen for this project was manufactured by Schaevitz. This transducer is of a special type for application in agressive environments, hermetically sealed, being water and humidity proof. The electrical cables were also water and humidity proof. The connections were sealed using a plastic casing filled with silicone grease.

'For details of Linear Variable Differential Transformer refer to Herceg, (1976).

Installation Procedure

The installation is carried out in two phases. Before the fill reaches the desired elevation of the instrument, plate "A" is bolted to the concrete wall.

After the fill has covered at least half of this plate, and good compaction is ensured in the region where the second plate will be placed, a small trench is dug and plate "B" positioned. Extreme caution is necessary in this phase to avoid excessive disturbance in the soil housing the plate. It is also important to ensure full contact between the plate and the soil.

With plate "B" in position, the LVDT is attached to plate "A" by means of two nylon screws and the inner core is screwed to plate "B".

It is important to notice that although plate "B" is a heavy plate, it prevents erroneous measurements by minimizing possibility of tilting of the plate which, in turn, would bend the inner core of the LVDT.

As a precaution, a protective device is suggested to prevent earth pressure acting against the inner core of the LVDT. Half a section of a plastic pipe filled with uniform round sand was used in this application.

The trench is then carefully backfilled, and the use of a hand held compaction device permitted only after the LVDT is completely covered.

A sequence of Plates (Plates 3.3a and 3.3b) illustrates the installation procedure.

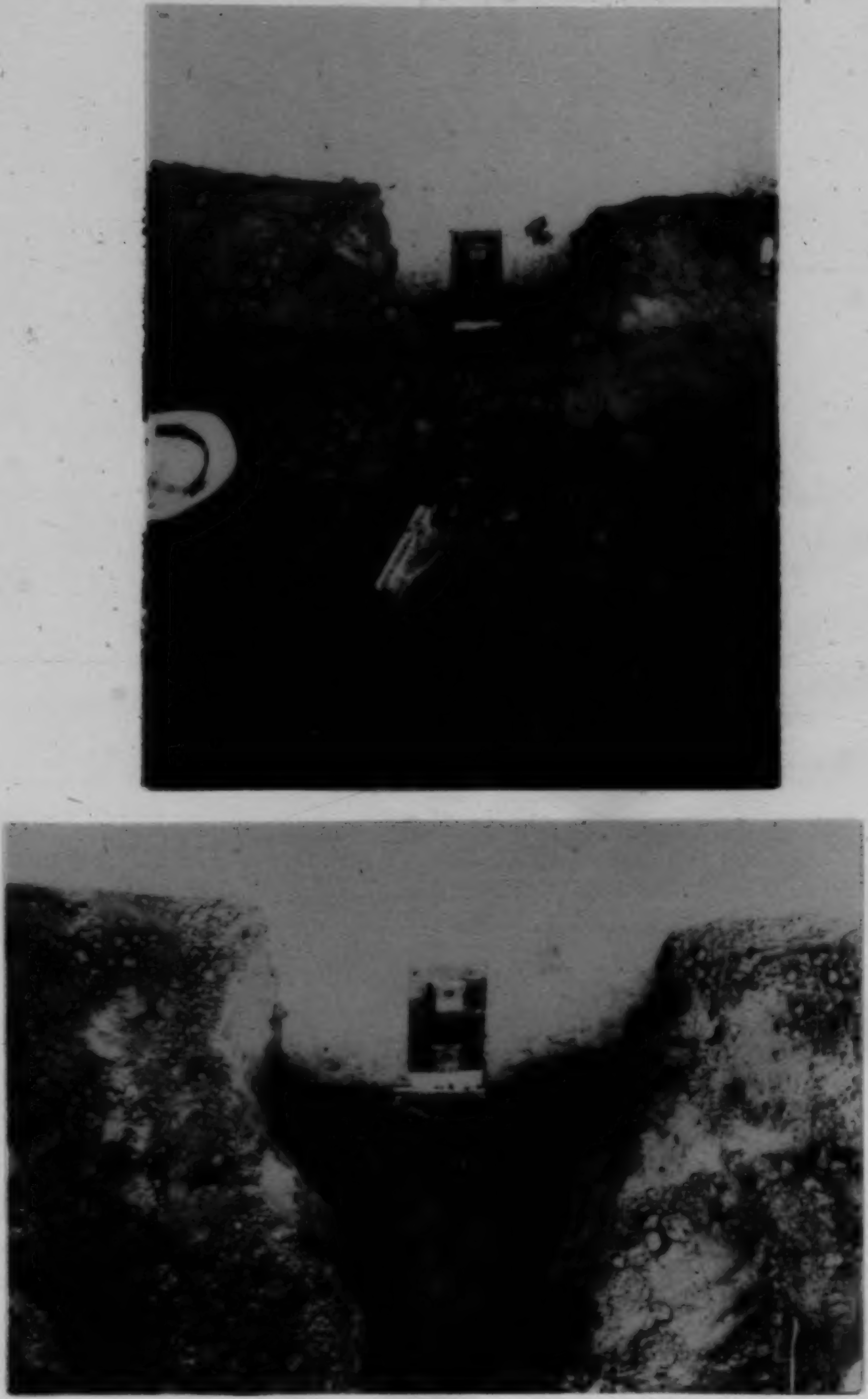

Plate 3.3 Sequence of Instalation - Shear Displacement Devices

Initial readings are taken after the trench is backfilled.

3.3.2.3 Shear Stress Device (S.S.D.)

Design Detail

The Shear Stress Device consists of a concrete block (in this particular case, 30 cm X 30 cm X 7.5 cm thick) placed inside a knock-out previously molded in the concrete structure. The knock-out is some 10 cm higher than the concrete block in order to accomodate two load cells, as shown in Figure 3.18. The concrete block is placed into position, resting on the load cells.

As in the previous instrument, friction is reduced by layers of teflon placed along any contact between the concrete block and the structure.

With the load cells and teflon sheets in place, the concrete block must fit snugly in the knock-out. This will prevent possible rotation of the concrete block, and consequent nonuniform distribution of loads to the load cells. Any gaps existing after the installation are filled with grease to prevent entry of soil into them. A wooden protection is used to avoid soil pressure acting laterally on the load cells.

The load cells to be used are a function of the anticipated load to be registered. For the test embankment, special alumminun load cells were built due to the small loads expected to be measured, since the embankment was relatively low (6 m high).

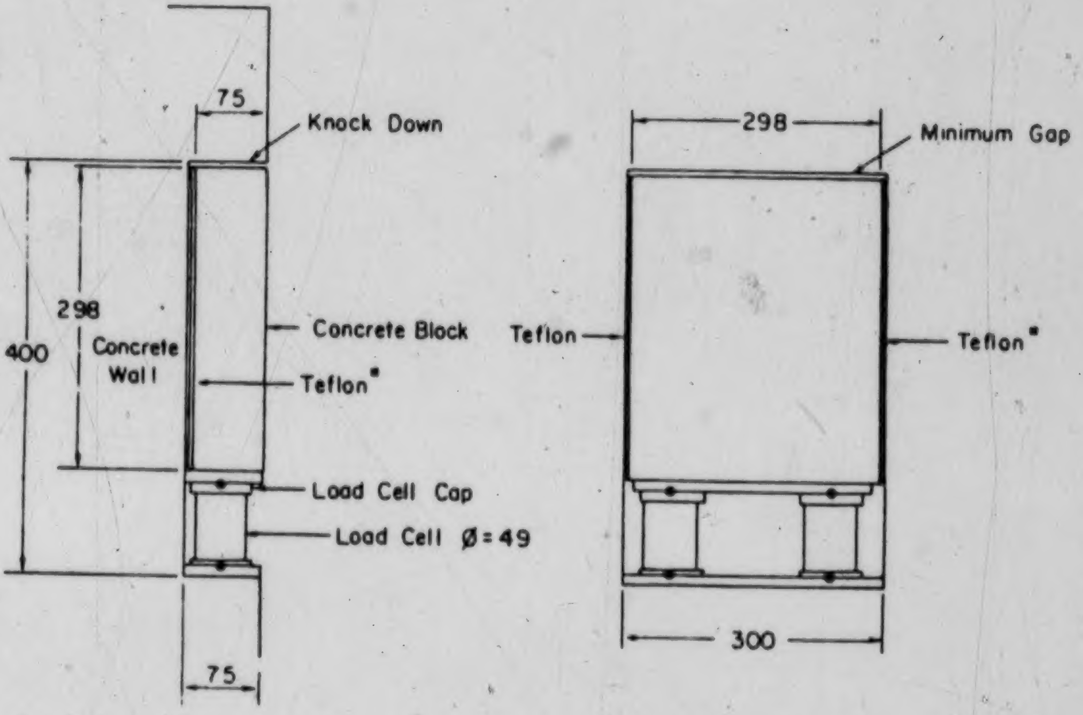
75
Knock Down
298
400
Concrete Wall
Concrete Block
Teflon*
Load Cell Cap
Load Cell Ø=49
75
298
Minimum Gap
Teflon
Teflon*
300

all dimensions — m m.
* two layers of teflon - 1.5 mm. each

Figure 3.18 Details of Shear Stress Devices

The value of shear stress is obtained by adding the loads in the two load cells and dividing the result by the area of the concrete block.

Calibrations

Two important calibrations have to be performed for each instrument, namely the calibration of the load cells individually, and calibration of losses by friction in the layers of teflon.

The first is a routine calibration, that can be performed either against a proving ring or dead weights and will not be discussed here.

A set up, similar to that used in the field, was reproduced in the laboratory to permit the second calibration to be performed. To make it feasible two modifications were introduced:

- the whole instrument was placed horizontally
- the concrete block was made thicker than the knock-out, to permit the shear load to be applied.

This set up is shown in Figure 3.19.

The calibration was carried out by applying normal loads, using weights, and pushing the concrete block at a very high rate of load application. The loads were registered by an external load cell placed at the position of load application and readings were obtained at 15 second intervals.

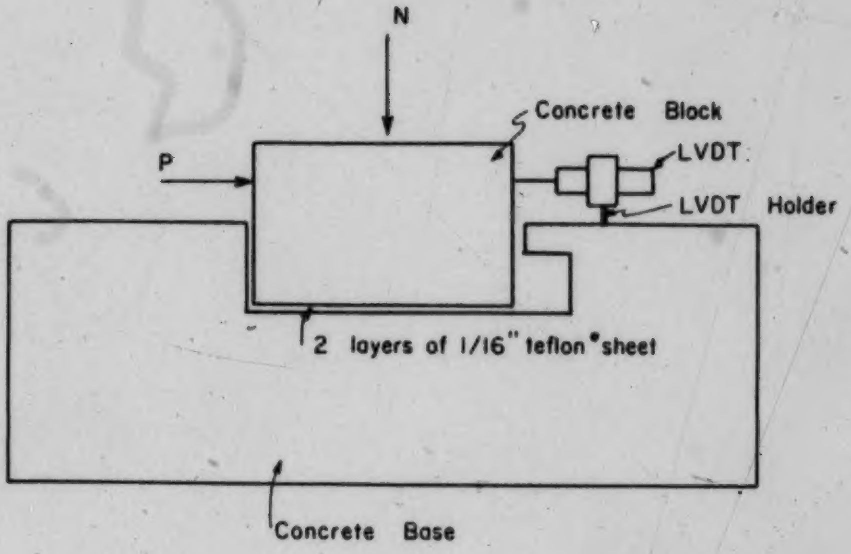
N
P
Concrete Block
LVDT
LVDT Holder
2 layers of 1/16" teflon*sheet
Concrete Base

N – Normal load
P – Incremental horizontal load

* inclusive laterally (parallel to the direction of movement)

Figure 3.19 Set Up for Shear Stress Devices Calibration

For each normal load shearing was maintained until constant readings of shear stresses were obtained and the block was translating freely. An example of a force-displacement curve is shown in Figure 3.20. After tests were performed for several normal loads the results were plotted in a stress space, as shown in the same figure. A value of 8° was found for the angle of static friction. The scatter observed in the results suggests a non-consistent behaviour of the teflon sheets.

Based on these results a major improvement in this equipment was suggested, in order to eliminate the use of teflon, as will be discussed in a subsequent chapter.

Installation Procedure

The installation procedure begins by molding a knock-out in the concrete structure during its construction. The dimensions of this knock-out had to be carefully measured in order to produce the smallest gaps possible on either side of the block, as discussed earlier.

Before the fill reaches the desired elevation, the concrete block is positioned but not allowed to come into contact with the load cells until they have been perfectly aligned, and the verticality of the load cells ensured. The concrete block is then released and allowed to rest on the load cells which are later protected. Initial readings are then taken.

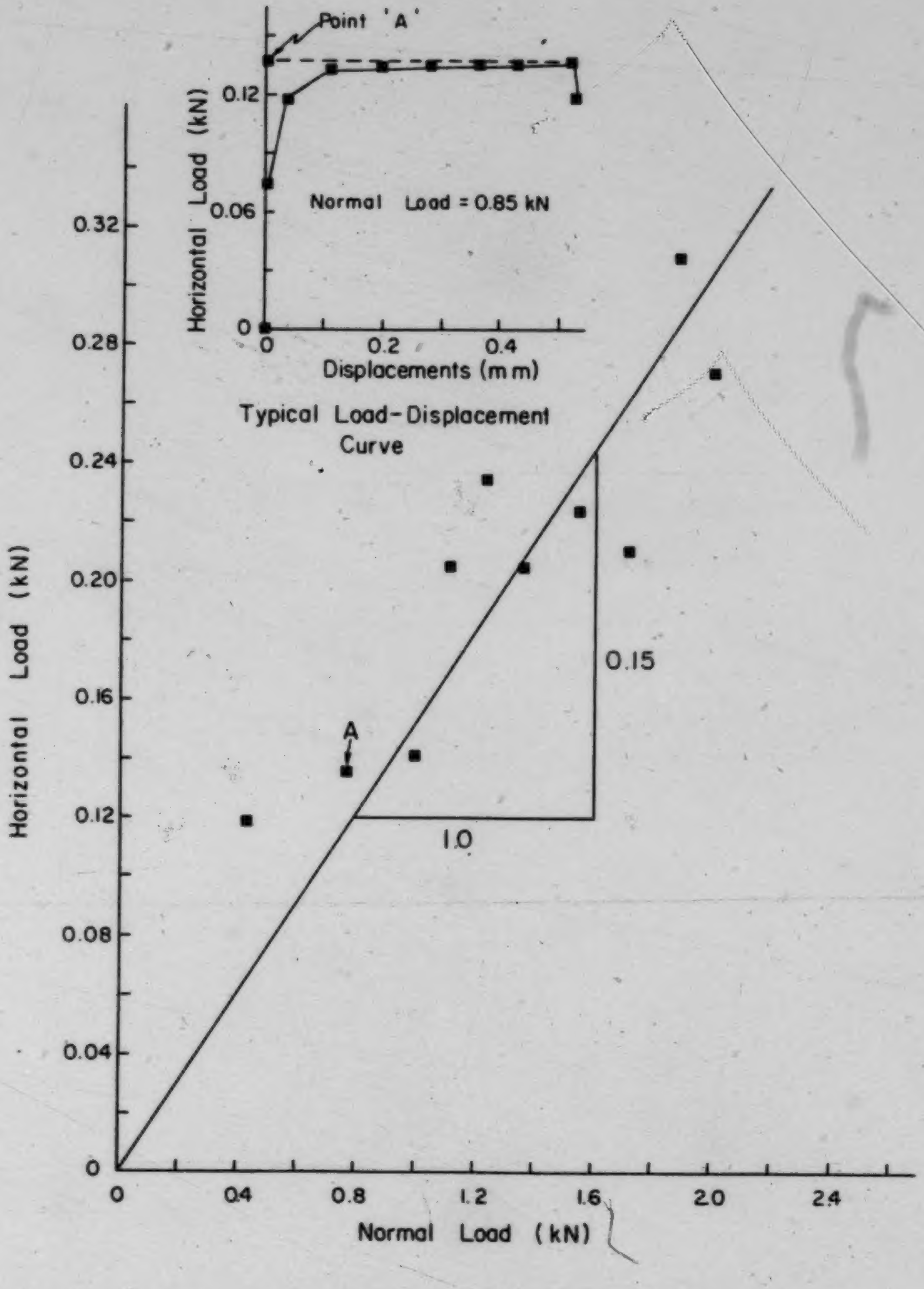

Figure 3.20 Calibration Results - Shear Stress Devices

Plate 3.4 Shear Stress Device after Instalation

Plate 3.4 shows the instrument after installation.

3.3.3 Additional Supporting Instruments

In addition to the basic instrumentation presented in the last sections, four other instruments provided supporting measurements for the test embankment. They were:

- slope indicator casing (installed inside the concrete wall)
- settlement points
- bench marks
- Piezometers

3.3.3.1 Slope Indicator Casing

In order to monitor possible deflections expected of the concrete wall, a slope indicator casing was installed inside the concrete wall. This casing was attached to the reinforcement during the wall construction and fixed in the bedrock.

Readings were obtained after every three layers of fill were placed and three sets of initial readings were performed before backfilling started.

Some results of deflections parallel to the centerline of the fill are shown in Figure 3.21. This results suggest that the structure first moved towards the fill (passive movement). After most of the fill was placed (in October 6 - see Figure 3.3) the movements reversed and approximatelly 0.3 cm of active movement was observed.

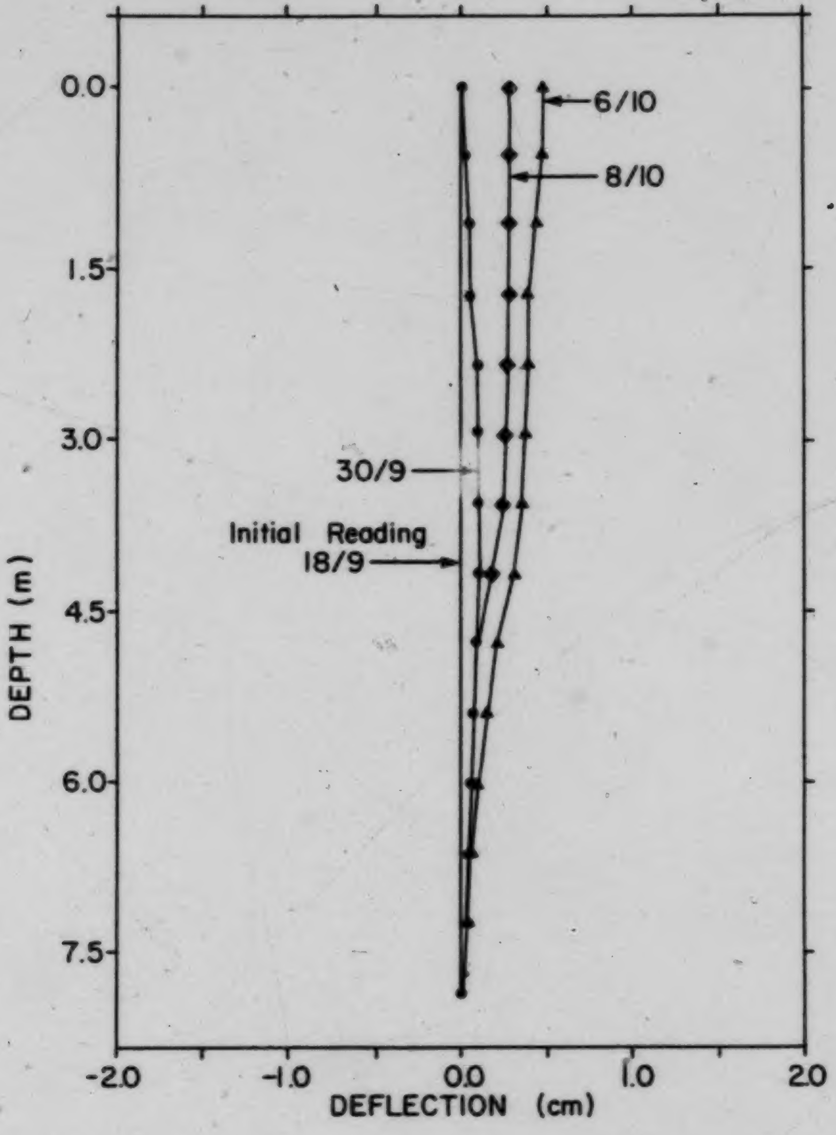

Figure 3.21 Results of Slope Indicator Casing Inside Wall

3.3.3.2 Settlement Points

Three settlement points were installed on the crest of the wall in order to monitor any possible settlement occuring during placement of the fill. They were made of steel, with a concave recess to fit the ball bearing welded to the bottom of the surveying rod.

The observed settlements were within the accuracy of the surveying equipment used to monitor settlements (± 1 mm) and therefore it is assumed that the settlements were negligible.

3.3.3.3 Bench Marks

Two bench marks were installed, grouted into the rock foundation at a safe distance behind the wall. They were used as references for leveling the settlement points, and the top of the access tube of the multipoint extensometers.

A 5 cm (2") hole was drilled, 2 m into the bedrock and sections of steel pipe 2.5 cm (1") in diameter placed inside. Grout was poured to fix the steel rods into the rock. A 3.8 cm (1 1/2") plastic pipe was used as casing for the steel pipe, and the area between the original ground and the borehole, above the bedrock level, filled with sand.

The steel rods were headed by a cap containing a concave recess to fit the ball bearing welded in the leveling rod, as mentioned previously.

3.3.3.4 Piezometers

Two piezometers, able to monitor both positive and (slightly) negative pore pressures (suction) were installed near the center and upper levels of the wall instruments and in contact with the concrete structure.

They were intended to measure possible pore pressure generation, in the vicinity of the wall, during placement of fill.

The instrument used was manufactured by Petur Instruments. It consists of a plastic diaphragm placed inside a 2.5 cm (1") long probe containing a "high air entry value" porous stone at one end. This probe was connected to the readout through a nylon pipe, embedded in the concrete wall.

Readings were taken after every new layer was placed and, for the rate of construction imposed on the test embankment, no excess pore pressure was observed in either instrument. It was therefore assumed that a drained condition occurred, at least in the region of the interface.

3.4 PRESENTATION AND DISCUSSION OF RESULTS

3.4.1 Fill Instrumentation

3.4.1.1 Settlement Measurement

Two different types of plots are used to present the results of the settlement measured with the multipoint extensometers, during the fill placement. The first is a settlement with time, as shown in Figure 3.22, for vertical ME-3. In the same figure the increase in the height of fill with time is presented.

In the second plot, the settlement profile at a certain elevation is plotted, as a function of the distance to the wall. This is presented, for all plates MP-4, in Figure 3.23 for two different times of the embankment contruction [2].

Three immediate observations arise from these two figures:

- The fill showed no significant time-dependent settlement during the period of study. It can be observed in Figure 3.22 that as soon as the fill was completed most of the settlement stopped, for all plates.

- The shape of the settlement profiles obtained (Figure 3.23) is not as anticipated. They show, in all cases, a maximum settlement somewhere between verticals of multipoint extensometers ME-2 and ME-3. The settlement was expected to curve monotonically up to certain distance from the wall where the settlement curves would become constant.

- The magnitude of the settlements is larger than

---

[2] Curves for all multipoint extensometers are shown in Appendix "B".

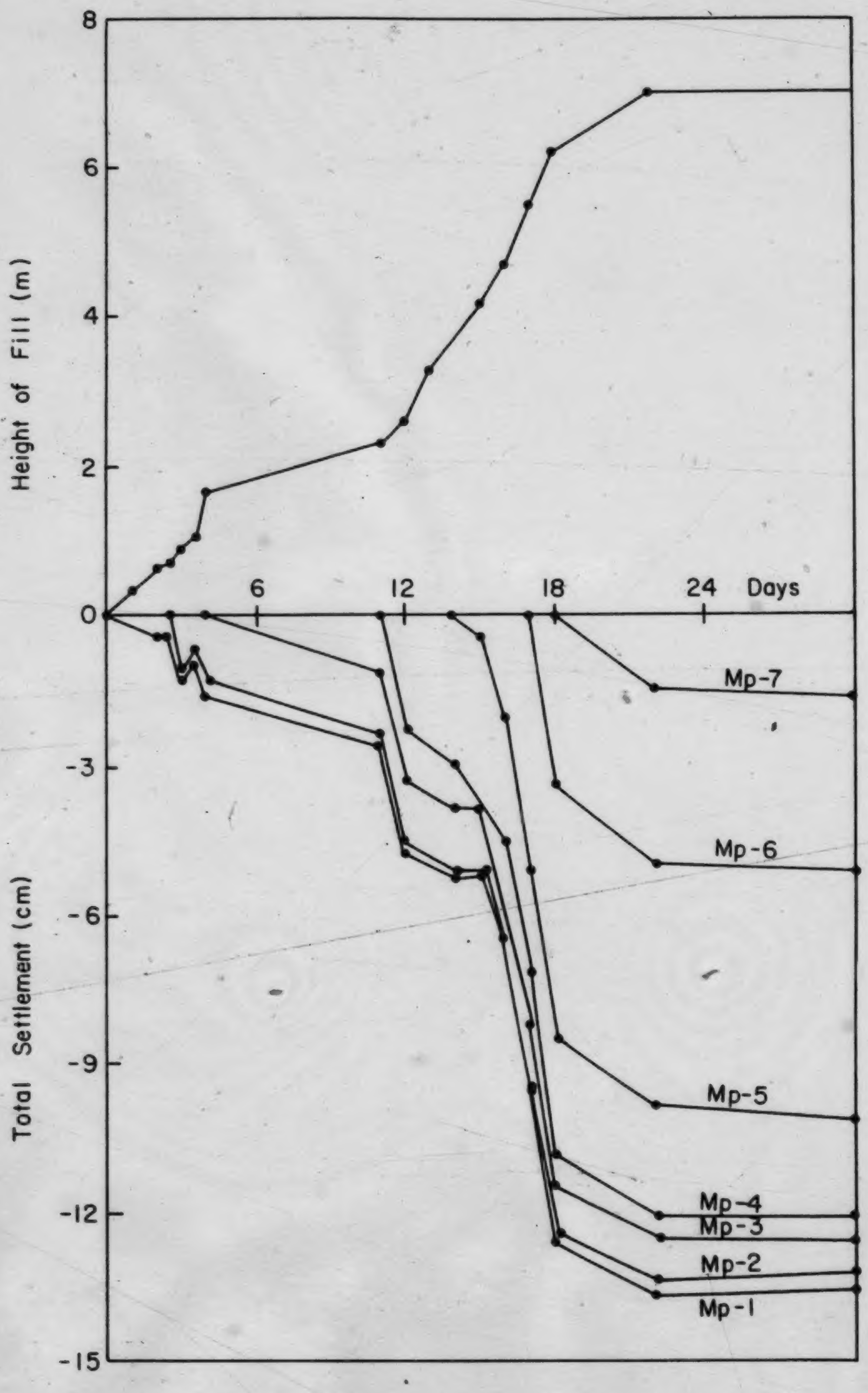

Figure 3.22 Total Settlement Versus Time - ME-3

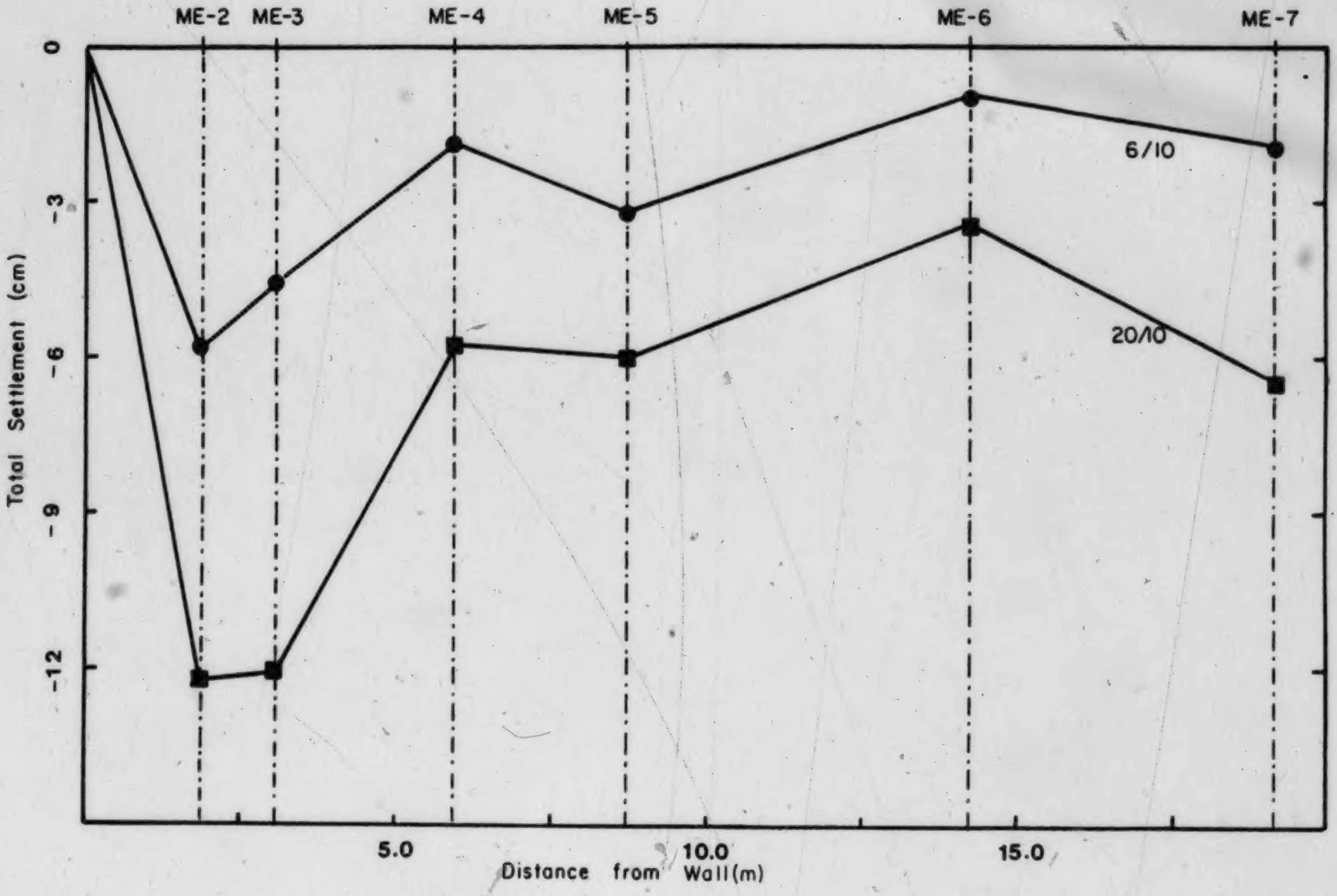

Figure 3.23 Total Settlement Versus Distance from Wall - MP-4

anticipated. As can be seen in Figure 3.23, the maximum settlement is about 0.12m, corresponding to 2% of the height of the fill. Similar cases reported, such as for Ilha Solteira (Celestino and Marechal, 1975) showed some 0.5% of the height of the fill, or Mica Dam (Eisenstein and Law, 1979) with similar percentage as in the previous example.

Since the foundation of the test embankment can be considered of poor quality (very fractured), most likely, this material is responsible for the shape and magnitude of the settlement profiles. It is probable that the excavation process caused excessive disturbance in the foundation material and promoted an increase in its compressibility.

This increased compressibility occurred as a consequence of the reduction in the vertical stresses caused by the removal of the excavated material. Since the horizontal stresses are not reduced in the same proportion, the foundation was subjected to a vertical "extension". This phenomena seems to be accentuated near the toe of the slope created by the excavation and, as shown by Dunlop and Duncan (1968), this region is the potential zone for yielding initiation.

Furthermore, the form of the settlement profiles (non-monotonic with a maximum settlement near ME-3) suggests that the construction of the concrete structure promoted a further increase in the compressibility as a result of increases in the horizontal stresses with no component in the vertical stresses (in the foundation adjacent to the wall base).

Moreover it can be expected that, even though all precautions were taken, some weathering (as discussed by Morgenstern and Eigenbrod, 1974) probably took place in the area covered by phase I of excavation (bounded by the vertical of multipoint extensometer ME-3).

As a confirmation of the above discussion, settlement profiles were recalculated using the magnetic plates installed at the interface fill-foundation as reference for the settlement of the subsequent sensors. The results for ME-4 are presented in Figure 3.24. It can be noticed that although not totally eliminated, the shape of the settlement curves are closer to the anticipated and the maximum displacement, as a percentage of the total fill height was reduced to 0.3%, suggesting that most of the settlement indeed occurred in the foundation.

It can also be noticed that a similar effect (increasing settlement) was observed near the slope opposite to the concrete wall (see Figure 3.23). For this region the effect was not as accentuated, and after the foundation settlement was removed, the curves became almost horizontal.

Another important point to be observed in Figures 3.22 and 3.23 is the high degree of straining developed in the soil near the wall. Note that, although the settlement measurements closest to the wall were obtained in the vertical of multipoint extensometers ME-1, it will be shown

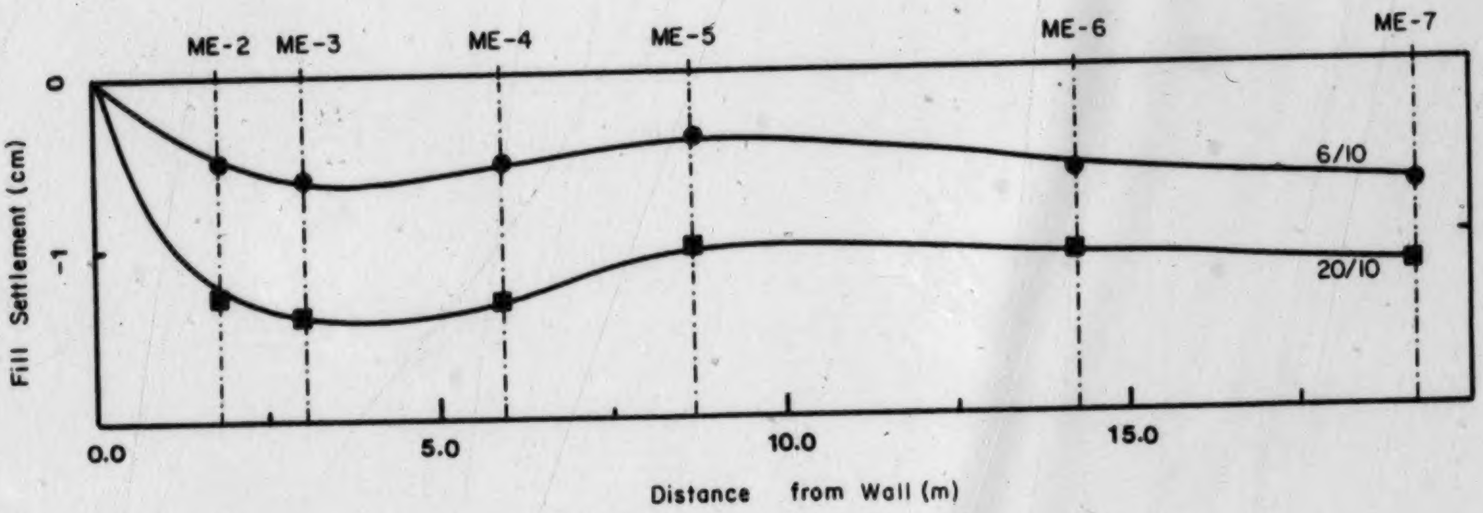

Figure 3.24 Fill Settlement versus Distance From Wall - MP-4

in subsequent sections that the relative movements between soil and structure were of very small magnitude, and in the scale of these two figures it would be shown as almost null movement, as depicted. This difference in settlement is translated as straining of the soil placed immediately adjacent to the wall and consequently very high shear stress should develop in this region.

As a consequence, it is expected that a load transfer mechanism could have been formed, as proposed by Kulhawy and Gurtowski, (1976):

> "...the phenomenon of load transfer occurs.. (in zoned dams).. because of the different stiffnesses of adjacent zones. Consider, for example, a zoned dam with a soft core (low modulus) and a stiff shell (high modulus). During the construction of this dam, the zone of low modulus will settle with respect to the zone of high modulus and if no separation occurs along the zone boundaries, the core will tend to "hang" on the shell. The placement of sucessive layers of fill accentuates this process..."

In general, load transfer would occur towards the concrete wall (stiffer material) caused by the accentuated angular distortion observed in the soil near the structure. In particular in the test embankment it is believed that a second mechanism occurred due to the higher settlement measured in the fill near the wall. In this second mechanism loads were transfered from the wedge of soil, bounded by the vertical of multipoint extensometers ME-3, towards the remaining soil. This point will be further discussed in the light of the pressure cell results, presented in the next section.

3.4.1.2 Earth Pressure Cells.

The results of the two clusters of earth pressure cells are presented in terms of principal stresses.

If the direction of one of the three principal stresses is assumed to be known, one cell can be used to monitor the magnitude of this stress. For the other two principal stresses (with assumed unknown directions) three cells are sufficient to determine both their directions and magnitudes. A fourth cell is generally used as a check of these values. Therefore, a cluster of five cells is necessary and sufficient to determine the directions and magnitude of the three principal stresses (if one direction is known).

According to Eisenstein and Law (1979) the principal stress ratio, $K=\sigma_3/\sigma_1$, based on Finite Element Analyses, should present a linear correlation for points within a compacted soil mass. This ratio, for the center line of a dam, should be around 0.53.

Charles, (1976) who presented field evidence obtained for Winscar Dam during construction, measured, using a cluster of five cells, ratios between σ_3 and σ_1 of the order of 0.39 to 0.47.

Although some scatter can be found in the data provided by the Glöetzl cells, the ratio K for the cells installed remote from the wall was found equal to 0.32 and 0.21 for the other group, as can be seen in Figure 3.25. In both cases, as proposed by Eisenstein

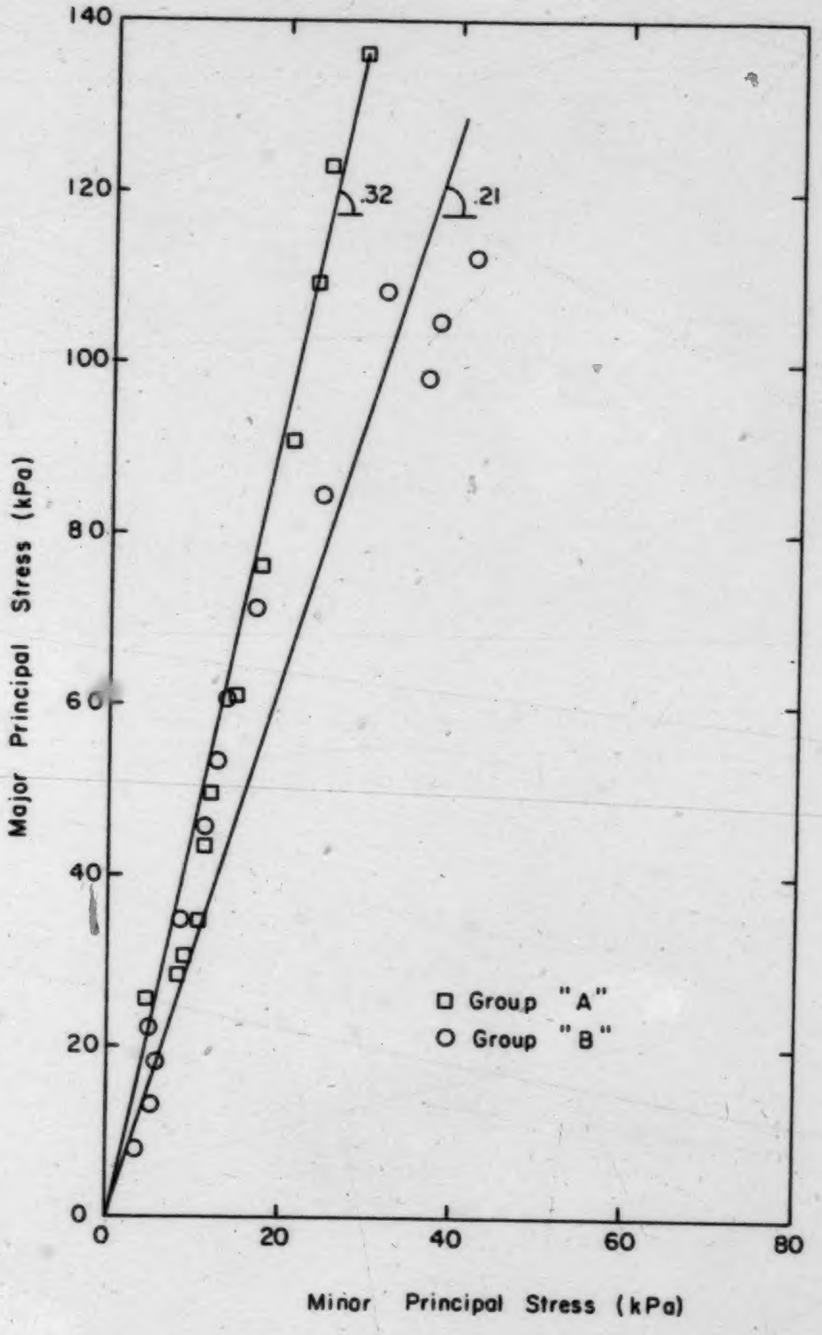

Figure 3.25 Stress Path - Earth Pressure Cells

and Law (1979), an almost linear relationship was found.

Poulos and Davis, (1974) presented a parametric study for the ratio of vertical stress to overburden ($\sigma_v/\gamma h$). For the case of an embankment sloping at 30° and for a Poisson Ratio of 0.3 they found the ratio $\sigma_v/\gamma h$ to be 0.8 for the centerline and near the foundation of an embankment. Figure 3.26 presents the plot of vertical stress versus overburden (γh) for both groups of pressure cells. The ratio $\sigma_v/\gamma h$ was measured to be equal to 0.82 for the group not influenced by the structure (group "B"). For group "A" the ratio was found to be equal to 0.91.

Since the values for group "B" are in perfect agreement with the theoretical solution proposed by Poulos and Davis (op.cit.), it is assumed that the cell measuring the vertical stress was not affected by the boundaries of the test embankment (concrete wall from one side and opposite slope of excavation at the other end - see Figure 3.15). Therefore, the higher ratio $\sigma_v/\gamma h$ observed for group "A" can be attributed to a second load transfer mechanism. In this mechanism, load transfer occurs from wedge I towards the remaining soil mass (as measured by the earth pressure cell). The final load transfer mechanism is shown schematically in Figure 3.27. Unfortunately the stress field at the wall can not be fully defined using contact pressure cells only, leaving the question of whether or not the load transfer

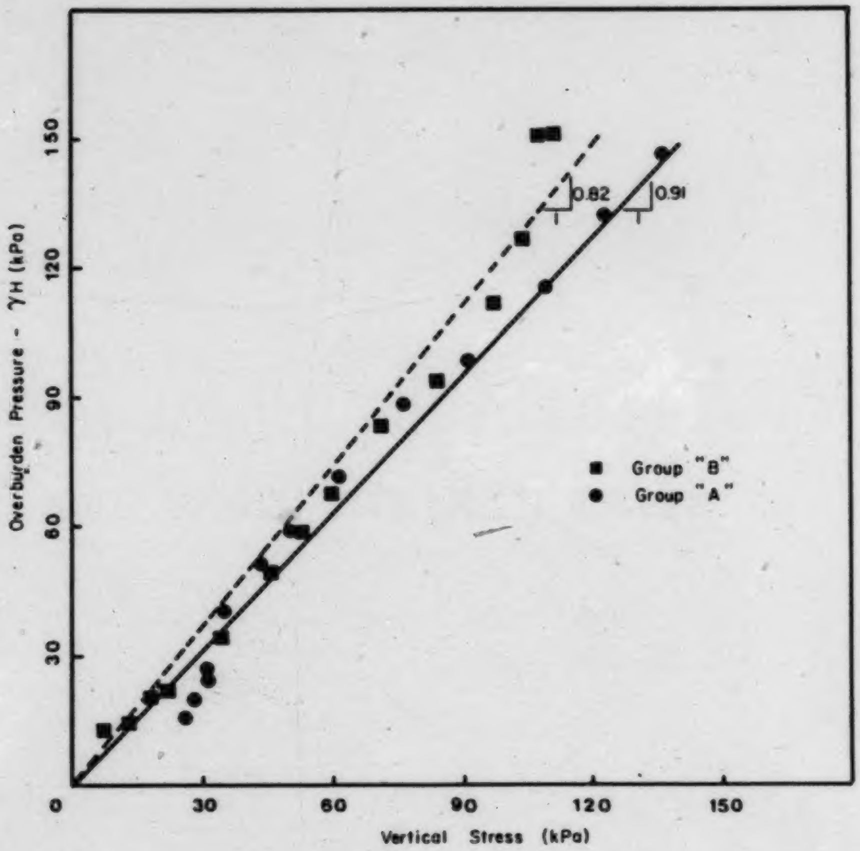

Figure 3.26 Overburden Pressure versus Vertical Stress

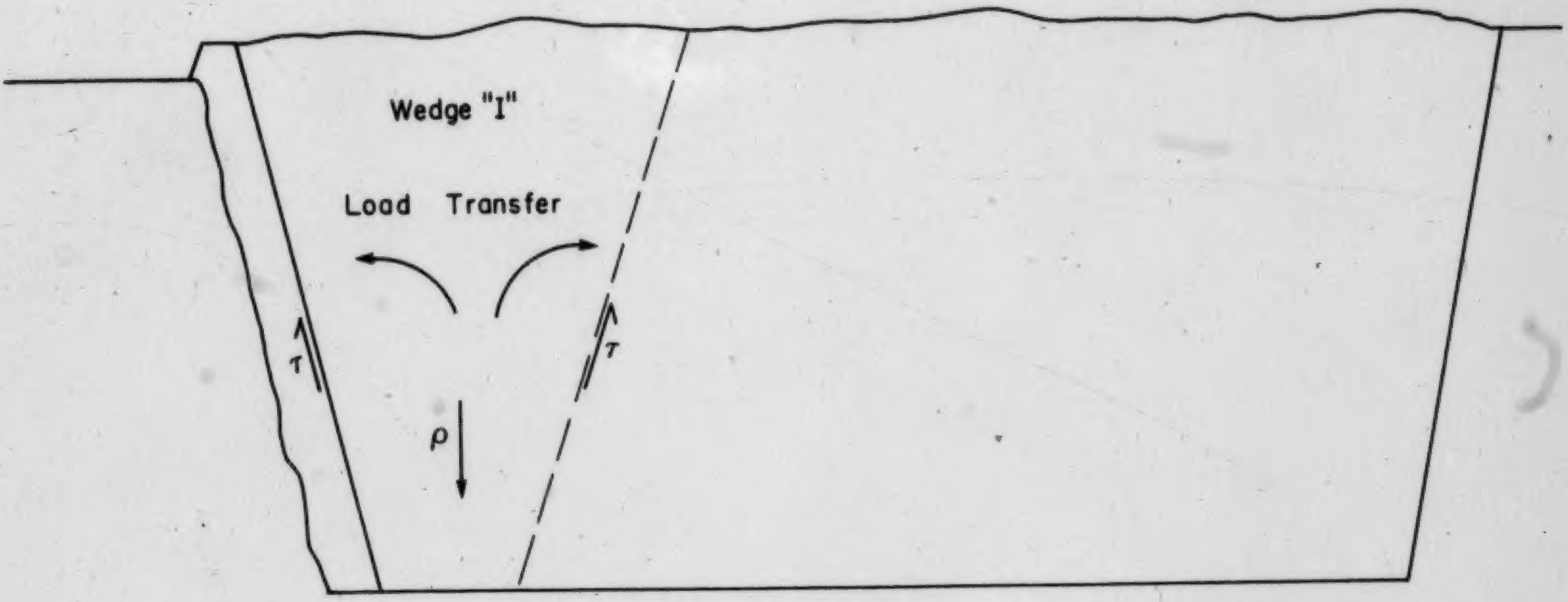
Wedge "I"
Load Transfer
τ
τ
ρ

Figure 3.27 Sketch for Proposed Load Transfer Mechanism

really occurred towards the wall.

On the other hand, the results of the Glöetzl cells suggest that the hypothesis of plane strain for the center line of the test embankment does not hold and the fill cannot be considered "infinite" in the direction parallel to the wall. Neverthless, the hypothesis of plane strain condition will be maintained for the analyses presented in subsequent chapters.

The load tranfer mechanism is further discussed in Chapter 6 in the light of the results of the finite element analyses.

3.4.2 Wall Instrumentation

In this section the wall measurements are presented. As mentioned before, each line of instruments is referred to as lower instrument, center instrument and upper instrument depending on the elevation of installation (4.5m, 3.0m, and 1.5m, from the top of the wall respectively).

3.4.2.1 Contact Pressure Cells

Several articles have been published, describing experiences with the use of different types of contact pressure cell such as, Vaughan and Kennard, 1972; Coyle et al, 1974; Felio, 1980.

The normal stresses measured in the test fill, plotted versus the height of the wall, are presented in Figure 3.28, for the last three days of measurements.

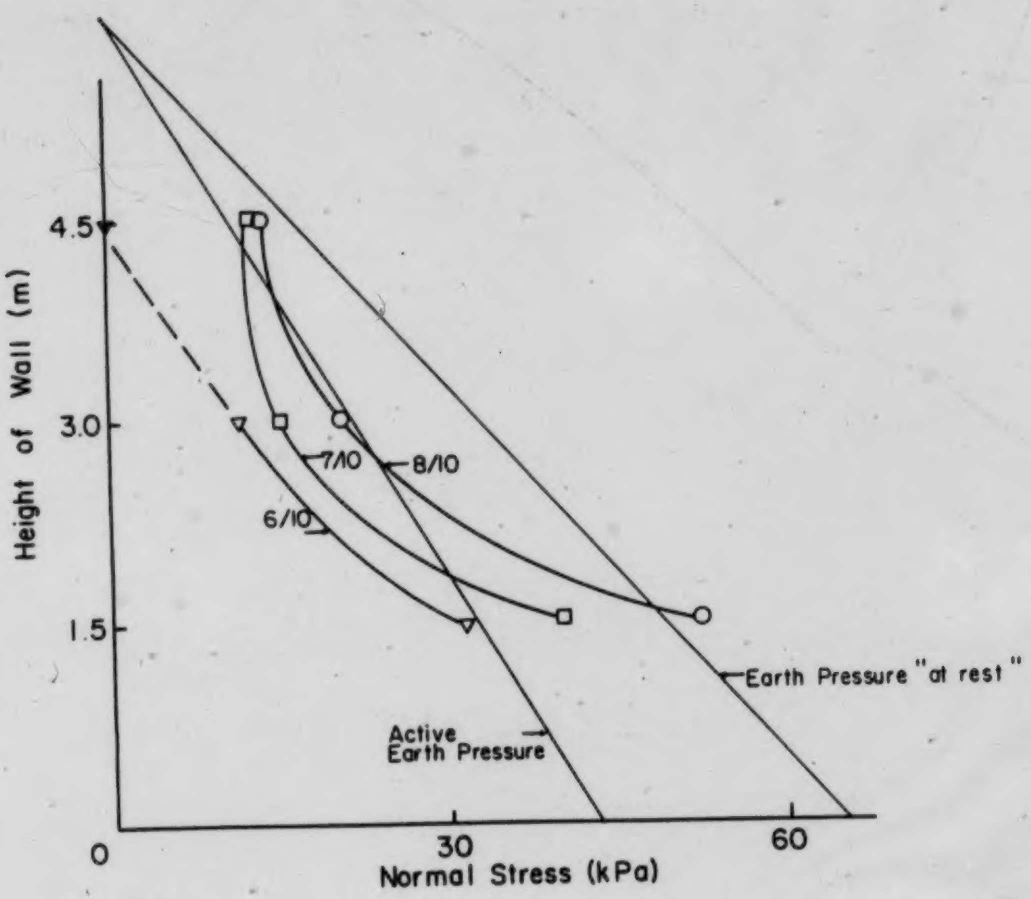

Figure 3.28 Normal Stress versus Height of Wall

It is of interest to observe that the readings obtained are not consistent with the type of wall deflections measured. According to the slope indicator passive movements occurred until October 6th (near the end of backfilling - see Figure 3.3) when they reversed to active movements along the entire height of the wall. Neverthless, the measurements for the upper and lower instruments show an almost "at rest" condition whereas the center instrument measured a near active condition, as shown (Figure 3.28).

Although explanations for this results are not apparent, it is worth mentioning that, due to problems during the construction of the concrete structure, the recess for the center contact pressure cell was made too deep. At the end of installation it was observed that the cell was seating approximately 1 cm inside the recess. This inappropriate installation could have caused poor contact between the soil and the cell, leading to reduced readings during early stages of fill construction (low normal loads).

3.4.2.2 Shear Displacement Devices

The average reading obtained by the two shear displacement devices installed in the same row of wall instruments is plotted versus the time (or increasing height of fill) in Figure 3.29.

It is of interest to notice the magnitude of the displacement registered. They represent approximately

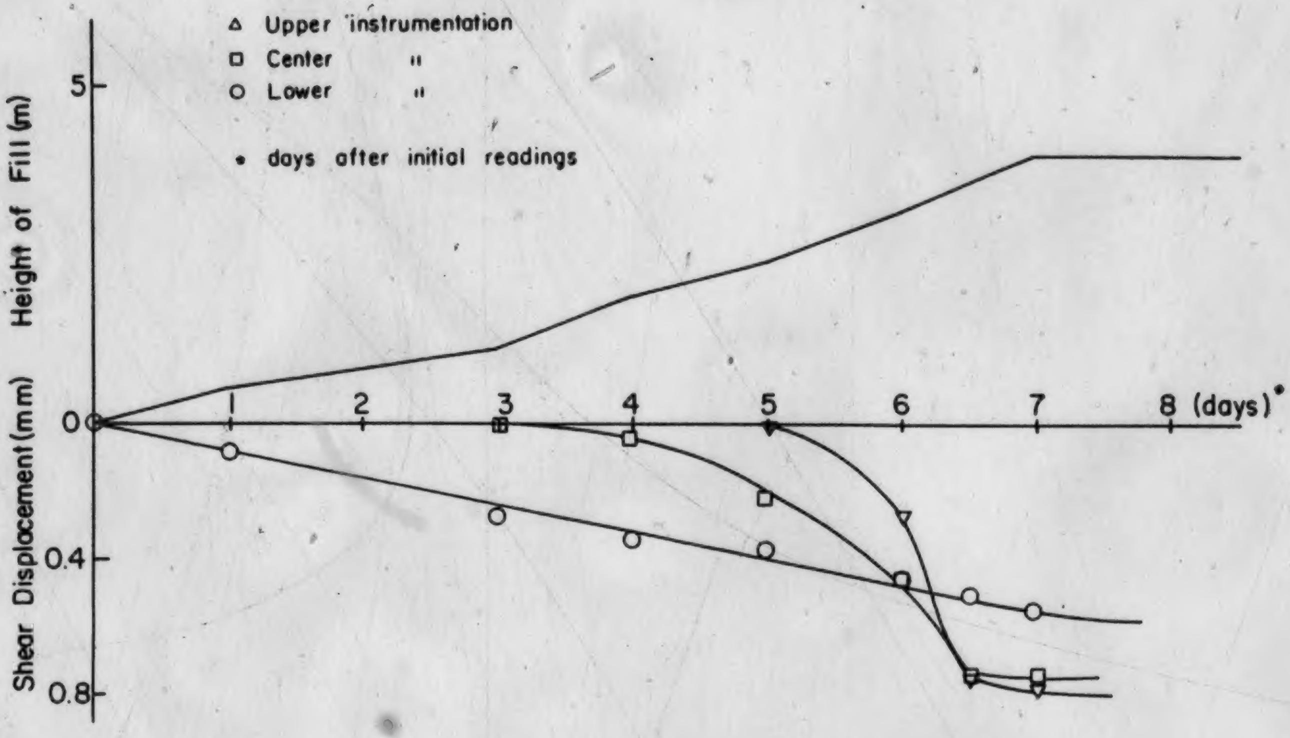

Figure 3.29 Shear Displacement versus Increasing Height of Fill

10% of the displacement measured in the fill, suggesting a very high adhesion between the soil and the concrete structure.

Figure 3.30 presents the development of relative displacement with height of the wall. Although measurements of shear displacement have not been reported in the literature, Cook and Price, (1973), testing a horizontal inclinometer found a similar trend for the shear displacement measured during an axial loading test of a pile.

3.4.2.3 Shear Stress Device

As depicted in Figure 3.31 the shear stress showed an increase with time and no significant time-dependent behaviour was registered. Furthermore, an immediate response to an increase in the rate of construction was detected, contributing to a measure of the quality of the equipment.

By plotting the values of Figure 3.31 versus the height of the wall, Figure 3.32 was obtained.

Once again, only in foundation engineering some effort has been reported to obtain similar measurements. Vesic, (1970) presents results for shear stress obtained by back analysis of axial loading test of piles. Although in a rather different problem, similar qualitative results were obtained for skin friction of the pile.

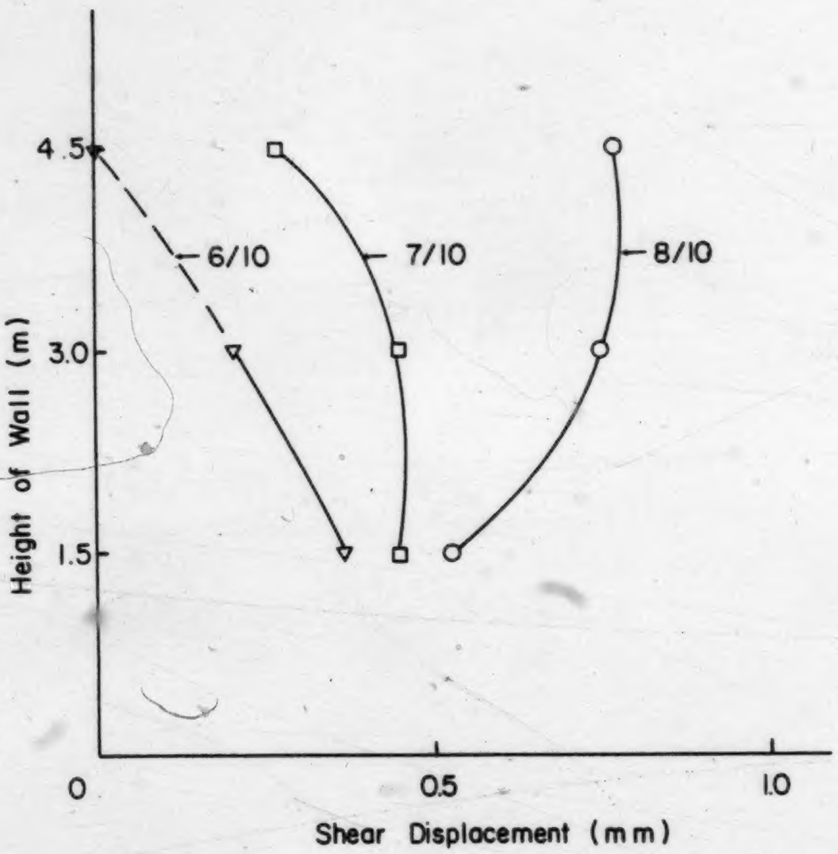

Figure 3.30 Shear Displacement versus Height of Wall

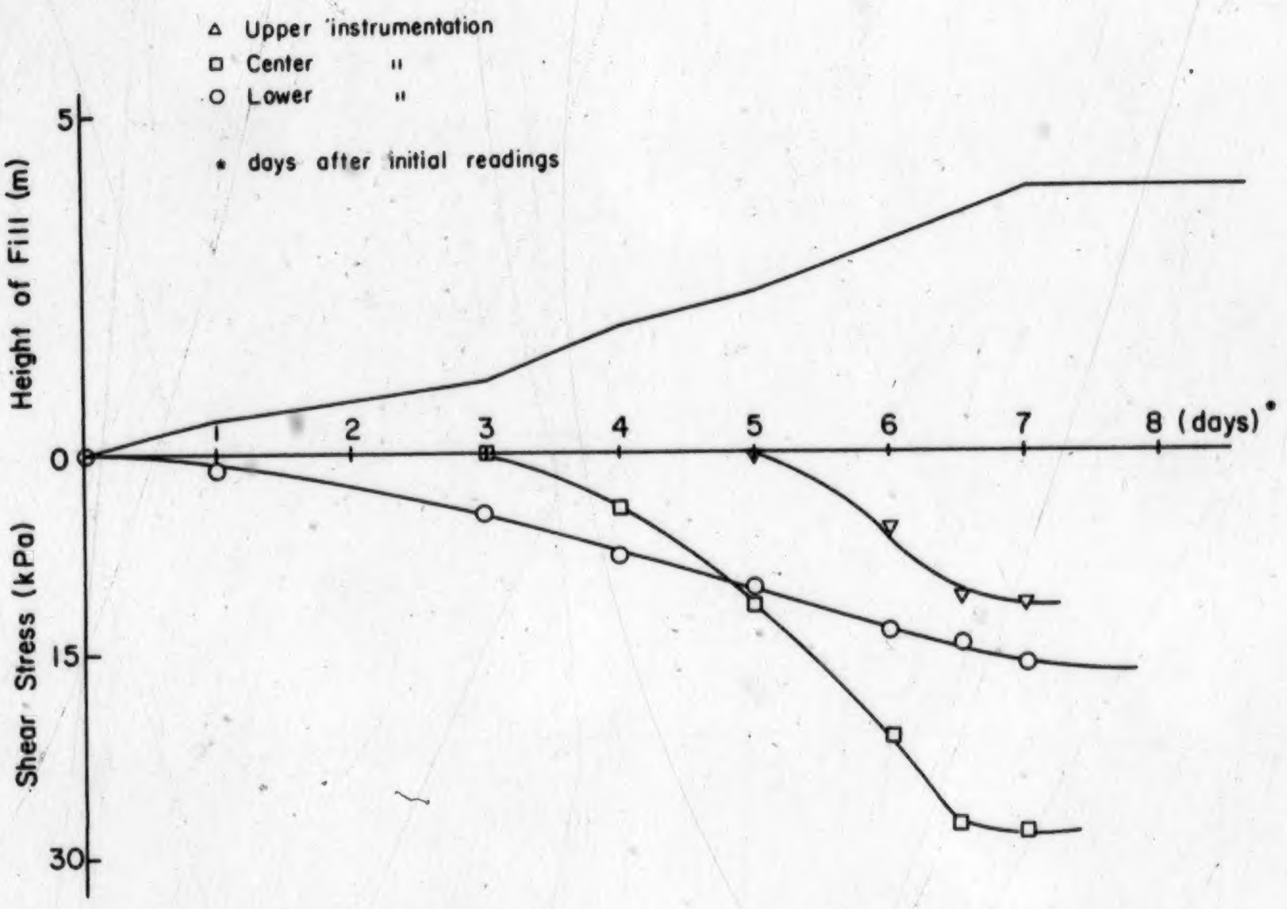

Figure 3.31 Shear Stress vesus Increasing Height of Fill

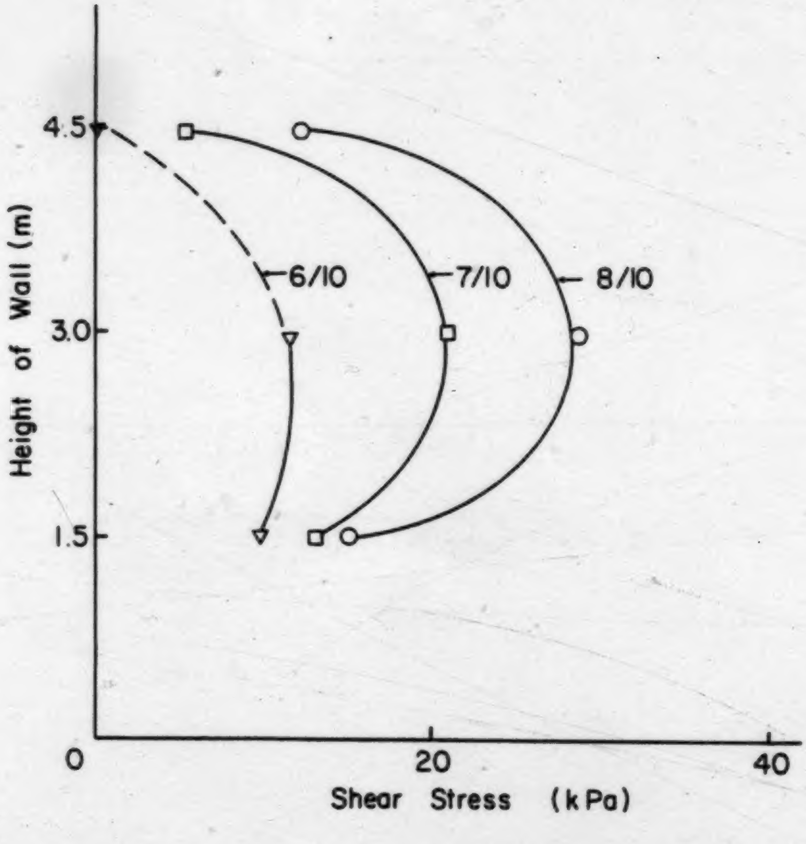

Figure 3.32 Shear Stress versus Height of Wall

Based on Figures 3.28, 3.30 and 3.32, Figure 3.33 can be produced. In this figure, the measured shear stress, normalized with respect to the measured normal stress, is plotted versus the shear displacement. As can be seen, disregarding the scatter, the interface behaviour seems to be well represented by a linear function intercepting the τ/σ axis at a finite value (denoted by $(\tau/\sigma)_0$). This tendency suggests a high adhesion between the concrete structure and the soil for early stages of loading. This trend is further discussed in following chapters.

3.5 CONCLUSIONS

The behaviour of a fill compacted against a concrete wall presents some interesting features, most of them likely occurring in actual engineering projects. These are:

- excavation for construction of concrete structures can increase the foundation compressibility. This phenomena is more pronounced if the horizontal stresses are very high or increased, such as for a deep excavation or if a massive structure is built near the slope created by the excavation. As a consequence, settlements higher than expected can be observed.
- in the most general case, load transfer mechanism is expected to occur at soil-concrete interfaces. This load tranfer is a consequence of the

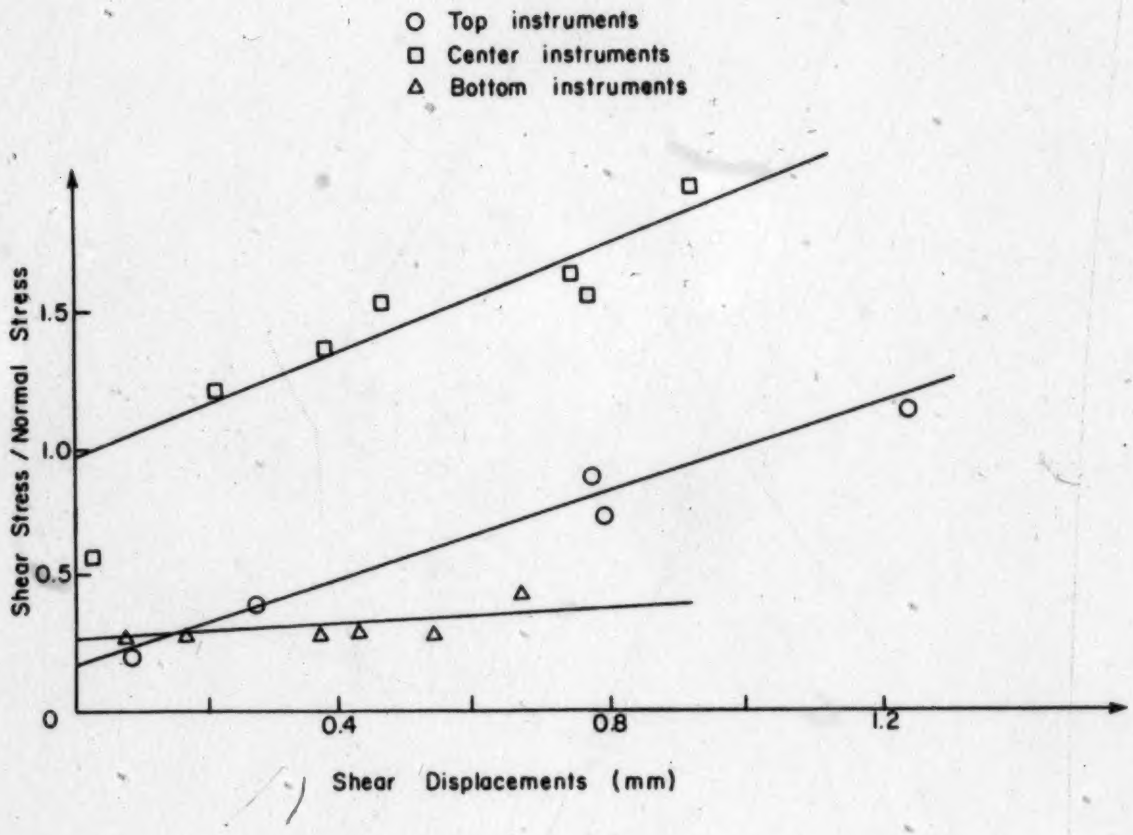

Figure 3.33 Normalized Stress-Displacement Curve

differential settlement observed between the structure and the adjacent soil. This load tranfer can cause formation of cracks in the soil near the structure accentuating water infiltration (if any). This undesirable effect is of special concern in junctions between earth and concrete dams.

- in particular for the test fill reported in this chapter a second mechanism was detected, as a consequence of the excessive settlement measured in the fill near the concrete wall. In this second mechanism loads were tranfered towards the soil adjacent to a hypothetical wedge bounded by the vertical of multipoint extensometers ME-3 (see Figure 3.27). This second mechanism can accentuate the crack generation described above.
- the wall instrumentation helped to define the "macro" behaviour of soil-concrete interfaces.

It was concluded, based upon these results that high adhesion between the soil and the wall is expected to occur, at least for initial stages of loading. This high adhesion is translated by a very high (in certain cases, infinite) **tangential stiffness** (K_t defined in Chapter 2).

Confirmation of these results remains. This may be done with the aid of numerical techniques, such as the finite element method. However, in order to obtain parameters for these analyses, laboratory tests have to be performed.

Ideally, the most representative test for the behaviour of soil-concrete interfaces should follow a similar stress-path as that measured in the field and shown in Figure 3.34. The curves presented in this figure do not resemble the stress-path for a direct shear box test. However, one of the objectives of this research is to discuss the use of these tests as input parameters for interface modelling. Therefore direct shear box tests were performed in the laboratory and are discussed in the next chapter.

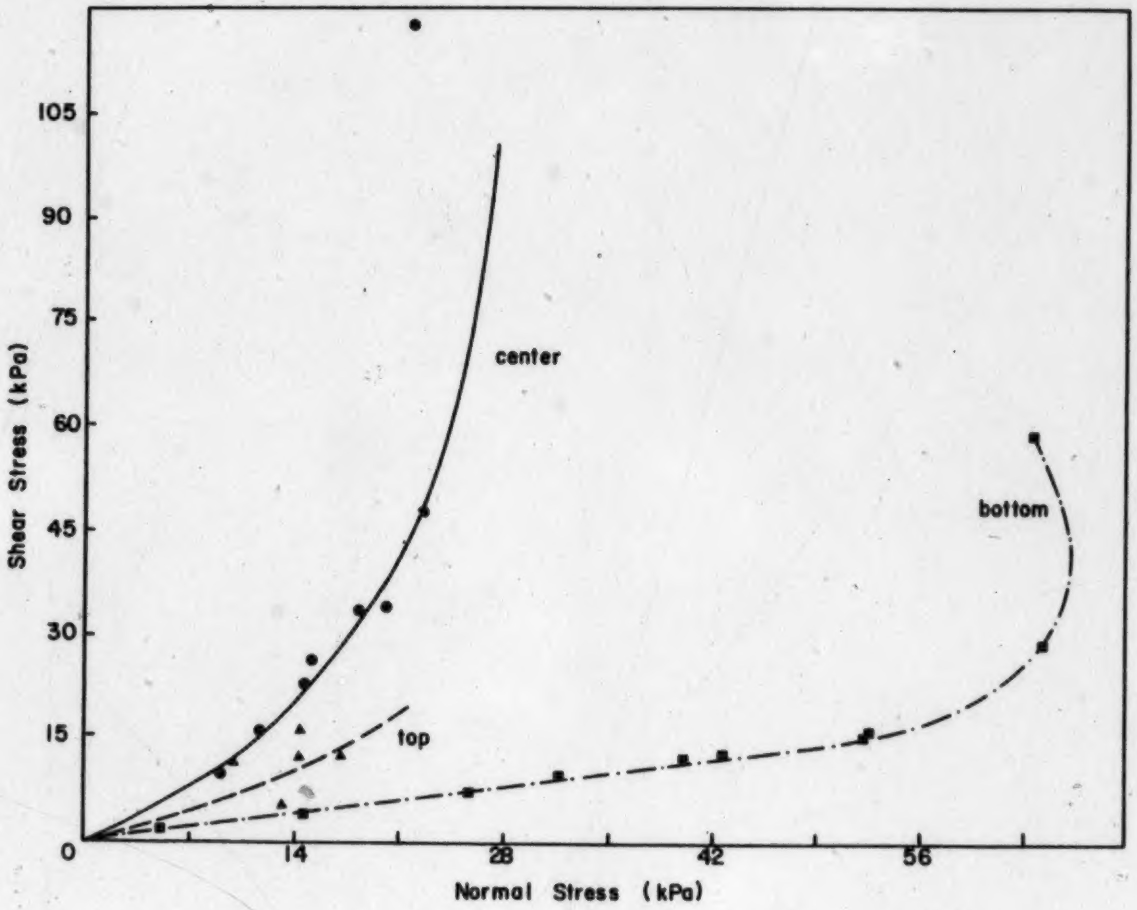

Figure 3.34 Stress-Path Observed at the Concrete Wall

4. LABORATORY TESTS

4.1 INTRODUCTION

The primary aim of the laboratory test program presented in this chapter is twofold:

1. Obtain further evidence of the behaviour of soil-concrete interfaces.
2. Access the methods to obtain parameters for Finite Element analyses.

Since the materials chosen for this research can be reproduced in the laboratory and no undisturbed samples are necessary, several tests were performed including a large shear box test in a newly developed apparatus. In this chapter, this large shear box test will be fully described and discussed.

Apart from the results provided by these large tests, other two routine tests were performed and will also be discussed. They were:

- Conventional compressive triaxial tests.
- Direct shear box tests (using combined samples).

The first type of test is used as the material model for the elements representing the soil mass in the Finite Element analyses. Its necessity is discussed in Chapter 6 and the routine adopted and the results are reported in Appendix "C".

The shear box tests were run in order to analyse their applicability in designing interfaces, as proposed by Clough and Duncan (1971) and later by Roa (1981). The routine followed and the results obtained are presented in the following section.

4.2 CONVENTIONAL DIRECT SHEAR BOX TESTS

4.2.1 Equipment and Procedures

The tests were performed in a Wykeham Farrance Direct Shear Apparatus. A square box 6 cm x 6 cm was used, having the lower half filled with concrete.

Two series of tests were run in order to evaluate the influence of the sample preparation.

In the first series (series 100) ten tests were performed using five different normal loads. The samples were compacted inside a Standard Proctor Mold at optimum moisture content. During the extraction operation, a square cutter was used to trim the sample to be used in the test. All samples were obtained from the center of the cylinder and only one sample per compacted cylinder.

After both ends had been trimmed to the desired height (1.7 cm), the sample was pushed inside the upper half of the box (against the concrete) and the normal load applied.

Shearing started 24 hours later, allowing enough time for the vertical movements to virtually stop. The rate of shearing of 0.0045 mm/min was chosen in order to match the requirement of full drainage, as suggested by Lambe (1951).

concrete roughness and soil gradation. Based on the experience of Kulhawy and Peterson (1979) it was decided to use 2 mm spacing in both series of tests reported in this thesis. A visual inspection of the samples after shear showed that, using this gap, failure was occurring at the interface.

4.2.2 Presentation and Discussion of Results

The stress displacement curves for four of the tests of series 100 are shown in Figure 4.1. Figure 4.2 presents similar curves for the 200 test series. Table 4.1 summarizes all 22 direct shear box tests performed.

It is of interest to notice the difference in behaviour presented by both series of test. While the curves for the first group present a strain-hardening behaviour (shear stress increases monotonically), the second group shows a strain-softening pattern (shear stress shows a peak value).

Since both series of tests were performed using the same concrete block and the same soil placed under similar conditions (optimum moisture content and maximum dry density), differing only in the method of sample preparation, two major factors are considered to explain these differences:

- disturbance caused by the sampling procedure adopted in the first case,
- higher "degree of bonding" (adhesion) developed in the second method.

In the second series of tests (series 200) the soil was compacted inside the upper box, avoiding extracting and trimming procedures. For this series a higher upper box was chosen allowing enough loose soil to be placed during sample preparation and still obtain a soil sample with the same height as in the previous series.

The sample preparation consisted of placing approximately 75 gm of loose soil in the upper half of the box (and in contact with the concrete) and applying 4 blows against a compaction head, using a Standard Proctor Hammer. Subsequently, another 75 gm of loose soil was compacted in a second layer, by applying 5 blows. This procedure ensured that a uniform sample was obtained at the maximum dry density. In this series, 12 tests were performed using the same normal loads as in series 100.

All 22 tests were performed using material collected during the construction of the Test Embankment and the concrete block used in both series was the same. The concrete block was molded inside the lower half of the box and against a plywood form, thus reproducing as close as possible the roughness of the concrete wall.

Kulhawy and Peterson (1979) pointed out the influence of spacing between the two halves of the shear box, in tests involving soil-concrete interfaces. They emphasized the importance of ensuring that the interface was actually being tested by selecting the proper spacing. These authors concluded that the spacing must be varied depending on the

Table 4.1 Summary of Direct Shear Box Tests

Ser.	Test #	σ_n (kPa)	γ_t (kN/m^3)	w_i (%)	w_f (%)	τ_p (kPa)	τ_R (kPa)
100	1	15.00	20.7	13.0	12.8	12.1	-
	2	15.00	20.9	12.8	12.3	7.0	-
	3	30.0	22.0	12.9	12.9	20.3	-
	4	30.0	20.0	13.5	13.2	26.0	-
	5	60.0	20.8	14.3	14.0	47.2	-
	6	60.0	20.9	14.1	14.1	43.6	-
	7	90.0	20.5	13.5	12.9	74.0	-
	8	90.0	21.1	13.6	13.0	66.0	-
	9	120.0	21.3	12.9	12.9	100.3	-
	10	120.0	20.9	13.3	12.9	97.7	-
200	1	30.00	20.5	13.4	13.2	21.6	18.5
	2	30.00	21.2	14.5	14.0	32.2	22.2
	3	30.0	19.5	12.0	12.0	16.6	16.6
	4	30.0	21.5	13.2	13.0	39.7	34.5
	5	30.0	22.0	13.7	13.7	56.6	35.8
	6	60.0	19.5	13.8	13.5	49.4	43.2
	7	60.0	20.0	13.5	13.2	54.4	39.0
	8	90.0	20.7	13.7	13.6	69.0	64.0
	9	90.0	20.3	12.8	12.5	83.3	70.0
	10	120.0	20.0	13.5	13.2	103.3	90.1
	11	120.0	21.5	14.0	13.8	112.3	103.5
	12	120.0	20.9	13.8	13.7	75.9	75.7

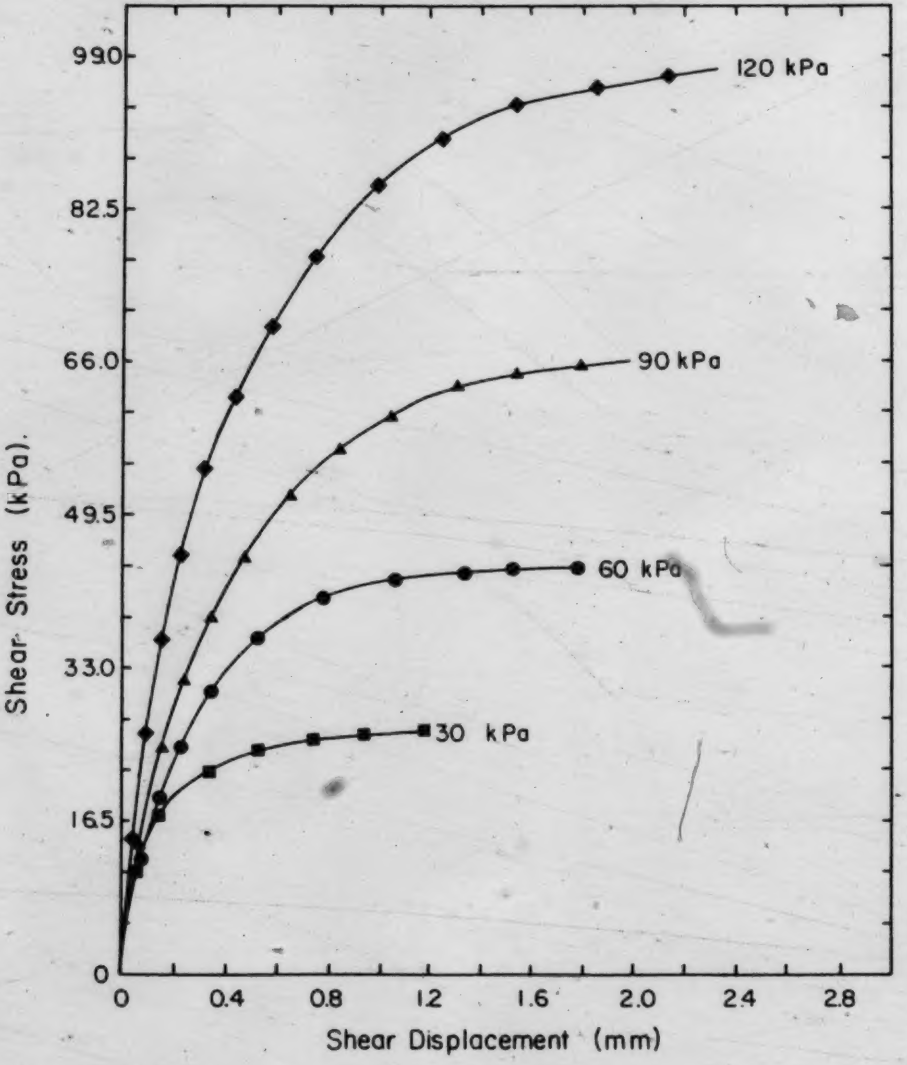

Figure 4.1 Results of Direct Shear Test - Series 100

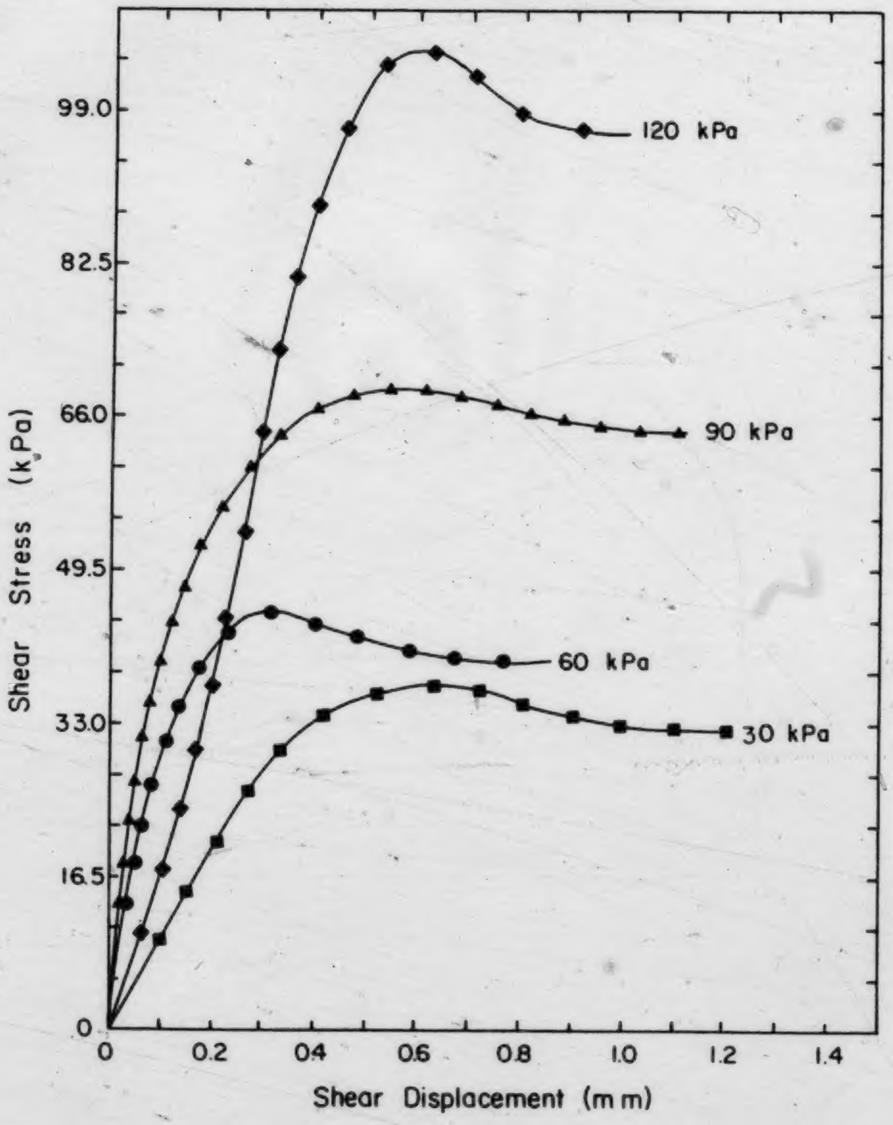

Figure 4.2 Results of Direct Shear Test - Series 200

As explained previously, in the sample preparation for series 100 the soil was compacted in a Standard Proctor mold and then subjected to a "**sampling procedure**" . All sampling procedures cause disturbance that, in most cases, can play an important role in the stress-strain behaviour of soils. The effect of sampling has been extensively studied in the past. Broms, (1980) pointed out that the effect of sampling disturbance has a large effect on stress-strain curves of brittle material. This author has shown evidence that this type of material can present a ductile behaviour as a consequence of disturbance. Similar experiences have been reported by Milovic, (1971) and La Rochelle and Lefebvre, (1971) for different types of soil.

The second method was developed to minimize disturbance and consequently to obtain a "**more intact**" sample.

The higher **degree of bonding** can be established in two different ways:

- First the type of contact between soil and concrete developed by compacting the soil directly against the concrete is different from that developed in the first case. In the second method it is expected that all recesses existing in the concrete will be filled with soil. Consequently, for this case, failure will occur partly across the soil and partly across the interface. This difference is shown schematically in Figure 4.3.

- Second, if the tests are plotted in a τ - σ stress space, as shown in Figure 4.4, it can be seen that while the results for group 200 show some intercept in the τ axis, the first group shows no intercept. This intercept suggests a higher degree of adhesion.

Furthermore, it is believed that samples cut from the compaction mold (as in series 100) develop different soil fabric (arrangement of grains) at the interface when compared to the structure developed by the second method.

Seed and Chan, (1959) have studied the effect of fabric on the behaviour of compacted soil. The authors have shown that materials compacted drier than the optimum moisture content develop a more flocculated fabric and the stress-strain curves, in a triaxial apparatus, show a strain-softening behaviour. This type of behaviour is characteristic of "unstable" fabrics. On the other extreme, samples compacted wetter than the optimum moisture content present a more disperse arrangement and show strain-hardening stress-strain curves.

Based on the above discussion and since the stress-displacement curves for the shear box tests performed in samples of series 200 showed a strain-softening behaviour, it can be expected that this method of sample preparation induced a more flocculated structure (unstable stucture). However this conclusion is not supported by the analysis presented by Seed and Chan (1959) since the energy

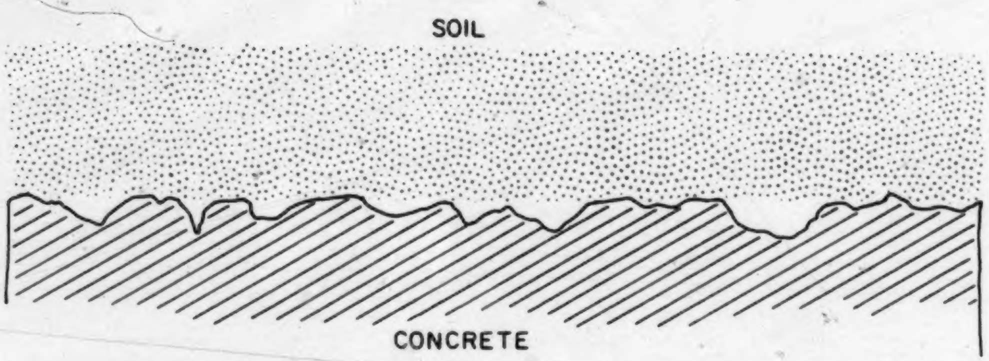
SOIL
CONCRETE

TYPICAL INTERFACE FOR SERIES 100

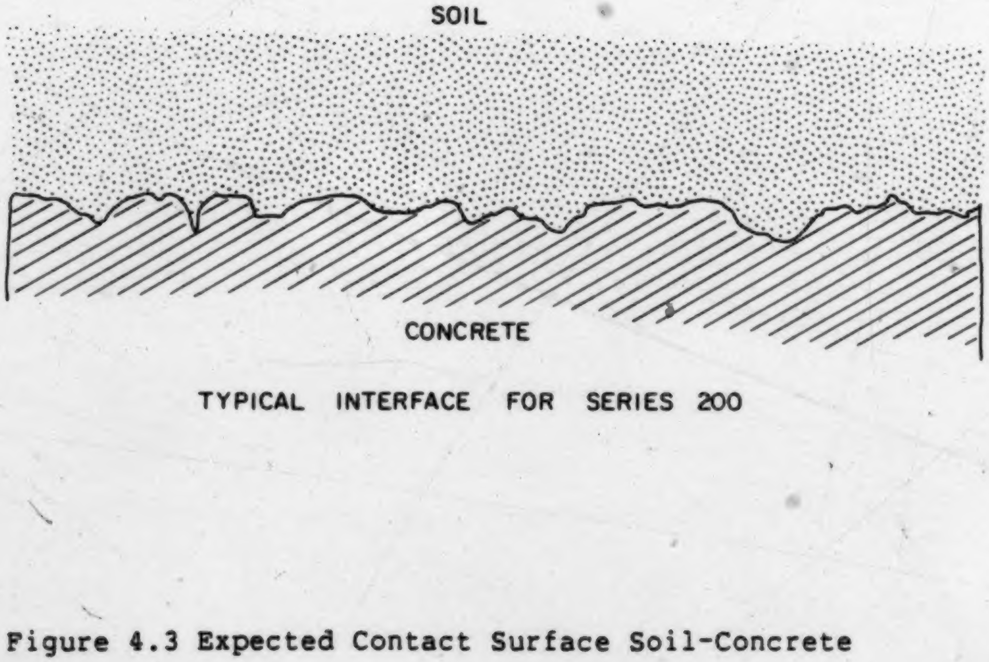
SOIL
CONCRETE

TYPICAL INTERFACE FOR SERIES 200

Figure 4.3 Expected Contact Surface Soil-Concrete

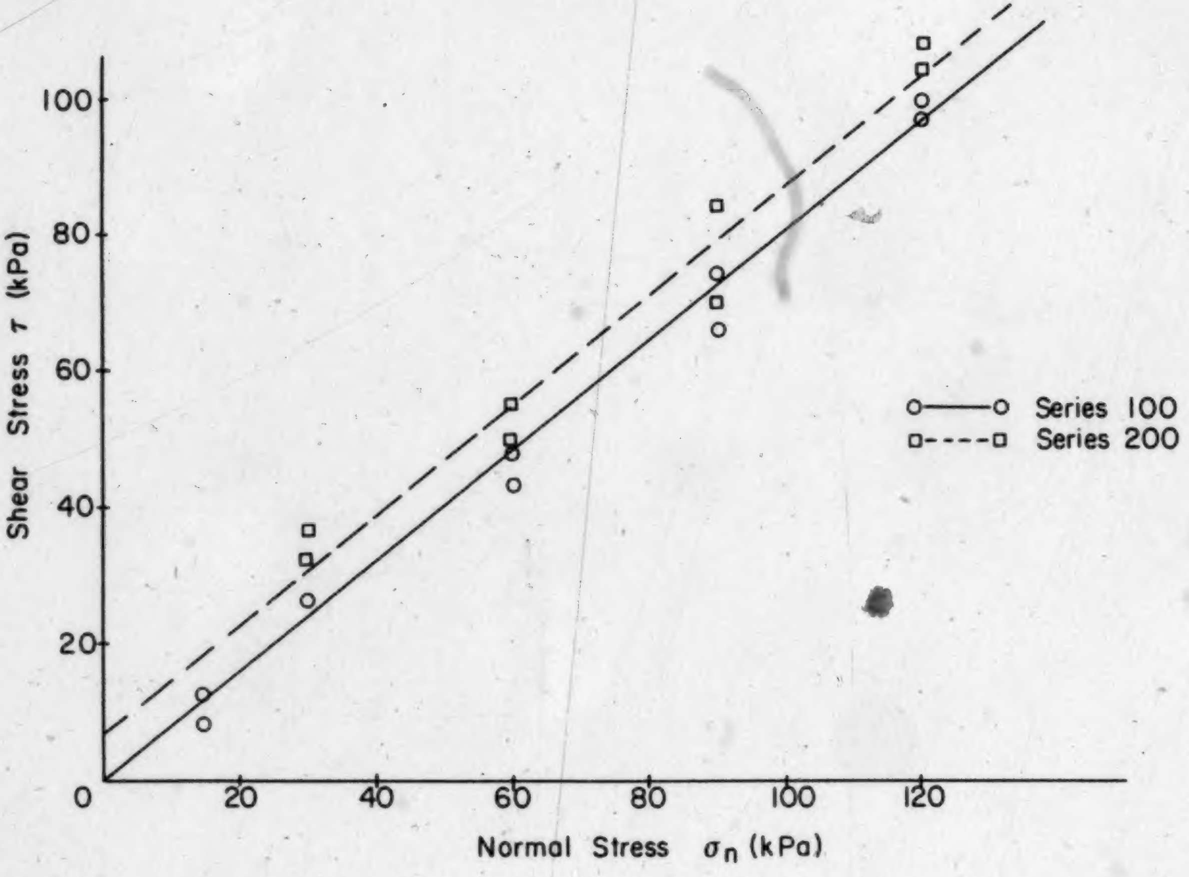

Figure 4.4 Envelope for Direct Shear Tests

imposed on the samples of series 200 is higher than that used in series 100. Therefore, for the same moisture content and unit dry density used in series 100 the increased compactive energy should impose a higher degree of dispersion and a more stable structure should be expected and not the opposite.

These factors contributed, in different proportions, to create a more brittle material, that showed slightly higher shear stress and very low displacement for failure, when the second method was used.

It is of interest to mention that the stress-displacement curves for the second group of samples have demonstrated a **"sensitivity"** to disturbance created by mishandling or any small variations in the moisture content (± 0.5%). Since, in the field, the moisture content is seldom controlled within this range, it is difficult to rely on the peak strength for design purposes. Moreover, it is difficult to anticipate the displacement path followed by a grain of soil during compaction, and consequently it is difficult to anticipate which method of sample preparation better represents the field behaviour. One possible path, used here as an example to explain what was mentioned above, is shown in Figure 4.5. In this figure, AB represents the displacement caused by compaction, bringing the grain of soil closer to the structure. This is followed by removal of the load (BC). Subsequent passes of the compaction machine will cause the grain of soil to came into contact with the

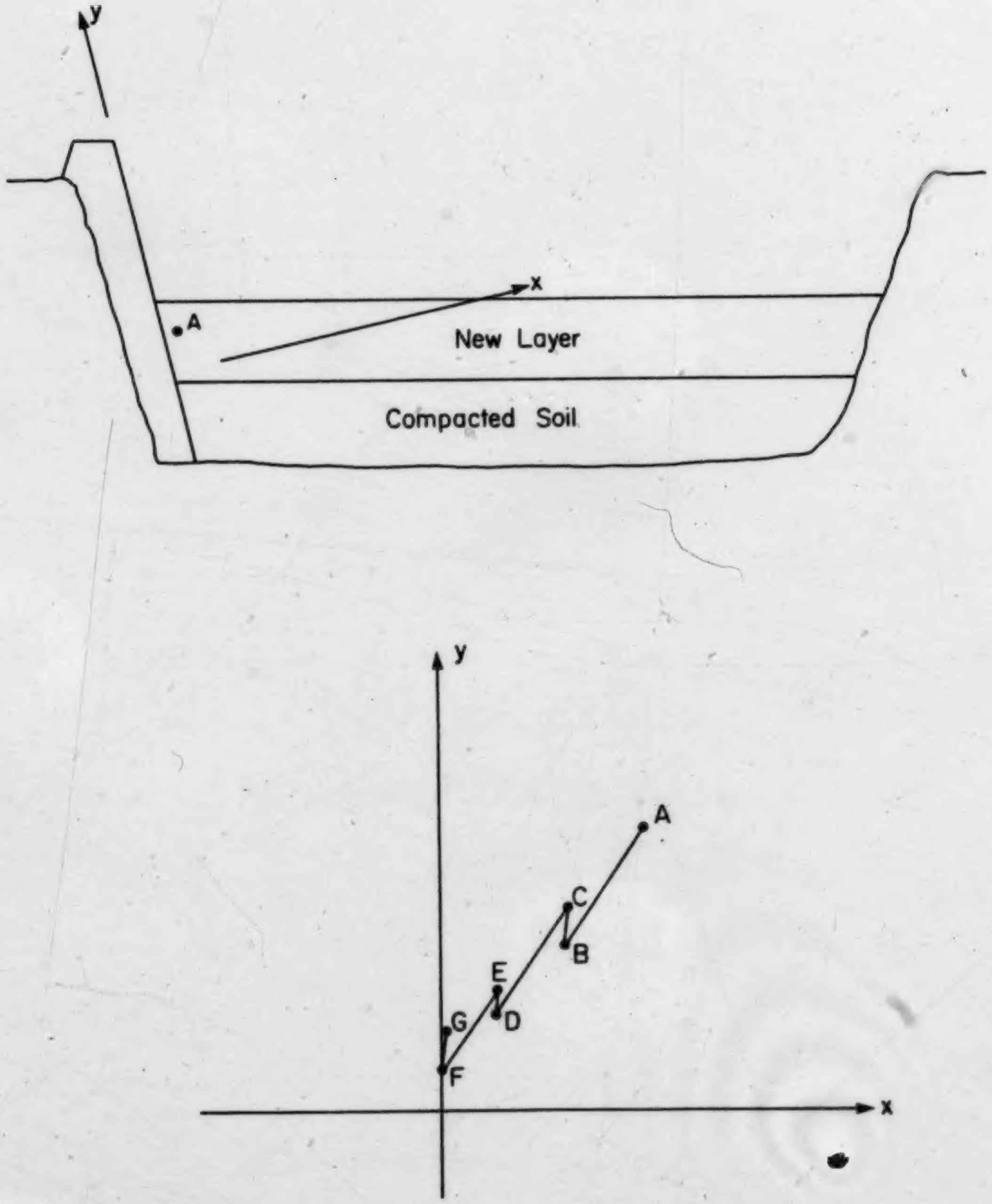
y
x
A
New Layer
Compacted Soil
y
A
C
B
E
D
G
F
x

Figure 4.5 Suggested Displacement Path for Grain of Soil

structure (CD, DE,...,etc), and eventually to displace parallel to it. During this process, it is believed that the soil will suffer displacements relative to the concrete wall, sufficiently high to disturb any possible adhesion.

This discussion, although hypothetical, provides an idea of what type of contact should be expected in a soil placed near a concrete structure.

Therefore, in practice, before any measurement can be obtained, the fill will have already been subjected to "loading cycles" due to compaction and superimposed layers and it is probable that the field behaviour will not be similar to that observed in series 200. On the other hand, some adhesion will probably develop due to increases in normal stresses caused by the newly placed layer, and consequently series 100 will also misrepresent the actual behaviour. This discussion will be extended in Chapter 6 based on the results of the finite element analyses.

4.3 LARGE SHEAR BOX TEST

4.3.1 General

The equipment was idealized to reproduce a section of the concrete wall, containing a row of instruments, as described in the previous chapter.

In this section the apparatus will be presented in detail, followed by a discussion of the equipment performance, tests performed and conclusions drawn.

4.3.2 Design of the Laboratory Apparatus

The large shear box apparatus is composed of three basic components:[3]

- A reinforced concrete base and sample container
- A vertical loading system
- A horizontal loading system

4.3.2.1 Concrete Base and Sample Container

The reinforced concrete base was molded inside a plywood form which had dimensions 1.0 m x 1.0 m and 0.25 m deep.

Attached to the reinforcement 12 threaded rods were placed, each driven through the form and extending 20 cm outside the form. These rods were used to hold an inverted U-frame that served as reaction for both vertical and horizontal loads.

At the center of the base, a knock-out was molded to accomodate a Shear Stress Device (as discussed in Chapter 3), having dimensions 0.29 m x 0.29 m x 0.075 m deep.

Three modifications were introduced in the Shear Stress Device for laboratory use:

- the knock-out was molded by a steel box left in position before concrete pouring
- the concrete block (used in the shear stress device) was also molded inside a steel box

---

[3] Detailed drawings and plates showing the apparatus are presented in Appendix "D".

- roller systems were used between these two steel boxes, reducing the friction between the two parts to virtually zero.

Details of this modified version of the Shear Stress Device are presented in Appendix "D". Although it was designed for laboratory application it is perfectly suitable for field use.

The dimensions of the Shear Stress Device used in the laboratory were choosen based upon a simple finite element analysis, ran to simulate a cross-section of the proposed apparatus. A mesh was drawn, assuming the nodal points at the interface soil concrete to be the same (in other words, no slip was allowed at the interface). The results of this analysis have shown that, for a soil sample 1.0 m long, the center three-quarters of the sample would have almost uniform shear stress distribution. Based on this analysis it was decided to use a 0.29 m long device, corresponding to approximately the center 50% of the 65 cm of the soil sample.

The soil was placed inside a steel mold 0.7 m square and 0.25 m deep. The mold was made of 25 cm (10") channel sections and placed over steel rollers to minimize friction at their contact with the concrete. It is important to note that although the mold was 0.25 m high, the soil sample was only 7.5 cm thick. The remaining height was used to provide safety against possible failure of the vertical loading system.

The soil container was constrained from rotating horizontally by means of two pairs of castors welded to a 7.5 cm (3") steel angle section, bolted to the concrete base.

Friction between the container and the soil sample was reduced by using two layers of silk at the contact. Although not commonly used for this application, silk seems to be most efficient in reducing friction under these circumstances.

In order to evaluate the performance of the silk to reduce friction, Figure 4.6 presents the results of direct shear box tests between two blocks of wood containing two layers of silk at their contact. In the same plot, results of similar tests for layers of teflon and for a uniform round sand are shown. As may be seen, the two layers of silk showed the smallest angle of friction, about 8% of the value for sand, whereas two layers of teflon amount some 20% of the angle of friction for sands.

It is worthwhile mentioning that the gap between the steel mold and the concrete base was filled with foam. This foam helped to maintain the moisture content during the test as well as avoiding flow of loose soil under the box before compaction of the first layer.

A view of the whole assembly is sketched in Figure 4.7 and Plates 4.1a and 4.1b. Further details are in Appendix "D".

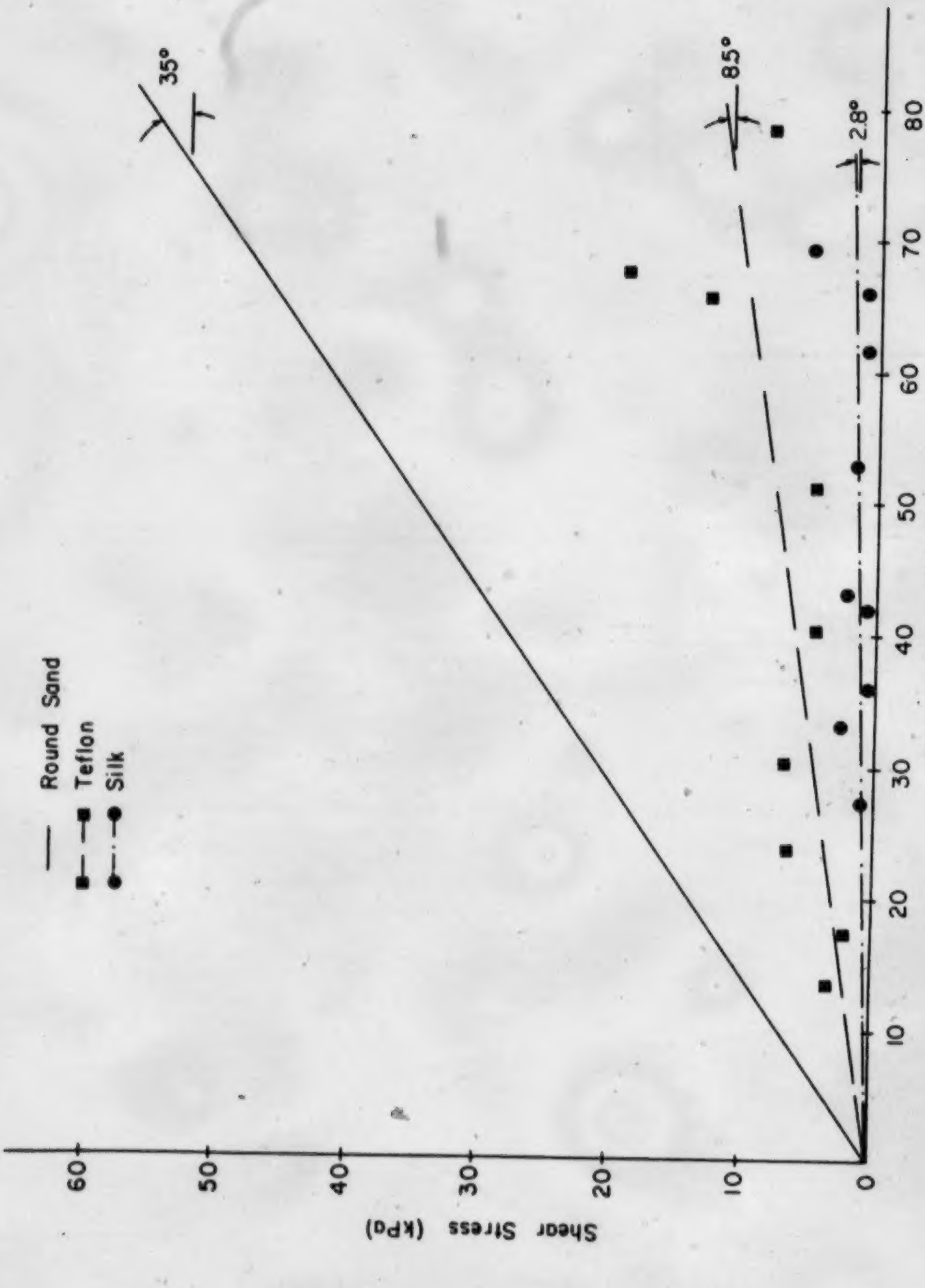

Figure 4.6 Evaluation of Method of Friction Reduction

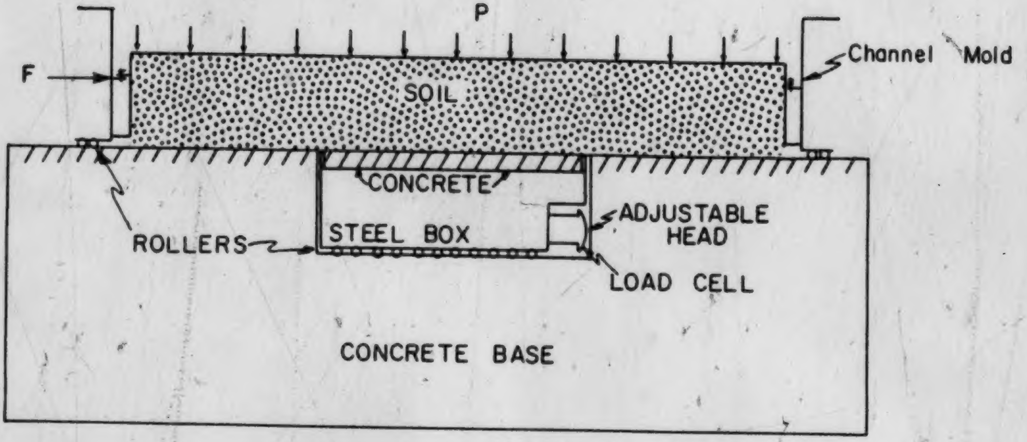
P
F
SOIL
Channel
Mold
CONCRETE
ADJUSTABLE HEAD
STEEL BOX
ROLLERS
LOAD CELL
CONCRETE BASE

Figure 4.7 Sketch of Large Shear Box Apparatus

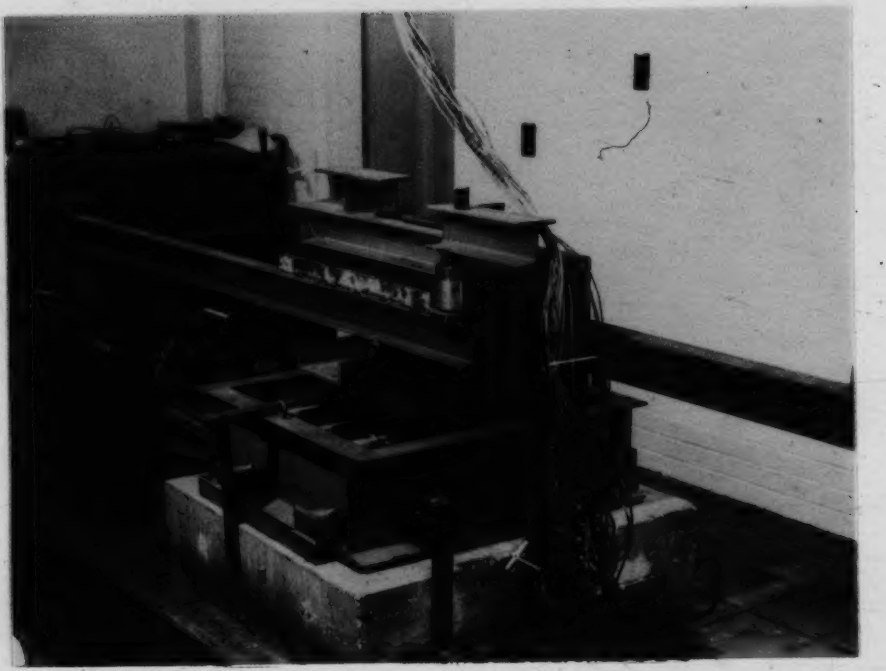

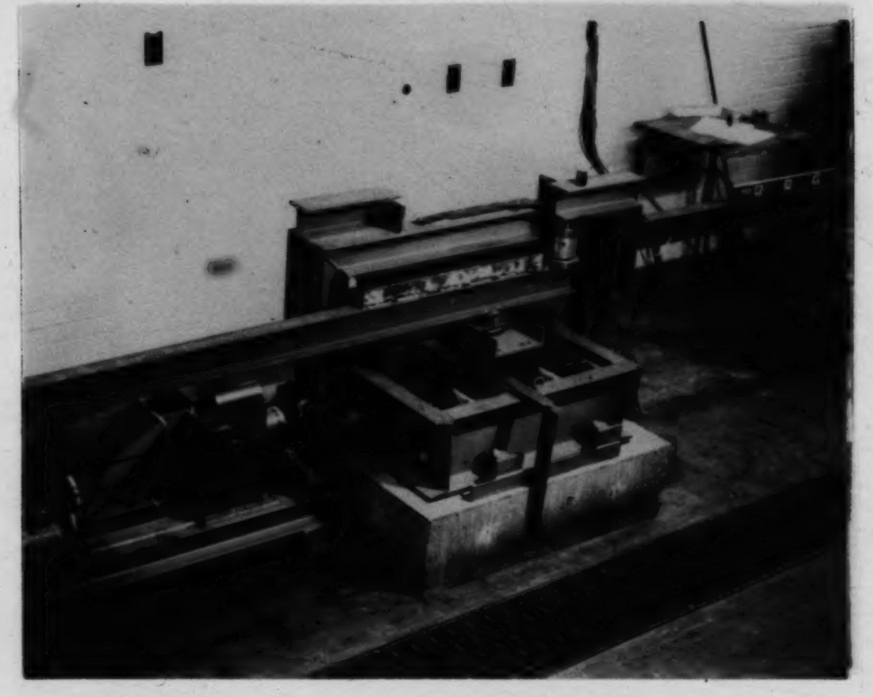

Plate 4.1 General View of Large Shear Apparatus

4.3.2.2 Horizontal Loading System

All tests were performed in a strain-controlled mode. The strain rate was imposed by a piston attached to a gear box by means of a drive chain. This system enables different rates of shearing to be used.

The whole system was mounted in a frame welded to the reaction frame. An overview of the loading system connected to the concrete base is shown in Appendix "D".

4.3.2.3 Vertical Loading System

In order to allow for differential settlement (due to nonhomogeneities in the soil sample) and to ensure a uniform distribution of normal stress, a rather complex loading system was designed.

After several unsuccessful trials, the final system imposed the following measures:

1. Reducing the area of the soil sample but maintaining the loaded area.
2. Reducing the height of the sample
3. Application of the load through a series of prismatic elements forming a pyramid shaped loading head.
4. Load applied by two symmetrical lever systems and weights.

The first measure was accomplished by welding a steel member near the base of the molde with dimensions

2.5 cm wide x 5 cm high (1"x 2"). A 5 cm x 2.5 cm (2"x 1") angle section was bolted against the first member and served as a collar to hold the loose soil before compaction. After the sample was compacted, the angles were removed and the final sample was approximately 7.5 cm deep (refer to Appendix "D" for details).

The pyramid shape is a well-known efficient method for distributing concentrated loads. This shape is frequently used in shallow foundation design as the most appropriate configuration for transfering loads from pillars to soil masses. A second common application can be found in the laboratory, where pyramid shaped loading heads are used in most conventional shear box apparatus to transform the vertical point load into a uniform stress. In particular at the University of Alberta a similar problem was faced during the development of a model test for tunnels (Kaiser, 1980). Here also, the lateral loads, applied by hydraulic jacks, were tranformed into uniform stresses by means of a series of prismatic elements with triangular cross-section, forming a pyramid.

Following the experience of Kaiser (op.cit.), rows of prismatic elements made from steel were used to form the pyramid. In the first row (bottom row) 64 prismatic elements were used to cover the whole area of the mode. For the second row, 32 elements were used, each transfering their loads to two of the previous row.

Subsequently, another 16 prisms were placed, again each resting on two of the previous row. The last row was headed by 8 steel flat bars (dimensions 5 cm x 2.5 cm or 2" X 1") located at the center of the pyramid element apex. These 8 bars received their load from another 4 steel bars (again 2" x 1") that were headed by 2 bars (2"x 2") and finally 1 bar (2 $^1/_2$" x 2 $^1/_2$") received the point load from the lever system. Figure 4.8 and Plate 4.2 illustrate the loading system.

It is important to note that the contacts between the flat bars were made through ball bearings, thus ensuring tranfer of normal loads only. Friction between the loading head and the container was reduced by using two layers of teflon.

Another important detail concerns the difference between the dimensions of the base of the loading system (0.7 m x 0.7 m) and the soil sample (0.65 m x 0.65 m). This procedure was adopted based on the results of sucessive calibrations, using different arrangments. Since this configuration resulted in a more uniform load distribution, it was adopted.

Vertical loads were applied using two symmetric lever systems and weights. The levers were composed of two 10 cm (4") I-beams reacting against the reaction frame. The ratio of the levers were 8:1 and the they were 2.5 m long, allowing for application of 58 kN (12000 lbs) of total load (29 kN or 6000 lbs per

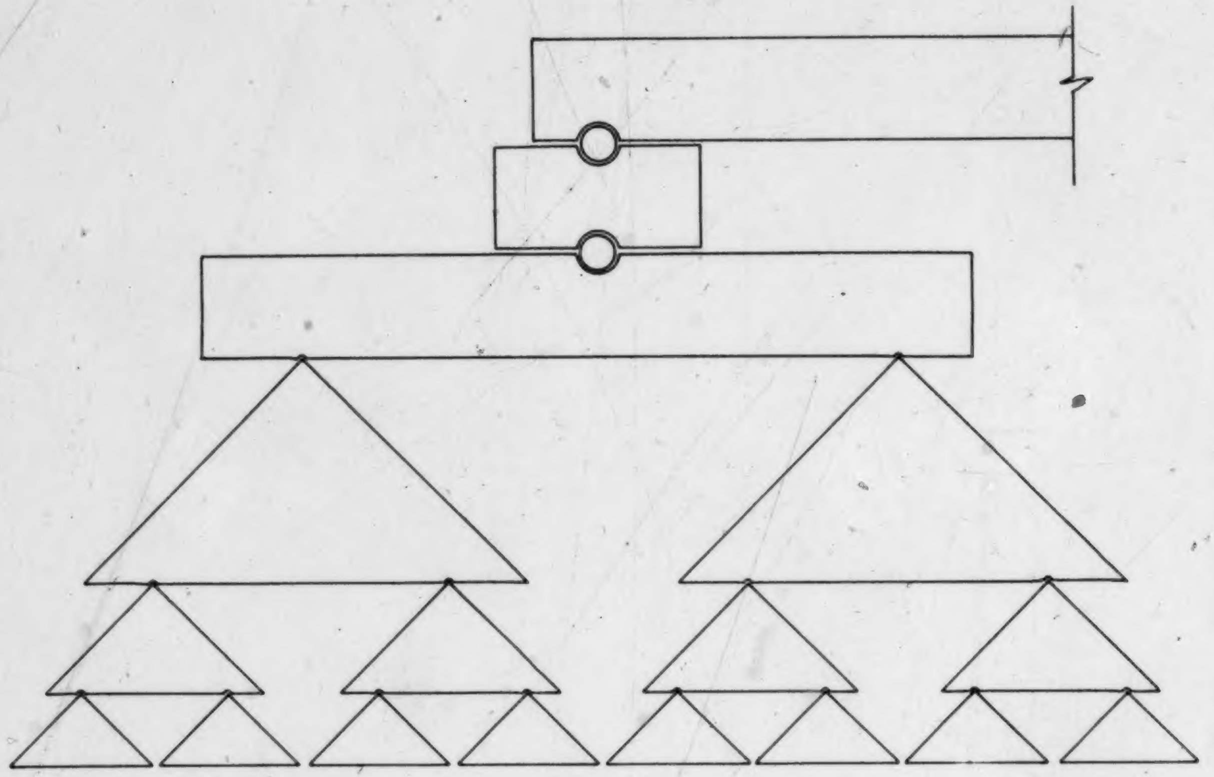

Figure 4.8 Loading Head for Vertical Load

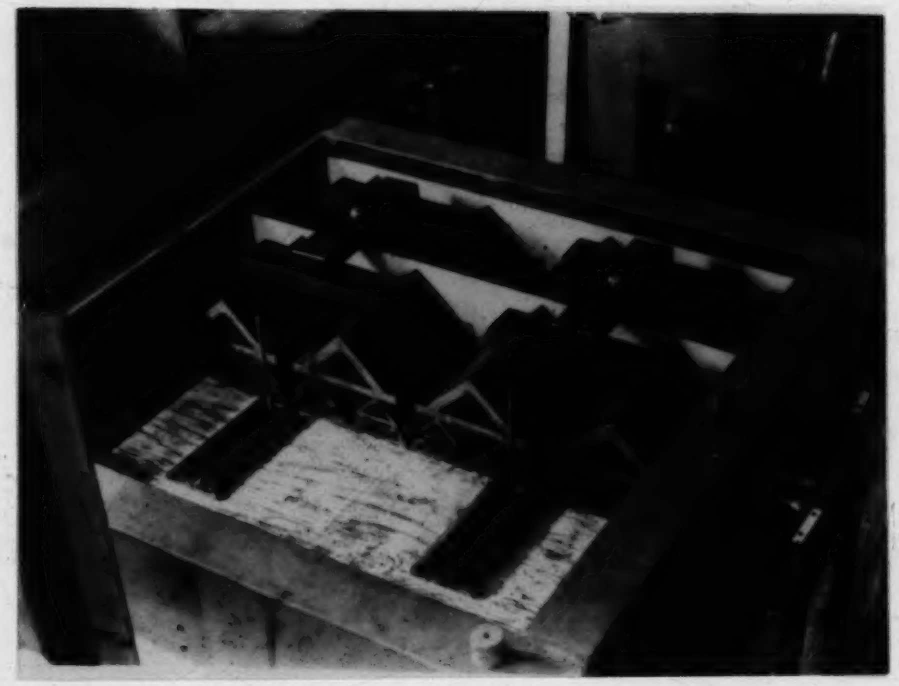

Plate 4.2 Loading Head for Vertical Stresses

lever).

In order to correct the level of the levers during test, their reaction points were mounted on screws. (see Plates 4.1)

The reaction frame was built using extended web steel "H" sections, 10 cm (4") high and 10 cm (4") wide, forming an inverted "U" frame, and attached to the concrete block by means of 12 threaded rods, as explained before.

4.3.3 Instrumentation

Each sample tested was instrumented to allow a comparison between internal and external measurements. By internal measurements it is understood that they are similar to measurements obtained in the field, i.e., shear stress at the interface (using the Shear Stress Device in both cases) and relative displacement. The external measurements are those compatible with the conventional shear box test i.e., applied external force and displacement of the box.

The external shear stresses were obtained by a calibrated load cell at the point of application of the load. This load divided by the total area of the soil sample equals the "external shear stress". The displacements were measured using a calibrated LVDT in contact with the steel box, and on the opposite wall to the load application (see Figure 4.7).

For the "internal measurement" of displacements, a modified "Shear Displacement Device" was designed. It was composed of a 1/16" stainless steel rod having a small 5 mm x 25 mm plate welded to one end and threaded at the other end to couple to a LVDT. Two of these devices were installed inside each sample, after the first layer of the sample had been compacted (refer to section 4.3.4)

The installation procedure began by opening a groove 2 cm wide and approximately 26 cm long. The rods, protected by a 3/16" aluminum casing, were placed in position, extending to the outside of the box through the gap between the box and the concrete base. The small plates were then pushed into the soil in order to ensure full embedment in the soil mass (full contact between the plate and the soil). Finally, the grooves were covered and a small hammer was used to compact the soil inside the trench.

Using the procedure described above it was possible to ensure that the Shear Displacement Devices were installed in similar positions in all the tests. On average, the instruments were laid approximately 5 cm from the base of the Shear Stress Device (see Figure 4.10) and 2 to 3 mm from the concrete base.

The average measurements obtained by these two devices were plotted versus the shear stress readings of the shear stress devices to comprise the "internal" curve, discussed in the presentation of results.

Vertical movements were also monitored for each test, both externally and internally. In both cases two measurements were obtained, using four calibrated LVDT's.

For the external measurements the LVDT's were in contact with the steel member receiving the vertical load.

The internal displacements were measured approximately 0.5 cm from the concrete. Again for this instrument a 1/16" stainless steel rod with a 2.5 cm x 2.5 cm aluminum plate was built. They were installed inside small trenches opened after the second layer was compacted. After positioning, the rods were protected by 3/16" stainless steel casing and the trenches refilled using compacted material. The opposite extremity of these rods were coupled to the inner core of the LVDT. This LVDT had to be mounted on a roller system in order to displace with the sample and avoid bending the inner core of the LVDT, which would lead to erroneous measurements. Details of these rollers are presented in Figure 4.9 and Plates 4.3a and 4.3b. These measurements allowed the observation of vertical displacements during shearing.

Figure 4.10 shows a sketch of a sample with the instruments in position.

4.3.4 Sample Preparation

As mentioned previously, each sample was composed of two compacted layers. A trial and error method had demonstrated that, to obtain the maximum dry density, 400

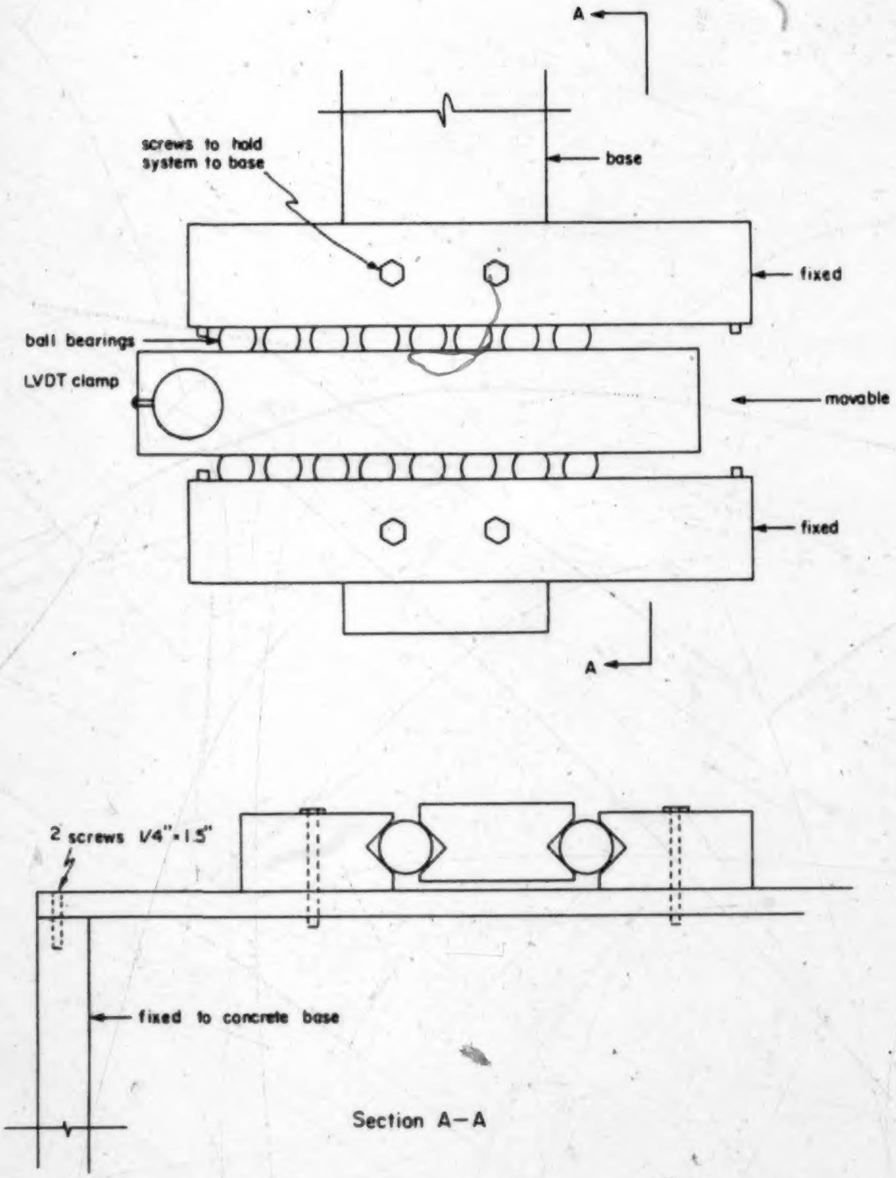
A
screws to hold system to base
base
fixed
ball bearings
LVDT clamp
movable
fixed
A
2 screws 1/4"×1.5"
fixed to concrete base
Section A–A

Figure 4.9 Device to Measure Vertical Displacement during Shear

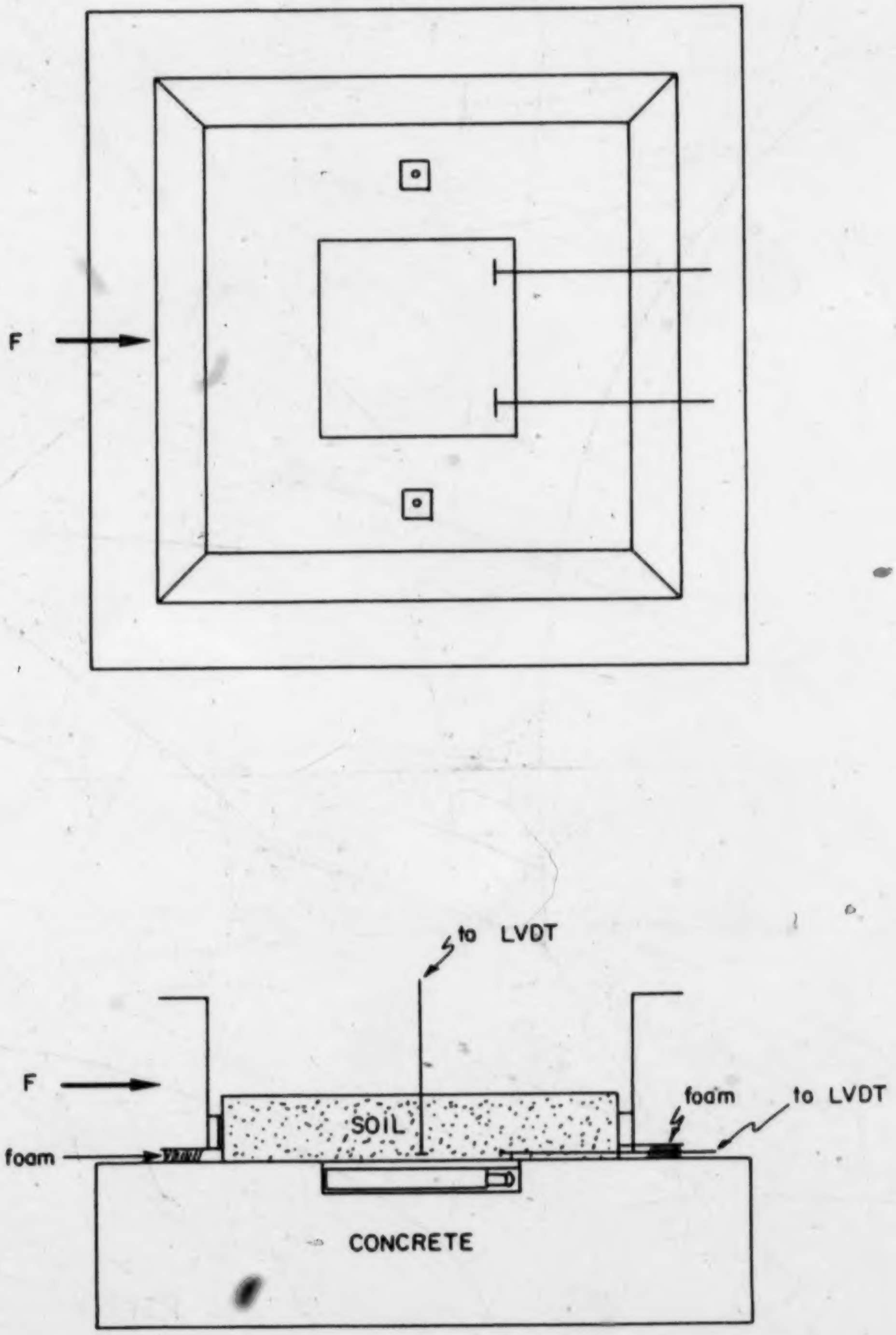
F
to LVDT
F
foam
SOIL
foam
to LVDT
CONCRETE

Figure 4.10 Position of Instruments in a Typical Sample

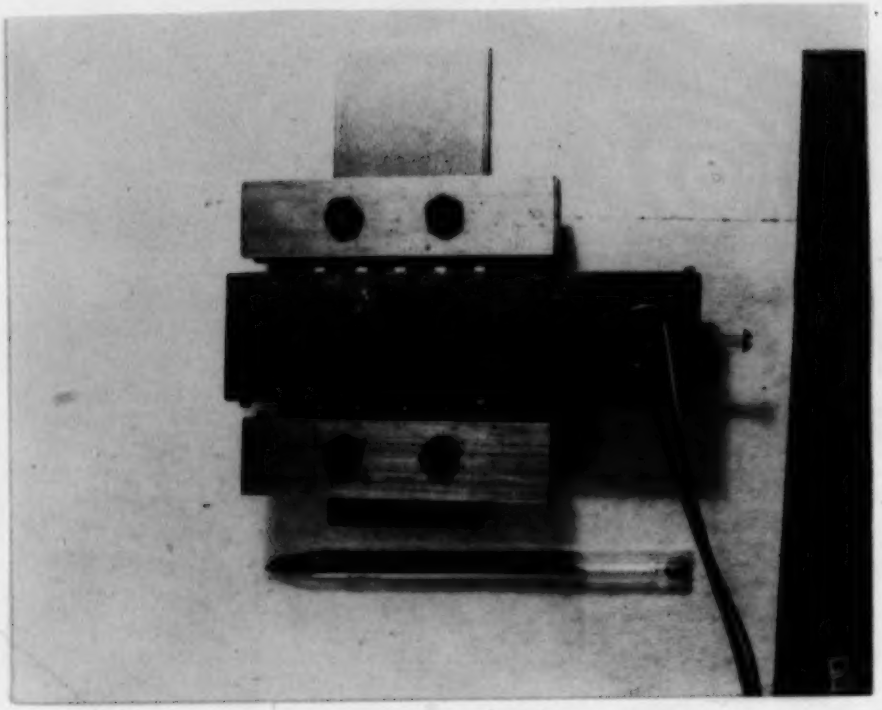

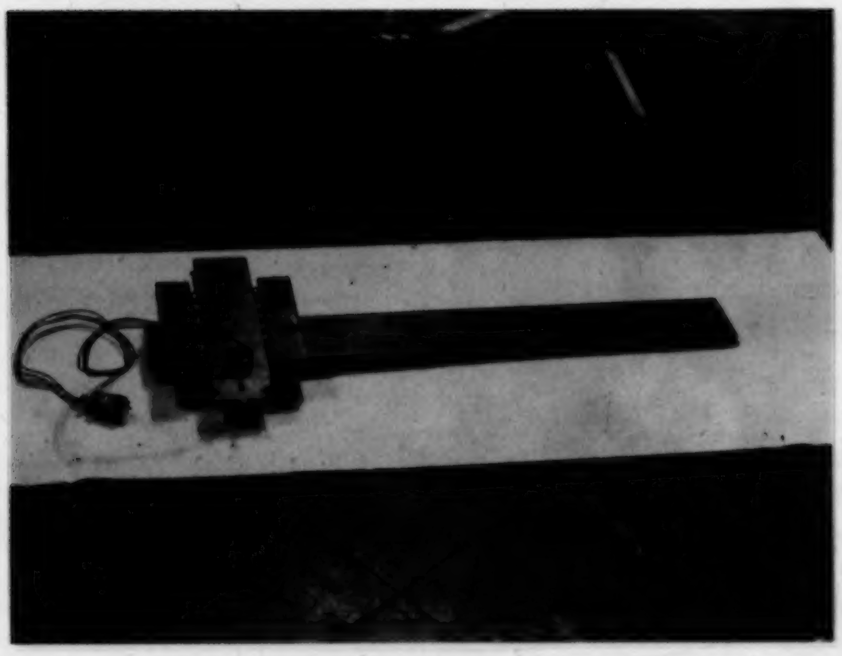

Plate 4.3 Device to Measure Vertical Displacement during Shear

blows per layer had to be applied using a modified Proctor hammer.

To facilitate the compaction procedure, a 30 cm x 30 cm (12"x 12") steel compaction foot was attached to the hammer, increasing the contact area between the hammer and the soil.

The sample preparation included the following steps:

a. Positioning of the steel mold including cleaning the equipment from the previous test and replacement of the foam in the gap between the steel box and the concrete base.

b. Placement of approximately 5 cm uniform layer of loose soil.

c. Compaction of the first layer by applying the blows in four series of one hundred blows in alternate sides with respect to the reaction frame.

d. Installation of the two Shear Displacement Devices.

e. Placement of loose soil up to the top of the removable angle (discussed previously).

f. Compaction following similar procedure as described in "c".

g. Installation of the two sensors for vertical displacement measurements.

h. Removing angles and placement of the vertical loading system, without lever.

i. Adjustment of all LVDT's.

j. Placement of levers and subsequent application of load.

The zero readings for the two load cells measuring the internal shear stress were obtained before the vertical loading system was positioned.

4.3.5 Testing Procedure and Tests Performed

A total of 47 tests were performed, 37 of them considered preliminary tests, carried during the development of the apparatus. The remaining 10 tests were performed using the final version of the equipment. A summary of the final tests is presented in Table 4.2.

All 10 final tests were conducted with four different normal loads and followed the procedure described below.

For all tests, the normal load was kept constant for 48 hours, to ensure that vertical displacements had been reduced to negligible amounts. After this period of time, shearing commenced at a rate of 0.0045 mm/min and maintained until failure had occured. Failure was considered to be an increase of less than 0.5% of the total external load over a period of 30 minutes. On average this condition was reached after 24 hours of shearing.

With the procedure described above, each test had a duration varying from four to five days, including sample preparation and cleaning from the previous test.

One additional test was performed primarily to study effect of rate of shearing on the strength parameters. Since the same special instrumentation was installed in this

Table 4.2 Summary of Tests - Large Shear Box Test

Test #	σ_n (kPa)	γ_t (kN/m)	Wi (%)	Wf (%)	τ_e (kPa)	τ_i (kPa)
1	29.25	17.6	13.0	12.5	34.0	20.0
2	29.25	19.8	13.5	13.1	36.0	16.0
3	59.4	18.7	14.0	13.8	63.0	29.0
4	59.4	19.0	12.5	12.1	64.0	27.0
5	85.8	18.9	13.0	12.5	91.0	39.0
6	85.8	17.6	13.5	12.9	81.0	42.0
7	106.8	18.0	13.4	12.5	121.0	59.0
8	106.8	16.5	14.0	13.9	122.0	54.0
9	29.3	17.8	13.5	12.6	37.5	17.6
10	54.9	19.0	13.5	13.2	74.0	23.0

sample, several other features could be observed. This test, hereafter referred as Test#11, will be extensively discussed in subsequent chapters.

4.3.6 Presentation of Results

As mentioned, each test provided two stress-displacement curves, viz, "external measurements" (total applied shear stress versus total displacement of the steel box) and "internal measurements". The latter were obtained by averaging the displacements measured by two Shear Displacement Device, and plotting against the shear stress registered by of the Shear Stress Device. These curves are shown in Figure 4.11 through 4.14, for four of the tests performed.

Several important immediate observations arise from these figures:

1. The shear stresses for failure are not the same for internal and external measurements.
2. The shear displacements for failure are considerably smaller on the internal curve.
3. The internal plot shows a strain-softening behaviour whereas the external plot presents a strain-hardening pattern.
4. The tangential stiffness (K_t or k_{st}, as discussed in Chapter 2 and defined as the slope of the stress-displacement curve) is not the same for internal and external curves, for a given horizontal

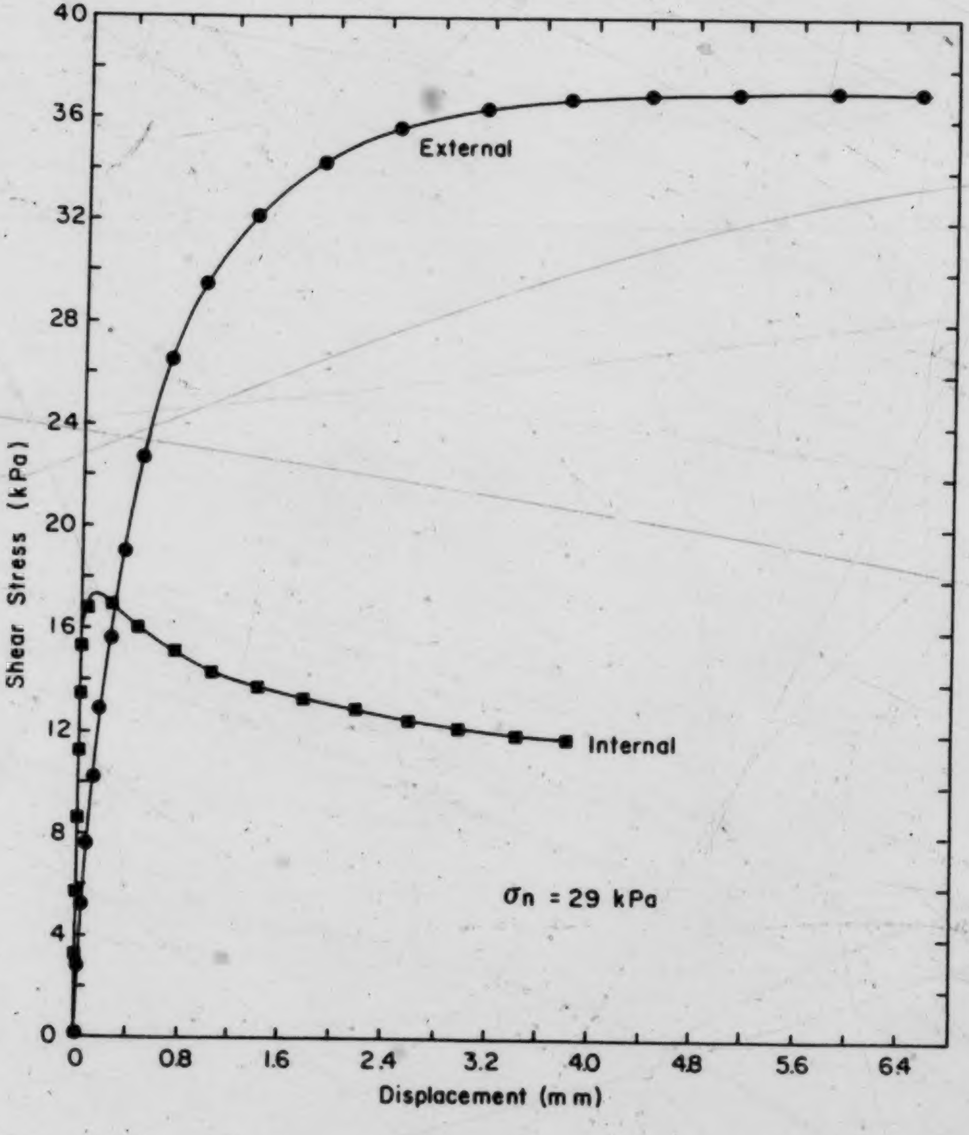

Figure 4.11 Results of Large Shear Test - Test#9

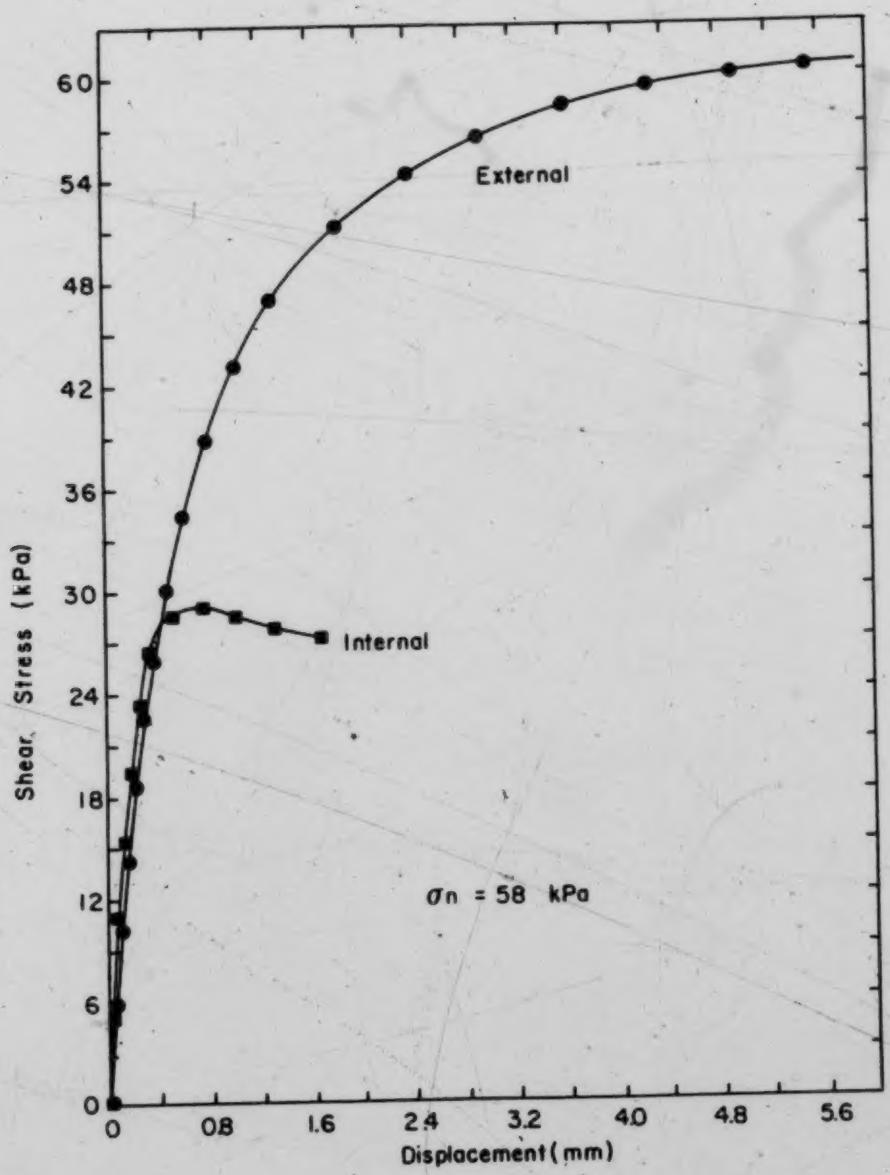

Figure 4.12 Results of Large Shear Test - Test#3

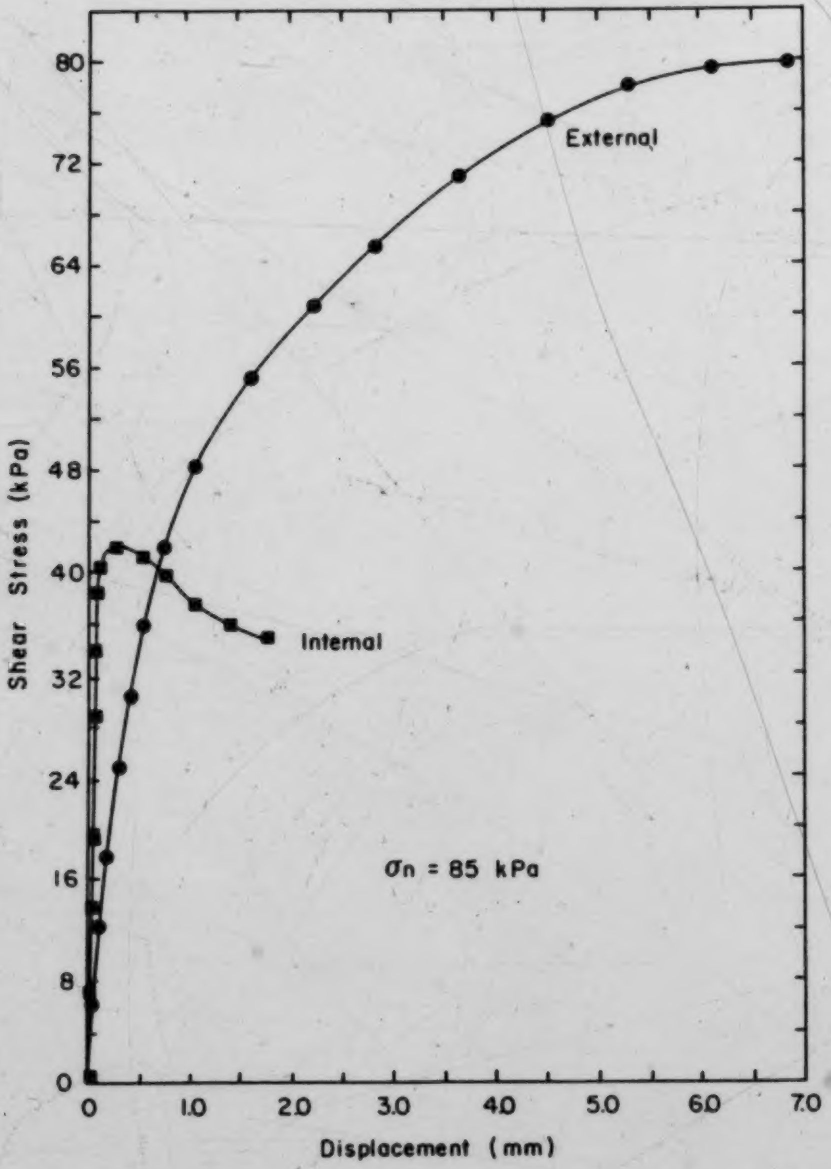

Figure 4.13 Results of Large Shear Test - Test#6

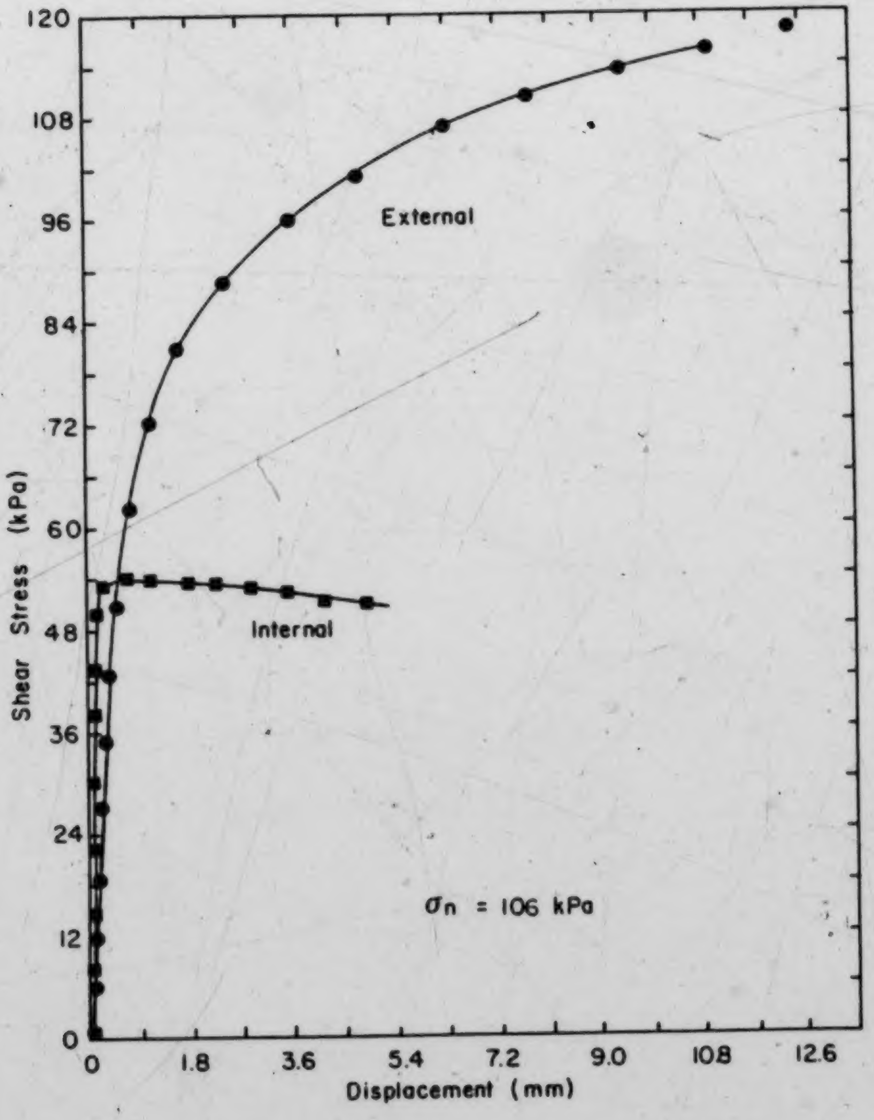

Figure 4.14 Results of Large Shear Test - Test#8

displacement. A detail of the initial portion of the stress-displacement curve for Test#3 (σ_n = 58 kPa) is shown in Figure 4.15. As can be seen, there is a significant difference in the shape of both curves.

Some of these features do not offer an immediate explanation but will be considered in subsequent chapters. Neverthless, some of these features can be discussed with the analyses of the test results.

The results of vertical displacements are shown in Figure 4.16. These measurements were obtained in test#8 (σ_n = 106 kPa). Some of the remaining curves are shown in Appendix "E". It is important to mention that the internal vertical monitoring displacement devices, in most cases, measured displacements within the accuracy of the LVDT used. This fact made difficult a precise analyses of the vertical displacements within the sample. Neverthless, the trends measured are as expected and tests performed at lower normal stresses show some upward movement. This trend reversed for samples tested under higher normal stresses. A transition from one type of behaviour to another can be observed for intermediate normal stress levels.

Figure 4.17 shows the tests plotted in a τ - σ stress space. In this figure the solid lines present a band of possible peak envelopes for the internal measurements and the dashed lines bound the external measurements.

It is important to notice that, although the inclination of these straight lines are different, their

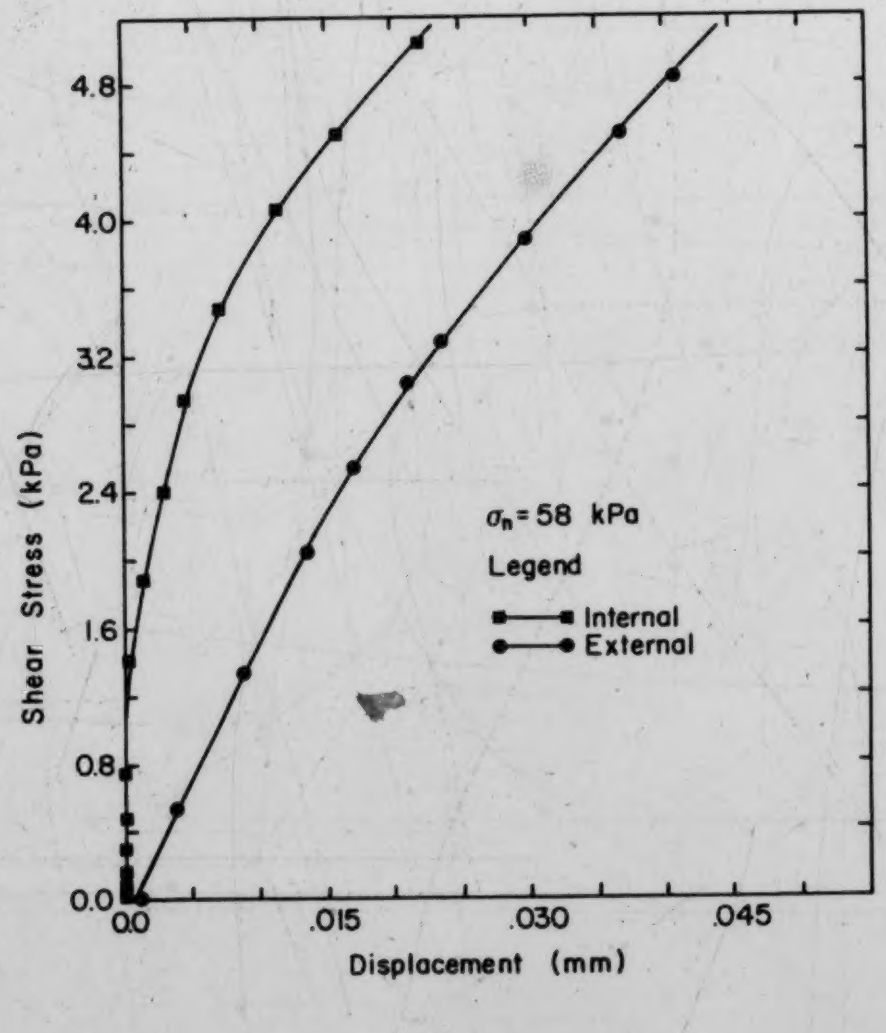

Figure 4.15 Detail of Stress Displacement Curve - Test#3

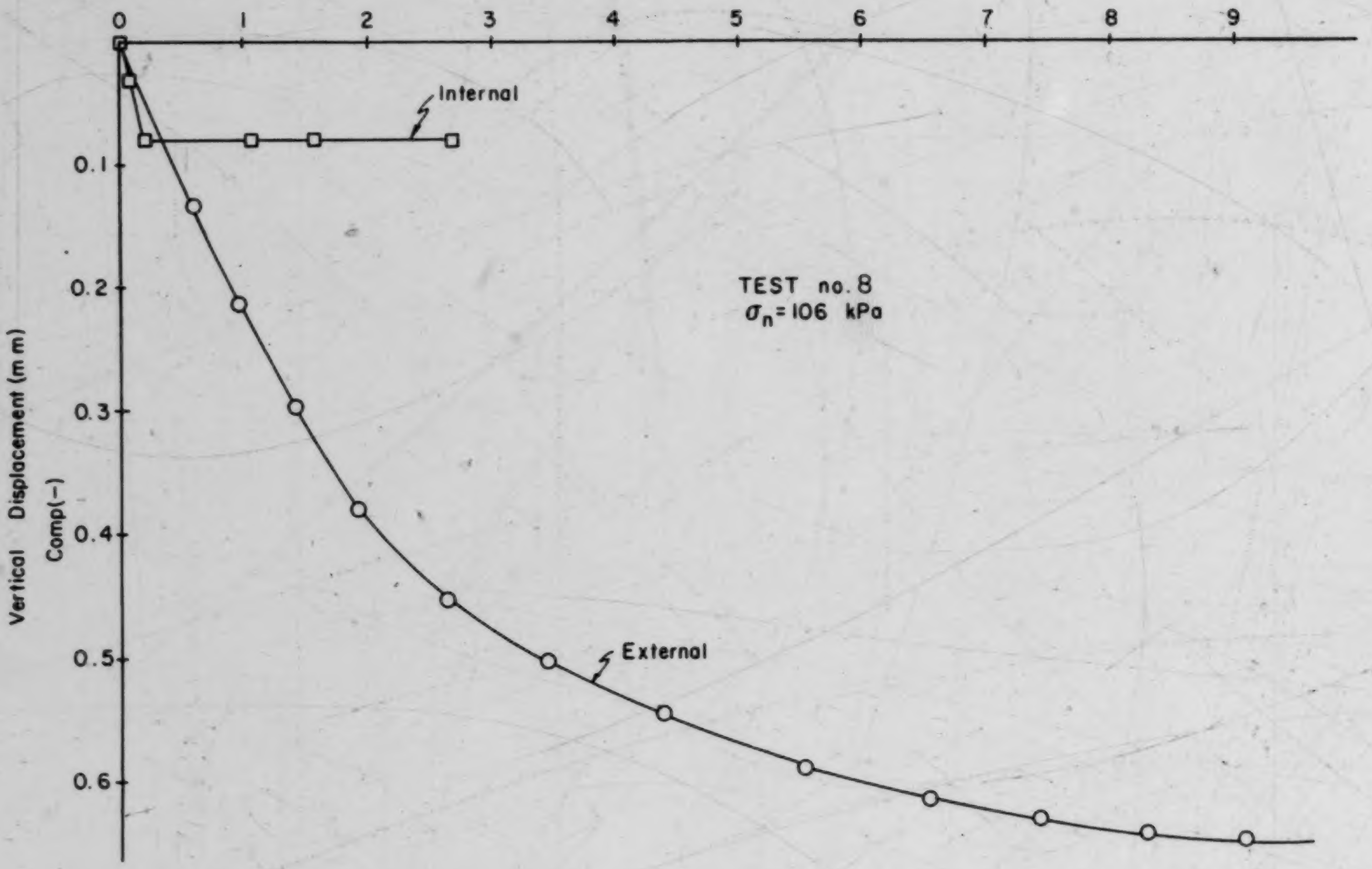

Figure 4.16 Vertical Displacement During Shear - Test#8

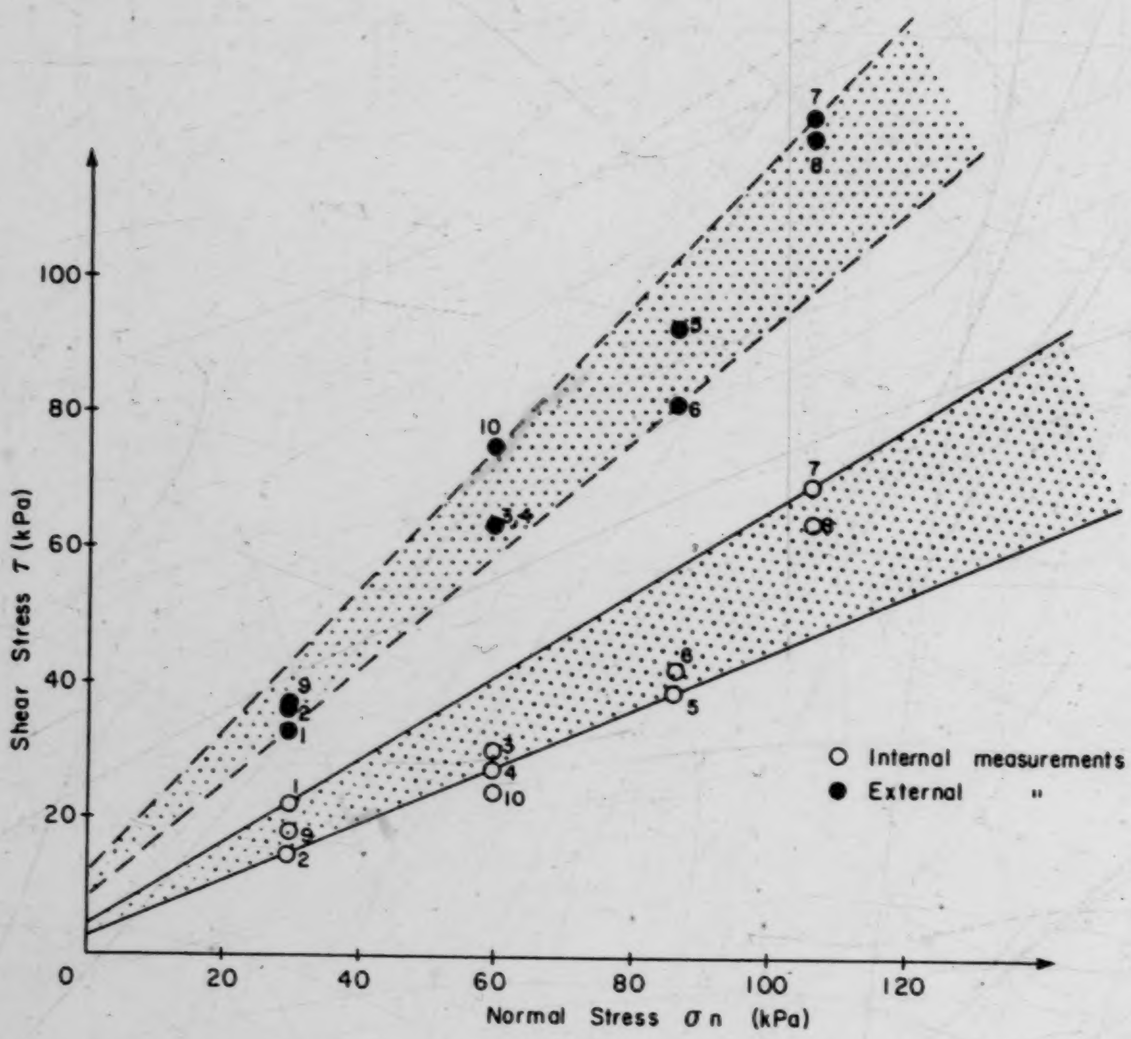

Figure 4.17 Strength Envelope for Large Shear Tests

intercepts are almost the same. The scatter presented in the results can be attributed to heterogeneity introduced in the sample, during its preparation.

Figure 4.18 presents the results of Test #3 and Test #11 plotted together. From these two tests, Test#3 was considered one of the final tests (and was presented earlier in this chapter) and Test#11 was performed to study the effect of rate of shearing. As can be seen from this figure, the rate effect is significant and for a rate approximately 7 times faster, the shear strength increased by 32%. Moreover, if the faster rate is used, the maximum shear stress is reached for negligible values of the shear displacement (approximately 0.001 mm). In any case, the rate of shearing was chosen to allow complete drainage during shear, as measured by the two piezometers installed at the soil-structure contact in the test embankment.

4.4 PERFORMANCE OF APPARATUS AND DISCUSSION OF RESULTS

4.4.1 Difficulties in Designing the Apparatus

During the preparation of the equipment described in this chapter, several difficulties had to be overcome, most of them due to lack of background in designing large scale test apparatus. Therefore most of the problems were solved by trial and error.

In the next few paragraphs, a brief discussion of these problems and the solutions adopted will be presented, hoping

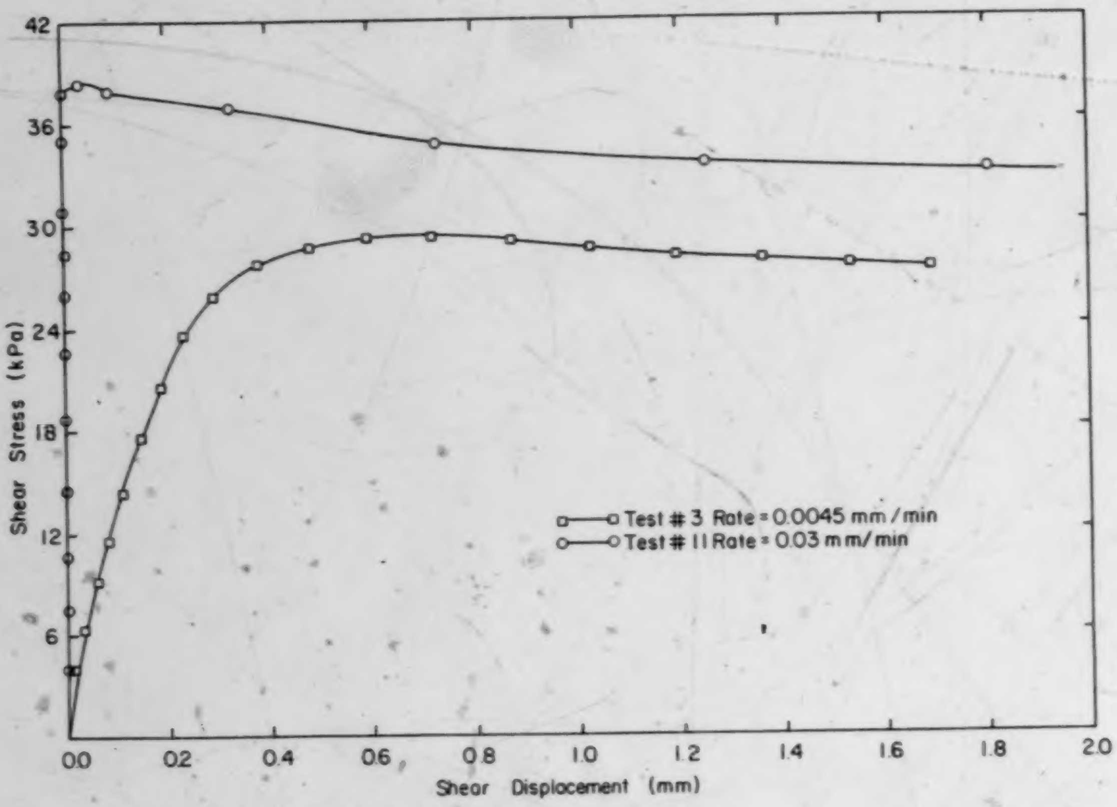

Figure 4.18 Study of Rate Effect - Large Shear Test

that the experience gained here can be of some help for future researchers facing similar situations.

Certainly the large dimensions of the soil sample were responsible for most of the problems faced. Even in order to apply a relatively small normal stress (up to 120 kPa) the magnitude of the total loads had to be relatively high (up to 58 kN or 12000 lbs). In other words, the vertical loading system had to be able to apply high total loads but be sufficiently sensitive to keep the pressure constant (with an acceptable variation of ± 2% of the total load). Unfortunately the hydraulic equipments available were capable of fulfilling only one of the requirements. After several trials it was finally decided to use a lever system, since it proved to be the only way to fulfill both requirements.

Another problem that had to be faced concerns the distribution of normal stress. The task of transforming a concentrated load into a uniform stress is rather difficult. Several methods have been tried, varying from a rigid, 2.5 cm (1") thick single plate covering the entire area of the sample to a more flexible system capable of accomodating differential settlements, as described before. It was finally concluded that none of the methods were totally effective. Reasonable results were obtained using the configuration presented in section 4.3.2.3. It seems that the ideal configuration should have followed with prismatic elements (instead of flat bars) up to the point of aplication of the concentrated load. This would have required another 4 rows of these elements, with a total of another 16 elements. Moreover the reaction frame would have had to be twice as high (2 m high), and consequentely requiring a different steel beam section, hence considerably more expensive.

The application of horizontal loads presented similar problems. The ideal test should be performed under stress-controlled conditions, to better simulate the field conditions. To accomplish this, the loading system would have to be able to apply forces up to 98 kN (10 tons) but sensitive enough to apply small initial increments to allow a detailed examination of the initial portion of the stress-displacement curves. Several different hydraulic systems were tried, but none were completely satisfactory. Some of the hydraulic pumps tried were very sophisticated. They are provided with "servo-systems". These servo-systems are able to apply a large range of loads and maintain the load constant within small variations. For each system a prestablished range of loads is set, according to the expected loads. Unfortunately, the mechanism that provides these characteristics also implies in an unavoidable "in-built" load in the pump. This load is activated, and transfered to the ram as soon as the hydraulic pump is switched on. The higher the range of the prestablished loads, the higher is the in-built load. To accomplish the range required for the large shear tests, this load was too high, excessively disturbing the initial portion of the stress-displacement curve.

It was then decided to perform strain-controlled tests. Although less representative, the stress-displacement curves are far more accurate and detailed when compared to the tests conducted under the stress-controlled mode.

In order to overcome friction in various regions of the apparatus, several systems of rollers had to be provided. These roller systems were designed after layers of teflon had been tried and proven to be inadequate for these circumstances. Rollers had to be designed for:

a. shear stress device (base and sides)
b. under the steel box in the contact with the concrete block.

These rollers reduced the friction to negligible values.

In conclusion three important lessons were learnt from the design of this equipment:

a. Whenever friction is to be reduced to negligible values, the use of teflon is inadequate. It presents a "slip-stick" behaviour and relatively high static friction. The use of rollers (steel balls or steel cylinder) is suggested.

b. Although the hydraulic systems available were very sophisticated they were still not adequate to apply loads over a large range and still accurate for small increments. Mechanical systems are strongly suggested.

c. The task of transforming a point-load into a uniform stress is very difficult. A reliable system should have a pyramid shape and be sufficiently flexible to allow differential movements (due to heterogeneities). The pyramid should receive the point load at its apex.

4.4.2 Normal Stress Distribution

As mentioned before the system for applying normal loads was designed on a trial-and-error basis. The evaluation of whether or not one particular system was adequate, was based on a simple calibration.

The calibration consisted of replacing the Shear Stress Device by an earth pressure cell composed of an aluminum block resting on three load cells. The load cells were made of aluminum pipe each having four strain gauges. All twelve gauges were wired forming one full Wheatstone bridge producing an amplified output. The aluminum block had a recess where concrete was placed to reproduce a roughness similar to that of the Shear Stress Device. The earth pressure cell was calibrated separately using weights.

With this earth pressure cell replacing the shear stress device, a sample was compacted in a similar fashion as for the tests. After compacting the sample, the load head was placed and loads applied. Each load was maintained until constant readings in the pressure cell were obtained.

Figure 4.19 presents the results of the calibrations, using two different loading heads. In the first case, a 2.54 cm (1") rigid plate was used. The second curve was obtained for the loading system proposed earlier. In both cases the sample size was already reduced with respect to the loading area. In this figure it can be seen that, although not ideal, the pyramid shape represented an improvement compared to the single rigid plate.

Ideally the relationship between applied and measured stresses should follow a 45° line. Departures from this line means that the load is not being uniformly distributed (assuming no losses by friction between soil and mold).

According to this calibration (Figure 4.19) load transfer was observed from the center of the sample (location of the measuring device) towards the remaining sample. This reflects a nonuniform normal stress distribution. This effect is accentuated for higher normal loads and the maximum difference between measured and applied stresses was 13% for the highest normal stress. This load transfer can be caused by nonhomogeneities in the sample (the central portion of the sample was the most difficult to compact because of the position of the reaction frame) or by some flexibility of the measuring system (deformability of the load cells used in the calibration) that creates conditions for the mechanism to occur. In any

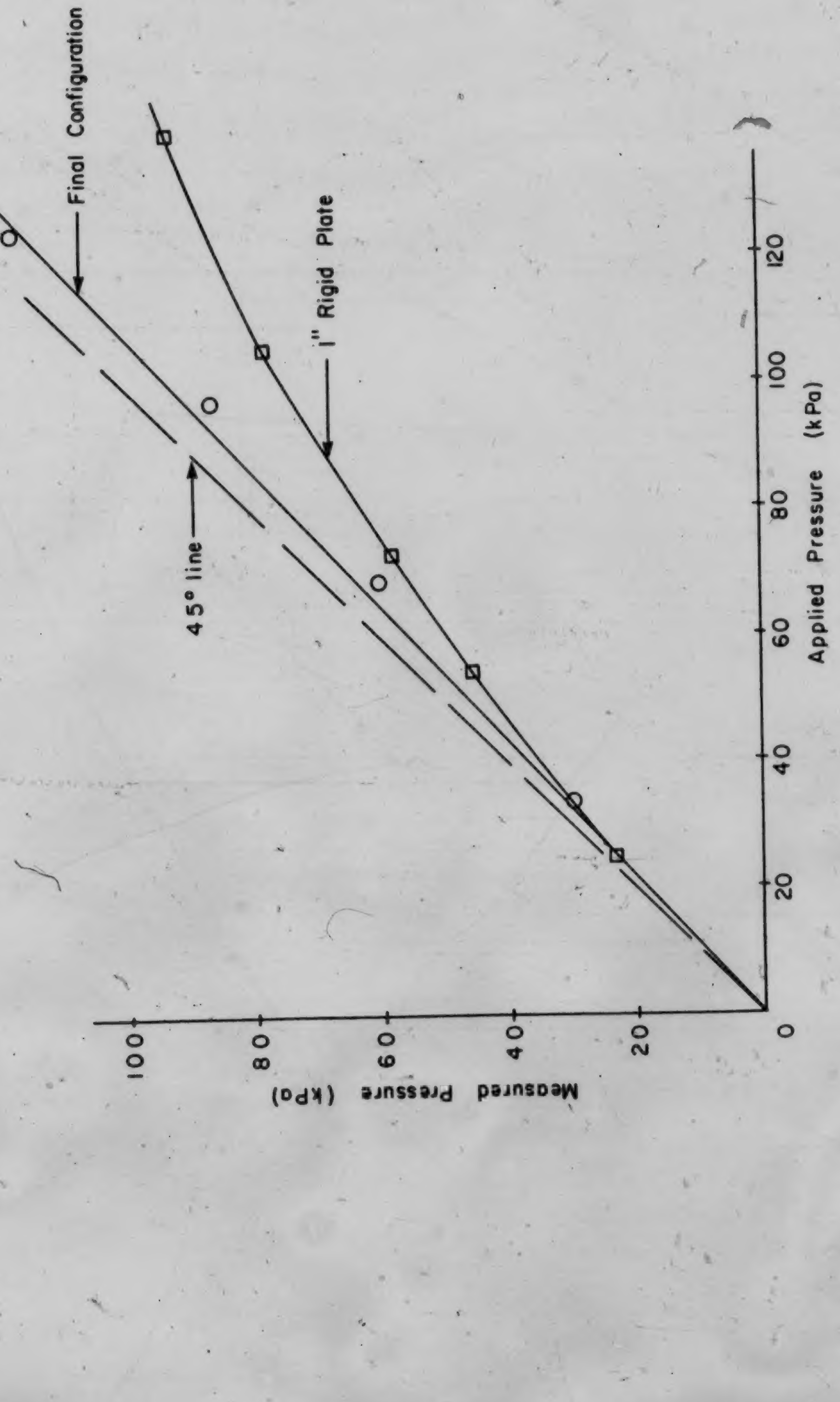

Figure 4.19 Comparison Between Two Loading Systems

case, it is believed that both conditions contribute to this mechanism not only during the calibration but also during the actual test, and lower stresses in the center of the samples were expected.

For the analysis of the test results it was assumed that the normal stresses remained constant during the application of the shear forces.

4.4.3 Shear Stress Distribution

The distribution of shear stresses in the plane of failure of a sample is recognized as being complex and so far these stresses have never been fully determined.

In particular for direct shear box tests, Morgenstern and Tchalenko, (1967) have demonstrated that failure occurs in a complex mode. Furthermore, Hvorslev, (1960) pointed out that, in a shear box test, failure is progressive and the stress conditions are not known to a high degree of accuracy.

Regardless of the preceding comments, some speculative analysis of the stress distribution will be presented, with the view of presenting a better understanding of the test results.

Assume, for the sake of simplicity, a uniform shear stress distribution across the sample (simulating full development of shear strength throughout the interface), as shown in Figure 4.20.

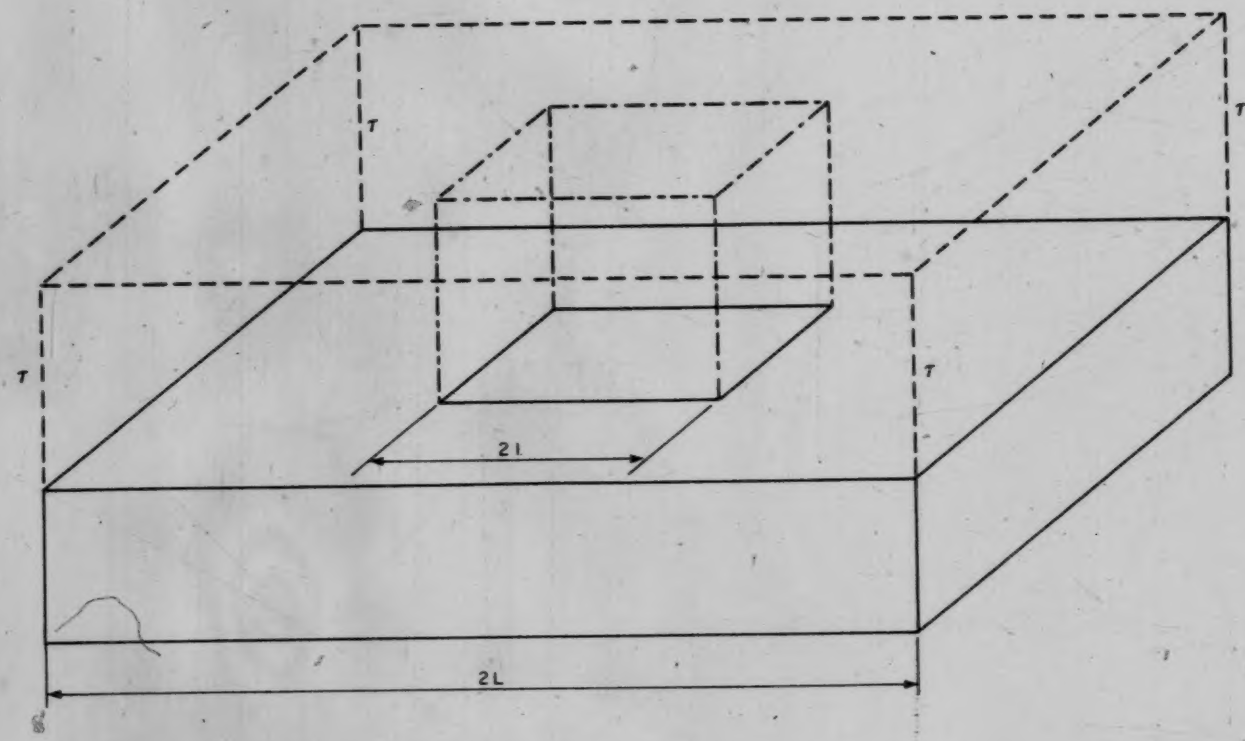

Figure 4.20 Idealized Shear Stress Distribution

The integral of the volume under the total area of the sample results in the total force being applied in order to shear the sample, while the integral of the volume over the region of the internal sensor represents the total force measured by two load cells of the Shear Stress Device.

Evaluating these integrals, it is concluded that:

$$V_t = L^2 y$$

and

$$V_i = l^2 y$$

where:

V_t - Total volume (or total force)

V_i - Internal volume (or internal force)

y - shear stress

L - semi length of the concrete base

l - semi length of the concrete block

or,

$$V_t / V_i = L^2 / l^2$$

Substituting the values of L and l (from the equipment geometry and shown in Figure 4.20) in this expression, the theoretical ratio between the forces is:

$$V_t / V_i = F_t / F_i = 5.376$$

On the other hand, Table 4.3 presents the ratio between measured internal and external forces. In this table the average ratio between measured total forces (F_t^m) and measured internal forces (F_i^m) was found to be 11.35. In

Test #	σ_n (kPa)	τ_e (kPa)	τ_i (kPa)	Fe[1] (kN)	Fi[2] (kN)	Fe/Fi
1	29.25	34.0	20.0	14.3	1.6	8.85*
2	29.25	36.0	16.0	15.2	1.3	11.67
3	59.4	63.0	29.0	26.6	2.4	11.25
4	59.4	64.0	27.0	27.0	2.2	12.32
5	85.8	91.0	39.0	38.4	3.2	12.10
6	85.8	81.0	42.0	34.1	3.4	10.00
7	106.8	121.0	59.0	51.0	4.8	10.65
8	106.8	122.0	54.0	51.4	4.4	11.71
9	29.3	37.5	17.6	15.8	2.4	11.05
10	54.9	74.0	23.0	31.2	1.9	16.68*
					average	11.35

1 - area = 0.42146 m2
2 - area = 0.0081225 m2
* - unused for average

Table 4.3 Ratio Between External and Internal Forces

other words, the theoretical ratio is only 48% of the measured ratio for the assumed distribution of shear stresses.

Depending upon the assumed function representing the shear stress distribution and the values of shear stresses at the boundaries, the theoretical ratio V_t/V_l (or F_t/F_l) can be increased or decreased. However, it can be shown that, regardless the function used for the shear stress distribution, the theoretical ratio will never approach the measured ratio, if reasonable assumptions are specified. Reasonable assumptions are considered to be hypothesis such as:

1 - At any point of the sample, the shear stress can overcome the maximum shear strength,

2 - The function representing the distribution of shear stress is monotonic,

3 - The shear stress at x=0 is larger or equal to the shear stress at x=L (see Figure 4.20).

Based on this discussion, it can be concluded that the measurements of the internal shear stresses were consistently smaller than expected.

This conclusion is in close agreement with the discussion presented earlier concerning the normal stress distribution. Since the outer region of the sample was subjected to higher normal pressures and aparently to higher densities due to difficulties during compaction, it will "attract" more shear stress.

Hence, the two curves obtained for one sample (internal and external) are not comparable. They can, however, be interpreted separately, among similar curves for different normal stresses. In fact, it seems that these two curves represent two different tests and that the internal is more a "interface test" since it seems to be least influenced by the test device.

Furthermore, these two measurements have another basic difference. While the external curve is essentially a conventional shear box test, using a large sample, the internal curves were obtained by measuring shear stresses and shear displacements remote from the boundaries. This feature assumes considerable importantance if a comment presented by Kisiel (1964) and emphasized by Morgenstern and Tchalenko (1967) is recalled. These authors call attention to the high stress concentration and degree of straining caused by the loading sides in the shear box test. This concentrated stress is averaged in the shear stress calculation. On the other hand, with the measurements obtained remote from the boundaries, this concentration of stress is attenuated, and a more uniform shear stress distribution, near the center of the sample, should be expected.

Finally, another two characteristics of the apparatus should be pointed out:

a. The pressures in the central area of the sample (internal sensor) are applied by a flexible boundary as oppose to rigid boundary (steel box) applying the external pressure.

Rigid boundaries impose, in a nonhomogeneous soil sample, even displacements from point to point and nonuniform stresses. On the other hand, flexible boundaries create nonuniform displacements but uniform stress distribution. Since nonhomogeneities are expected in the samples used in the large shear test, the flexible boundary improves the shear stress distribution in the area of the sensor.

b. Despite the fact that flexible boundaries improve the distribution of shear stresses in the large shear box, this "loading system" seems to be more representative of the field condition. In the field, the Shear Stress Devices were loaded by layers of soil (flexible boundary) rather than by a rigid boundary.

Based upon the summary of characteristics presented above and regardless of the dissimilarities in the stress-path followed in the field and in the laboratory tests, it can be concluded that the internal shear stress-shear displacement curves, obtained in the large shear box tests, are the most representative of the field behaviour (at least among the curves presented in this chapter). Therefore these curves should be used to obtain the parameters for the numerical analyses.

However, the "type of behaviour" observed in these curves (strain-softening) make their use rather complex. Modelling of strain-softening has motivated extensive research and is still under active consideration (e.g. Chan, 1985). Consequently, only limited application will be given to the internal measurements obtained in this series of tests, and mainly in Chapter 5, where a theoretical model is introduced.

4.5 CONSTITUTIVE LAW - DISCUSSION

Constitutive relationships are equation or groups of (mutually exclusive) equations relating strains and stresses.

The most widespread constitutive law is Hook's law for linear elastic materials. In geomechanics, the hyperbolic model (Duncan and Chang,1969) is one of the constitutive relationships most used in practice, whenever material nonlinearity is to be considered.

Restricting this discussion to the elastic behaviour of soils or joints, and not including the effect of fabric or arrangement of grains, these relationships should account for the influence of some important factors, such as:

- effect of normal stress
- effect of roughness
- effect of sample dimensions

The effect of normal stress is shown in Figure 4.21 where the stress-displacement curves for four tests are plotted. It can be seen that the influence of the normal stress is remarkable.

The roughness should include not only the asperities of the concrete structure but the relative size of the concrete asperities with respect to the gradation of the soil. It should also consider the relative density or degree of compaction of the sample. These effects were studied by Kulhawy and Peterson (1979) based upon a series of direct shear box tests conducted on combined samples sand and concrete. The objective of the laboratory program was to compare the results of these tests (tests along interfaces) with those performed using soil alone. The authors present results of tests using four different roughness of concrete, ranging from a very smooth precast concrete to a very rough surface. The sand used in the upper half of the box had also different gradations, varying from a uniform round sand to a well graded angular material.

Although the author's major concern was the shear strength of the interface, most of their conclusions can probably be used to understand the general influence on the roughness of the shear stress-shear displacement curves.

The results have shown that the friction angle (Φ) increases with decreasing void ratio and is lowest for the smooth interface. The results also show interface friction angles higher than those obtained for soil alone for the

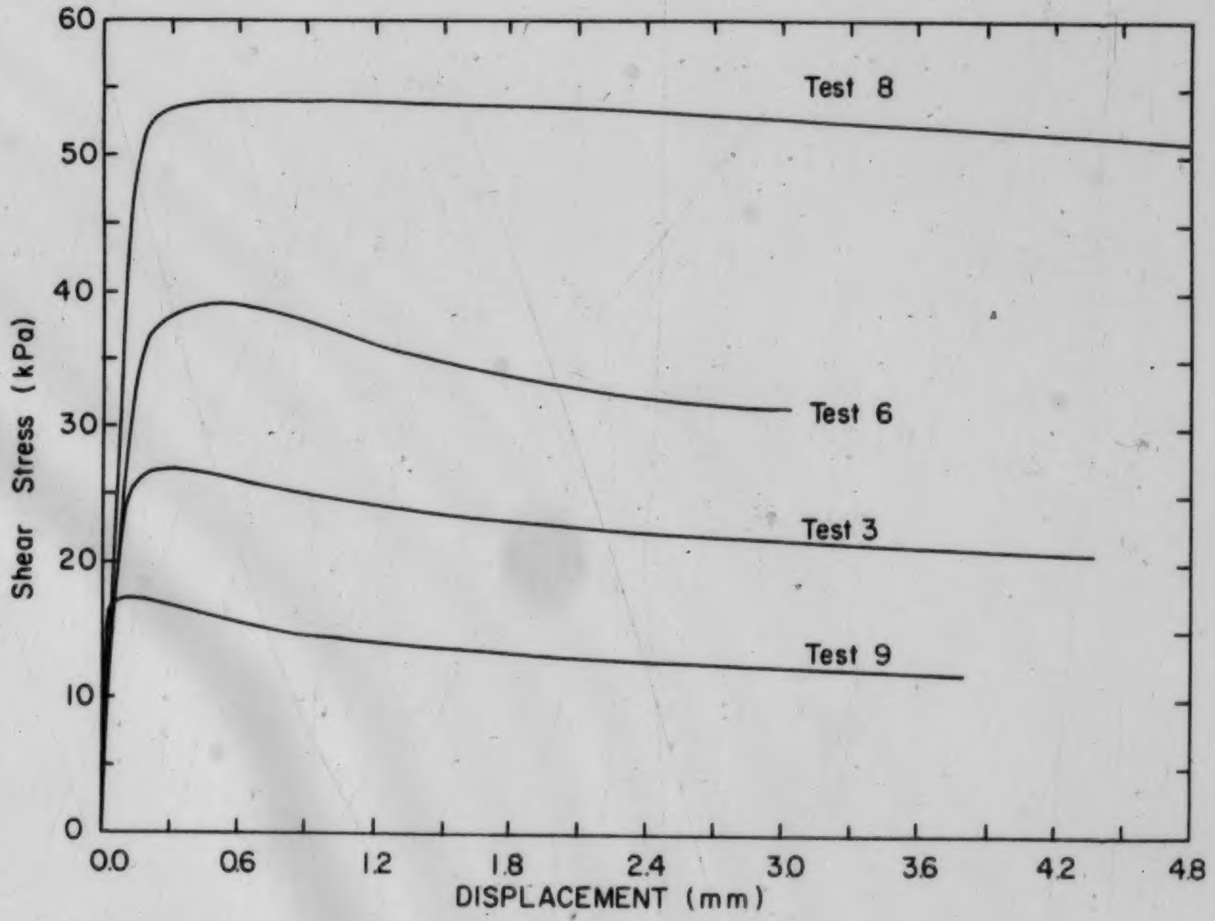

Figure 4.21 Stress Displacement Curves - Large Shear Test (Internal)

dense state, while in the loose state the values were equal or slightly lower than for pure soil samples.

In conclusion, it was shown that the strength of the interface is governed not only by the roughness of the face of the structure, but also depends on the "relative roughness" between the concrete and the soil. Furthermore, the degree of compaction (or relative density) should also be considered, since this can change the interface shear strength.

Similarly, it should also be expected that both factors (relative roughness and degree of compaction or relative density) would influence the general shape of the stress-displacement curves and consequently the parameters extracted from them (tangential stiffness, K_t).

The mathematical determination of the "relative roughness" is not simple and the only reported effort considering this effect in the behaviour of soil-concrete interfaces was presented by Kulhawy and Peterson (1979).

Grain size analyses were conducted on the soil and on the aggregate used in the concrete. The "roughness" of each of these materials was defined as:

$$R = (D_{60} \text{ x } D_{10}) / D_{50}$$

where,

R - roughness of structure.

D_{60}, D_{50} and D_{10} are respectivelly particle sizes at 60%, 50% and 10% finer.

The relative roughness was defined as:

$$R_r = R_{structure} / R_{soil}$$

Although easy and convenient, among the results of 178 tests performed by Kulhawy and Peterson (1979) the shear strength showed no relationship with the relative roughness, as defined above. One possible reason for the poor relationship could be the definition of the "structure roughness".

Since all the tests performed for the present research work made use of one roughness, representing the texture of the concrete wall built for the field instrumentation, no attempt will be made to determine this parameter.

Neverthless, it is possible that some of the methods used in rock mechanics can be useful in this discussion. Parameters such as the JRC (Joint Roughness Coefficient) defined by Barton and Choubey (1977) may be applicable. Furthermore, the authors provide two very simple tests to determine the JRC. The "Tilting Test" for joints with small degree of bond (such as rock joints with no soil filling) or the "Push Test". Note that in both cases, the parameter obtained is a measure of the relative roughness of the two sides of the joint or, for the case of interfaces, is a measure of the "relative roughness" between the two interfacing materials.

Another interesting feature of these tests is that they are, in someway, a measure of the static friction of the joint, as discussed in the introduction of this thesis (Section 1.3).

The effect of sample size also has to be considered. For the sake of organization of this thesis, this effect will be discussed in Chapter 5.

Finally and most difficult, a law to represent the results considered to be the most reliable in this chapter, namely the internal measurements in the large shear tests, would have to consider loss of strength after peak (strain-softening behaviour). This point has already been discussed and the implementation of complex laws is not part of the scope of this research.

Nevertheless, a simple law is proposed based upon the results obtained in the tests presented herein. Note that the influence of the roughness is not considered, since the concrete used in the laboratory tests represented the roughness of the prototype and perhaps typical of most practical situations and nothing is said about sample size.

Figure 4.22 reproduces Figure 3.33 with a slight difference in interpretation. An analyses of Figure 4.22 shows that the relationship between the normalized shear stress with respect to normal stress versus shear displacement resembles two straight lines.

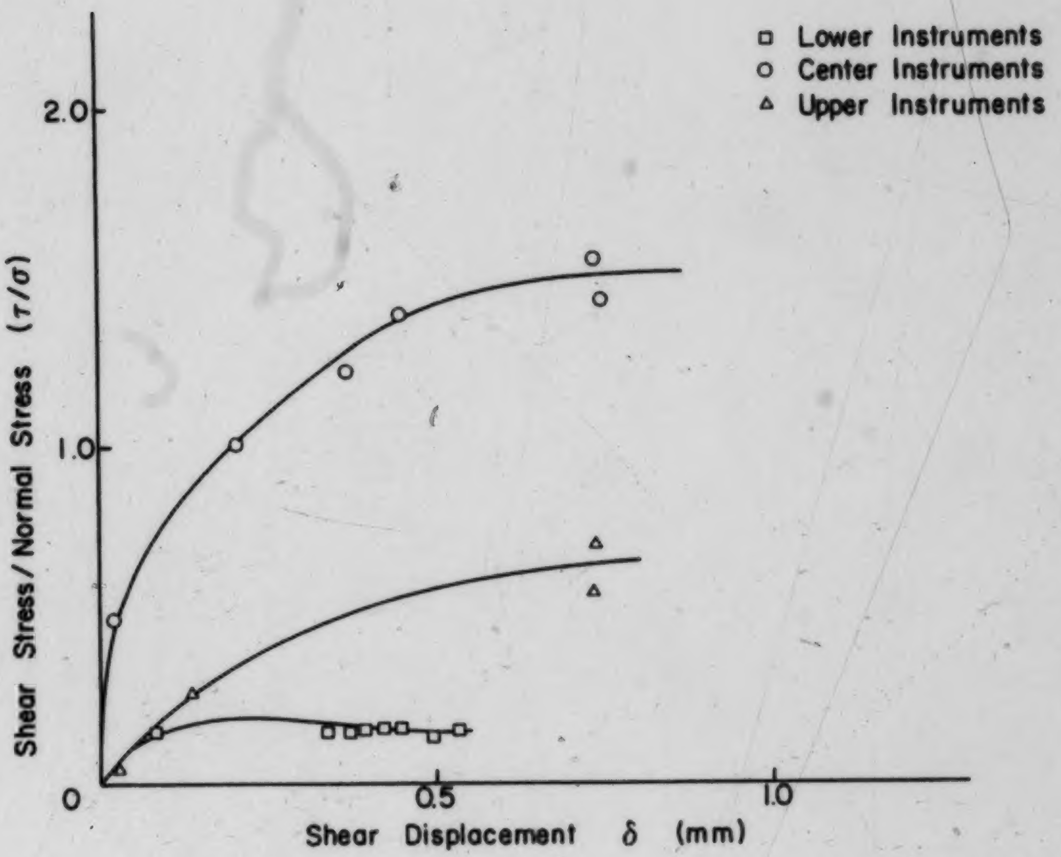

Figure 4.22 Normalized Shear Stress-Displacement Curves

Similarly, the results of the laboratory tests can be plotted in this form. These curves are shown in Figures 4.23 through 4.26 for conventional shear tests series 100 and 200 and for large shear tests (internal and external measurements) respectively. In these figures the range of test results are plotted and the field measurements are presented, allowing for comparison.

For practical purposes all the "bands" of test results can be replaced by two average lines, represented by:

- two inclinations
- one point of change in inclination

Hence, the joint stiffness can be determined by simply knowing these parameters or:

$$(\tau/\sigma) = \delta \tan \Phi_i \quad \text{for } \delta > \delta_o$$

$$(\tau/\sigma) = (\tau/\sigma)_o + (\delta - \delta_o) \tan \Phi_t \quad \text{for } \delta \le \delta_o$$

where:

$(\tau/\sigma)_o$ - value of the ratio for changing inclination

(τ/σ) - current value for the ratio τ/σ

δ - current displacement of the interface

δ_o - value of δ for changing inclination

Φ_i - variation of τ/σ with respect to displacement for $\delta \le \delta_o$

Φ_t - variation of τ/σ withrespect to displacement for $\delta > \delta_o$

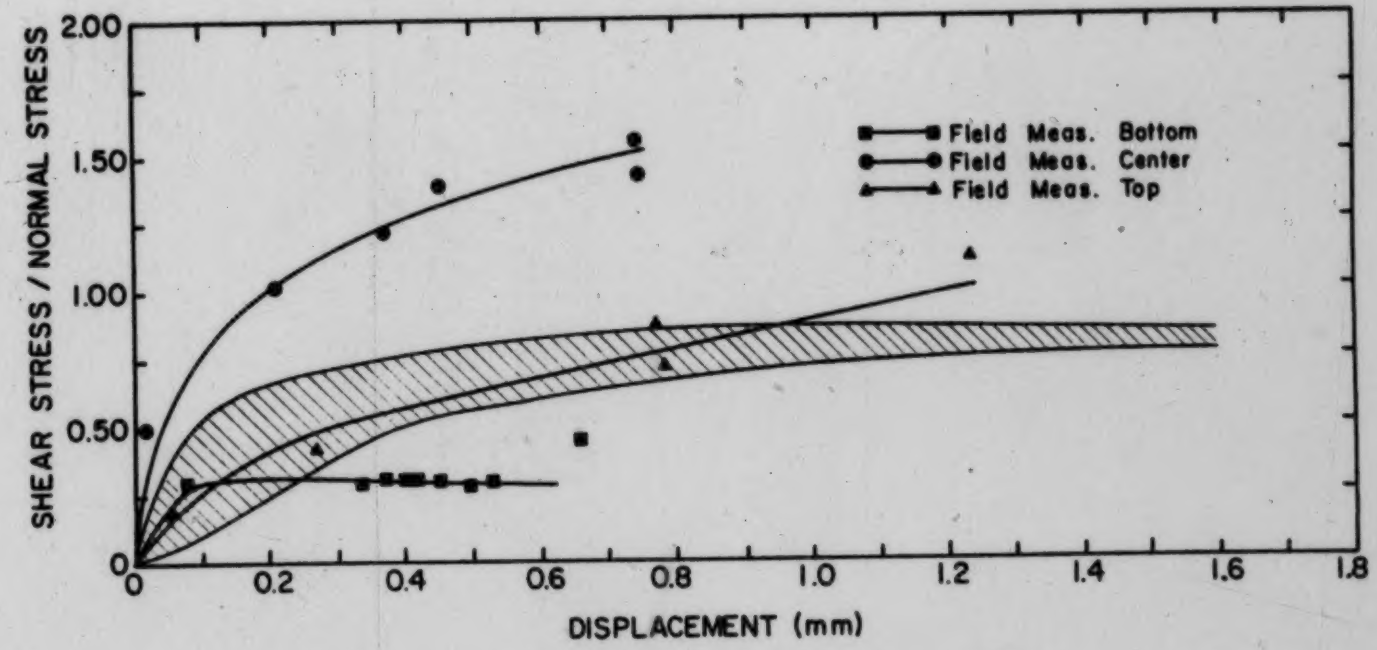

Figure 4.23 Normalized Stress-Displacement Curves - Series 100

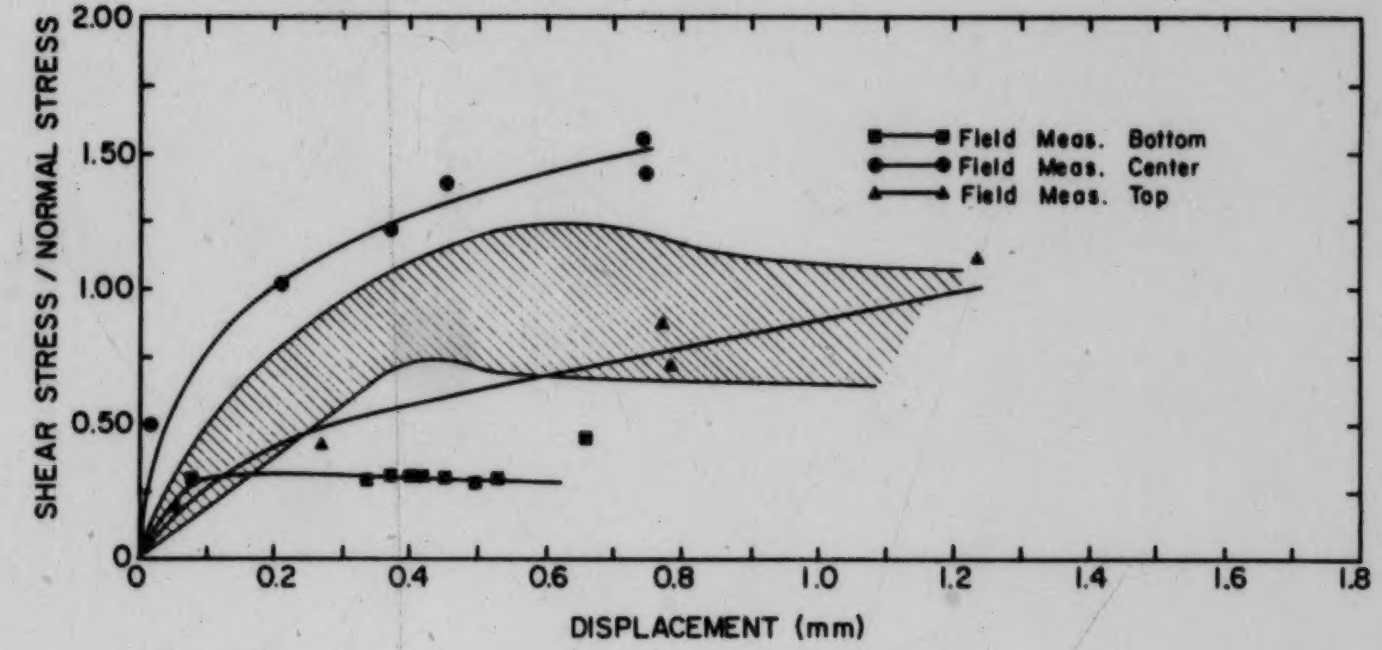

Figure 4.24 Normalized Stress-Displacement Curves - Series 200

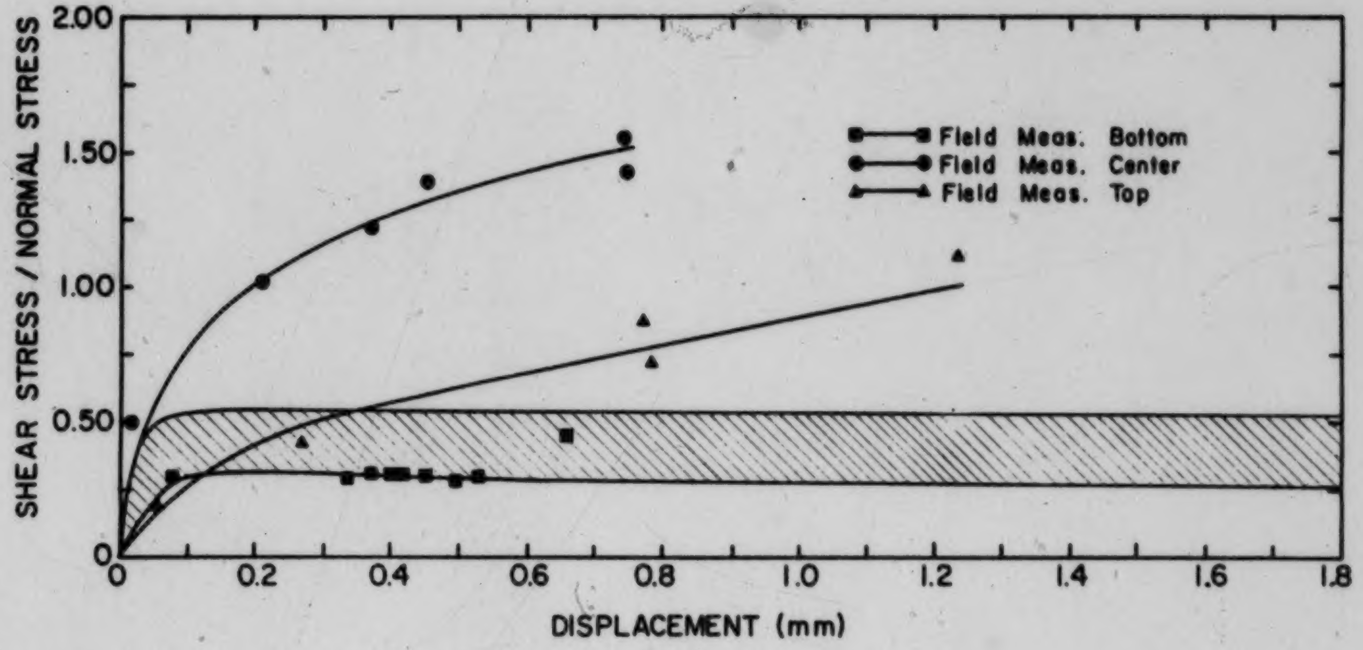

Figure 4.25 Normalized Stress-Displacement Curves - Internal

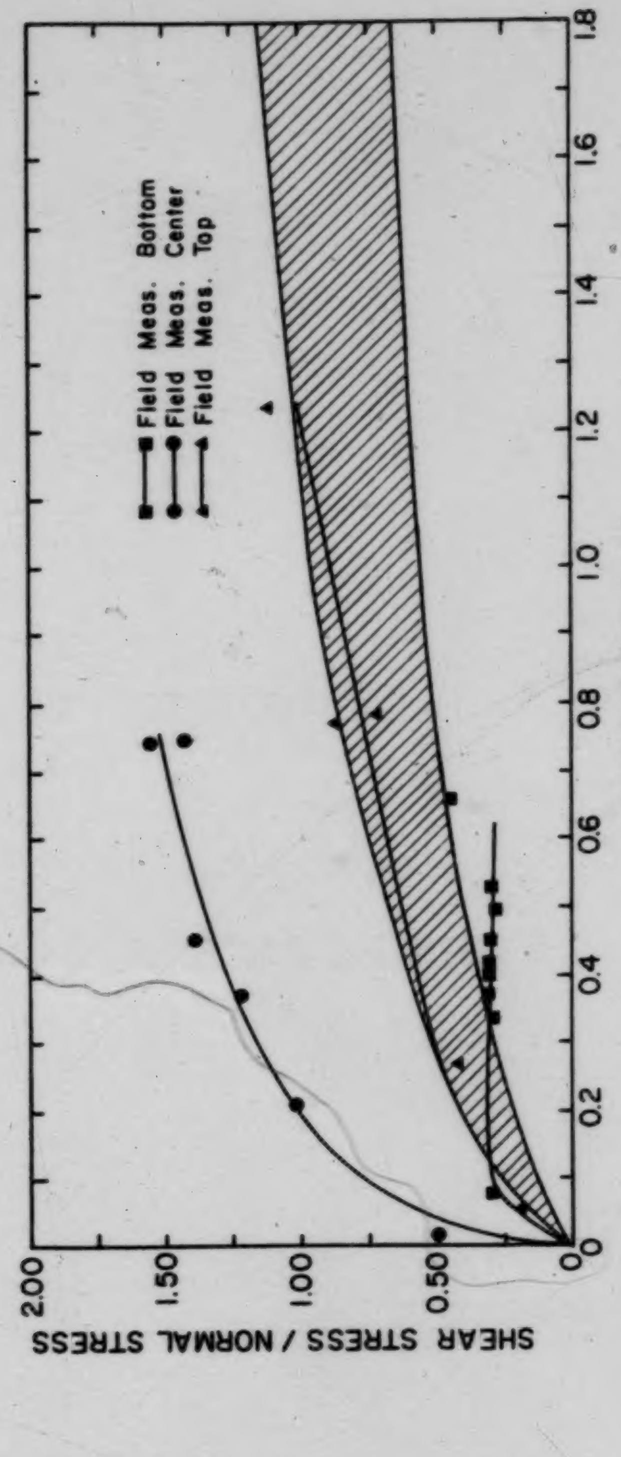

Figure 4.26 Normalized Stress-Displacement Curves - External

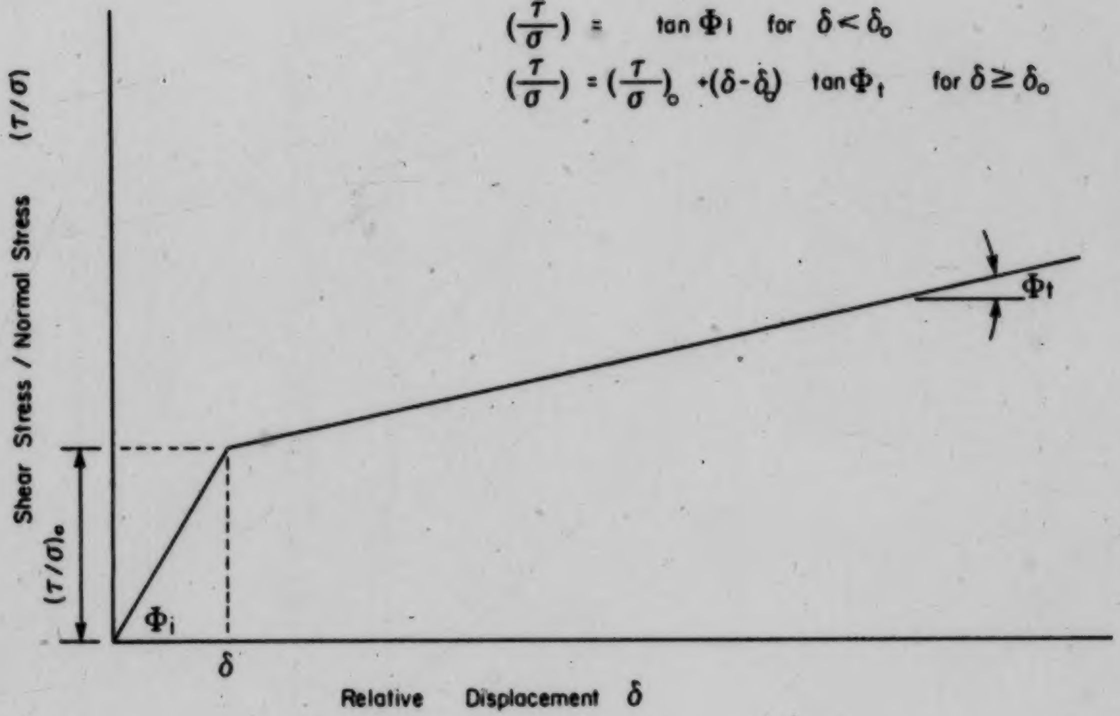

Figure 4.27 Proposed Constitutive Relationship for Interfaces

If the normal stress is known, the shear stress can be determined and the joint behaviour can be completely described.

This procedure was introduced in the Finite Element Program described in Chapter 6 and will be further described there.

4.6 CONCLUSIONS

Based upon the tests described in this chapter, some conclusions can be presented. They are listed below:

1 - The method of sample preparation strongly affects the results of direct shear box tests. A brittle material (unstable structure) is obtained if the soil is compacted directly against the concrete.

2 - Analyses of the effect of compaction procedure close to the wall indicated that, in the field, the interface will probably present a behaviour that falls between the extremes represented by compacting the soil directly against the concrete or compacting the soil in a compaction mold and trimming the sample for the direct shear box test.

3 - The "internal" behaviour (remote from the boundaries) in the large shear box test differs from the "external" behaviour in several points. Reasons for these dissimilarities are presented and evidences provided showing that the internal measurements are more representative of the field

condition.

4 - Using the results of both conventional and large shear tests, the mechanical behaviour of the soil-concrete interfaces was assessed. Furthermore, these tests (in particular Test#11) provided enough information for the derivation of a **phenomenological model**, which is discussed in the next Chapter.

Furthermore, in this Chapter the discussion of the effectiveness of the "conventional direct shear box test" as a tool for obtaining parameters for design of certain interfaces was introduced. Further discussion will be presented in Chapter 5, based upon the model.

5. PHENOMENOLOGICAL MODEL

5.1 INTRODUCTION

Phenomenological, mechanical and rheological models are simple tools used frequently in research. Models such as those developed to explain the pore-pressure dissipation (Craig, 1974), creep of soils (Bowles, 1979), progressive failure in rock (Kovari, 1977) or time-dependent strength of rocks (Kaiser, 1980) are some examples of their use.

In most cases, the models are developed because some **complex mode of behaviour** can not be fully understood or explained based only on observations. Therefore, most mechanical models make use of simple "**units**" with well-known behaviour and, after assembly in a pre-established pattern, capable of reproducing complex behaviour.

In this chapter, a "**Phenomenological Model**" will be introduced and used to explain some features observed in previous chapters. Examples are provided to assess the characteristics of the model and the ability to represent the behaviour of a soil-concrete interface. Finally the use of direct shear box test as input for joint elements in numerical analyses, using the finite element method, is discussed based on the model.

5.2 PRESENTATION OF THE MODEL

5.2.1 Required Properties

The model was idealized from the results of Test#11 which was performed primarily to study the effect of the rate of shearing.

Apart from the study of the rate effect described previously, four internal sensors to measure shear displacement were installed in this sample, instead of two as in the other 10 tests presented in Chapter 4. Each of these sensors was installed at different positions with respect to the boundary where the load was applied, as shown schematically in Figure 5.1 (face X-X in the insert). Also in this figure the measured shear displacements are plotted versus the time from the start of the test.

Based in this figure, some observations can be obtained, viz:

a. Points located at different positions with respect to the wall where the load was applied (such as points A, B, C or D) started to displace at different moments of the test.

b. The displacement-time curves are initially nonlinear. After some displacement had occured the curves became linear and tended to be parallel.

c. The final displacements are different for all four sensors.

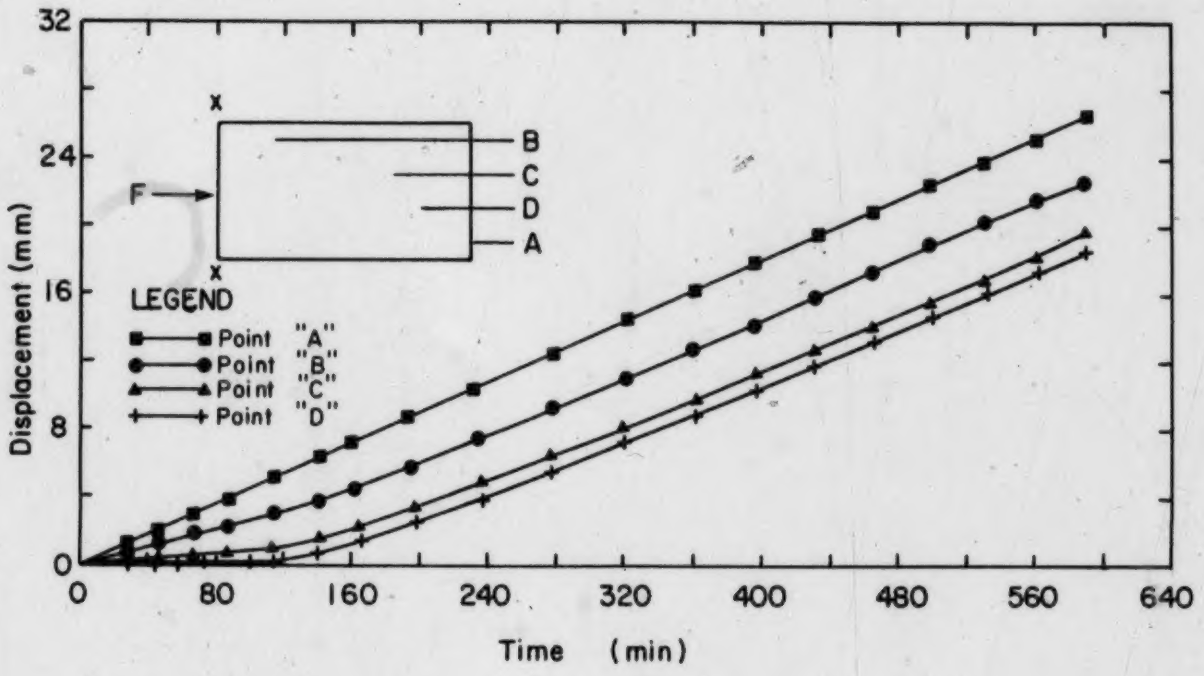

Figure 5.1 Shear Displacement versus Time - Test # 11

The first comment implies a nonuniform degree of mobilization of the shear displacement and consequently a nonuniform mobilization of the shear stress along a plane parallel to the direction of the movement. From a mechanical point of view, this phenomena is similar to a **progressive failure behaviour** (Simmons, 1981). Similar conditions have been observed in the past by Hvorslev (1960) for conventional direct shear box test. This behaviour is responsible for the nonlinearity of the curves shown in Figure 5.1.

After the maximum shear strength is reached at all points at the interface, the soil sample translates as a rigid body with no further increase in the shear stress (or with some decrease if strain-softening occurs). This translation is represented by the linear portion of the curves.

Finally, the fact that the curves show different total displacement suggests that some "compression" had occurred during the shearing process, in the direction of the shear forces. This **change in length** (for planar interfaces) due to the applied shear force will be called **"longitudinal compression"**.

In summary, three important effects were observed from the results of Test#11 and a model capable of reproducing the behaviour of the large shear tests has to accomplish these **minimum requirements**. They are:

a. A "progressive failure like" behaviour.

b. Longitudinal compression during shear.

c. Rigid body motion after full failure has occurred.

Furthermore, the effect of normal stress has to be considered. This effect is similar to that discussed during the derivation of the constitutitve law (see Chapter 4).

5.2.2 Proposed Model and Its Elements

In this section a one dimensional mechanical model is described and the elements composing it defined.

In order to fulfill the minimum requirements specified in the last section, a model composed of a series of "**blocks**" is proposed. Each **block** has independent properties and consists of two elements: a **spring** and a **frictional unit**, as shown in Figure 5.2(a).

The "**frictional units**" are similar to the "St. Venant" model presented by Lombardi (1979). As such, they are able to represent the shear strength at the interface. The sum of the areas of these units (in this case length, since the model is one dimensional) equals the total area of the interface and the shear stress acting at the interface is the shear stress determined by these units and defined as the load applied on each frictional unit divided by the area (length) of the individual unit.

The **spring** elements have a well known behaviour and the mechanical behaviour need not be discussed further. As in several cases reported in the past (e.g. Kovari, 1977) the

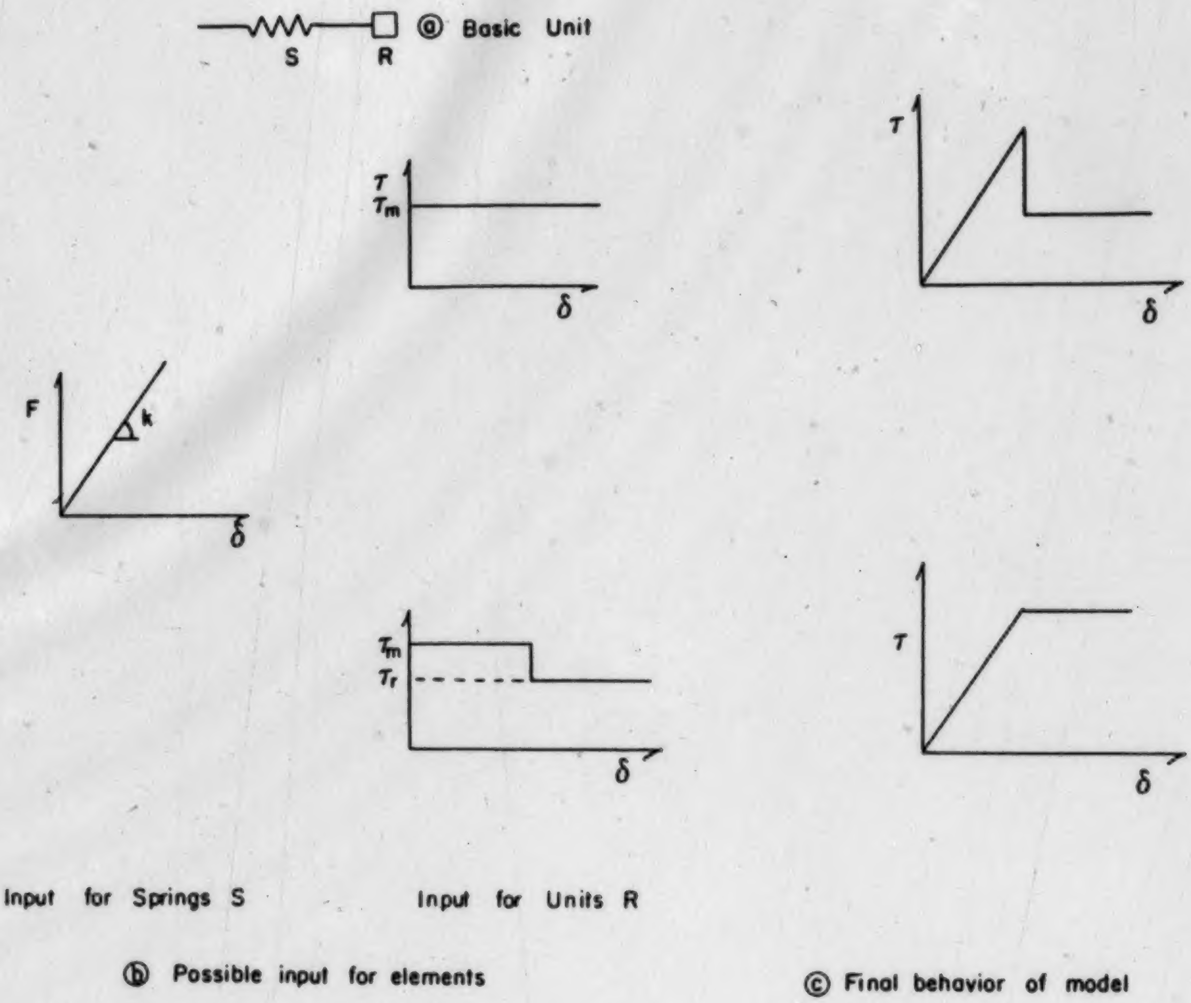

S
R
ⓐ Basic Unit
F
k
δ
τ
τ_m
τ_r

Input for Springs S

Input for Units R

ⓑ Possible input for elements

ⓒ Final behavior of model

Figure 5.2 Units Composing the Phenomenological Model

springs can be assumed to have piecewise linearity to incorporate a nonlinear behaviour in the model. These springs will be referred as **even springs** since they will receive even indices in the final assemblage.

Depending upon the expected behaviour at the interface, different properties can be assigned to the spring elements. A simple example is presented in Figure 5.2(b).

By assembling these two units to form a **"block"**, the final behaviour is, for example, that shown in Figure 5.2(c).

The final assemblage of the model has to account for the compressibility of the system (longitudinal compression). This can be accomplished by introducing a second **spring element** between two consecutive blocks. These springs will be referred as **odd springs** since they will be assigned odd indices. The assembled configuration of the model is shown in Figure 5.3. The physical interpretation of the spring elements is presented in later section (Section 5.3.2).

By assigning adequate properties to the elements composing the model, it can be shown that a sequential failure takes place. Failure will first take place in the elements of lower index (R_1) and progresses towards those of higher index (R_n). Furthermore, for each increment of load applied (ΔF), spring S_1 will contract (see Figure 5.3). Part of the load reaching node 2 will be absorbed by element R_1 (proportional to the spring constant) and part will be

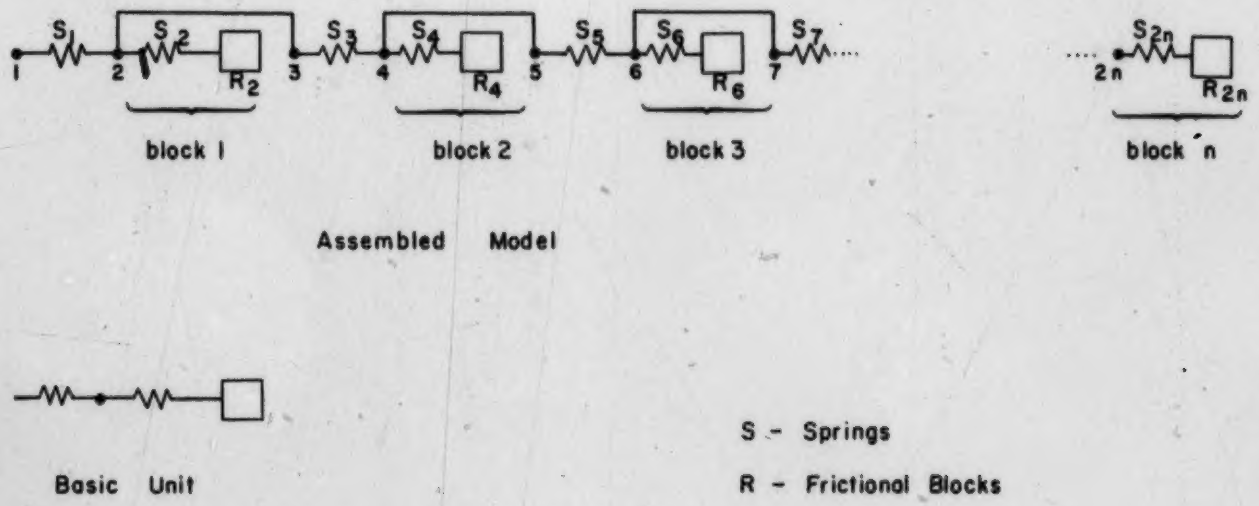
S1
S2
S3
S4
S5
S6
S7
S2n
R2
R4
R6
R2n
1
2
3
4
5
6
7
2n
block 1
block 2
block 3
block n
Assembled Model
Basic Unit
S - Springs
R - Frictional Blocks

Figure 5.3 Final Configuration of the Proposed Model

transfered to the subsequent block. This process will be repeated until a residual force (if any) is absorbed by the last unit R (R_n). It is important to notice that the load reaching each block is always smaller than that applied to the previous one. Consequently each unit "R" will be subject to different loads and will develop uneven shear stress. The mode of behaviour described above characterizes the different degree of mobilization discussed earlier (or the progressive failure-like behaviour).

If the displacement of the first and second blocks are assumed to be represented by the displacements of points 2 and 4 respectivelly (Figure 5.3), it can be shown that the final assemblage is displacing and changing length since these nodes are subjected to different loads and consequently will present differential displacement.

This discussion shows that all three minimum requirements described before have been fulfilled.

In order to resolve the model, a computer program was written which is the scope of the next section.

5.2.3 Mathematical Solution

The model, as presented in Figure 5.3, seems difficult to solve mathematically due to its complex geometry. Hence, a simpler geometry had to be idealized, preserving all the properties discussed above. This new configuration is shown in Figure 5.4. By comparing Figures 5.3 and 5.4 it can be concluded that they represent exactly the same model and the

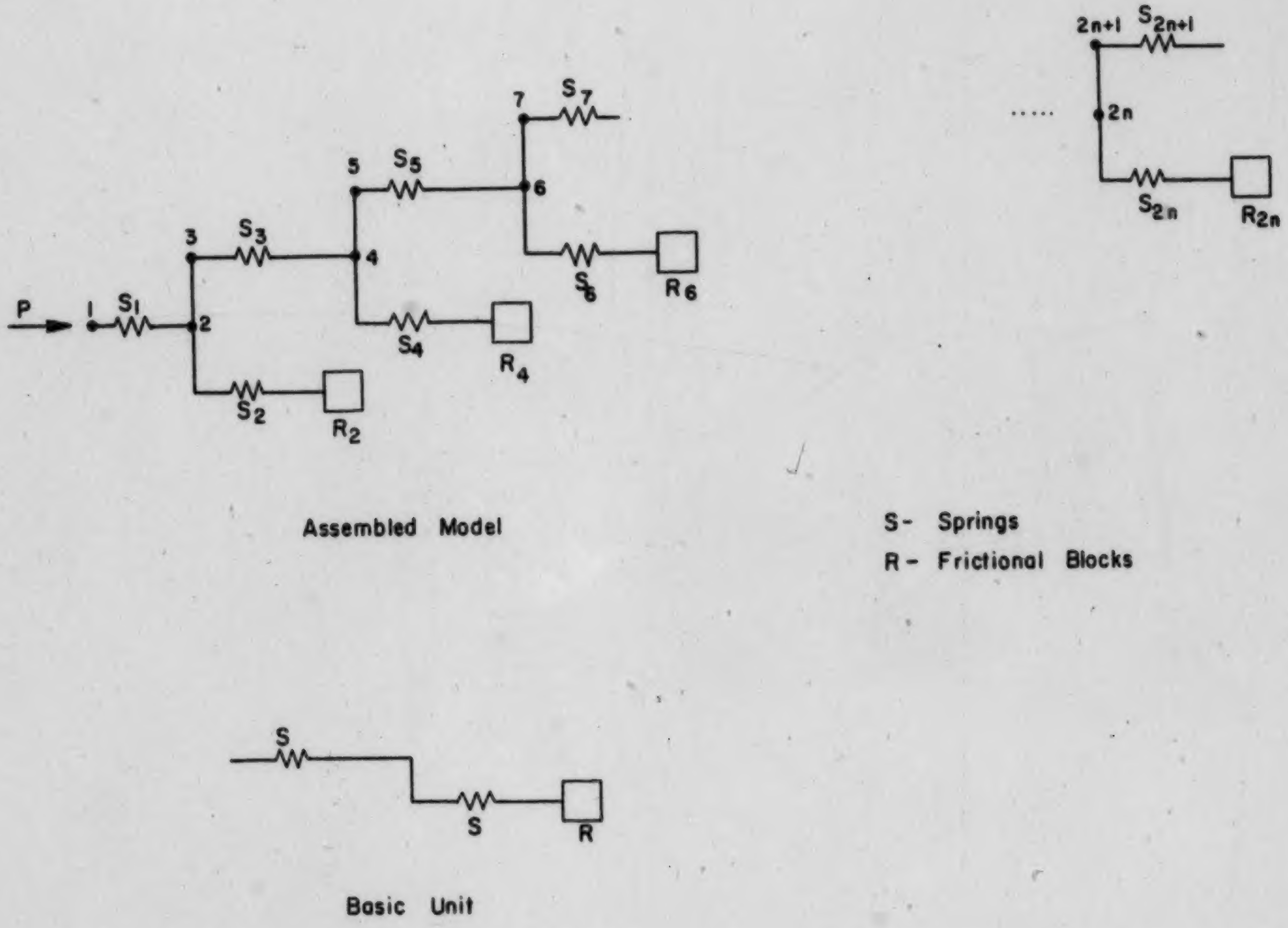
P
1
S1
2
3
S3
S2
R2
4
5
S5
S4
R4
6
7
S7
S6
R6
.....
2n+1
S2n+1
2n
S2n
R2n
Assembled Model
S- Springs
R- Frictional Blocks
S
S
R
Basic Unit

Figure 5.4 Simplified Phenomenological Model

configuration shown in the latter figure can be treated mathematically, since it represents springs assembled in series and in parallel alternately.

To facilitate the solution, a computer program was written and is presented in Appendix "F". It consists of a subroutine capable of determining the "**equivalent stiffness**" for each node of the assembled model.

The term **equivalent stiffness** can be understood by referring to Figure 5.5. Assume that the configuration shown in Figure 5.5a is subjected to a force F. Due to this force node 1 will displace a certain amount δ. This displacement δ is a function of the values imposed to the springs constants to the right of node 1. However, the same displacement δ can be obtained in the assembly shown in Figure 5.5b if the spring S assumes a constant equal to:

$$KE = F/\delta$$

This value of spring constant KE that produces the same displacement (δ) to an applied force (F) as the entire system is called **equivalent stiffness** for node 1. The value of the constant for each spring in the assembly is referred as "individual stiffness".

The calculation of the equivalent stiffness of each node in the model is performed starting with the last spring, having an equivalent stiffness equal to the individual stiffness, or:

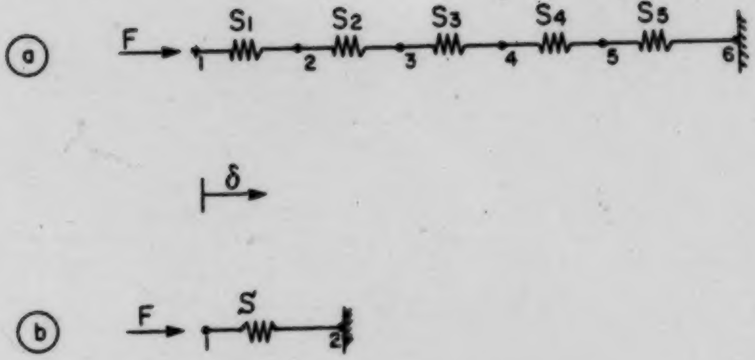
a
F
S1
S2
S3
S4
S5
1
2
3
4
5
6
δ
b
F
S
1
2

Figure 5.5 Definition of Equivalent and Individual Stiffnesses

$$KE(2n+1)=K_{2n+1}$$

where:

$KE(2n+1)$ - equivalent stiffness for node $(2n+1)$

K_{2n+1} - stiffness of spring S_{2n+1}

For the preceeding node (node 2n), the spring is assembled in series with the remaining system, or:

$$1/KE(2n) = 1/K_{2n} + 1/KE(2n+1) \quad \text{.........} \quad (5.1)$$

Subsequently, the next spring is in parallel with the system and the equivalent constant is:

$$KE(2n-1) = K_{2n-1} + KE(2n) \quad \text{.............} \quad (5.2)$$

By using equations (5.1) and (5.2) alternately, the equivalent stiffnesses for all nodes can be determined.

A main program solves the system for stresses and displacements. An iterative procedure ensures that the units "R" will never be subjected to stresses higher than the maximum shear strength.

5.2.4 Details of the Mathematical Solution

The representation of displacement of each unit (before failure of the unit) and translation of the entire system after complete failure has occurred, made it imperative that some special features be used in the mathematical model.

First, it is important to notice that the displacement of the blocks of lower indices equals, for continuity reasons, the sum of the displacement of all the subsequent blocks plus the translation of the system, if any. After a particular block fails, it stops compressing, since there is no increase in the shear stress, (no increases in the reaction) and only translates due to the incremental load. An extreme condition happens after all the blocks have failed. The model should be able to represent a **"rigid body motion"**. To accomplish that, a **"dummy"** block is automatically introduced in the model. This block does not receive any load until the last block fails. Thereafter, all the force is transmited to this dummy block, and consequently it moves. This movement is transfered to all the blocks, to represent the translation

It is worth mentioning that the dummy block is not assembled in the model as all the other blocks. This block is only present in the model after all the blocks actually composing the model have failed.

5.3 IDEALIZED INPUT PARAMETERS

5.3.1 Even Springs and Frictional Blocks

Consistent with the discussion presented in Chapter 4, the conventional shear box test will be used to determine the parameters for the analysis presented here. In a later section this assumption will be discussed.

Nevertheless, the results of these tests have to be utilized with caution, to avoid misinterpretation. In other words, the size of the sample used in the tests has to be considered when the parameters are obtained.

In the proposed model, this effect can be accounted for by assuming that the parameters obtained from the direct shear box tests represent the behaviour of one **"block"** (basic unit). Hence, the dimension of each block equals the size of the sample tested. By making this assumption, and knowing the geometry of the interface to be studied, the **"number of blocks"** composing the model is uniquely defined. In practical terms, if the interface is 1.00 m long and the parameters were obtained from a 5 cm (2") square sample, the model to represent this interface should have 20 blocks.

The input for the elements of the model can be obtained by plotting the results of the direct shear box test on two different plots: a plot "shear force versus shear displacement" and a plot "shear stress versus shear displacement". These two curves are shown in Figure 5.6 for a generic test. It is worth mentioning that since the model is one dimensional, the forces to be plotted are the forces per unit of width of the box used in the test. The inclination of the first curve provides the **"spring constant"** K for the spring elements. The maximum and residual values of the shear stress - shear displacement curve provide input for the **"frictional element"**. This

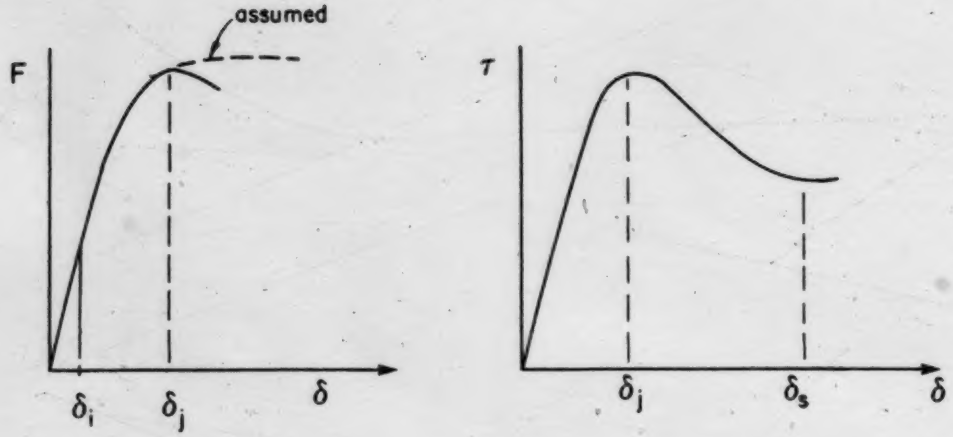

a- HYPOTHETICAL TEST RESULT

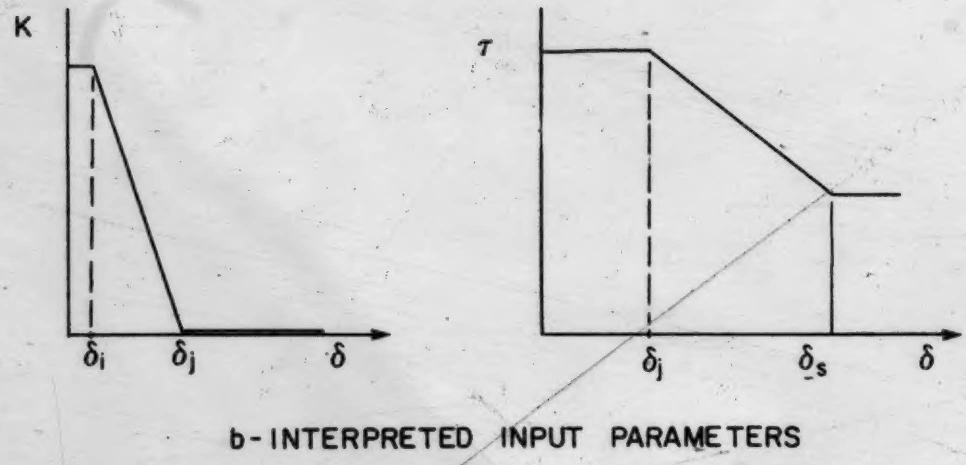

b-INTERPRETED INPUT PARAMETERS

Figure 5.6 Idealized Input Data for Model

interpretation is shown in Figure 5.6(b) for the hypothetical test presented in Figure 5.6(a)

In this figure the spring constants are assumed to be constant within the linear region of the curve (up to δ_i). Thereafter, the constant decreases until the peak force is reached (δ_j). After that the spring constant is assumed to decrease to zero. Note that even though the force-displacement curve shows a negative slope after failure, for this model, the spring constant is maintained equal to zero.

For the second curve, the shear strength equals the maximum shear strength until the shear stress in the units "R" reach this value (at $\delta = \delta_j$). Thereafter this value drops to the residual shear strength, in case the test shows a strain-softening behaviour, otherwise it is kept equal the maximum shear strength.

Also of interest is the fact that the value of the shear strength can vary from peak to residual in increments, instead of in a sudden drop. For this simulation, a "relaxation factor" is introduced and the elements "R" will only reach the residual shear strength at shear displacements beyond δ_k.

5.3.2 Odd Springs

In order to discuss the input parameters for this group of springs it is imperative to understand their physical meaning in the model. Therefore, two extreme cases are considered:

a. Consider that the constant assumed by the odd springs are very high values: in this case, as can be seen from Figure 5.4, the even springs behave as if they were assembled in parallel, and connected by a **rigid member** (spring with a very high constant).

If a force is applied to node 1 (Figure 5.4), all the nodes will displace the same amount and therefore all even springs (assumed to have identical constants) will receive an equal portion of the applied load. Consequently, all blocks "R" will be subjected to equal shear stresses.

This type of behaviour is similar to that assumed to occur in a conventional shear box test where the shear stress is considered to be uniform throughout the sample and the value is the applied load divided by the total area of the sample (sum of the area of the units "R" in the model). Furthermore the displacements are also assumed to be uniform and equal the movement of the upper half of the box. Therefore, the even springs represent a **frictional translation mode of deformation** and the parameters should be obtained from a test that does not allow longitudinal compression. As mentioned before and also observed by Hvorslev (1960), compression does occur in the conventional shear box test although, in the test interpretation, this compression is neglected. Neverthless, its influence on the parameters obtained from the shear stress-displacement curves can not be avoided and consequently these tests seems not to be the most appropriate to derive this parameter. This will be further discussed in later sections.

b. At the other extreme let the even springs have zero stiffness and the odd springs assume a finite value. Again, by analysing this condition in Figure 5.4 it can be seen that this is equivalent to having all the odd springs assembled in series. This assemblage can be regarded as representing a **compression test** (not considering time dependence).

In analogy to an ideal oedometric test, if the height of the sample is increased, the displacements of the loading head increases, and vice-versa. In the model, this is represented by an increasing number of blocks and consequently the displacements of node 1 ("loading head") will increase since the equivalent stiffness will decrease.

Hence, the input to be assigned to the odd springs has to represent a **compressibility parameter** of the soil placed in contact with the structure. Unfortunately, this parameter cannot be obtained from the same test from which the other two were derived. This is due to the nature of the shear box test in which constant stress is assumed and no compression occurs in the direction of the shear stress. Furthermore, among the tests performed for this research and presented in Chapter 4, none seems to be appropriate for derivation of the parameters for these units. Therefore, in the following examples, these values are arbitrarely set to match the results of the large shear box tests, and the values that provides the "best fit" will be used for the analyses of the experimental embankment.

5.4 APPLICATIONS OF THE MODEL

The validity of the model will be discussed by analysing three different cases. In each case one additional difficulty will be introduced.

5.4.1 Analyses of Large Shear Test

In the first example, the large shear tests will be simulated using the proposed model.

Since the method of sample preparation for the large shear test and the conventional tests performed under series 200 is the same, (see Chapter 4) these tests will be used to obtain the parameters for the even springs and frictional blocks.

The large tests selected for this simulation were performed at 59 kPa and 106 kPa (Tests #3 and #8 respectively) and the input parameters obtained in the corresponding (same normal stress) conventional direct shear box test.

Due to the one dimensional nature of the model, it is not possible to reproduce the two curves obtained simultaneously in the same test (internal and external - see Chapter 4, section 4.3.3). Therefore, this analysis will focus only the internal measurements, since these are considered to be more representative of the interface behaviour, as discussed in the preceding chapter.

As mentioned before, the size of each block has to be compatible with the dimension of the test used as input. For this example, where 6 cm tests were performed, eleven blocks are necessary to represent the large shear box test (65 cm long). The internal sensor is represented by the central 5 blocks. These are the values used in the following discussion.

The results of the simulation are presented in three different curves. First, Figure 5.7 shows a plot of shear stress versus shear displacement. In this figure, the solid lines represent the test results and the dashed lines represent the theoretical approximation. The agreement is remarkable and hence it can be concluded that the model is able to reproduce the behaviour of the large shear tests for the set of parameters imposed for the odd springs.

Subsequently the distribution of shear stress developed along the soil-concrete contact, plotted for different steps, is presented in Figure 5.8. Each step in this figure corresponds to a load increment and therefore is equivalent to a "time interval" in Test#11. This figure shows that, for a particular step, points located at different distances from the applied load (represented by nodes 2, 4, 6,..., 20 and node 0 is the face where the load is applied) are subjected to different shear stresses. Therefore, this figure demonstrates that the requirement of differential degree of mobilization has been fulfilled.

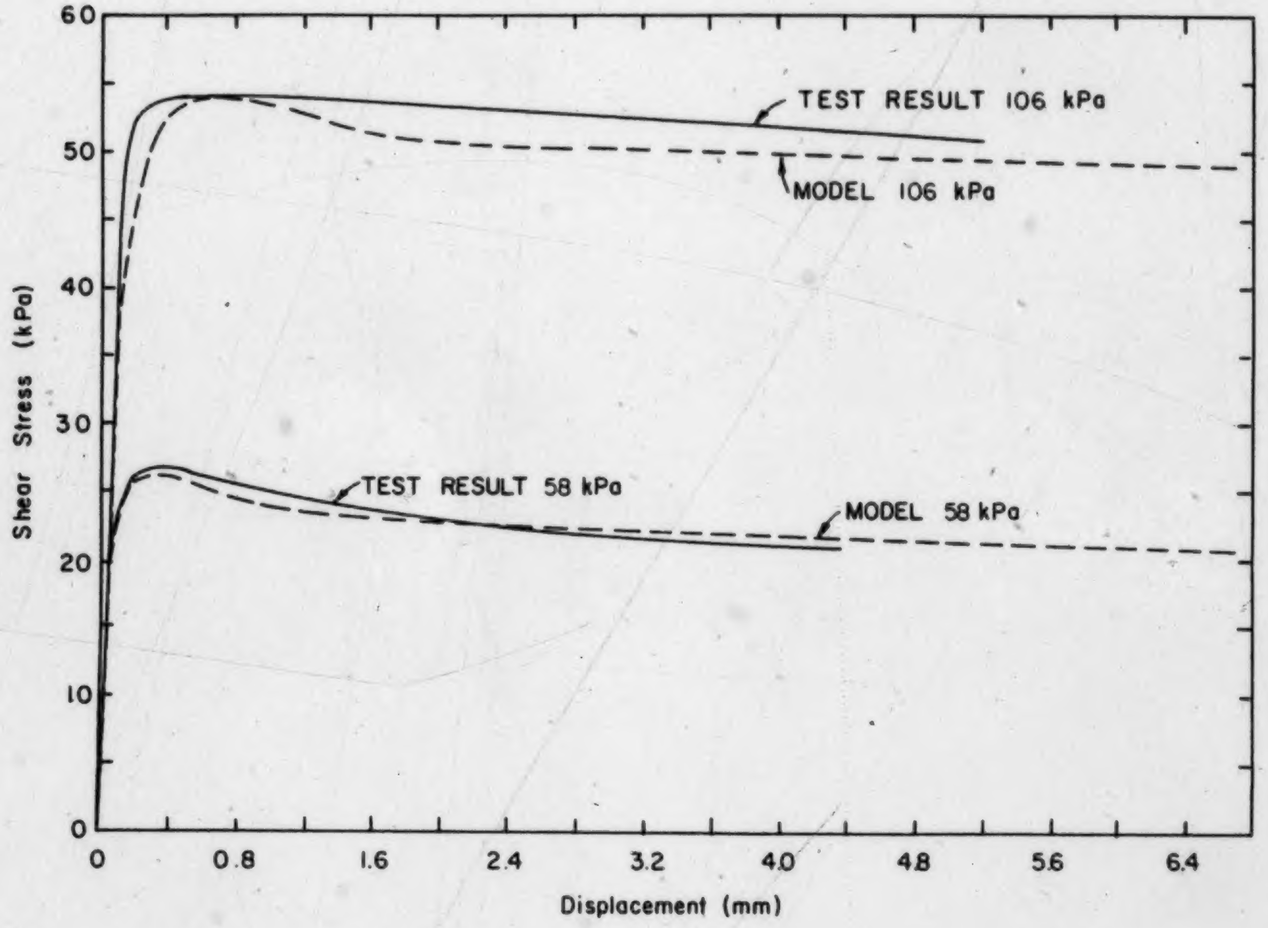

Figure 5.7 Large Shear Test Simulation - Stress-Displacement Curve

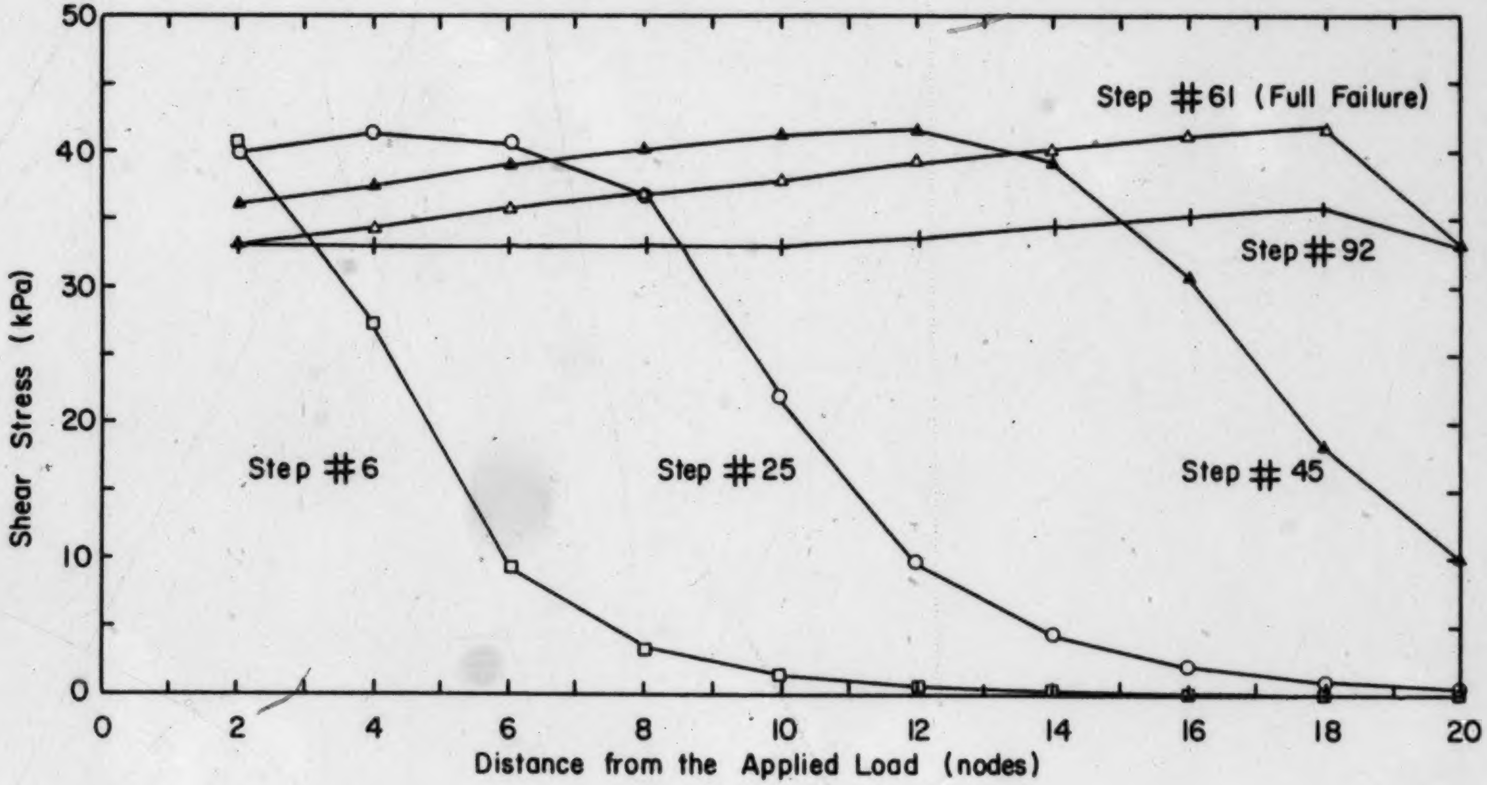

Figure 5.8 Shear Stress Distribution Along Interface

It should be pointed out that these results support the hypotheses which considered "reasonable assumptions" for the shear stress distribution proposed in Section 4.4.3.

In Figure 5.9 the development of shear displacement is plotted along the interface. Once again it can be observed that points located at different positions with respect to the applied load are subjected to different displacements. It can also be noticed that the curves for early stages of the test (e.g. step#6) are nonlinear and tend to became linear with increasing load.

Another important comment is that points where failure has occurred have equal incremental displacements. This represents the "translation" discussed before. In the extreme, where all the points at the interface have failed, this translation is represented by a **rigid body motion**.

In conclusion, the model seems to accomplish all the requirements discussed earlier in this chapter and therefore it can be used for further analyses, involving more complex problems. Moreover, the input for the odd springs have been calibrated using this example.

5.4.2 Behaviour of Frictional Piles

"Frictional Pile" is understood to mean deep foundations whose bearing capacity relies on frictional behaviour and assumes that the point resistance is negligible.

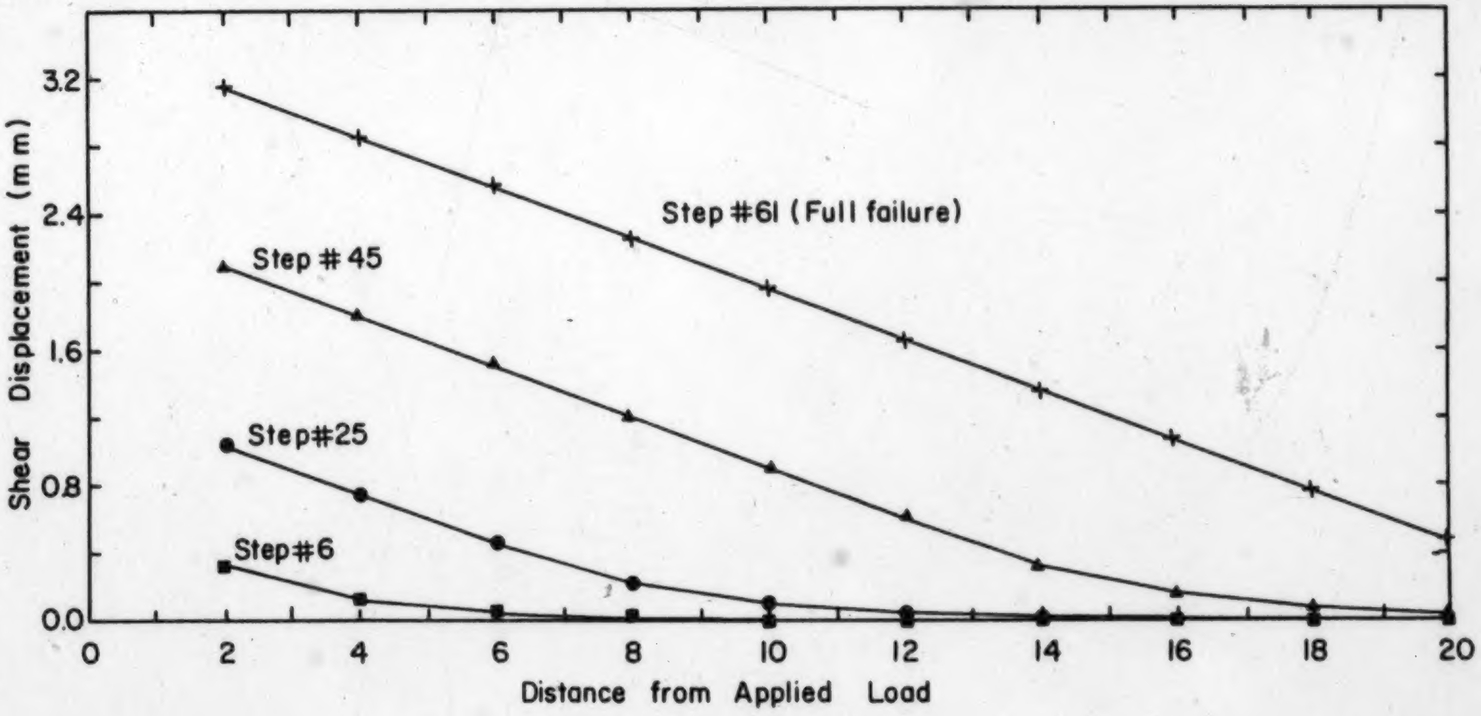

Figure 5.9 Shear Displacement Distribution Along Interface

In designing frictional piles it is important to know the shear stress distribution along the pile. Given this distribution, the depth of the pile can be optimized and the minimum pile length necessary to support the design loads, can be obtained.

In this example one additional difficulty is introduced: the normal stress is not constant along the interface and consequently the shear strength of the units "R" can not be assumed to be constant as in the previous example.

Since the properties of the elements in the model are assigned independently, this difficulty can be overcome by assuming a function which represents the shear strength distribution along the pile. For simplicity, a linear function, increasing with depth, was assumed. Furthermore, the pile was assumed to be hollow with a unit wall thickness and 3.0 m long. The input parameters were obtained from a series of shear box test reported by Kulhawy and Peterson, (1979). The tests were run in a 10 cm (4") square box and consequently 30 blocks were necessary to represent the pile. For the odd springs a relatively high stiffness was assumed, since they represent the compressibility of the sand.

The result of an axial loading test is presented in Figure 5.10 where the total applied axial load is plotted against the displacement of the pile (displacement of the first node or loading head of the pile). This curve presents a distinct shape and similar field test results have been

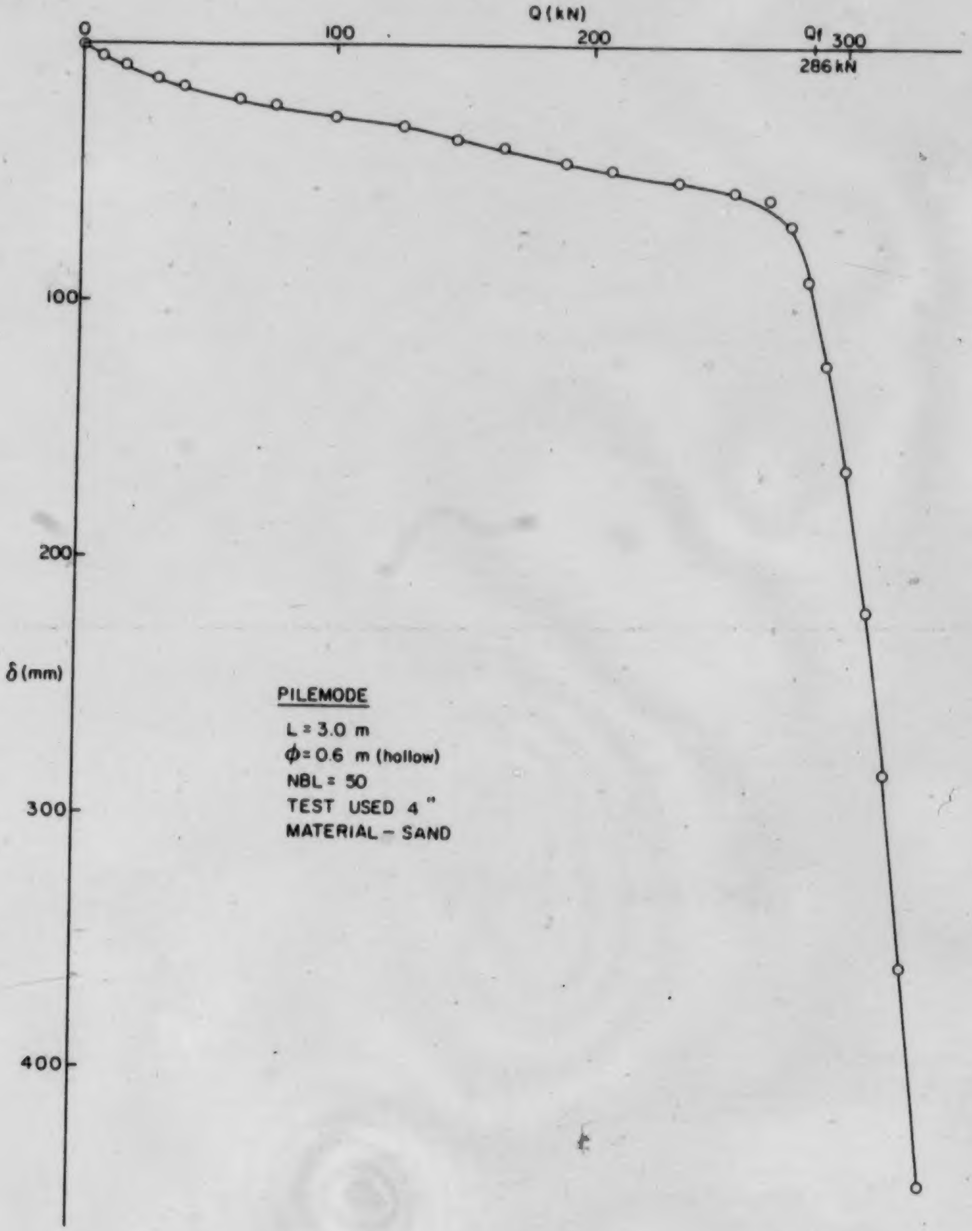

Figure 5.10 Results of Axial Loading Test in Frictional Piles

extensively reported. In particular, Vesic (1970) presented results of loading tests in piles driven in cohesionless material and the shape of the curve reported by Vesic is similar to that presented in Figure 5.10.

As mentioned before, the shear stress distribution along the pile shaft allows the length of the pile to be defined. For the theoretical simulation this can be seen in Figure 5.11. Again the shape of these curves are similar to that reported by Vesic (op.cit.). The author obtained the curves by interpolation of several load cells installed in an experimental pile. The difference in reading between two consecutive load cells was considered to equal the load lost by friction in this section of the foundation.

The similarity of the qualitative results observed between the theoretical and experimental results supports the model proposed in this chapter.

5.4.3 Behaviour of the Test Embankment

As a final example, the test embankment is analysed using the proposed model. In this example several assumptions are necessary since the number of unknowns is larger than in the two previous examples.

First, for the field instrumentation the distribution of loads acting in the model are unknowns of the problem. These loads represent the "shear loads" acting at the interface. At the same time, this shear load distribution is the most important factor influencing the model results

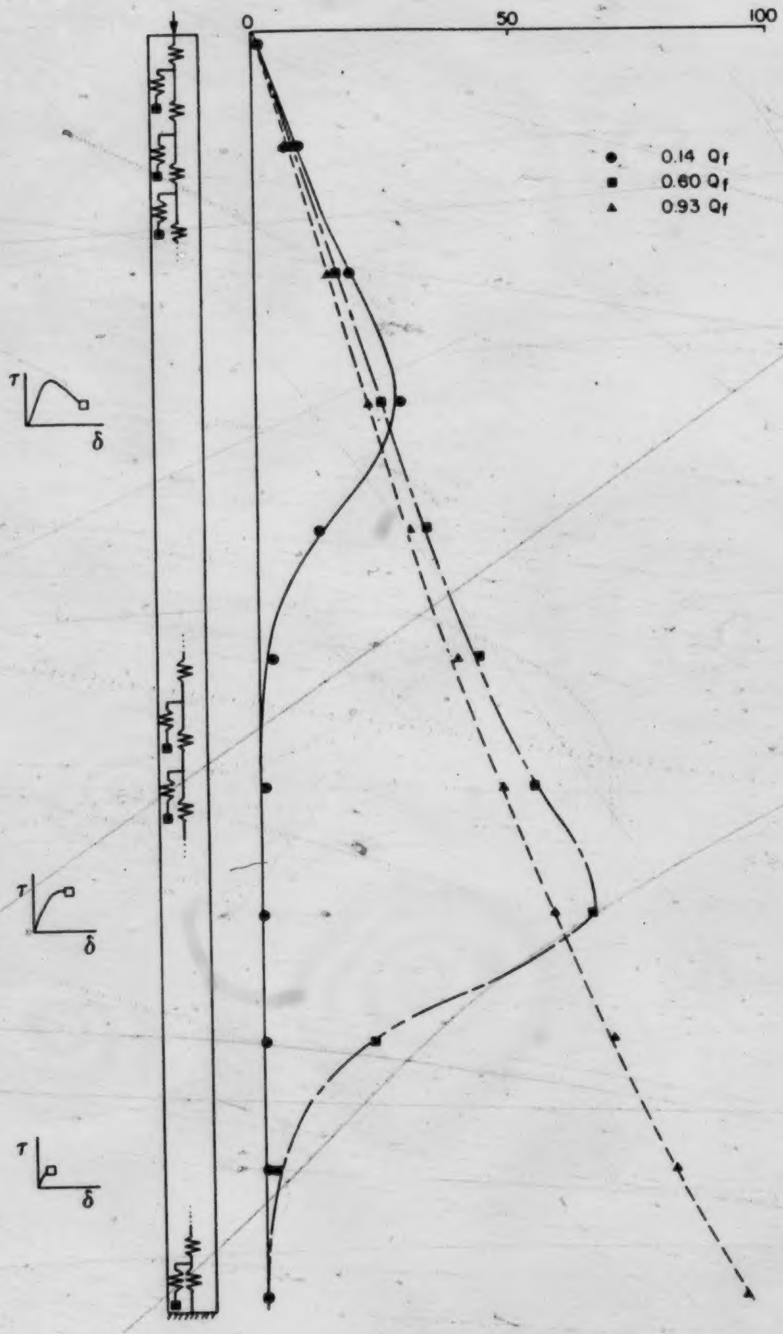

Figure 5.11 Shear Stress Distribution Along Pile

since it provides the distribution of shear stresses along the interface. Therefore, a trial method had to be used and different functions imposed to represent the distribution of applied shear load. The most representative function will be that providing the **best fit** between the theoretical and measured shear stress distributions.

Another important feature arises in this example: the loads are originated from soil being placed in consecutive layers. From the point of view of the model this means that, for each layer, a certain number of blocks have to be introduced in the analysis. For this example, the simulation in five "layers" of 1.2 m each was chosen. This corresponds of introducing 20 blocks for each construction step, totaling 100 blocks (6 m high concrete wall represented by 6 cm shear box tests).

Consistent with the discussion presented in Chapter 4, the results of the shear box tests performed in the series 100 were used as input data. For the odd springs the values obtained in the first example were adopted.

Similar to the frictional pile simulation, all input values should vary with depth and linear variations were adopted, for the sake of simplicity. For the odd springs the parameters were interpolated, as a function of the normal load (assumed to increase linearly with depth), between the two values obtained during the simulation of the two large shear tests.

Three functions were used to represent the shear force distribution, starting with one unlikely to happen, to assess the fidelity of the model.

The results for a linear, monotonically increasing function is shown in Figure 5.12. In this figure the values of shear stress are plotted along the concrete wall. In the same figure the values obtained in the field are also presented. It can be seen that the function used is not representative of the shear load distribution since the field measurements and simulated values show opposite trends.

A second, more realistic linear function was chosen and the results are presented in Figure 5.13. In this plot it can be noticed that the simulation is more representative of the measured values, although it seems that linear functions are not likely to occur.

As a final trial, a hyperbolic function was used as shown in the upper part of Figure 5.14. For this function some assumptions had to be made and are listed below:

a. Two different functions were used, one representing the layer being placed and a second for the existent material (see the insert in Figure 5.14).

b. Both functions were assumed to be tangent to the structure (first derivative equal to zero at x=0 for the first function and at x=l in the second function, where l is the thickness of the existing

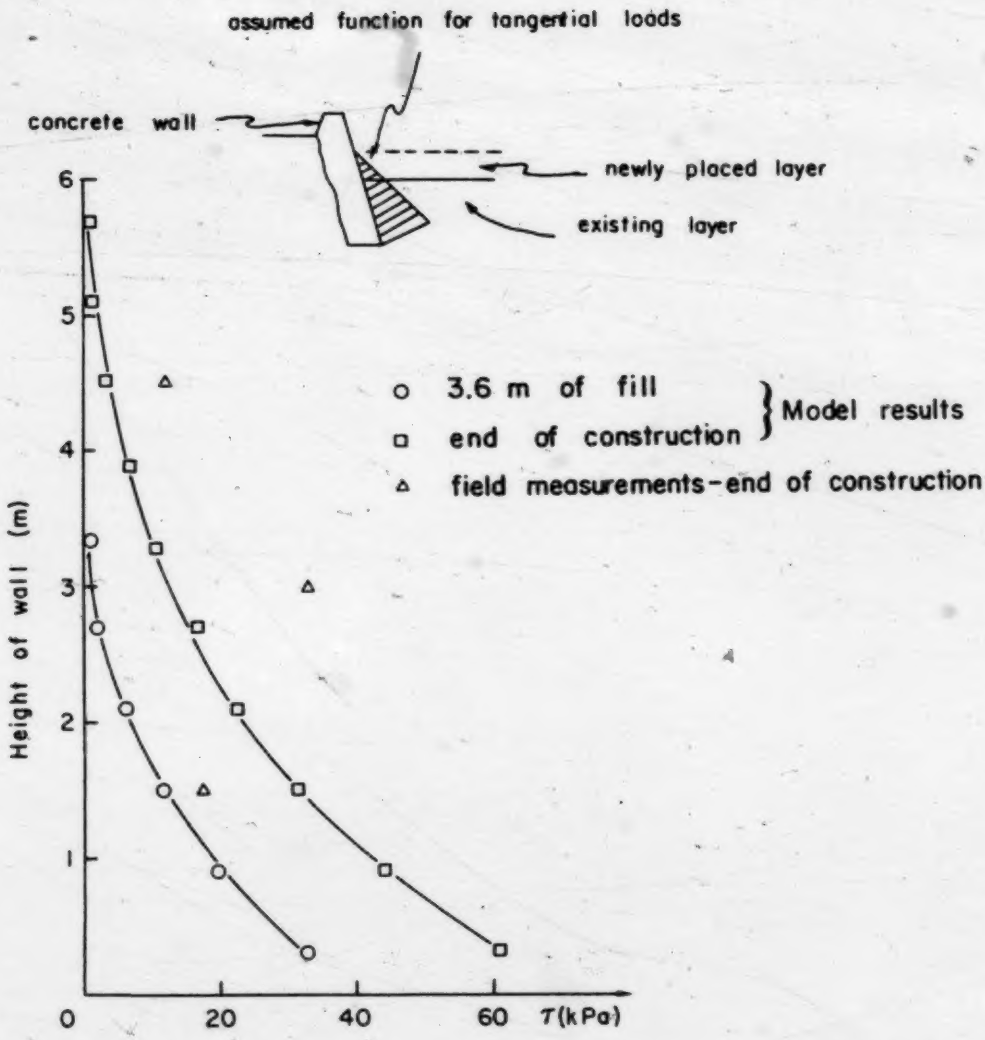

Figure 5.12 Field Measurements Simulation - Linear Function

I

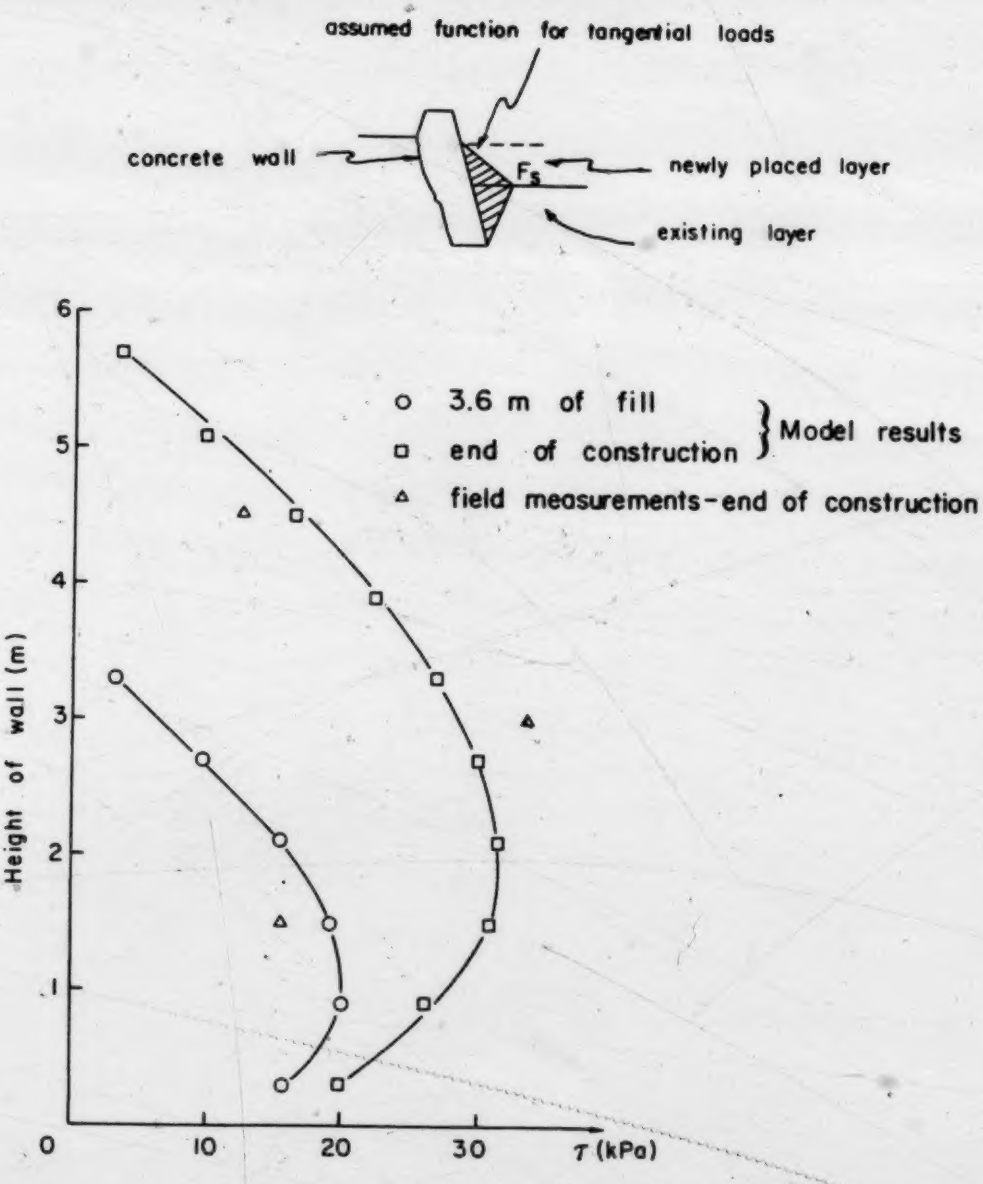

Figure 5.13 Field Measurement Simulation - Linear Function II

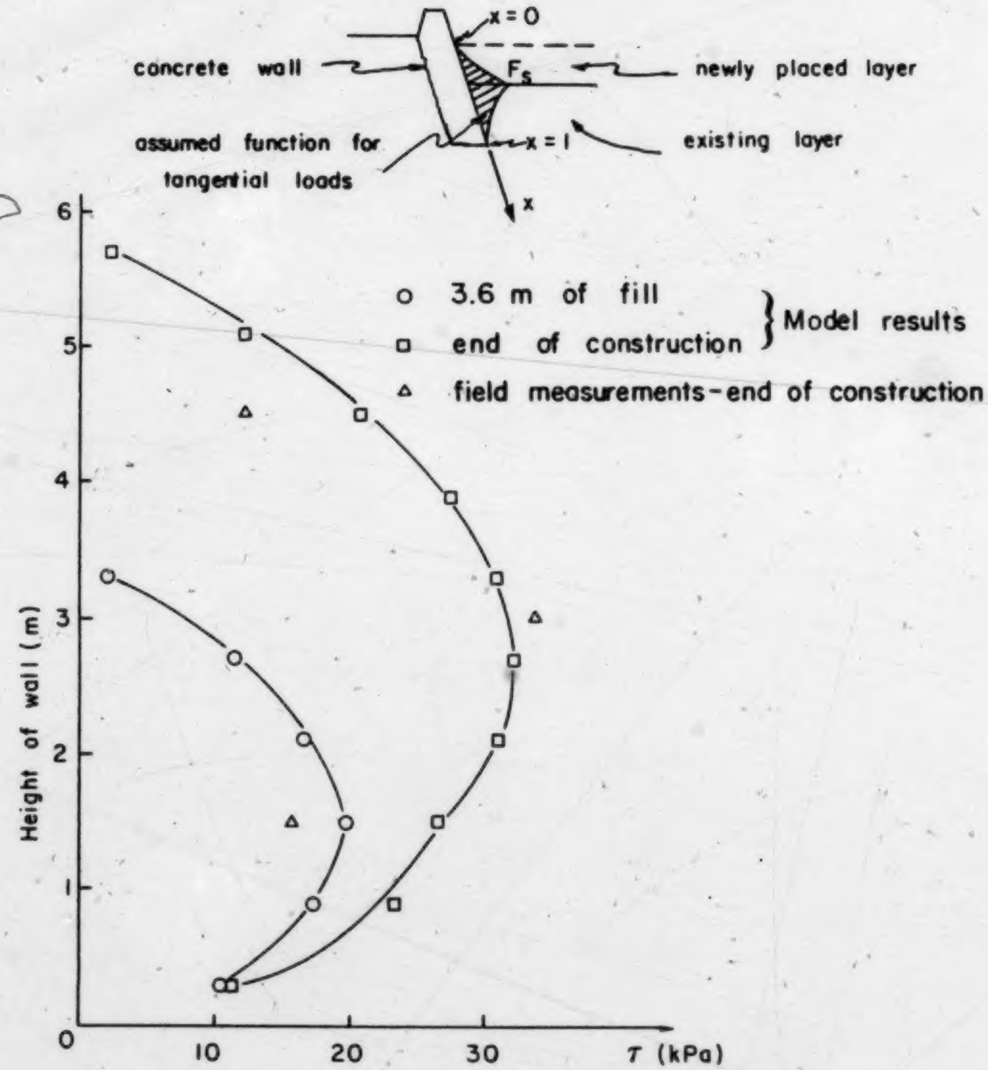

Figure 5.14 Field Measurements Simulation - Hypebolic Function

material).

c. Both functions have identical values at the interface between the newly placed layer and the existing layers (denoted by F_i in the figure).

Although a slightly better agreement was obtained, the results still do not match completely. Neverthless, qualitatively both results show similar trends and due to the simplified nature of the model better quantitative agreements should not be expected.

However, despite the larger number of hypotheses necessary for the last example, all three examples presented in this section seem to support the model to represent the behaviour of soil-concrete interfaces.

5.5 THE USE OF DIRECT SHEAR BOX TEST AS INPUT FOR JOINT ELEMENTS

From the analyses of the **"phenomenological model"** presented in this chapter, it was concluded that two different parameters should be used to represent the interface behaviour: one representing a **"frictional translation"** mode of deformation and one similar to a **"compressibility"** parameter. The former should be a pure representation of the ability of one side of the continuum to displace with respect to the other side, or a purely **frictional parameter**. The latter is a property of the soil itself. Both parameters are influenced by several factors such as, normal stress level, roughness of the structure, grain size of the soil and relative density.

In the past, the most common procedure adopted to obtain parameters for joint elements was to perform conventional shear box tests and obtain the inclination of the shear stress - shear displacement curve. This value was assumed to be the desired input for the joint element for the Finite Element analyses.

However, some factors that have been recognized in the results of these tests, such as the longitudinal compression, have to be analysed to assess its effect on the interface behaviour. For rock mechanics applications where the rigidity of the rock masses is large, for most ranges of normal stresses, the influence of compression seems not be relevant and the shear box test can be used to define the parameters for the numerical analyses. Neverthless, it is important to choose an element that follows the same assumptions adopted in the interpretation of the tests, the most important being the constancy of shear stresses inside the sample.

On the other hand, for soil application, the use of the shear box test should be considered with some restrictions. First it has to be recognized that the results of the shear box tests, in combined samples are affected by the geometry of the test and by the soil used. Therefore, the parameters extracted from these tests are not unique. This effect can be evaluated, in practical terms, by comparing the results of the tests presented in Chapter 4 (conventional shear box tests series 200 and large shear tests), reproduced in Figures 5.15 and 5.16. The latter figure includes a third test dimension (30 cm sample) reported by Neden, (1984). This test was performed on a similar soil using similar concrete sample and the sample preparation followed the specifications as described in the previous chapter for samples in series 200.

It can be seem from both figures that the larger the sample size, the smaller will be the value of the **"tangential stiffness"**, for the same soil.

Further evidence can be obtained by the theoretical solution presented by Noonan and Nixon (1972). The authors described a procedure for determining the Young's Modulus (E) based upon the results of shear box tests.

According to these authors, the **shear forces** (per unit of width of the shear box, since their analysis was plane-strain) should be proportional to the Shear Modulus (G) as follows:

$$T = k' \delta G$$

where:

T - shear force/unit of width

k' - constant

δ - shear displacement

G - shear modulus

Since:

$$G = E/2 (1 + \nu),$$

it follows that:

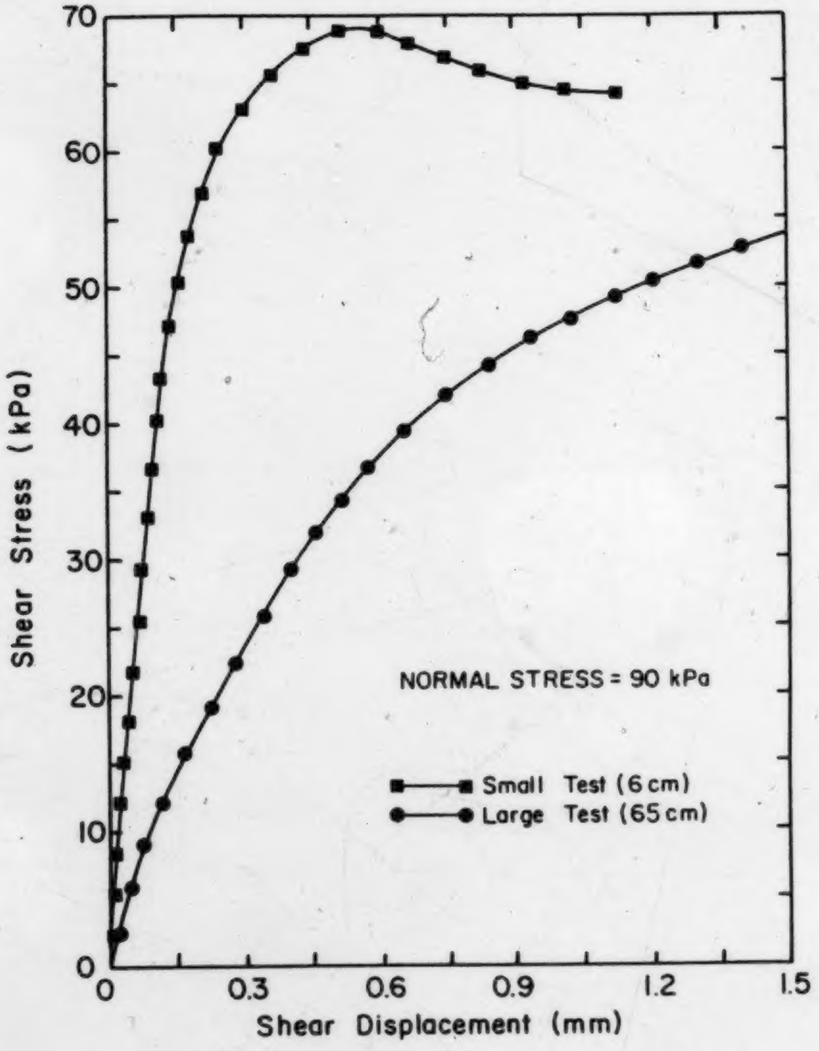

Figure 5.15 Comparison Between Two Sizes of Shear Box Tests

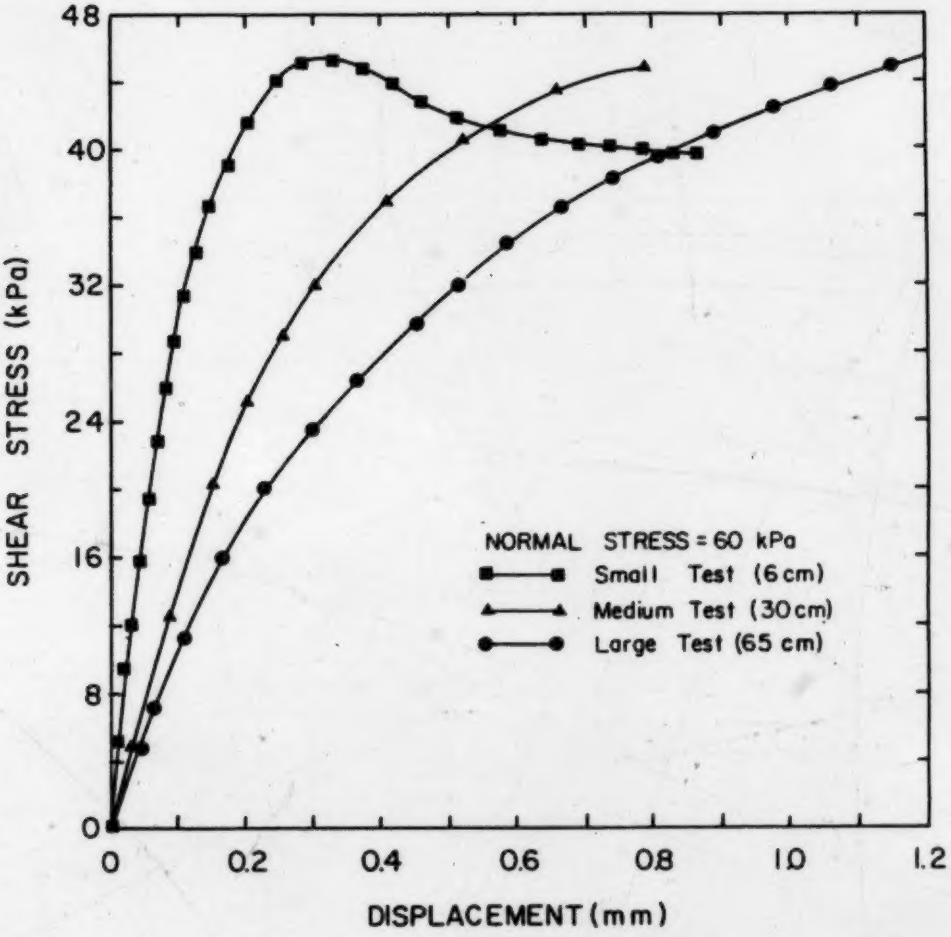

Figure 5.16 Comparison Between Three Sizes of Shear Box Tests

$$T = k\ E\ \delta \quad \text{.............................} \quad (5.3)$$

where:

k - constant = f (ν, geometry)

E - Young's Modulus

Or, the last expression can be written:

$$E = T/\ (k \times \delta) \quad \text{..........................} \quad (5.4)$$

By varying the geometry of the test (basically the height of the sample (H), the length (L) and the gap between boxes (B)) the authors provided a series of charts allowing the determination of the constant k.

By knowing the geometry of the test (and consequently k from the charts) and the values of T and δ within the linear portion of a shear stress shear displacement curve, the Young's Modulus (E) can be determined using expression 5.4.

Based upon the definition of **tangential stiffness** (K_t) presented in Chapter 2, and using similar notation as Noonan and Nixon (1972), the following can be written:

$$K_t = \tau/\delta = T/\ (A \times \delta) \quad \text{...................} \quad (5.5)$$

or:

$$K_t \times A = T/\delta \quad \text{...........................} \quad (5.6)$$

where:

T - shear force/unit of width

A - area (length for plane strain) of test

δ - shear displacement

Expression 5.4 can be rewritten:

$$T/\delta = k \times E \quad \ldots\ldots\ldots\ldots\ldots \quad (5.7)$$

Comparing equations (5.6) and (5.7) it follows that:

$$K_t \times A = k \times E \quad \ldots\ldots\ldots\ldots\ldots \quad (5.8)$$

Since the constant k is a function of the geometry and Poisson's Ratio only, expression 5.8 becomes:

$$K_t = (K \times E)/A$$

or:

$$K_t = K \times E \quad \ldots\ldots\ldots\ldots\ldots \quad (5.9)$$

where:

K - constant = f(ν and geometry)

E - Young's Modulus

According to expression 5.9, the tangential stiffness is a function of the geometry and elastic constants. By varying either the geometry of the test or the elastic constants (E and ν) of the soil, the tangential stiffness will change. Therefore, the value of K_t is not unique.

The influence of the soil properties has also been studied, using laboratory tests. Kulhawy and Peterson, (1979) have reported shear box tests performed on combined samples of sand-concrete and have shown that the relative density plays an important role in the shear strength and in the shear stress - shear displacement curves, and therefore in the tangential stiffness derived from these tests.

It is important to note that the difference in behaviour mentioned above is a direct consequence of differences in the measured shear displacement. Palmer and Rice (1973) arrived at an identical conclusion when trying to derive a model for a shear band. According to the authors, the shear displacement is not a parameter independent of the sample size, such as strain.

However, the primary reason for the differences in the shear displacements can be atributed to the "longitudinal compression" described in early sections. In an extreme situation, if a sample of rock is tested, for most ranges of stress state, the longitudinal compression will be negligible and a uniform distribution of shear stress is expected. Therefore displacements will not be observed (other than compliance of the testing apparatus and adjustments of the sample) until maximum shear stress is reached over the entire interface (or joint).

This discussion suggests that, for soil application, the ideal test would be performed on a sample with very small dimensions to minimize the effect of the compression. Such a test would, most likely, present a rigid-plastic behaviour, since deformations prior to failure would not be measurable. In fact, the rigid plastic mode is probably the most realistic mode of behaviour to be adopted for analyses of soil-concrete interfaces.

This type of behaviour has been illustrated in the introduction of this thesis, using a simple example of an elastic body resting in an inclined plane. It was stated, at that time, that displacements would not be observed until the maximum shear strength of the interface had been reached. Moreover, it was also mentioned that shear stresses would develop, as a reaction, even before any measurable movement had occurred.

The major factor contributing to the behaviour described in the example of section 1.3 (elastic body on an inclined plane) seems to be the magnitude of the stress level. Since only body forces were considered the compression of the elastic body was negligible and uniform shear stress along the interface assumed.

This example is probably an illustration of a mode of behaviour that seems to be realistic for any soil-concrete interface. Displacements of any point at the interface should only occur after the maximum shear strength of the interface have been reached at all points. Prior to failure (slippage) movements are consequences of recoverable adjustments to the new equilibrium condition (created by the increase in the stresses by placing a new layer). In other words, prior to failure the soil is in "perfect bond" with the structure and a "no slip" (rigid) mode of behaviour seems to be the best representation for this phase of the simulation. After failure has been reached at a particular point of the interface, the soil can move freely with respect to the structure and a "full slip" (plastic) condition occurs with no further increase in the shear stress.

From the finite element analysis point of view, this represents an assumed infinite value of the tangential stiffness prior to failure and a null value after failure. Simulations of this nature using joint elements have some drawbacks as will be discussed in Chapter 6.

In terms of the phenomenological model this is equivalent to removing the odd springs (defined in section 5.2.2) and the even springs will act as if arranged in parallel. If high constants are assigned to this set of springs, only small deformations will take place (equivalent to the recoverable movement discussed above) until the maximum shear stress is reached, and uniform shear stress distribution is obtained. Any load increment applied after maximum shear stress has been reached at all blocks "R", will promote a translation of the system with no further increase in the shear stress.

In conclusion, in the writer's opinion, the value of the tangential stiffness K_t as an intermediate condition between the "full slip" (no shear stress is developed at the interface) and the "no slip" (no displacement takes place at the interface) seems to have no support on physical grounds. The tangential stiffness is a pure response to a test condition and is strongly influenced by the dimension of the test and soil properties.

Although it is not the objective of this thesis to discuss all available joint element formulations, it is important to draw attention to a distinction that has to made between elements without and with thickness (see Chapter 2). In the first case, the element has no "material" and it is only an aid to describe a "difficulty" or "facility" concerning a pair of nodes (basically the same point) to displace with respect to each other in both directions (normal and tangential). Since the element has no **physical meaning** the discussion presented above holds in full.

For elements having thickness the joint is physically represented, and consequently both parameters discussed in connection with the phenomenological model have to be taken into consideration, viz: compressibility and translation (since the material existing inside the element can be subjected to longitudinal compression).

In one of the most recent developments for Finite Element analyses of soil-concrete interfaces the effect of the compression seems to have been recognized. Desai et al, (1984) have developed the **Thin Layer Element** (described briefly in Chapter 2) that makes use of a particular constitutive matrix [C], as shown below:

$$C = \begin{bmatrix} C_1 & C_2 & 0 \\ C_2 & C_1 & 0 \\ 0 & 0 & G_1 \end{bmatrix}$$

where, in this matrix:

$$C_1 = [E\ (1 - \nu)/(1 + \nu)(1 - 2\nu)]$$

$$C_2 = [\ E\ \nu/(1 + \nu)\ (1 - 2\nu)]$$

$$G_i(\sigma_n, \tau, \delta) = [\ \Delta[\tau(\sigma_n, \delta)]/\Delta\delta]\ x\ t$$

and,

τ - shear stress

σ_n - normal stress

δ - relative displacement

t - thickness

Δ - "variation" (of τ or δ)

The values of C_1 and C_2 are dependent only upon elastic constants (E and ν) and can be associated with the "compression" described before, whereas the value of G_i is defined in a form similar to the "tangential stiffness" (K_t) as has been defined previously (refer to Chapter 2) and represents the "frictional parameter". In their report, Desai and his co-authors give an indication that a new test has been proposed to determine the joint parameter G_i.

However, even in these circumstances, the interpretation value of the tangential stiffness K_t based on direct shear box tests is questionable.

From this point on, the discussions presented will focus on elements without thickness for the reasons presented in the next chapter (section 6.3.3) and in particular in the formulation proposed by Goodman (1968) since it is the most used joint element, as has been shown in Chapter 2.

5.6 CONCLUSIONS

With the aid of the tests reported in the preceeding chapter a theoretical model was proposed to provide a better understanding of the physical behaviour of soil concrete interfaces. Several requirements have been imposed on the model, and examples have been presented to show that the requirements have been fulfilled.

The model made possible the analyses of some simple examples, including the reproduction of the field test. The most important conclusions obtained during this analysis are:

1 - The behaviour of the large shear box tests is governed by two factors: one corresponding to a "frictional translation" and a second corresponding to a "compression". The first reflects a degree of difficulty for the soil to displace with respect to the structure, while the second represents a change in length that occurs in the direction of the shear.

2 - Although good agreement was not obtained between the simulated and measured shear stresses, the function describing the distribution of "shear forces" in a planar concrete structure, caused by the placement of sucessive layers of soil, seems to

be nonlinear.

The model also provided an important opportunity for the parameters obtained from the conventional shear box test to be critically reviewed. It was concluded that:

1 - The value of the tangential stiffness k_t is strongly influenced by the geometry of the shear box test used and the parameters of the material interfacing with the concrete. The **longitudinal compression** is the dominant factor responsible for these differences.

2 - The value of K_t seems to have no physical meaning for intermediate conditions (partial slip or partial bond) as proposed in the literature.

3 - The rigid-plastic mode of behaviour seems to be the most realistic for representing the behaviour of soil-concrete interfaces.

6. FINITE ELEMENT ANALYSES OF TEST EMBANKMENT

6.1 INTRODUCTION

The Finite Element method is an efficient numerical technique for solving continuous media problems since it permits to take into account complex features, such as, heterogeneity, anisotropy, nonlinearity and other complex properties existing in real soil masses (Rudykh, 1981).

The decisive rule of joints in the behaviour of jointed rocks masses imposed the formulation of a different type of element to account for relative displacement, rotation, opening of gaps and overlapping.

Most recently the use of these joint elements was adopted to simulate behaviour of interfaces between soil and concrete structures (Clough and Duncan, 1971).

The simultaneous use of joint elements to represent the behaviour of interfaces, with well developed solid elements to simulate the continuum, allowed one further complexity to be incorporated in the Finite Element analyses.

As discussed in Chapter 2, the literature review has demonstrated that a common procedure is used in analysis of soil-concrete interfaces using the finite element method. Most of the publications reviewed revealed that joint elements are used and the parameters for these elements obtained from conventional direct shear box tests performed on combined samples of soil and concrete. However, in Chapter 5 this procedure was contested since the value of the tangential stiffness K_t derived from the direct shear box test is not unique (Section 5.5). Therefore,it is the writer's opinion that the conventional method of analysis using the finite element method does not represent the actual behaviour of soil-concrete interfaces.

On the other hand, most of the examples provided in the publications referred in Chapter 2 have shown that the conventional method of analyses yielded good agreement between back analyses and field measurements.

In this Chapter a back analysis of the test embankment described in Chapter 3 is presented in order to discuss this method conventionally used. For this back analysis a Finite Element program was developed. The choice of type of elements, equation solvers, storage schemes, among other features were made primarily to accomplish an efficient program, with simple input data, and consequently inexpensive.

In this chapter a detailed description of the most important features will be presented. Simple examples will be provided to access both the efficiency of the program and the algorithms used in the implementation of these features. Subsequently, the test embankment is analysed and the results discussed.

It is worth mentioning that a plane strain condition is assumed throughout this analysis. This hypothesis is not supported by the results of the total pressure cells reported in Chapter 3, where a three-dimensional effect was observed.

6.2 FINITE ELEMENT PROGRAM

6.2.1 General

As part of this research work, a Finite Element program was developed, based on the program FENA-2D (Krishnayya, 1973) and labelled INTERDAM (Interfaces in Dam Design).

Several modifications were introduced to the original version to increase its efficiency or to fulfill specific needs. Among the modifications, the most relevant were:

- The equation solver was replaced by a Gauss elimination technique from Gauss-Seidel iterative procedure.
- The storage scheme was replaced from "banded" to One-Dimensional storage scheme using the Skyline method (Bathe and Wilson, 1976).
- Joint elements were introduced.

These features will be explained in more detail in the next sections. A listing of the program, user's manual and an example of its use are presented by Brandt (1985).

6.2.2 Capabilities of the Program

The available version of INTERDAM makes use of Constant Strain triangular elements and Constant Strain joint elements. It incorporates the following features:

a. Linear or nonlinear analysis can be performed to represent the behaviour of both the soil mass and the interface. The nonlinear behaviour of the soil is simulated using the results of conventional compressive triaxial tests. The stress-strain curves are input pointwise in a digital discrete form (Krishnayya, 1973).

In the original program FENA-2D measurements of volume change during shear were provided together with the stress-strain curves allowing the two elastic constants (K - Bulk Modulus and G - Shear Modulus) to be determined. Since in most conventional triaxial tests the measurement of volume change during the shearing phase is not routine, an option of imposing directly the value of Poisson's Ratio (ν) was incorporated. In this case the axial strain - volume change curves are not required and the Poisson's ratio is constant throughout the analyses. A detailed description of the method used to determine the elastic constants is presented by Krishnayya (1973).

Its important to note that, unlike FENA-2D, nonlinear analyses can include some linear elastic materials. This feature is particularly important in analyses of soil-concrete interfaces where the behaviour of the soil can be represented by a nonlinear law whereas the concrete is simulated by a linear relationship.

b. The program allows for the application of concentrated loads.

c. The initial stresses, during the "switch-on" gavity phase, are determined for the value of the coefficient of earth pressure "at rest", determined by the Poisson's ratio (ν), as

$k_0 = \nu / 1-\nu$.

d. Prescribed displacements can be applied.

e. Inclined boundary conditions can be specified.

f. The program presents a subroutine to reduce tension in the soil mass, as proposed by Zienkiewicz et al (1968). If this option is used, the elements under tension have their stresses redistributed to the entire mesh until a tolerable tension is reached in all elements.

g. The analysis is incremental and each increment (called "step") can be subdivided into subincrements. This feature is particularly important for nonlinear analyses and partially substitutes the need for iterations to ensure that the stress-strain curve is closely followed. It is important to notice that this procedure is "problem-dependent" and the ideal number of subincrements has to be sought for each particular problem. This can be accomplished by performing partial analyses of the whole mesh using an increasing number of subincrements. For linear analyses the number of subincrements is automatically set equal to one.

h. Mesh generation is also possible both for uniform and nonuniform patterns (see User's Manual for details).

Most of these features were available in the original version of FENA-2D. However in order to increase efficiency and consequently reduce cost, some procedures were modified and more up-to-date methods were used. Therefore, three additional modifications were introduced, and due to their importance for this program they will be discussed separately in the next section.

6.2.3 Additional Features

In most numerical analyses using the Finite Element method, the majority of the cost lies in storage and in solving the linear equations. In nonlinear analyses the stiffness matrix may have to be redetermined for every increment of load and assembling the stiffness matrix has to be redone several times. This is particularly true if elements are introduced in the stiffness matrix for every new step of loading, such as in the representation of a fill contruction. Therefore considerable savings can be obtained if the methods of assembling, storing and solving are efficient.

Although the methods used in FENA-2D are still widespread methods of storing (banded matrix) and solving

(Gauss-Seidel iteration), in recent years some new methods have been developed. The algorithm chosen to replace that used in the original FENA-2D code is discussed briefly in the next section.

Furthermore, to analyse the behaviour of interfaces, a joint element was incorporated in INTERDAM. The type of element, its mathematical formulation and advantages are also presented.

6.2.3.1 The Skyline Method

In computer calculations with matrices, it is necessary to choose a scheme of storing the elements of the matrices in a high-speed storage. An obvious way of storing these elements is by simply dimensioning, in the program, an array M x N to store all the elements a_{ij} of the matrix A(M,N). However in this procedure, several unnecessary zero terms are stored in the storage space.

In Finite Element analyses most large matrices (such as the stiffness matrix) present two important properties: they are symmetrical and "banded". Symmetry means that the elements a_{ij} are equal to the elements a_{ji} where i and j denote generic terms of the matrix. Consequently only half of this matrix need to be stored. Bandedness means that all elements beyond the the "bandwith" of the matrix are null terms (Bathe, 1976). Therefore, if advantage is taken of these two properties, only the elements above and including the mean diagonal have to be stored (due to symmetry) and only those elements inside the bandwidth (since the remaining are zero). Figure 6.1 shows a generic matrix and the elements that have to be stored.

By analysing the matrix shown in Figure 6.1, it is noticed that, although some of the zero terms have been eliminated, some null elements remain inside the bandwidth and will be stored. Since these elements have no influence in the overall solution of the problem, storing these elements can be avoided.

One method of avoiding this unnecessary storing is by using the Skyline principle. This method enables the computer program to recognize the first nonzero element of a particular column of the matrix and set an "imaginary line" above this element, as shown in Figure 6.2. The same figure presents the equivalent bandwith and it will be noticed that all unnecessary zero elements have been eliminated from storage.

In order to eliminate all these undesirable elements, the final storage scheme uses a one-dimensional array, and consequently the method has to provide a way for the computer to recognize the original position of each element storage in this final one-dimensional array. This is obtained with an "addressing matrix" that differentiates between active and nonactive degrees-of-freedom. This method is fully described by Bathe and Wilson (1976) and was implemented in the program INTERDAM. All the matrices involved in

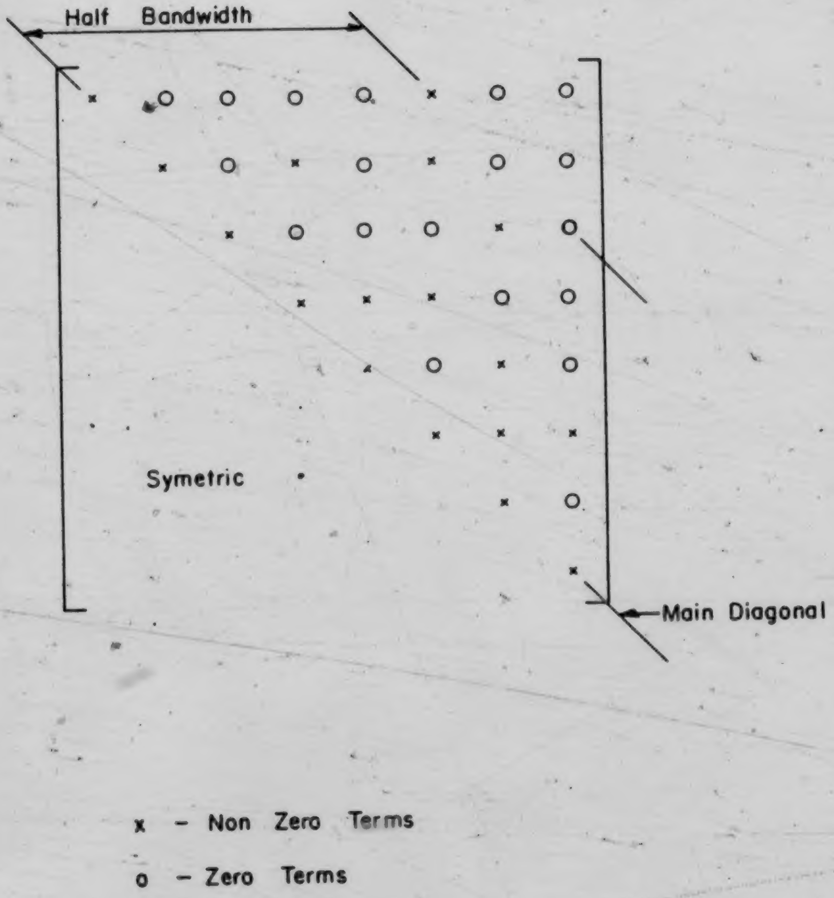
Half Bandwidth
Symetric
Main Diagonal
x - Non Zero Terms
o - Zero Terms

Figure 6.1 Example of Banded Matrix

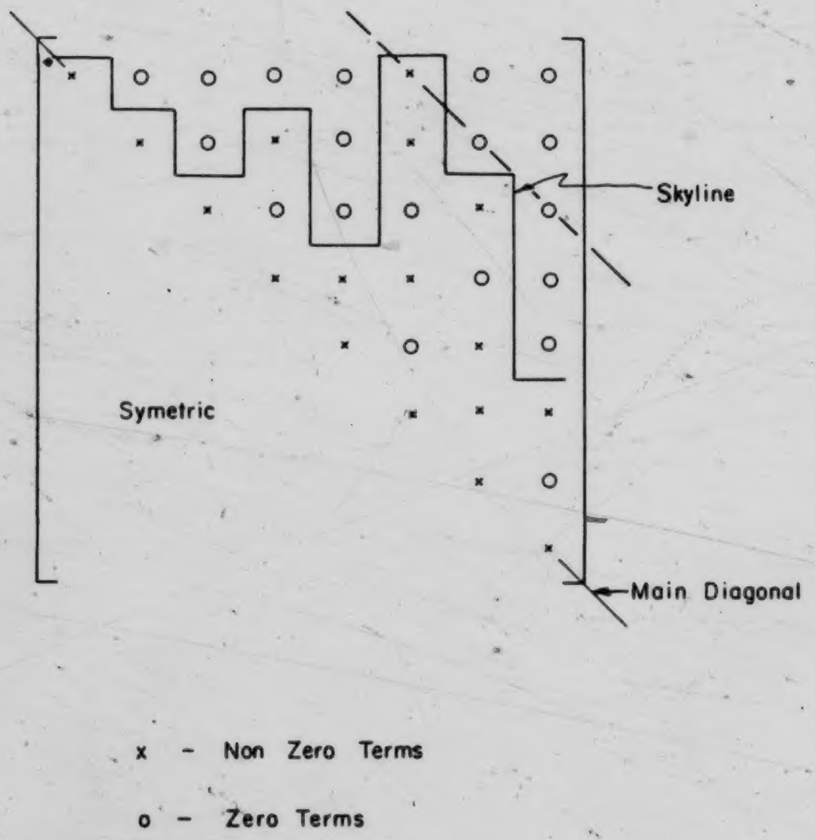
Skyline
Symetric
Main Diagonal
x - Non Zero Terms
o - Zero Terms

Figure 6.2 Example of Matrix with Skyline

the solution have to be set as one-dimensional arrays, such as the load vector and displacement vector.

The efficiency of the method will be assesed later in this chapter.

6.2.3.2 Equation Solver

A basic disadvantage of the Gauss-Seidel iterative method to solve a set of linear equations is that the time of solution can only be estimated approximately, because the number of iterations required for convergence depends upon several factors. In nearly all cases, direct methods of solution, such as the Gaussian elimination method, are more efficient. For this reason the Gaussian elimination method was chosen and implemented in the INTERDAM program.

Since both methods have been extensively described in the past (see for example Bathe and Wilson, 1976) no further details will be presented.

6.3 JOINT ELEMENT

6.3.1 General

As mentioned before, the numerical modelling of interfaces using Finite Element techniques requires the use of a special element. This element allows the representation of slippage, separation and overlapping. These modes of deformation are generally not permitted in conventional elements. Several of these elements have been briefly described in Chapter 2.

Among them, the element proposed by Goodman et al (1968) was chosen. The reasons for adopting this element were:

1. Simplicity
2. Zero thickness
3. Compatibility with triangular element (constant strain triangle)

6.3.2 Goodman's Joint Element

As mentioned in Chapter 2, the element proposed by Goodman et al (op.cit.) uses the directional stiffness formulation. This method implies a restriction of the relative movement of a pair of nodes (one on each side of the interface), initially in contact (physically the same point). Its formulation follows step-by-step the methods proposed for solid elements and therefore its implementation into existing Finite Element programs is a simple task. The most important points of its formulation are presented in Appendix "G".

6.3.3 Zero Thickness Assumption

The choice between a zero or finite thickness joint element depends upon the particular case to be analysed. In general this choice can be restricted to the recognition of whether or not the joint can be assumed to have material inside it. For example, for the case of jointed rocks, joints initially in contact and not filled with soil should be well represented using zero thickness joint elements, whereas joints with soil fillings would be more realistically represented with finite thickness joint elements.

In studying soil-concrete interfaces the choice is, in most cases, not as simple. The discussion should concentrate on deciding whether or not the presence of the concrete structure influences the properties of the soil adjacent to the structure up to a limit where different properties should be assigned to this region. Furthermore, the extension of the affected area should be analysed. These two observations will define the thickness and properties of the nonzero joint element to be used.

For the case presently under consideration, it seems that a nonzero joint element is inappropriate, since visual inspection of samples removed from the large shear box apparatus have shown that the thickness of the material involved in the shear zone was negligible.

Although some nonzero thickness joint elements derived allow for large aspect ratios (ratio between the length of the sides of the elements), such as the **Thin layer element** (Desai et al, 1984), the thickness to be assigned to the element remains to be determined. According to these authors, a parametric study is necessary, since the definition of the most appropriate thickness is not an easy task.

6.3.4 Constitutive Matrix

The **Constitutive Matrix** for the joint element has been presented in an earlier chapter and is defined, in its most general form (not considering rotation) as:

$$[C_j] = \begin{bmatrix} K_{ss} & K_{sn} \\ K_{ns} & K_{nn} \end{bmatrix}$$

Most of the applications of Goodman's joint element (see Table 2.1, Chapter 2) assume that the off-diagonal terms K_{ns} and K_{sn} are equal to zero and dilatancy is not explicitly considered. Desai et al (1984) describe these parameters as "difficult to determine". For rock applications, Goodman and Dubois (1972) proposed a method, for field and laboratory use, to determine the **coupling terms** K_{ns} and K_{sn}.

From the remaining terms (K_{ss} and K_{nn}), the normal stiffness (K_{nn}) is determined arbitrarily in order to avoid overlapping of adjacent solid elements (Clough and Duncan, 1971, Desai et al, 1984). Values ranging from 10^{8} to 10^{12} units have been suggested for this term, although no logical basis exists for such an assumption. Parametric studies are recommended for each specific problem, using the available computer (the maximum acceptable value depends on the machine used, as will be discussed later).

For the case reported in this thesis, a parametric study has shown that the normal stresses converge rapidly to constant values if the normal stiffness exceeds 10^8 kN/m^3. It has also been found that beyond 10^{10} kN/m^3 numerical problems occur and the normal stresses vary at randon. It was decided to assume a value 10^9 kN/m^3 for this parameter.

Finally, the tangential stiffness (K_{ss}) must be defined. Its influence in the overall behaviour of the problem is remarkable and the finite element simulation has to be made with caution, as will be discussed later.

Neverthless, some methods of determining this parameter were included in the finite element program. In particular for the INTERDAM code, five methods were implemented and are described in Appendix "H".

6.4 TESTS FOR INTERDAM PROGRAM

6.4.1 General

In order to verify the procedures adopted and the efficiency of the program, three simple examples are presented in this section. Due to the unavailability of closed form solutions (exact solutions based on theory of elasticity) the examples were obtained using the finite element method.

6.4.2 Test for Implementation of Joint Elements

The mathematical procedure used to introduce joint elements in the program INTERDAM were tested in a simulation of a shear box test in a combined sample.

The soil mass was subdivided into finite elements and the concrete was represented by a rigid boundary as shown in Figure 6.3. The analyses assumed a nonlinear behaviour for the joint element and a linear elastic soil sample.

The parameters for the joint element were obtained from the results of two conventional shear box tests, as shown in Figure 6.3 (curves for σ_n = 15 kPa and σ_n = 45 kPa).

The simulation was performed by applying an incremental displacement and observing the shear stresses. The results of a Finite Element analysis performed for a normal stress of 30 kPa is also presented in Figure 6.3. In the same figure a curve obtained by linear interpolation between the two input curves is shown. The agreement between the finite element approximation and the interpolated curve is remarkable and supports the procedures used to incorporate the joint elements in the program.

6.4.3 Test for INTERDAM Code

The reliability in the INTERDAM program was tested using a classical limit equilibrium problem for a retaining wall. This example was inspired by similar test reported by Clough and Duncan (1971) for a program with a comparable capability.

The mesh used is presented in Figure 6.4 together with the properties assigned for both, the joint elements and the soil mass.

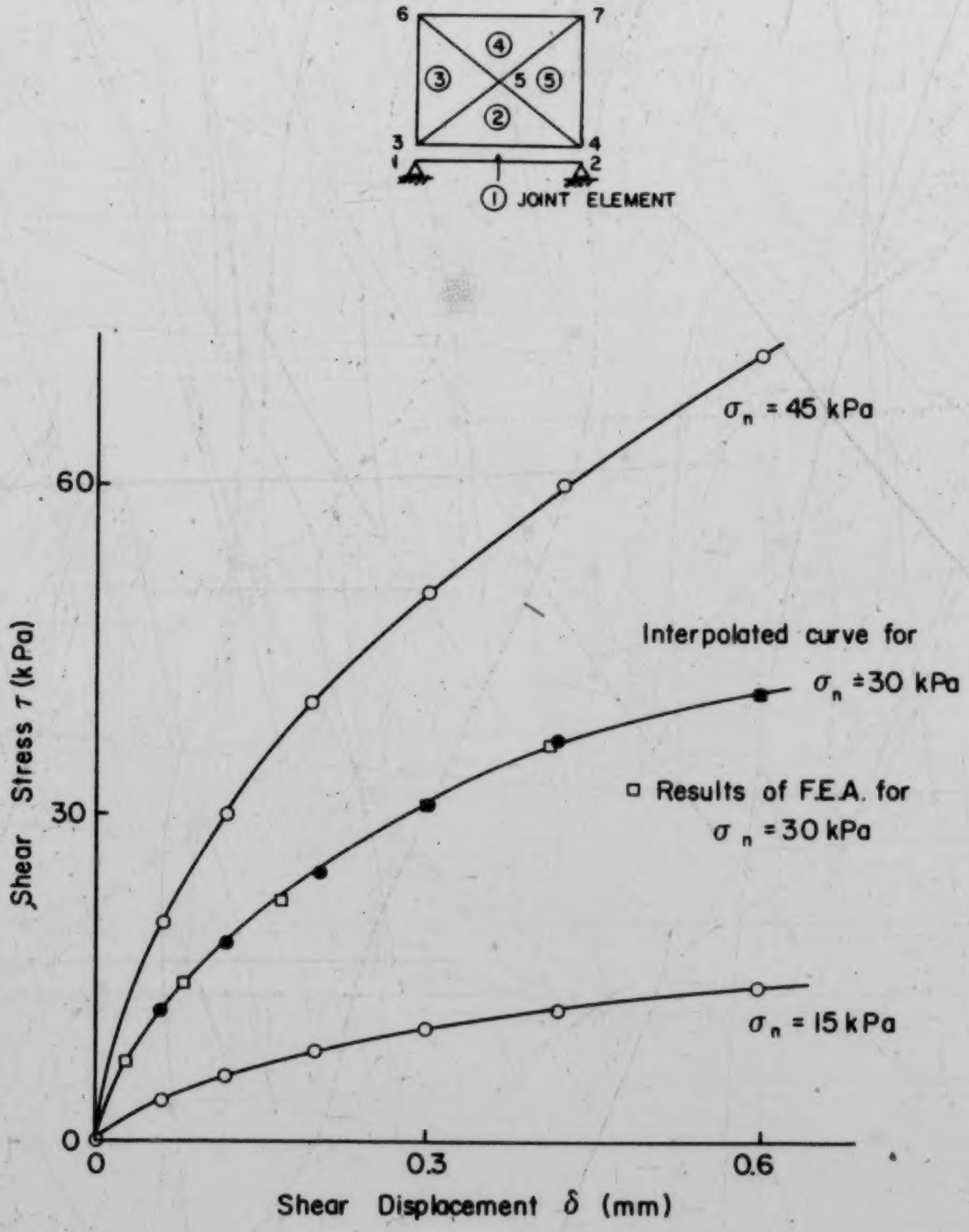

Figure 6.3 Input and Results of Shear Box Test Simulation

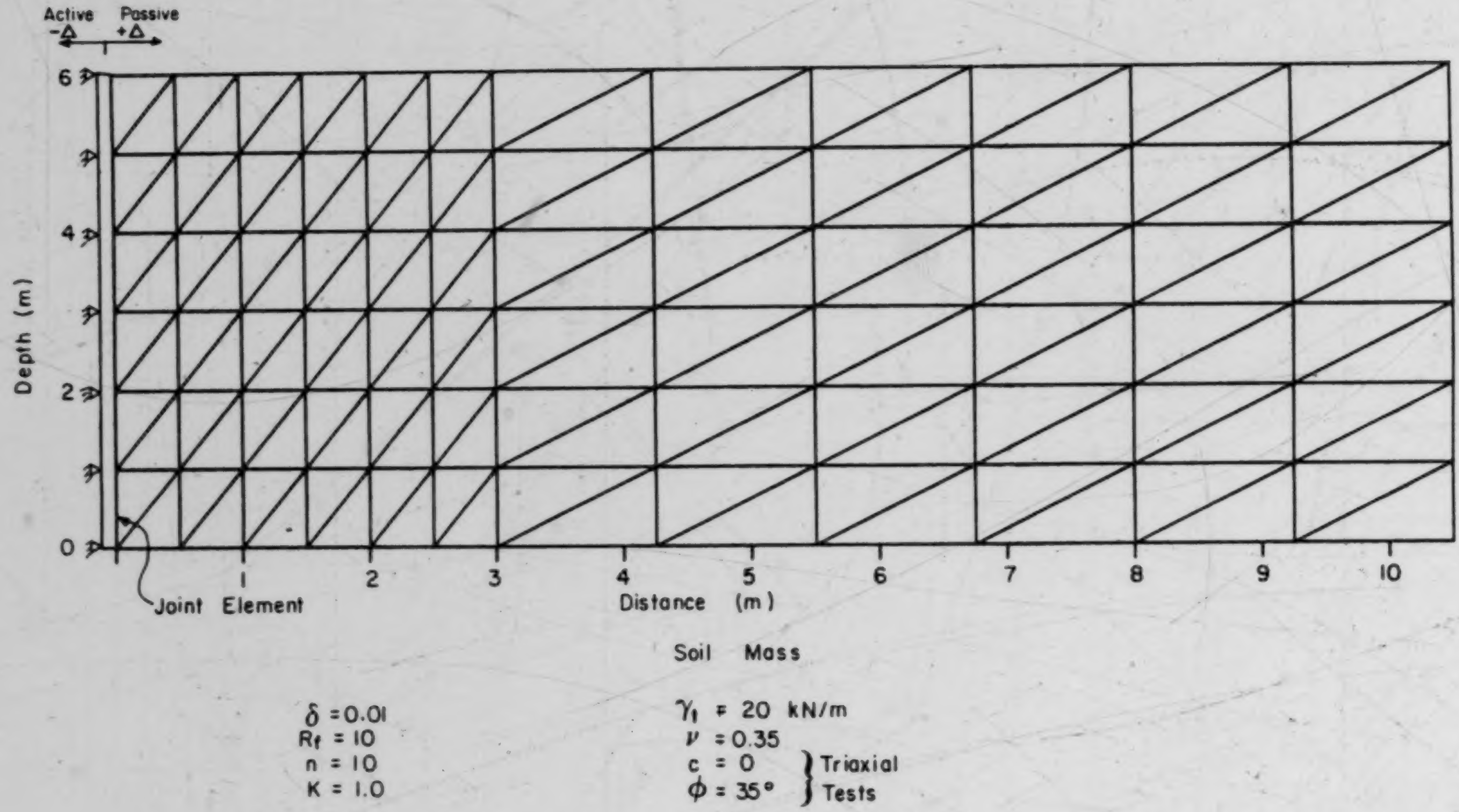
Active
−Δ
Passive
+Δ
6
4
2
0
Depth (m)
Joint Element
1
2
3
4
5
6
7
8
9
10
Distance (m)
Soil Mass
δ = 0.01
Rf = 10
n = 10
K = 1.0
γt = 20 kN/m
ν = 0.35
c = 0
φ = 35°
Triaxial
Tests

Figure 6.4 Mesh and Input Parameters - Tets for INTERDAM

The simulation was performed in two stages: in the first stage the fill was constructed in six identical layers. During this stage the wall was considered rigid. In the second phase translational movements were imposed on the concrete wall in order to develop active or passive conditions in two separate runs.

The resulting load-displacement curve is shown in Figure 6.5. In the same figure the values obtained using classical limit equilibrium solutions is shown.

It is important to note that the program does not incorporate any plastic model and therefore yielding can not be modelled. Neverthless, the shape of the curve resembles the expected results for the classical earth pressure theories and the extreme values are close to those obtained from the classical analyses. Furthermore, the results are very similar to those reported by Clough and Duncan (1971).

6.4.4 Efficiency of INTERDAM program

As mention in early sections, the methods of assembling and storing and the equation solvers were modified from the original FENA-2D code. The objective of these modifications was to reduce the execution time and consequently reduce the cost of the analyses.

To evaluate the gain in efficiency, the same problem was solved using both programs. The mesh was set as shown in Figure 6.6 and a total of eight runs were performed with increasing numbers of degrees-of-freedom.

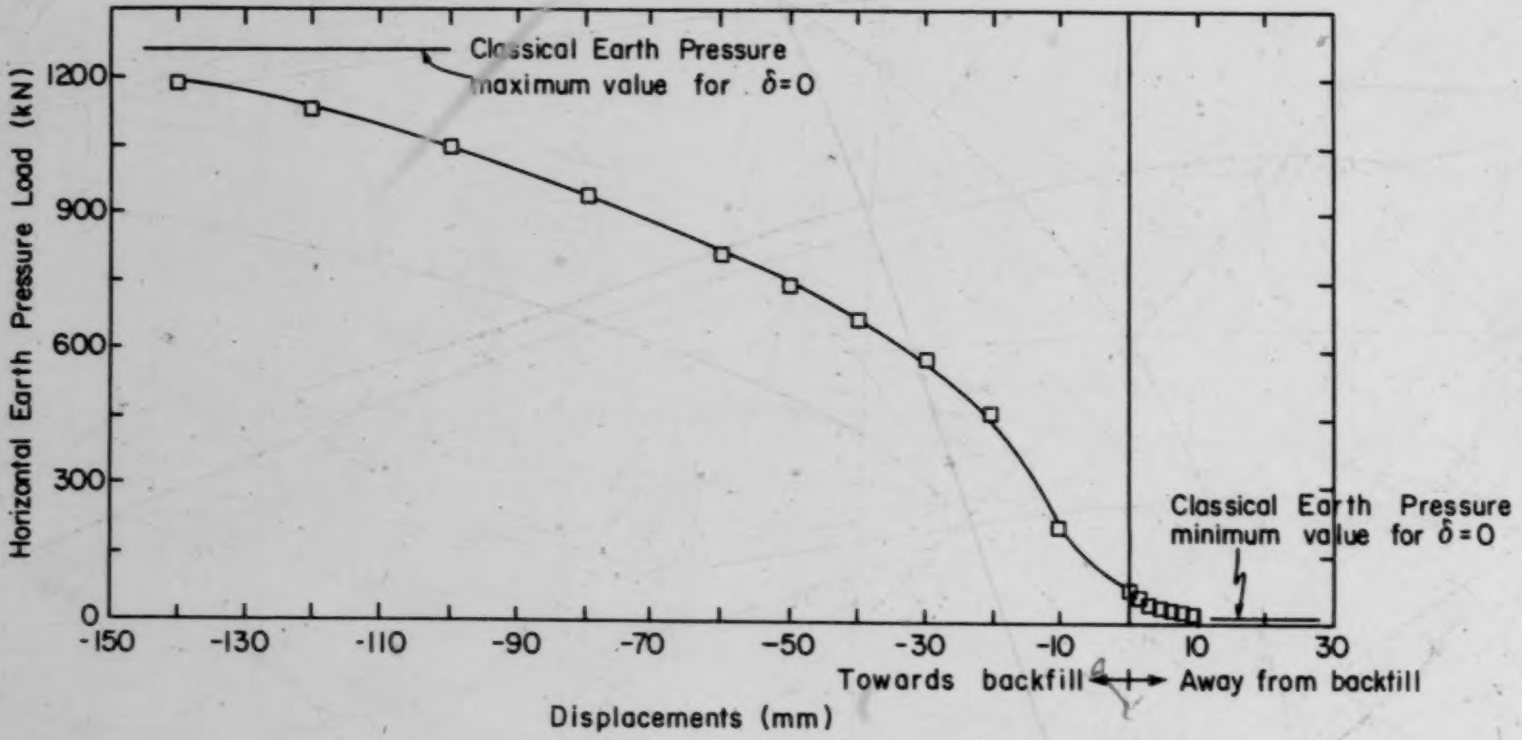

Figure 6.5 Results of Retaining Wall Simulation

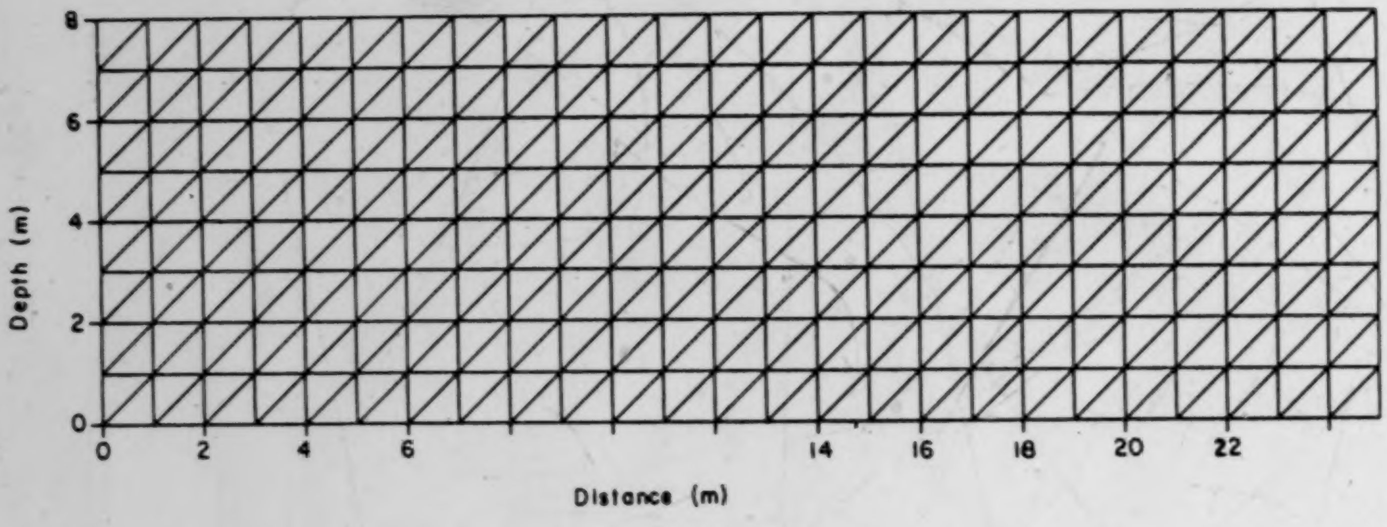
8
6
4
2
0
Depth (m)
0
2
4
6
14
16
18
20
22
Distance (m)

Figure 6.6 Mesh for Comparison Between INTERDAM and FENA-2D

The parameter used for this comparison was the CPU (Central Processor Unit) time recorded in two phases of the solution: immediately after assemblage and immediately after the equations were solved.

The results of this comparison are shown in Figure 6.7. It can be observed from these two curves that the assembly procedure used in the INTERDAM code is slower than the method used in FENA-2D. This is mainly caused by the necessity of generating a second matrix referred as the "addressing matrix" (Bathe and Wilson, 1976). However, the method of assembling permitted a more efficient storing scheme to be used (in a one-dimensional array) and consequently the entire procedure of assembling, storing and solving became considerably faster, as shown in the second curve of Figure 6.7. Furthermore, the assemblage procedure is only 25% more time consuming whereas the total solution represents up to 80% in savings, if the methods used in the INTERDAM code are adopted.

6.5 REVIEW OF THE MECHANICAL BEHAVIOUR OF WALL INSTRUMENTS

Most of the analyses performed in this chapter were intended to compare the results of the numerical solution with the field measured values. Therefore, it is imperative to judge which measurements are comparable.

For the numerical simulation, the input parameters for the joint elements were obtained from the results of direct shear box tests.

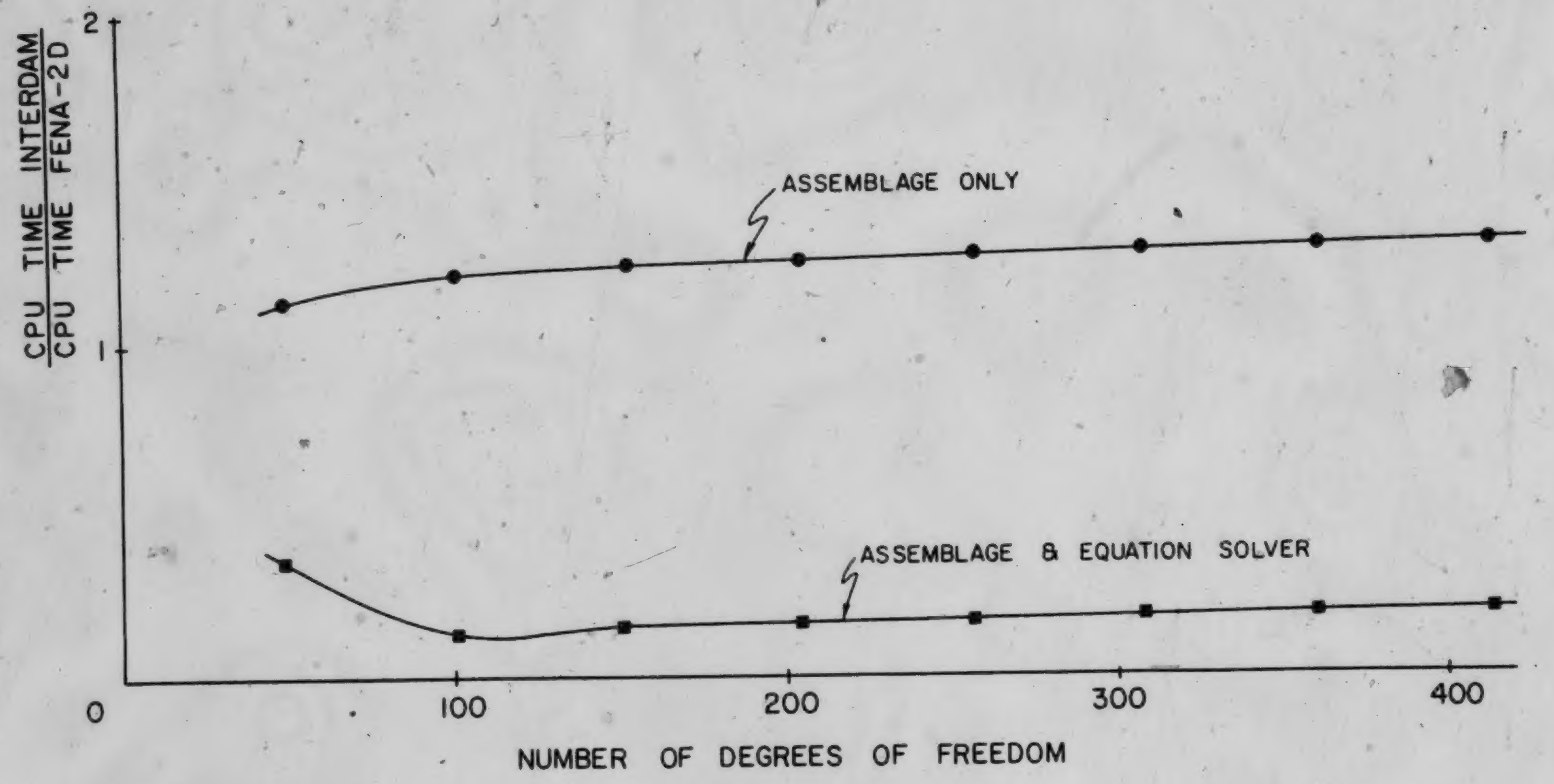

Figure 6.7 Comparison Between INTERDAM and FENA-2D

The use of these tests have been discussed in Chapter 5, section 5.5, and it was concluded that the tangential stiffness is a consequence of the geometry of the test and is influenced by the longitudinal compression. Therefore, only the instruments, used in the test embankment, influenced by similar effects, are comparable with the numerical results. Hence it is important to reanalyse these instruments, from this point of view, to identify which results can be used in this comparison.

Shear Stress Devices

As described in Chapter 3, the Shear Stress Device, designed to measure the development of shear stresses at soil-concrete interface, is composed of a 30 cm long concrete block resting on two load cells placed inside a knock-out molded in the concrete structure. With this configuration, the values registered by the load cells are the average forces acting on the concrete block and the instrument is not able to detect any concentration of stresses that occur in the sensor area. Therefore, these readings are definitely influenced by longitudinal compression.

Shear Displacement Devices

This instrument is composed of two steel plates, one bolted to the concrete structure and the second embedded in the soil. A LVDT is placed connecting these two plates and their relative movement is assumed to represent the relative movement between the soil and the structure.

Since the plate embedded in the soil is relatively thinner than one layer of soil, the displacements registered by the LVDT correspond to the movements of the soil immediately underneath the plate, and it is the displacement of a localized point. Therefore, regardless of any compression occuring in the material overlying the plate embedded in the soil, the measurements will respond to the movements of this localized point.

Therefore, it is expected that the trends in the shear stresses from the field instrumentation should be better reproduced than the trends from shear displacements.

Furthermore, the above discussion suggests that the joint elements should have the length of the shear box test used to obtain the input parameters. With this restriction both the shear stresses measured in the field and obtained in the finite element analysis would be equally influenced by the longitudinal compression.

6.6 ANALYSES OF TEST EMBANKMENT

6.6.1 General

In this section the back analyses of the Test Embankment, using the finite element method, will be presented. The aim of these analyses is to reproduce, numerically, the behaviour of the field instrumentation and to assess the usefulness of the method to predict the behaviour of interfaces. Therefore, the measurements at and in the neighbourhood of the concrete wall are of primary interest.

6.6.2 Finite Element Mesh

The mesh used in the analyses is presented in Figure 6.8. Some important comments regarding this mesh are:

1. The mesh is considered a "coarse" discretization.

In finite element techniques, the finer the grid of elements, the closer is the solution to the exact answer. However, by increasing the number of degrees-of-freedom the cost of each analyses increases in a similar proportion. Since it was desired to perform a parametric study, the use of a large mesh would not allow several runs due to the cost involved.

2. Finer local discretization.

The mesh was drawn primarily to study the interface behaviour. Therefore, in this area smaller elements were assigned.

3. Regions not included in the analyses.

Due to the lack of information of the properties of both the material existing behind the wall and the foundation material, these two areas have been excluded from the analyses.

4. Size of joint elements.

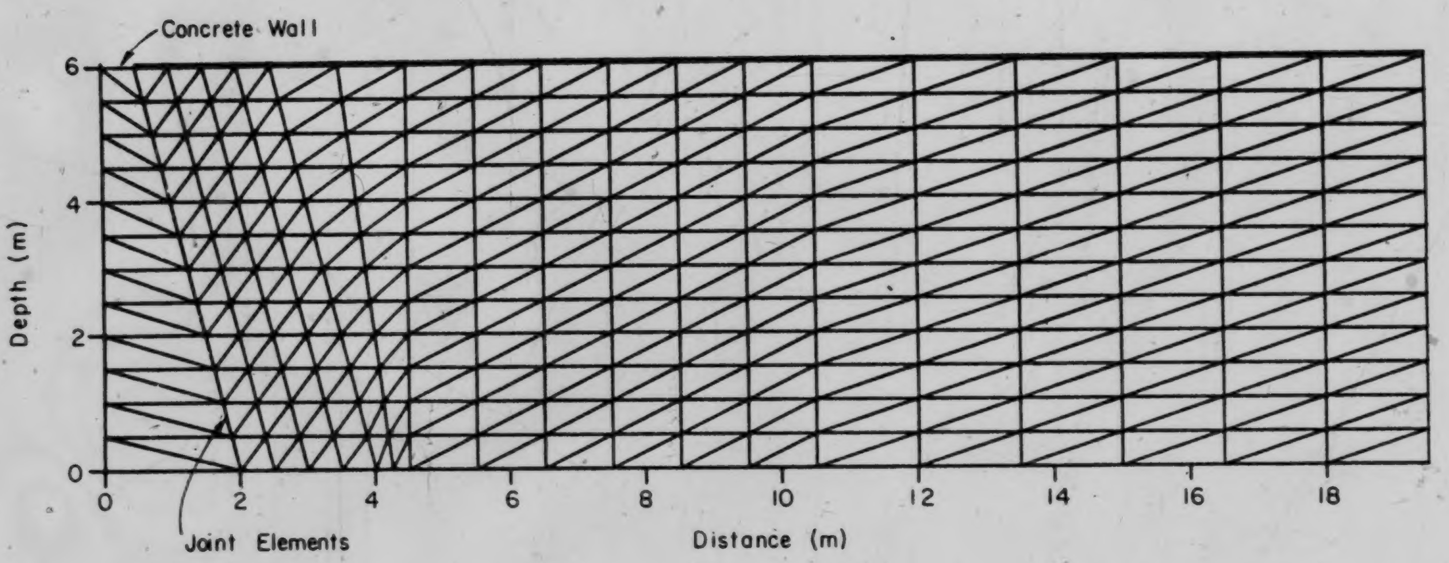
Concrete Wall
Depth (m)
6
4
2
0
0
2
4
6
8
10
12
14
16
18
Joint Elements
Distance (m)

Figure 6.8 Finite Element Mesh - Test Embankment Backanalyses

The joint elements are excessivelly long. As mentioned, ideally the joint elements should have a length equal to the tests used to determine the tangential stiffness.

However, the mesh to accomodate such small joint elements (6 cm long) would be considerably larger than that shown in Figure 6.8, and parametric studies would not be feasible.

6.6.3 Method of Simulation

The analyses of the test embankment was performed in fourteen steps. As pointed out by Clough and Duncan (1969), analyses in steps nomally yield better results than single-step "turn-on" gravity methods.

Therefore, the first step included the construction of the concrete wall (concrete was assumed to be linear elastic). From steps two through thirteen, twelve 0.5 m thick layers were placed completing the 6 m high test fill. Step fourteen was introduced to incorporate a suggestion proposed by Duncan et al (1980). According to those authors, the placement of a layer of soil is better represented by applying nodal forces, equivalent to the weight of the overlaying material, rather than by "switch-on gravity" method. To accomplish this, the layer being placed was assigned very small elastic properties to simulate the loads applied in the existing material. At the end of the calculation, the newly placed layer will have their (nodal) displacements and (element) strains zeroed.

On the other hand, it was observed that if the tangential stiffness of the joint element being introduced was not set to reduced values, high tension was created in the soil near the structure. This tension was caused by the excessively high degree of straining inside the elements adjacent to the wall, for early stages of loading. It is believed that this tension is a simulation effect rather than a physical phenomenon. Therefore, for each joint element entering the analyses, very low tangential stiffness was assigned.

It is important to note that, if the values of the elastic constants and/or tangential stiffness are reduced during the placement of a particular layer, the last step of construction would have zero displacements and strains. Therefore, it is necessary to finalize the analyses with a "dummy layer" with no weight to allow the last row of elements to have their displacements and strains determined. This is the fourteenth step.

6.6.4 Boundary Conditions

Due to the lack of parameters, the finite element mesh did not include the entire region affected by the test embankment and the material existing behind the wall and the foundation were ommitted. On the other hand, the discussion presented in Chapter 2 demonstrated that the presence of these two materials had a definite influence on the overall behaviour of the fill and the interface. Therefore, numerical analyses representative of both the behaviour of the interface and the behaviour of the fill, would only be possible if the entire region was discretized in the finite element mesh. In order to overcome this problem several possibilities have been considered such as:

- Use of a trial method to calibrate the parameters for these materials by matching the instrumentation measurements. This would probably lead to an endless procedure, primarily due to the nonhomogeneous characteristic observed in the foundation (see discussion in Chapter 2).
- Impose displacement boundary conditions along the fill-foundation interface and concrete wall rotations, based upon measurements. This method allowed the displacements inside the fill to match the measured values, but created a large zone of tension near the soil-concrete interface. As discussed in section 6.6.3, it is not believed that high tension had occurred in the test fill and again this high tension seems to be a consequence of the method of simulation (boundary conditions.

Therefore, it was decided to concentrate the analyses on the interface behaviour and fixed boundaries were imposed for the foundation of the fill. The concrete wall was allowed to move in both direction, but no displacements were imposed.

6.6.5 Back Analyses of Interface Behaviour

6.6.5.1 General

In order to analyse the influence of some factors on the results of stresses and displacements at the wall, the back analyses were performed as parametric studies.

These parametric studies comprised eleven runs with varying properties for both the joint elements and the soil mass. A summary of the properties used is presented in Table 6.1.

The major objective of this study was to demonstrate the influence of:

a. Comparison between linear versus nonlinear analyses

b. Variations in elastic properties for joint elements and soil mass

c. Method of sample preparation for shear box test

For the study of the "type of analyses" (item "a" above) four runs were performed as listed below:

Case #	Joint Element	Soil Mass
1	Linear	Linear
2	Linear	Nonlinear
3	Nonlinear	Linear
4	Nonlinear	Nonlinear

For cases 3 and 4 the parameters were obtained from results of the series 200 shear box tests and the "digital

Table 6.1 Summary of Parametric Study of Test Embankment

TABLE 4

CASE #	JOINT ELEMENT	SOIL MASS	
	Kt (kPa)	K (kN/m^2)	G (kN/m^2)
1	30000.0	7200.0	2400.0
2	30000.0	varies (triaxial)	
3	varies (series-200)	7200.0	2400.0
4	varies (series-200)	varies (triaxial)	
5	10000.0	28800.0	9600.0
6	10000.0	7200.0	2400.0
7	45000.0	7200.0	2400.0
8	varies (series-100)	7200.0	2400.0
9	varies (series-200)	7200.0	2400.0
10	0.00000001	7200.0	2400.0
11	100000000.0	7200.0	2400.0

method" for joint elements was used (see Appendix "I").

The influence of variations in the elastic properties for the joint elements and soil mass was studied in three runs. In all cases the interface and the soil mass were assigned linear elastic properties. The parameters for these runs are summarized in Table 6.1 and they were labelled Cases 5, 6 and 7.

Subsequently, the effect of the method of sample preparation was studied to support the discussion presented in Chapter 4 (section 4.2.2). For this purpose, in two different runs, the joint elements were assigned nonlinear properties and the input data obtained from series 100 and 200 conventional shear box tests. These cases are referred as Cases 8 and 9 respectively (see Table 6.1).

Finally the effect of the presence of joint elements was assessed using two extreme cases: first, the boundary between the soil and the concrete was free to move in the tangential direction (simulating a "full slip" condition). In the other extreme the same nodes were fixed in the concrete wall simulating a "no slip" condition. This cases are referred as Cases 10 and 11.

In terms of the finite element analyses, these two conditions were imposed by assigning extreme values for the tangential stiffness of the joint elements. Therefore, the full slip condition was simulated by assigning zero stiffness for the joint element and the no slip, by assuming an infinite stiffness. This procedure presented some drawbacks and will be discussed later in this Chapter.

6.6.5.2 Linear versus Nonlinear Analysis

The results of these analyses is presented in Figures 6.9 through 6.11.

In Figure 6.9 the normal stresses acting on the concrete wall are plotted versus the height of the wall. It is observed that the type of analyses does not influence the normal stress results and all four runs plot in a narrow band. This result was expected since the off-diagonal terms of the stiffness matrix of the joint element have been neglected. Therefore, the shear displacements do not influence the normal stresses and vice-versa (see section 6.3.4).

The same figure presents the pressure distribution for "at rest" and "active" conditions, calculated according to the classical earth pressure theories. Note that the lower half of the wall is subjected to normal stresses higher than the "at rest" pressures whereas the upper half the results are lower than the "at rest" condition. This trend suggests that stress tranfer is occurring and stresses are concentrating near the base of the wall.

Furthermore, the values measured in the field are also presented. These points are in acceptable agreement with the results of these four analyses, except for the center instrument. As discussed in Chapter 3, most likely this instrument suffered from a poor installation

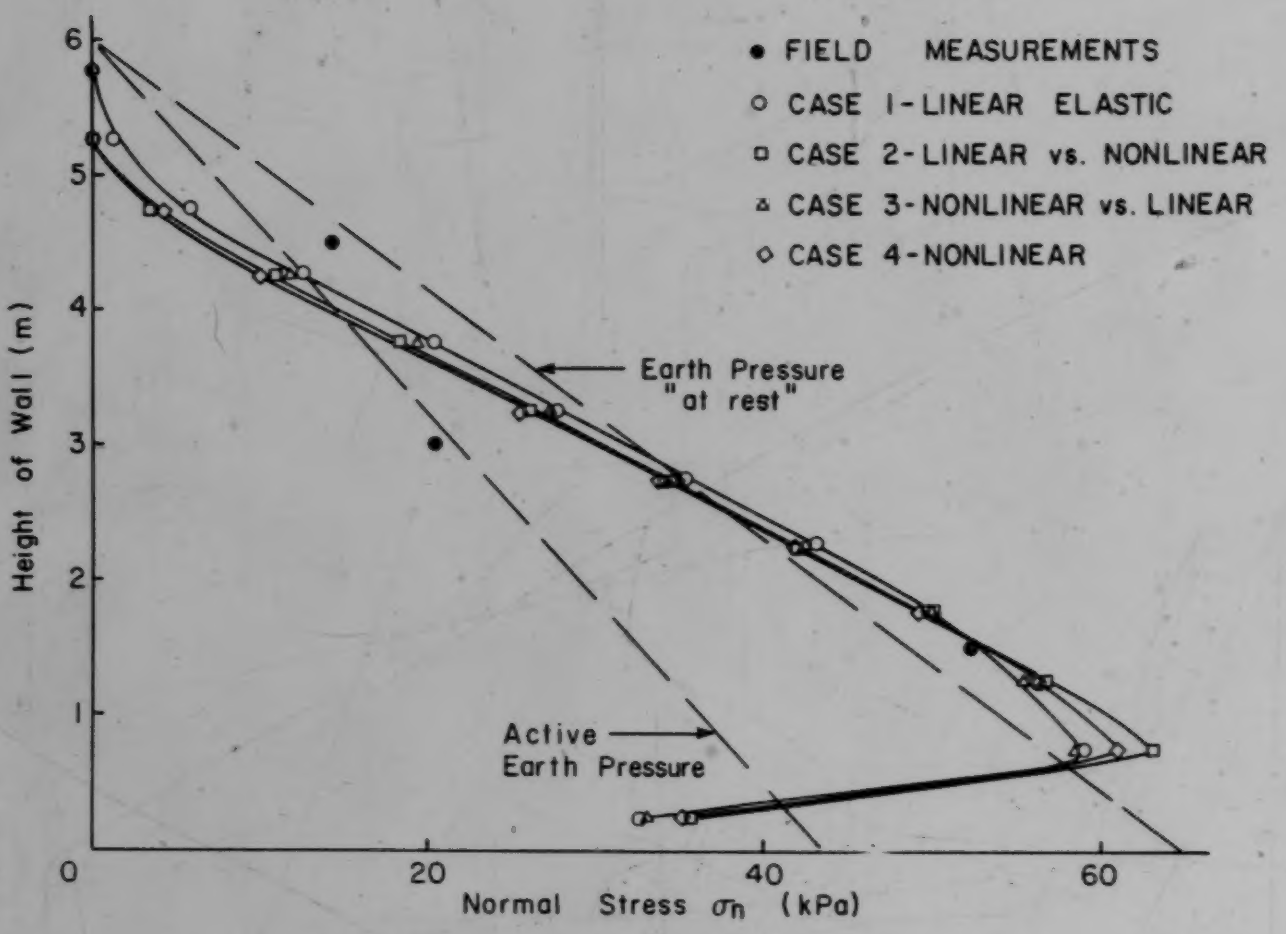

Figure 6.9 Back Analysed Normal Stresses Acting at the Wall

and therefore, these results are questionable.

Figure 6.10 presents the shear displacements obtained in the numerical simulation. Two distinct trends can be observed in this figure: when the joint elements were assumed to behave linearly (irrespective of the assumption made for the soil mass) the displacements showed a maximum value immediately below the center of the wall. For joint elements with nonlinear constitutive laws, this maximum value occurred near the upper one third of the wall.

Although the back analysed and measured displacements are of similar order of magnitude, the nonlinear analysis seems to reproduce the observed trends. However, as discussed previously, the instrument designed to measure these displacements is not affected by the longitudinal compression, and therefore better agreement should not be expected.

On the other hand, although the shear displacements are not the same for all four analyses, the shear stresses seem not to be affected by the assumption made. This can be seen in Figure 6.11, where the results of the shear stresses are plotted versus the height of the wall. In this figure the field values are also presented. It is observed that, in all cases, the numerical analyses tend to underestimate the shear stresses near the center of the wall and overestimate these values for the two extremes of the structure.

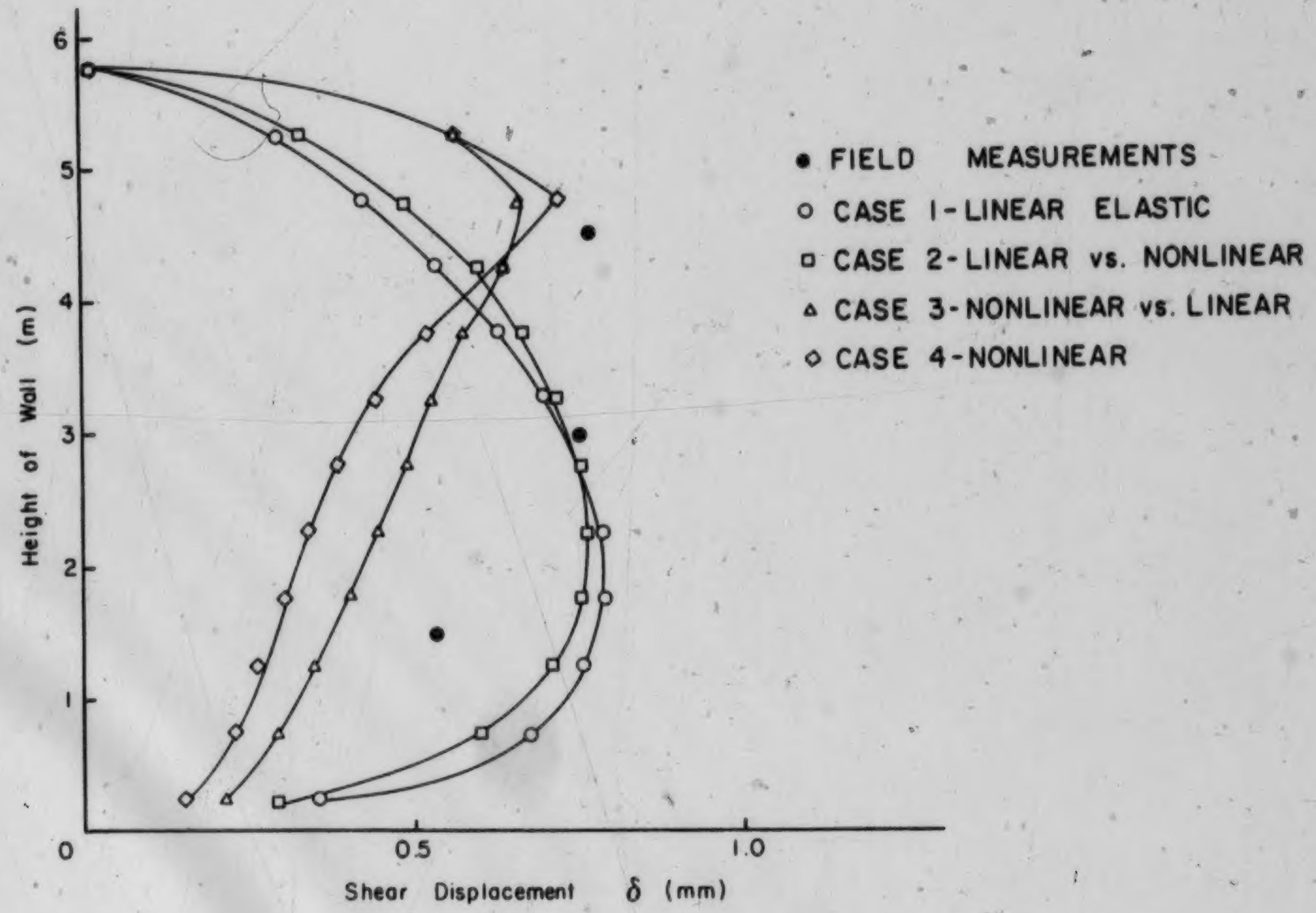

Figure 6.10 Back Analysed Shear Displacements

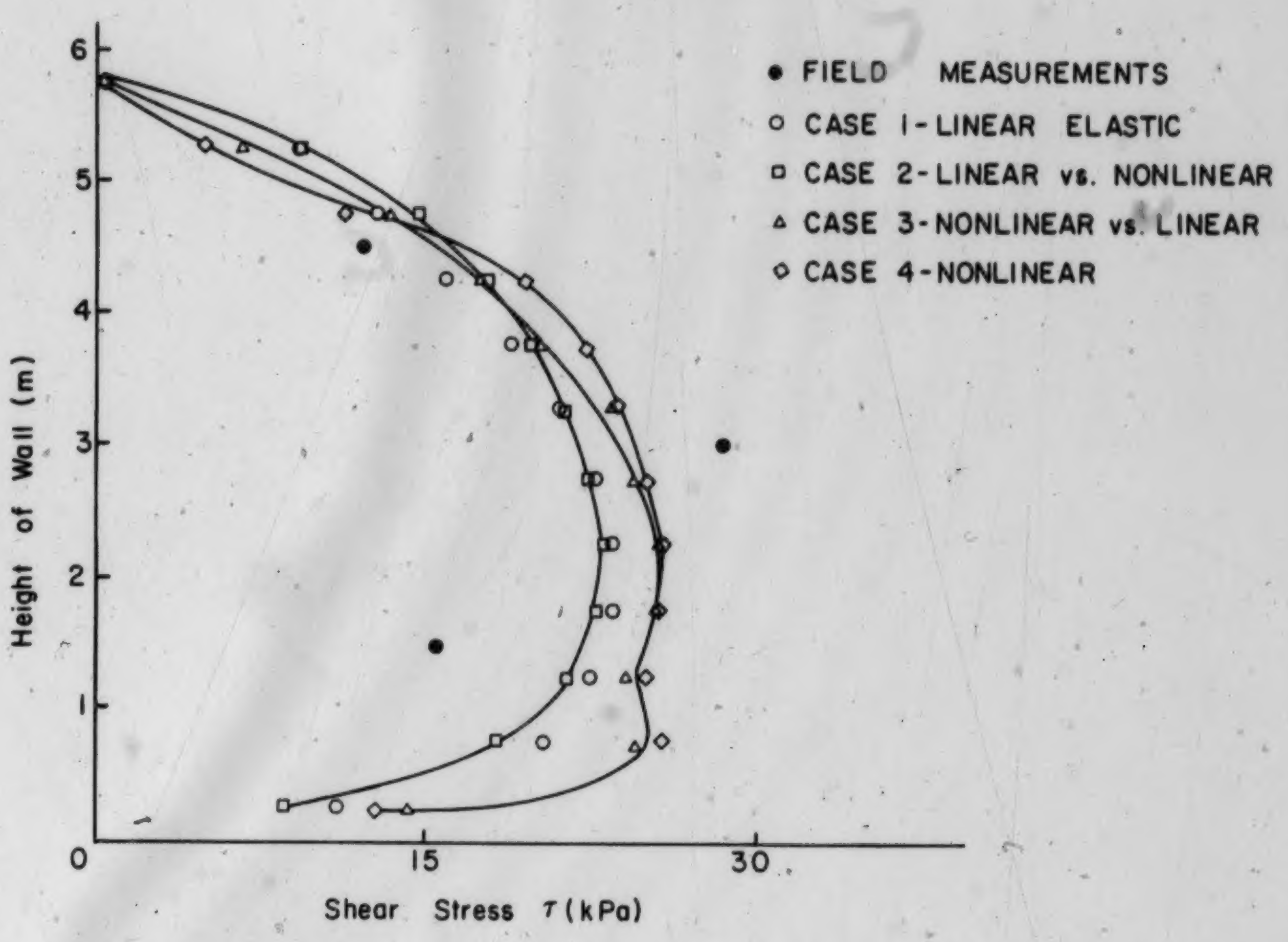

Figure 6.11 Back Analysed Shear Stresses

Neverthless, the trends are similar.

The insensitivity of the shear stress to the type of analyses can be explained if the expression used to determine these values is recalled from section 6.3.2. It was shown that the shear stress is a response of a shear displacement as follow:

$$\tau = K_t \times \delta$$

where:

τ - shear stress

K_t - tangential stiffness

δ - shear displacement

If the value of K_t is increased, the nodal displacements will decrease proportionaly, but the product of the stiffness and the displacement will remain almost unaltered. This effect is discussed further in the next section.

6.6.5.3 Effect of Variations in the Elastic Parameters

In this section three linear analyses are presented to evaluate, in more detail, the final comment of the previous section. Hence, the parameters for the joint elements were varied for two different runs and the soil parameters maintained unaltered. Subsequently the joint element stiffnesses were kept constant and the soil parameters changed to account for this effect. The results are presented in Figures 6.12 through 6.14

First, Figure 6.12 presents the results for normal stresses. Similar to the previous study, the effect is negligible for both cases (constant joint element properties or constant soil properties).

The shear displacements are shown in Figure 6.13 and it can be observed the variations in both, the soil constants or the joint element constants influence the results. However, the influence of variations in the joint element parameters is more pronounced and an increase of 4.5 times in tangential stiffness can reduce the displacements up to 80%.

However, as can be observed in Figure 6.14, the influence on the shear stresses is more sensitive if the soil parameters are changed. This is again expected since variations in these constants will impose different displacements for constant values of K_t, and therefore, the shear stress ($\tau = K_t \times \delta$) will vary.

The variation observed in the shear stresses for varying soil parameters are in perfect agreement with the discussion presented in section 5.5 and support the example presented in the introductory discussion of the mechanical behaviour of interfaces (section 1.3). It was stated that the shear stresses developed at soil-concrete interfaces should change if the materials of the mating bodies change (for the same state of stress). On the other hand the fact that the shear

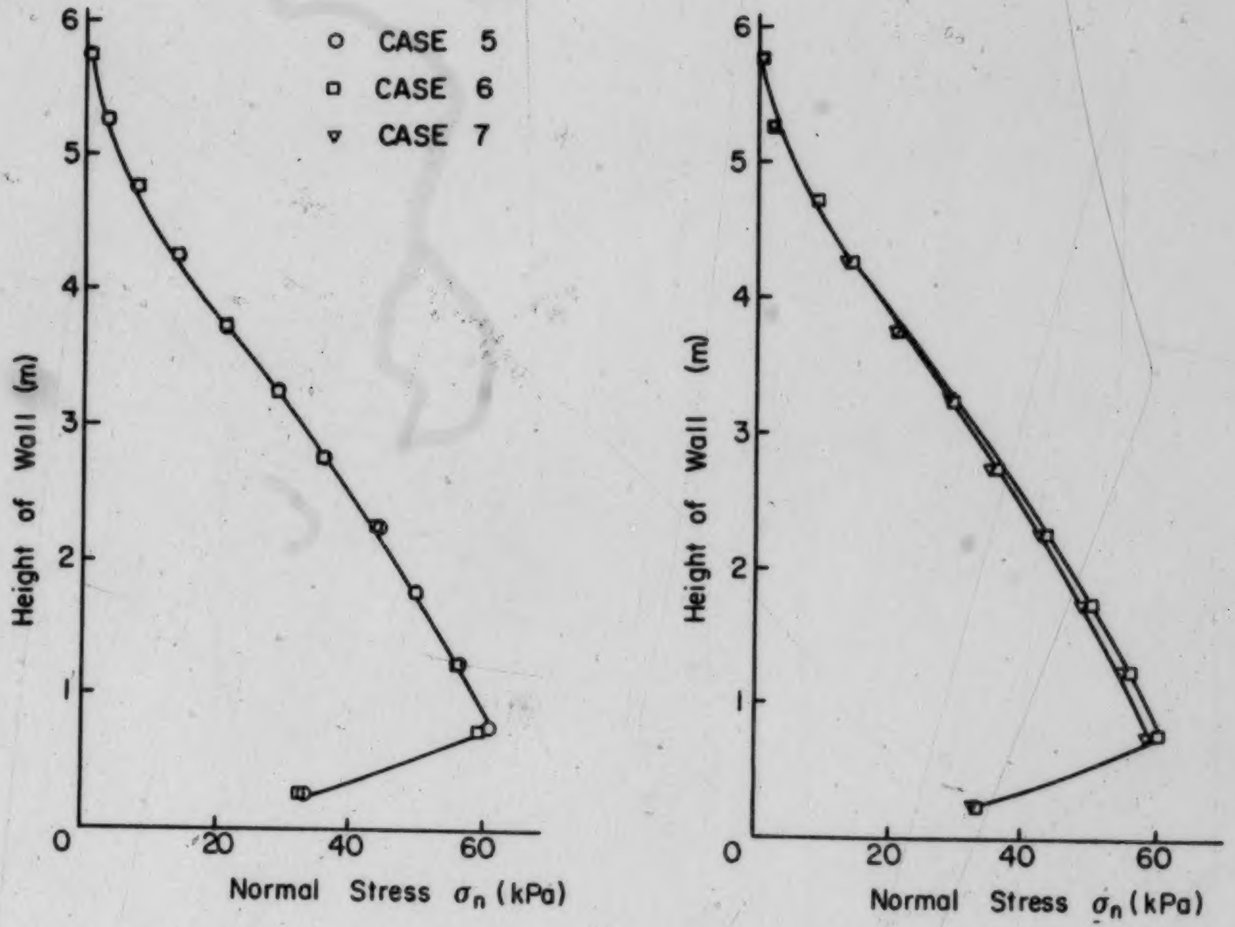

Figure 6.12 Effect of Variation of Elastic Parameter - Normal Stress

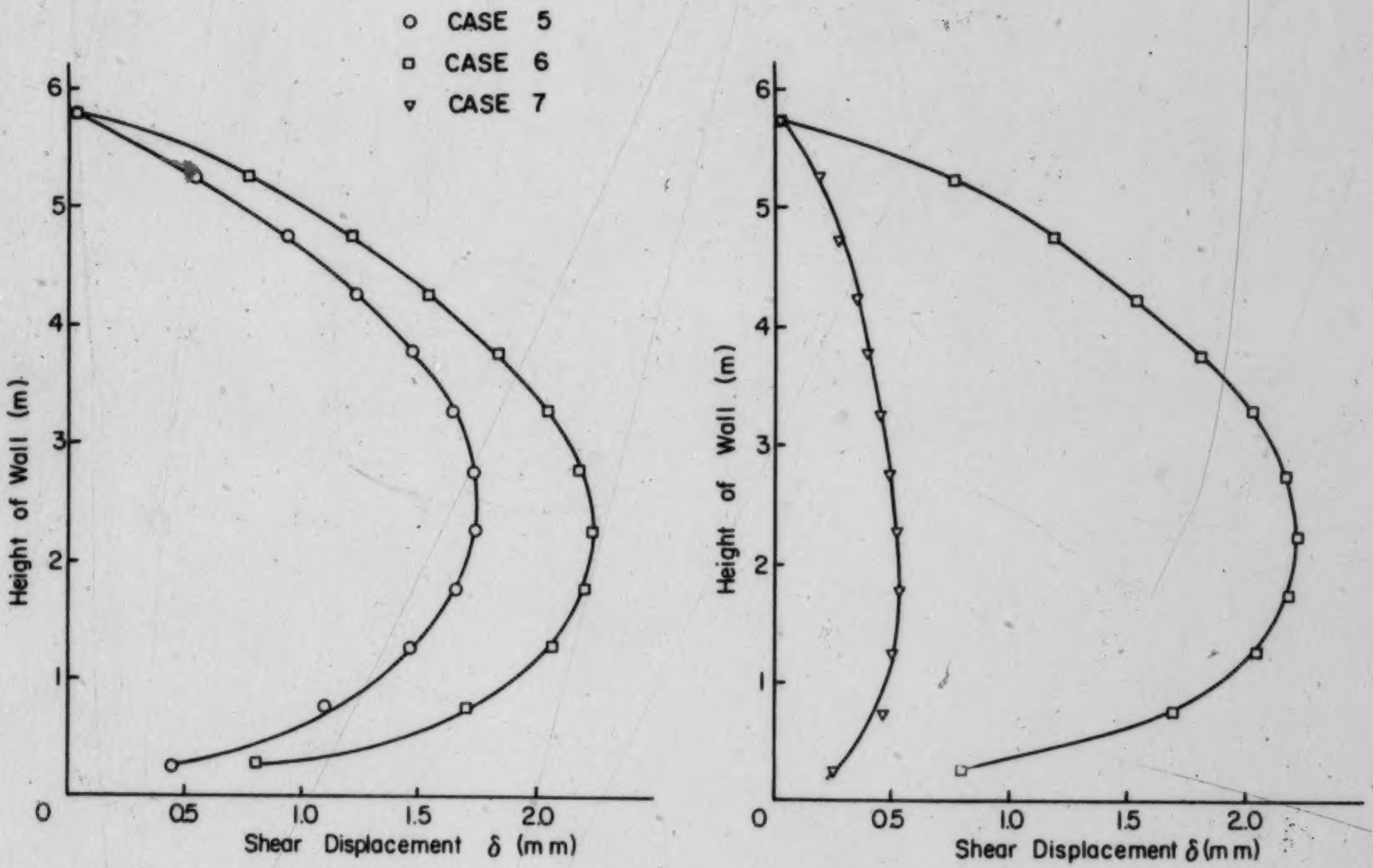

Figure 6.13 Effect of Variations of Elastic Parameters - Shear Displacements

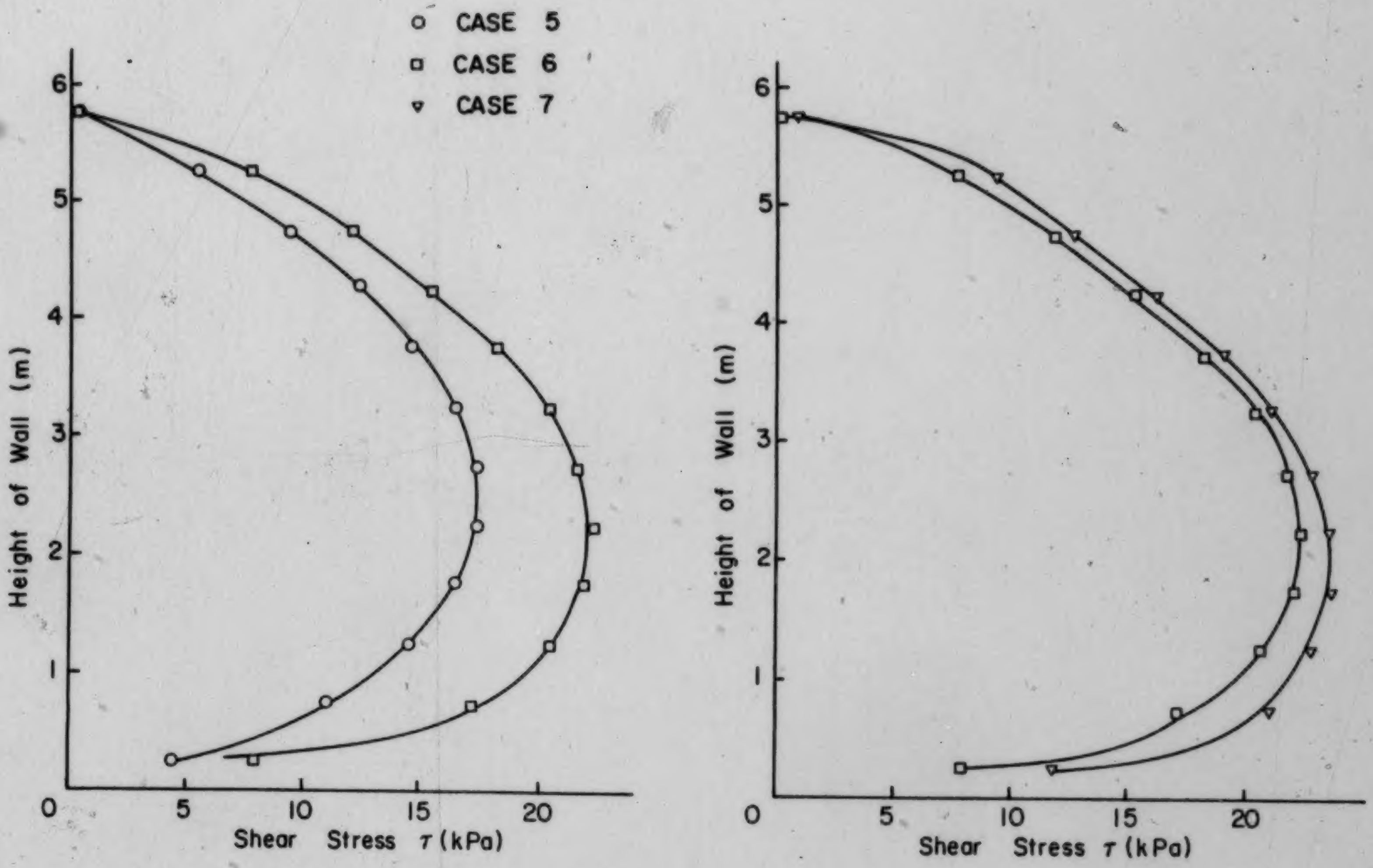

Figure 6.14 Effect of Variations of Elastic Parameters-Shear Stresses

stresses develop only as a response to a shear displacement is against this point of view.

6.6.5.4 Effect of Method of Sample Preparation

The results of the conventional direct shear box tests, presented in Chapter 4, are influenced by the method of sample preparation. In that chapter two methods were described and grouped into tests series 100 and series 200 (section 4.2). In the same section one possible displacement-path for a particle of soil being compacted near the wall was discussed. It was concluded that either of the two methods of sample preparation were not capable of closely reproducing the field condition. If these two series of tests are used as input for the finite element analyses, most likely the actual field behaviour will be between the results produced by these two boundaries.

In order to proceed with this discussion, the stress-displacement curves obtained in both series of tests were used as input for two different analyses. For series 200, the strain-softening behaviour was replaced by an almost zero stiffness after peak strength.

The results of the shear displacements from these analyses are shown in Figure 6.15. and it can be seen that the actual behaviour is somewhere between these two methods of sample preparation. Moreover the results suggest that series 200 tend to produce a better approximation. As expected, the shear stresses are

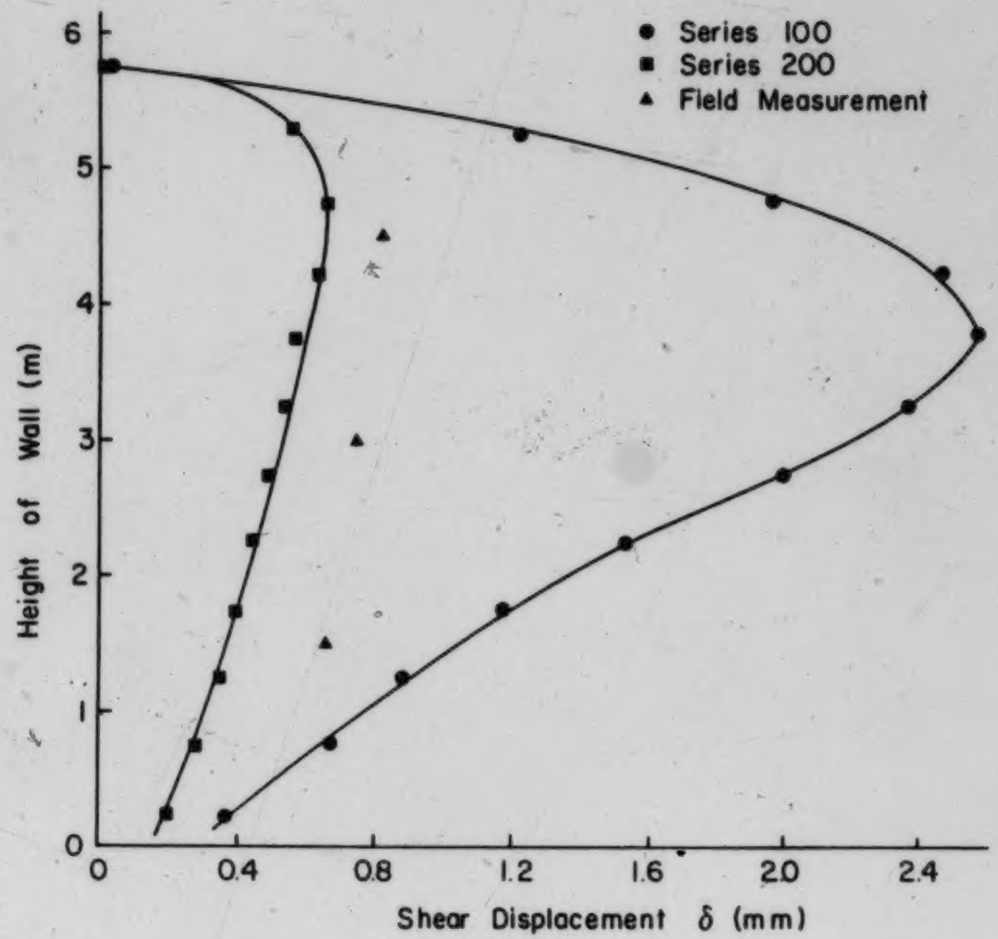

Figure 6.15 Effect of Sample Preparation - Shear Displacements

almost identical regardless of the method of sample preparation.

These results also support the theory discussed in Chapter 5, since the tests under series 200 present higher stiffnesses prior to failure and therefore are a better representation of the "no slip" condition (rigid behaviour).

6.6.5.5 Full Slip and No Slip Conditions

The analysis of soil-concrete interfaces can be performed for two extreme conditions. In one extreme the interface is considered to be "perfectly smooth" and no shear stresses develop. Relative movements between soil and concrete are free ("full slip" condition). At the other extreme, the interface is said to be "perfectly rough" and relative displacements are not allowed ("no slip" condition).

The use of the tangential stiffness (K_t), as defined in previous chapters, implies an intermediate condition, where some displacement can occur and, as a consequence, shear stresses will develop.

The simulation of these conditions was performed as an extreme case of the trend shown in the last section, and the analysis was performed with extreme values of the tangential stiffness. For the full slip condition the tangential stiffness was set equal to 10^{-8} kN/m^3 and for the no slip case this parameter was set equal to 10^{8} kN/m^3. The results are presented in Figures 6.16 and

6.17. The same figures show the field observed values.

The shear displacements, depicted in Figure 6.16, demonstrate once again that the assumption of infinite stiffness prior to failure seems to better represent the field behaviour. However, the no slip condition underestimates the displacements, probably because failure was not considered. If, however, for stresses higher than the maximum shear strength of the interface, the value of K_t was set at a very low value, higher displacements would have been obtained. This procedure is further detailed in later section.

In Figure 6.17, the shear stresses are plotted versus the height of the wall for the no slip condition (the other extreme implies zero shear stress). These values are identical to those obtained in the linear analyses, referred as Case 1 (Figure 6.11).

In conclusion, most of the cases reported in these sections tend to support the rigid-plastic behaviour proposed in Chapter 5 to represent the behaviour of soil-concrete interfaces.

However, it is important to realize the drawbacks in the procedure used to represent these two extreme conditions discussed in the last section (full slip and no slip). First, in some computers, the maximum possible value to be assigned to K_t may not be high enough to effectively simulate an infinite stiffness ("no slip" condition).

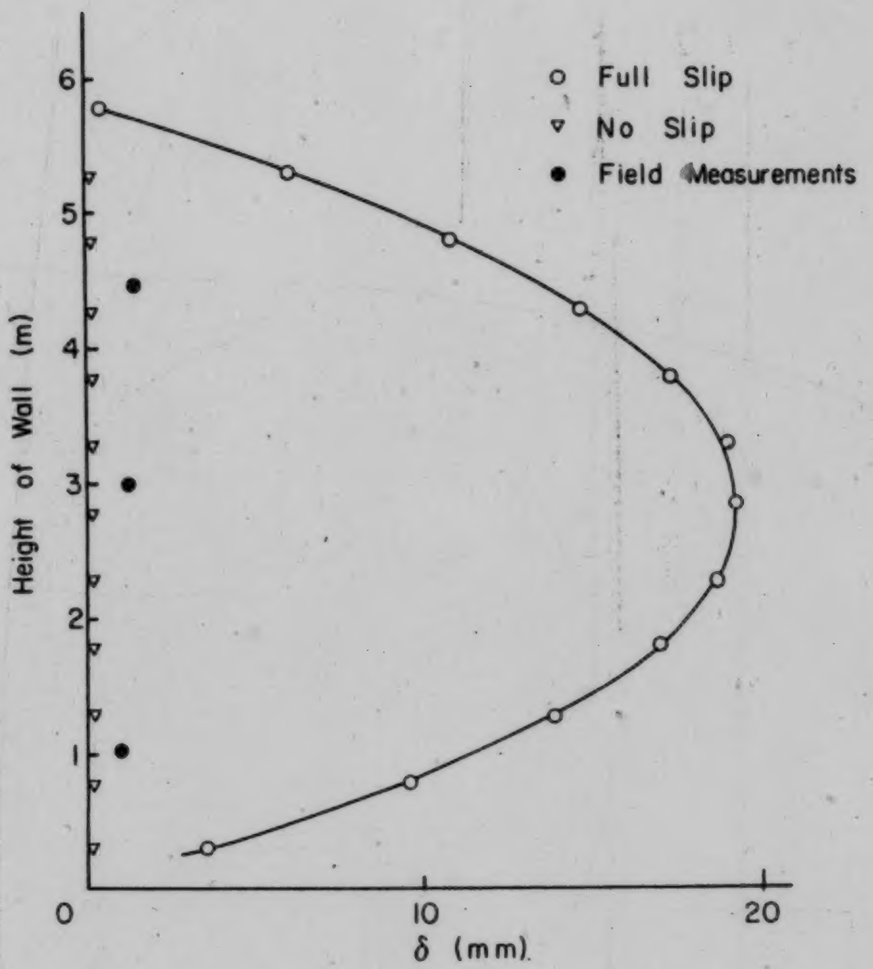

Figure 6.16 Shear Displacements - Extreme Conditions

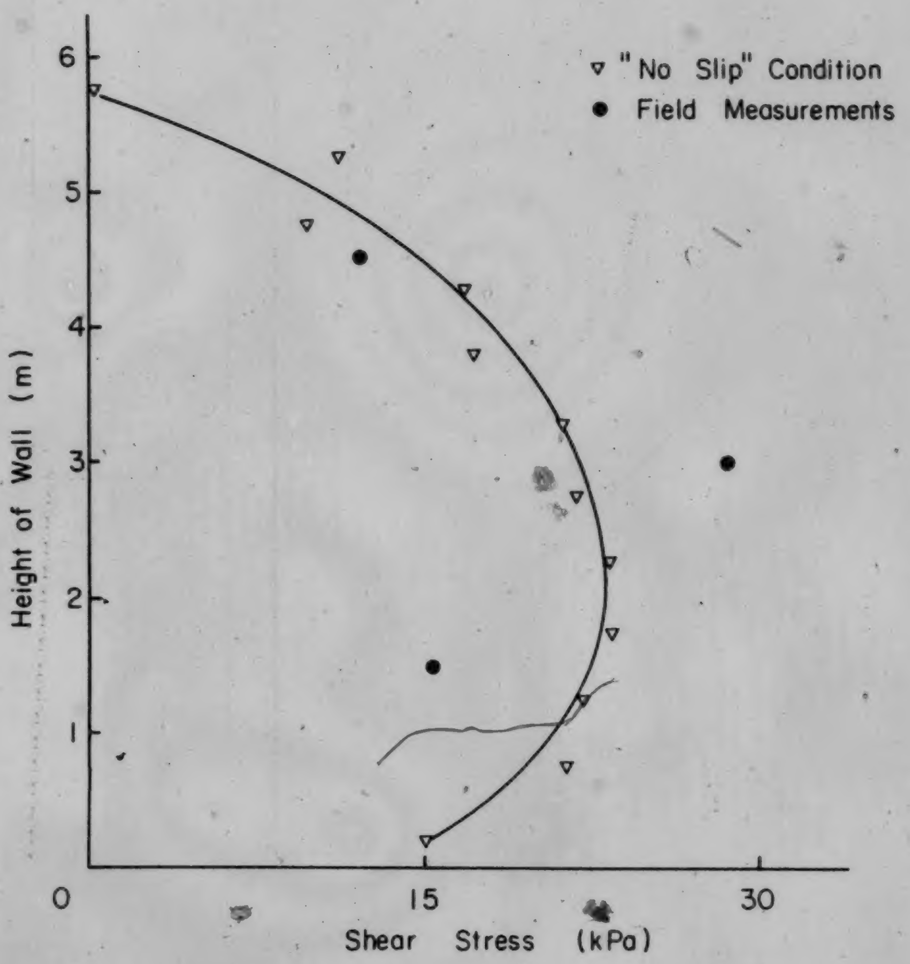

Figure 6.17 Shear Stresses for No Slip Condition

Second, and most important, by assigning an extremely high value to the tangential stiffness, numerical problems can arise. This potential problem is due to large terms in the stiffness matrix. These high values can numerically overshadow the contribution of the surrounding elements. In particular if these large terms occur in the main diagonal of the stiffness matrix, numerical instability can occur in the solution of the equations.

To overcome the first numerical problem it seems sufficient to adopt a joint element that uses relative displacements as independent degrees-of-freedom, such as the element proposed by Ghaboussi et al(1976). However this procedure does not ensure stability of the solution, since high stiffness elements may still exist in the main diagonal.

A more meaningful solution is proposed which avoids both numerical problems described and is physically correct. However, the methods of assembling the stiffness matrix used in the program INTERDAM have to be used (or similar a method with the same capability).

As described in Chapter 6, in the INTERDAM program an addressing matrix is created to define the active degrees-of-freedom for a particular step. Therefore, this matrix can be used to assign the same degree-of-freedom for two different nodes.

The method would impose similar discretization as if joint elements with zero thickness were to be used. In other words, at the interface, nodes would be specified in pairs, having the same coordinates.

The method is both incremental and iterative and the analysis would start by assigning identical degrees-of-freedom, in the tangential direction, for all pairs of nodes at the interface. Consequently, no relative movement would be allowed. At any stage of the analyses the state of stress of these joint elements can be checked and as soon as the maximum shear stress is reached, the nodes representing the soil side of the interface in the joint elements are assigned independent degree-of-freedom and relative movements can be observed.

Note that this approach is in perfect agreement with the physical concepts described in this research, but the definition of the best way of describing the resistance of the interface, remains.

Furthermore this procedure does not depend on any stiffness parameter determined from laboratory or field tests. A similar approach has been discussed by Herrmann (1978).

6.6.6 Back Analyses of Soil Behaviour

As a complement of this numerical analysis, some results of displacements and stresses in the soil placed adjacent to the concrete wall are discussed. This presentation analyses the possibility of stress transfer mechanisms or other adverse problems likely to occur in similar circumstances.

The phenomenon of load transfer in earth dams has been extensively studied and, as briefly outlined in Chapter 3, is mainly caused by the placement of materials with different compressiblities in adjacent regions. This difference in compressibility induces differential settlements in these areas, leading to arching effects.

As observed by Squier (1970), differential movements which develop within or between portions of a dam creates strain and, in some cases these strains may lead to the development of cracks. Differential vertical movements between the shell and the core of earth dams have caused longitudinal cracks parallel to the dam axis in several dams (Cary, 1950; Marsal, 1959; Leonard and Raine, 1960).

Casagrande (1950) had drawn attention to the possibility of another source of problems. The author has pointed out that differential settlements due to several factors, such as softer deposits in the river valley, can be the reason for cross-valley crack and consequent piping development.

Löfquist (1951) showed field evidence of load transfer measured with earth pressure cells in two dams (Hölle dam and Harspranget dam). Later, Leonards and Narain (1963) presented a comprehensive study of the causes of longitudinal cracks, supported by examples of several observations in the field (Reactor Creek dam, Woodcrest dam, Shell Oil dam, among others).

Squier (1970) studied qualitatively four modes of load transfer possible in earth dams. Some of these modes have been proven in field observations. Kulhawy and Gurtowski (1976) proposed a systematic way of defining the potential for load transfer by analysing the "load transfer ratio ($\sigma_1/\gamma h$)".

For the test embankment, it was shown in Chapter 3 that, most likely, load transfer occurred. Based on the pressure cells and settlement results two different mechanisms were suggested (section 3.4.1.2).

The results of the back analysis of the test embankment can provide an illustration for the discussion presented in Chapter 3. For this analysis only the cases labelled 1 to 4 were used.

Figure 6.18 presents the settlement profile for the four cases studied. It is important to mention that since the foundation was represented by a rigid boundary, the curves of Figure 6.18 are monotonic and, therefore, load transfer is observed only towards the concrete wall. The second mechanism, described in section 3.4.1, is not possible.

The mechanism observed in the results of the finite element analysis is caused primarily by the angular distortion in the soil adjacent to the wall. This settlement

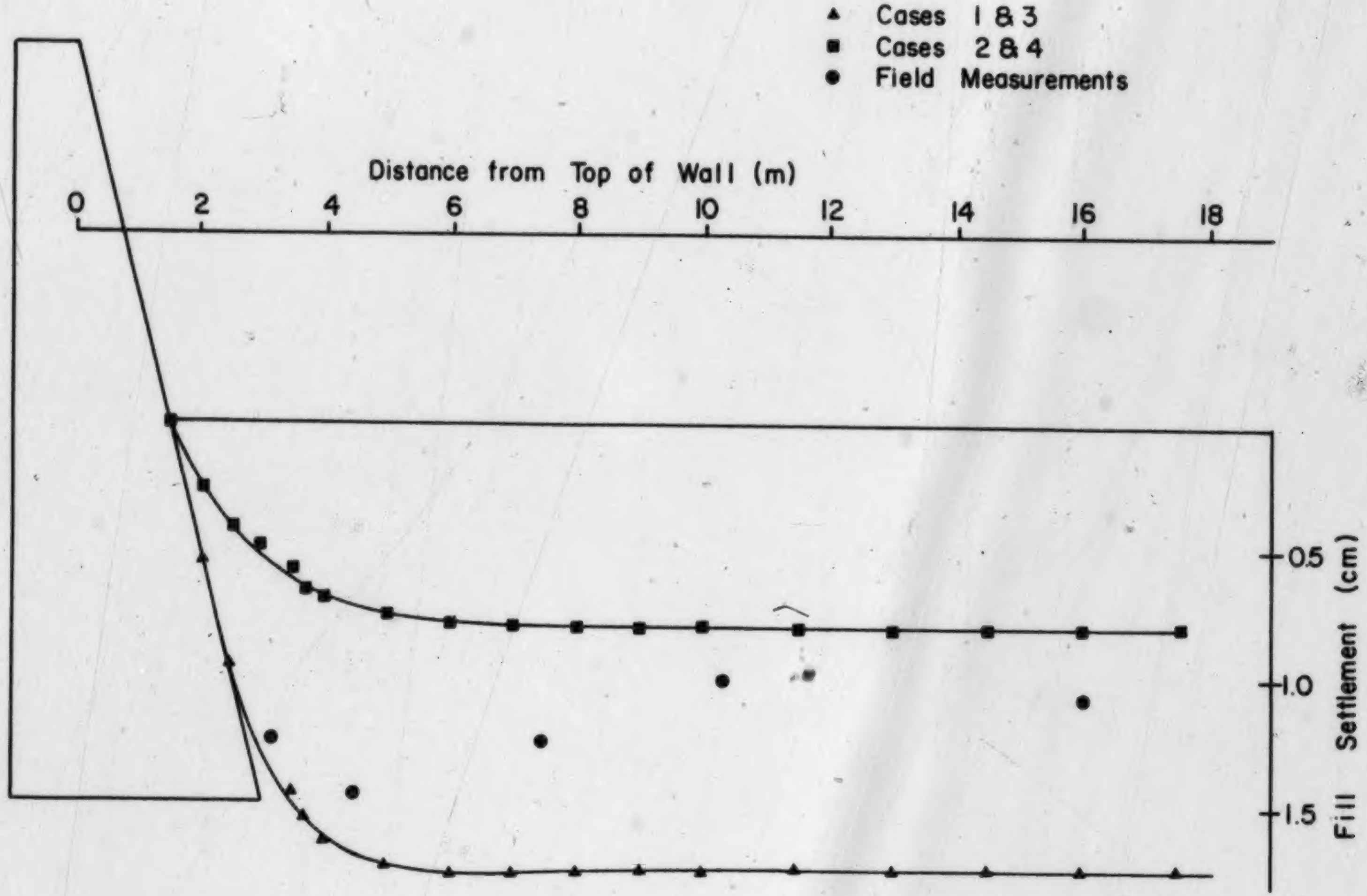

Figure 6.18 Results of Settlements of Fill - Back Analyses

generates high straining leading to load transfer and crack initiation (Squier, 1970).

Figure 6.19 depicts the load transfer ratio ($\sigma_1/\gamma h$) plotted versus the height of the wall. These values were obtained for the average of the major principal stresses in the pair of elements in contact with the wall (see Figure 6.8). This figure shows, for all four cases analysed, high load transfer near the toe of the concrete structure and ratios close to unit (no load transfer) near the crest of the wall.

All four cases have load transfer inside a very narrow range and the nonlinear analysis (case 4) seems to most favorable case (least load transfer).

The extension of the region subjected to load transfer can be evaluated in Figure 6.20. Since case 4 has proved to be the most favorable among the cases analysed, only this case is presented in Figure 6.20. From this figure it can be observed that, at least, load transfer will occur up to one full height of the wall (6 m) measured from the toe of the concrete wall.

The above discussion suggests that this region is at least as dangerous as any other junction in an earth dam. However, the contrast in compressibility between the soil and the concrete is among the highest that can be found in an earth dam. Consequently it should be expected that the region adjacent to a soil-concrete interface should represent one of the most critical regions for load

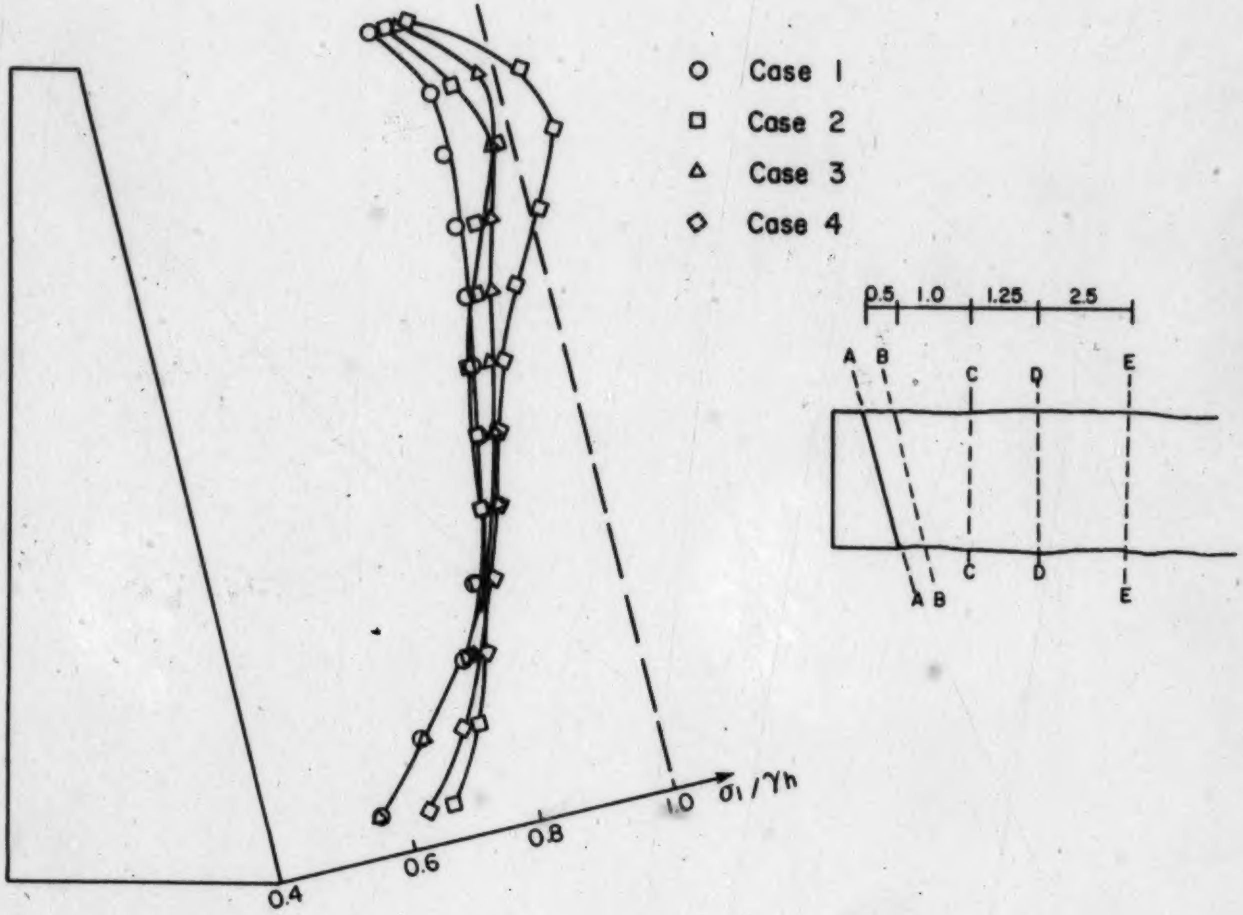

Figure 6.19 Load Transfer Ratio versus Height of Wall

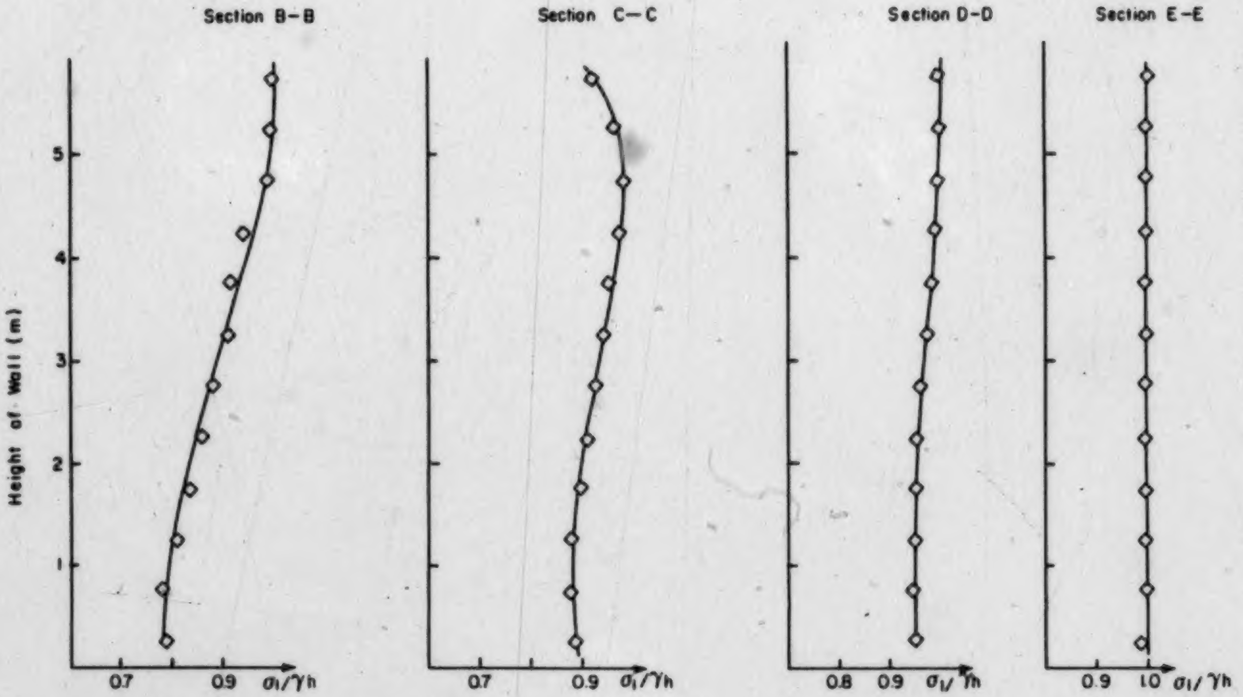

• For Position of Sections Refer to Figure 6.19

Figure 6.20 Extension of Region Subjected to Load Transfer

transfer, differential settlements and transverse cracks (vertical and perpendicular to the dam axis).

6.7 CONCLUSIONS

In this chapter back analyses of the test embankment were presented using the conventional analytical procedures; by representing the interface by a Goodman et al (1968) joint element and determining the parameters for these elements from results of direct shear box tests. Although it has been shown that, most likely, this method of analyses does not represent the physical behaviour of interfaces, this parametric study served two purposes:

1. To reafirm the conclusions drawn in Chapter 5
2. To obtain an insight into up-to-date analytical methods.

From the results of these analyses, several immediate observations were extracted and are summarized below:

1. The type of analysis (linear elastic or nonlinear elastic) has a minor effect on the shear stresses, although a significant effect can be observed in the shear displacements.
2. The normal stresses can be determined with any assumption for the interface and soil behaviour. The use of linear elastic, nonlinear elastic, full slip or no slip provides approximately the same

results (within ± 5%) for zero off-diagonal terms in the constitutitve matrix.

3. The influence of different parameters for both soil or interface is more significant for the shear displacement. Variation in the soil parameters affects, in the same proportion, the shear displacements and the shear stresses whereas variations in K_t imposes different values for the shear displacement only.

4. The influence of the sample preparation was also considered and the actual behaviour seems to fall between the two methods adopted, although it tends show better agreements with the method of sample preparation labelled "series 200".

5. The measurements obtained in the test fill (primarily the shear displacement) seem to be better represented by a "no slip" condition rather than by a "full slip" condition. Neverthless, the results are not in better agreement with the no slip case because failure was not considered.

6. A method was proposed, in brief, to avoid the use of the tangential stiffness. This method seems to better represent the physical phenomena of soil-concrete interfaces.

7. The soil placed adjacent to a soil-concrete interface seems to represent a potential region for crack initiation. Both the results of displacemnts

and stresses along the concrete wall suggests a high load transfer from the soil towards the concrete.

8. The conventional method of numerical simulation of interfaces (joint elements with parameters derived from direct shear box tests) seems to be able to reproduce the shear stresses, shear displacements and normal stresses measured in the field, within ±50%. These differences can be acceptable as "predictions" of the interface behaviour. For design purposes large factor of safety have to be specified.

However,in the writer's opinion the agreement observed in these analyses was caused by the fact that both, the laboratory tests used as input for the finite element program as well as the field instruments are subject to similar effects, and in particular influenced by the longitudinal compression. However, as pointed out before, the physical behaviour of interfaces seem not to be represented by a "tangential stiffness". This parameter has been proven to be a test response and not an "interface property".

At the same time, part of the differences observed between measured and back analysed stresses and displacements can be a consequence of the "three-dimensional effect", not considered in a plane-strain anlysis.

7. CONCLUSIONS AND SUGGESTIONS FOR FURTHER RESEARCH

7.1 GENERAL

The main objectives of this chapter are twofold:

1. Summarize the main conclusions drawn throughout this research.

2. Propose material for subsequent research.

In the first part the most important conclusions for both the mechanical behaviour and physical interpretation of interfaces soil-concrete are summarized.

In the second part, the writer's point of view of the trends that should follow this work will be presented, as an aid to future researchers involved in similar studies.

7.2 SUMMARY OF CONCLUSIONS

1. The literature available presents several joint element formulations, most have been proposed to simulate the behaviour of jointed rocks. Some have been used to represent soil-concrete interfaces. However, no account of the appropriateness to these elements of these applications has been found in the literature.

2. The literature review has demonstrated the need for field observations. Whenever field measurements have been reported at interfaces, only normal stresses have been

measured at the contact. No reports could be found describing either shear stresses or shear displacements at interfaces or measurements in the soil adjacent to the structure.

3. The magnitude of the observed interface (relative) shear displacements is of a very small order of magnitude (approximately 1 mm).

4. Since the shear displacements at the interface are considerably smaller than the settlement of the fill (approximately 10%), high straining occurs in the soil placed near the concrete structure. This can cause cracks in the soil and consequently excessive water flow (if any).

5. In particular for the case history reported in this thesis, two load transfer mechanisms were identified near the concrete structure. One caused by the soil "hanging" on the concrete structure and a second towards the soil placed away from the wall, caused by the excessive settlement observed in the fill near the wall. Both mechanisms are likely to happen in an actual engineering project, particularly if the foundation is of poor quality. However, evidence has been presented indicating that, in most cases, load transfer will be observed at least towards the concrete structure.

6. The results of the shear box tests along soil-concrete interfaces are strongly influenced by the method of sample preparation. If the soil is compacted directly against the concrete a strain-softening behaviour

should be expected. If the soil is compacted in a mold and subsequently trimmed to the desired dimensions, a strain-hardening behaviour is likely to be obtained.

7. The **tangential stiffness** (K_t) is not a **fundamental parameter** defining the behaviour of soil-concrete interfaces. It is affected by several factors such as the size of the test used to determine this parameter.

8. A compression, occuring in the direction of the shear, was recognized in the shear box test. This effect led to the conclusion that the value of the **tangential stiffness**, as defined in most of the literature available, seems to have no physical meaning and does not properly describe the physical behaviour of soil-concrete interfaces, but is rather a function of the test itself.

9. Evidence has been given to demonstrate, on a theoretical basis, that the rigid-plastic model seems to be a more realistic constitutive law for the behaviour of interfaces. In this simulation "slippage" has to be considered as soon as the shear stress acting at the interface reaches the maximum shear strength.

10. The conventional methods of numerical modelling using the finite element method (using joint elements and shear box test to obtain the parameters) have proven to be adequate to match the field results. However, better agreement was obtained between field measurements and numerical results for instruments influenced by the same factors as the test used as input data for the joint

elements. The most important seems to be the effect of the longitudinal compression.

11. The conventional methods of numerical modelling using the finite element analyses seems not to represent the physical behaviour of soil-concrete interfaces.

7.3 SUGGESTIONS FOR FURTHER RESEARCH

The suggestions proposed in this section will assume that the value of the tangential stiffness is no longer considered as an interface parameter and therefore the rigid-plastic model is the most appropriate to describe the interface behaviour. Consequently in terms of laboratory tests, the determination of the test and/or apparatus best able to determine a "fundamental parameter" for the interface, remains. This parameter seems to be more of a "strength type" rather than a "rigidity type" (stiffness). Among the existing parameters the coefficient of static friction seems to be the most promising.

Second the method described at the end of section 6.6.5.5 must be tried and the ability to represent the behaviour of interfaces verified. A similar approach has been described elsewhere (Herrmann, 1978) and can be used as starting point.

From the practical point of view analyses of the geometry of the concrete structure are necessary in order to avoid the high angular distortion observed and consequently the risk of cracking in the soil adjacent to the structure.

Again, the finite element method can provide an essential tool for parametric studies of different geometries.

The Shear Stress Device, designed to measure shear stresses at interfaces soil-concrete has to be reconsidered. In order to confirm the "local" behaviour of soil-concrete interfaces an instrument able to measure shear stresses but that avoids the effect of longitudinal compression is highly desirable.

Finally the three-dimensional effect should be considered. In this sense, geometries such as the "wrap-around" type of junctions between earth and concrete dams should be studied.

Another important point to be considered, particularly for earth dams, is the study of flow of water through soil-concrete interfaces.

REFERENCES

Alberta Environment (1980) "Contract Specification for Dickson Dam Main Dam and Emergency Spillway", Contract n. #8-81-0044, May, 1980.

American Society for Testing and Materials (1961) "Nuclear Methods for Measuring Soil Densities and Moisture", ASTM-STP 293, Philadelphia, 1961

American Society for Testing and Materials (1971) "Standard Methods of Test for Soil and Soil-Aggregate in Place by Nuclear Methods (Shallow Depth)", ASTM D 2922-71, pp. 854-861

Arthur, J.R.F. and Roscoe, K.H. (1961) "An Earth Pressure Cell for the Measurement of Normal and Shear Stresses", Civil Engineering and Public Works Review, 56(559), pp. 765-770.

Askegaard, V. (1984) "Design Basis for Cells Measuring Shear Stresses in an Interface", Geotechnical Testing Journal, vol. 7, n.2, pp. 94-98.

Barton, N. and Choubey, V. (1977) "The Shear Strength of Rock Joints in Theory and Practice", Rock Mechanics, vol. 10, pp. 1-54.

Bathe, K.J. and Wilson, E.L. (1976) "Numerical Methods in Finite Element Analyses", Prentice Hall, Inc., New Jersey.

Bauer, G.E.A.; Shields, D.H.; Scott, J.D. and Nwaboukei, S.D. (1979) "Normal and Shear Stress Measurements on Strip Footing", Canadian Geotechnical Journal, vol. 16, n.1, pp. 177-189.

Belcher, D.J., Cuykendal, T.R. e Sack, H.S. (1950) "The Measurement of Soil Moisture and Density by Neutron and Gamma-Ray Scattering", Technical Development Report 127, U.S. Civil Aeronautics Admin., Washington, D.C., 1950, 20 pp.

Bishop, A.W. and Henkel, D.J. (1962) "The Measurement of Soil Properties in the Triaxial test", Edward Arnold (Publisher) Ltda, 2nd. edition.

Bowles, J.E. (1979) "Physical and Geotechnical Properties of Soils", McGraw Hill, Inc.

Brandt, J.R.T. (1985) "User's Manual for INTERDAM Code", Geotechnical Computer Programs, Department of Civil Engineering, University of Alberta.

Broms, B.B. (1980) "Soil Sampling in Europe: State-of-the-Art", American Society of Civil Engineers, vol. 106, GT1, pp. 65-97.

Brown, S.F and Pell, P.S. (1967) "An Experimental Investigation of Stresses, Strains and Deflections in Layered Pavement Structures Subjected to Dynamic Loads", Proc. 2nd. Int. Conference on the Struct. Design of Asphalt, pp. 487-504.

Burland, J.B.; Moore, J.F.A and Smith, P.D.K. (1972) "A Simple and Precise Borehole Extensometer", Geotecnique, vol 22(1), pp. 174-177.

Carder, D.R.; Pocock, R.G. and Murray, R.T. (1977) "Experimental Retaining Wall Facility - Lateral

Measurements With Sand Backfill", Transport and Road Research Laboratory, Laboratory Report 766.

Cary, A.S. (1960) "Rockfill Dams: Mud Mountain Dam", Transactions, American Society of Civil Engineers, vol. 25, Part 2, pp. 185-189.

Casagrande, A. (1950) "Notes on the Design of Earth Dams", Proc. Boston Society of Civil Engineers, vol. 37, n4, pp. 405-429.

Celestino, T.B. and Marechal, L.A. (1975) "Stress and Strain in The Ilha Solteira Dam", Proc. 5th. PanAmericam Conference of Soil Mechanics and Foundation Engineering, Buenos Aires, vol. 2, pp. 189-198.

Charles, J.A. (1976) "The Use of One-Dimensional Compression Test and Elastic Theory to Predict Deformations of Rockfill Embankments", Canadian Geotechnical Journal, vol. 13, n.3, pp. 189-200.

Christian, J.T. (1980) "The Appication of Generalized Stress-Strain Relations", Proc. of the Symposium on Limit Equilibrium, Plasticity and Generalized Stress-Strain Relations in Geotechnical Engineering, American Society for Civil Engineers, Hollywood, Florida, Oct.1980, pp. 182-205.

Clough, G.W. and Duncan, J.M. (1969) "Finite Element Analyses of Port Allen and Old River Locks", U.S.Army Engineers Waterway Experimental Station, Vicksburg, Mississipi, Contract Report S-69-6.

Clough, G.W. and Duncan, J.M. (1971) "Finite Element

Analyses of Retaining Wall Behaviour", American Society of Civil Engineers, vol. 97, SM12 pp. 1657-1673.

Cooke, R.W. and Price, G. (1973) "Horizontal Inclinometers for the Measurement of Vertical Displacements in the Soil Around Experimental Foundations", Field Intrumentation in Geotechnical Engineering, Symposium of the British Geot. Society, pp. 112-120.

Coulomb, C.A. (1776) "Essis Sur Une Application de Regles a l'Architeture, (An Attempt to Apply the Rules of Maxima and Minima to Several Problems of Stability Related to Architecture)", Mem. Acad. Royal de Sciences, Paris, 3, pg. 38.

Coyle, H.M.; Bartoskewitz, R.E.; Milberger, L.J. and Butler, H.D. (1974) "Field Measurements of Lateral Earth Pressures on a Cantilever Retaining Wall", Transportation Research Council, Publ. #517, National Research Council, Washington D.C.

Craig, R.F. (1977) "Soil Mechanics", Van Nostrand Reinhold (Publisher) Ltd.

de Mello, V.F.B. (1977) "Reflection on Design Decisions of Practical Significance to Embankment Dams", 17th. Rankine Lecture, Geotechnique, vol. 27(3), pp. 279-355.

de Melo, F. and Direito, F.T. (1979) "The Behaviour of Roxo Dam", 13th. Int. Congress on Large Dams, New Delhi, Q52, vol. 2, pp. 387-401.

Desai, C.S.; Phan, H.V. and Perumpral, J.V. (1982) "Mechanics of Three-Dimensional Soil-Structure

Interaction", American Society of Civil Engineers, Journal of the Engineering Mechanics Division, vol. 108, EM5, pp. 731-747.

Desai, C.S.; Zaman, M.M.; Lightner, J.G. and Siriwardane, H.J. (1984) "Thin-Layer Element for Interfaces and Joints", Int. Journal for Numerical and Analytical Methods in Geomechanics, vol 8, pp. 19-43.

Doohan, J.P. (1975) "Earth Pressure Cell to Measure the Distribution of Shear and Normal Stresses on a Footing", M.A.Sc. Thesis, University of Ottawa, Ottawa, Ontario.

Duncan, J.M. and Chang, C.Y. (1969) "Nonlinear Analyses of Stress and Strain in Soils", American Society of Civil Engineers, Journal of the Soil Mechanics and Foundation Division, vol. 96, SM5, pp. 1629-1653.

Duncan, J.M. and Clough, G.W. (1971) "Finite Element Analyses of Port Allen Lock", American Society of Civil Engineers, Journal of the Soil Mechanics and Foundation Division, vol. 97, SM8, pp. 1053-1068.

Duncan, J.M.; Byrne, P.; Wong, K.S. and Mabry, P. (1980) "Strength, Stress-Strain and Bulk Modulus Parameters for Finite Element Analyses of Stresses and Movements in Soil Masses", Report n. UCB/GT/80-01, Department of Civil Engineering, University of California, Berkeley.

Dunlop, P.; Duncan, J.M. and Seed, H.B. (1968) "Finite Element Analyses of Slopes in Soil", U.S. Army Engineers Waterway Experimental Station Corps of Engineers, Contract n. DA-22-079 - CIVENG 62-47, Report n. TE 68-3.

Eisenstein, Z. and Law, S.T.C. (1979) "The Role of Constitutive Laws in Analysis of Embankments", Proc. 3rd. Int. Conf. Numerical Methods in Geomechanics, Aachen, vol. 3, pp. 1413-1430.

Felio, G.Y. (1980) "Monitoring of a Bridge Abutment Founded on a Granular Compacted Fill", M.Sc. Thesis, Carleton University, Ottawa, Oct. 1980.

Ghaboussi, J.; Wilson, E. and Isemberg, J. (1973) "Finite Element for Rock Joints and Interfaces", American Society of Civil Engineers, Journal of the Soil Mechanics and Foundation Division, vol. 99, SM10, pp. 833-848.

Goodman, R.E.; Taylor, R.L. and Brekke, T.L. (1968) "A Model for the Mechanics of Jointed Rock", American Society of Civil Engineers, Journal of the Soil Mechanics and Foundation Division, vol. 94, SM3, pp. 637-659.

Goodman, R.E. and Dubois, J. (1972) "Duplication of Dilatancy in Analyses of Jointed Rocks", American Society of Civil Engineers, Journal of the Soil Mechanics and Foundation Division, vol. 98, SM4, pp. 399-422.

Goodman, R.E. (1976) "Methods of Geological Engineering", West. Publ. Company.

Gurr, C.G. (1962). "Use of Gamma Rays in Measuring Water Content and Permeability in Unsaturated Columns of Soil", Soil Science, vol 94,(4), pp. 224-229.

Hamilton, J.J. (1960) "Earth Pressure Cells - Design, Calibration and Performance", Technical Paper n. 109, Division of Building Research, Ottawa.

Hilf, J.W(1961) "A Rapid Method of Construction Control for Embankment of Cohesive Soils" Engineering Monograph n. 26, U.S. Bureau of Reclamation, Setember 1961

Herceg, E.E. (1976) "Handbook of Measurement and Control; An Authoritative Treatise on the Theory and Application of the LVDT", Handbook HB-76, Published by Schaewitz Engineering, Pensanken, New Jersey.

Herrmann, L.R. (1978) "Finite Element Analyses of Contact Problems", American Society of Civil Engineers, Journal fo the Mechanical Engineering Division, vol.104, EM5, pp. 1043-1057.

Heuze, F.E.; Goodman, R.E. and Bornstein, A. (1971) "Numerical Analyses of Deformability Tests in Jointed Rock - 'Joint Perturbation' and 'No Tension' Finite Element Solutions", Rock Mechanics, vol. 3, pp. 13-24.

Heuze, F.E. (1979) "Dilatant Effects of Rock Joints", Proc. 4th. Int. Congress on Rock Mechanics, Montreaux, Suisse, vol. 1, pp. 160-175.

Heuze, F.E. and Barbour, T.G. (1982) "New Models for Rock Joints and Intrfaces", American Society of Civil Engineers, Journal of the Geotechnical Division, vol. 108, GT5, pp. 757-776.

Holmes, J.W. (1966). "Influence of Bulk Density of the Soil on Neutron Moisture Meter Calibration", Soil Science, vol. 102,(6), pp. 355-360.

Hvorslev, M.J. (1960) "Physical Components of the Shear Strength of Saturated Clays", Shear Strength Conference, American Society for Civil Engineers, Boulder, Colorado, pp. 116-273.

Jones, C.J.F. and Sims, F.A. (1975) "Earth Pressure Against the Abutments and Wing Walls of Standard Motorway Bridges", Geotechnique, vol. 25(4), pp. 731-742.

Kaiser, P.K. (1979) " Time Dependent Behaviour of Tunnels in Jointed Rocks", Ph.D. Thesis, Department of Civil Engineering, University of Alberta, 395pp.

Katona, M.G. (1981) "A Simple Contact-Friction Interface Element with Application to Buried Culverts", Proc. Implementation of Computer Procedures and Stress-Strain Laws in Geotechnical Engineering, Editors Desai and Saxena, Illinois, vol. 1, pp. 45-63.

Kaufman, R. and Sherman, W. (1964) "Enginreering Measurements of Port Allen Lock", American Society for Civil Engineers, Journal of the Soil Mechanics and Foundation Engineering, vol. 90, SM5, pp. 221-247.

Kisiel, J. (1964) "On Experiences Acquired in the Course of Tests Carried Out With a Shear Box", Archwn Hydrotech, vol. 11, pp. 415-421.

Kovari, K. (1977) "Micromechanics Models of Progressive Failure in Rock and Rock-like Materials", The Geotchenics of Structurally Complex Formations, Associazione Geotecnica Italiana, Capri, vol. 1, pp. 307-316.

Krishnayya, A.V.G. (1973) "Analysis of Cracking of Earth Dams", Ph.D. Thesis, University of Alberta.

Kulhawy, F. and Gurtowski, T. (1976) "Load Transfer and Hydraulic Fracturing in Zoned Dams", American Society of Civil Engineers, Journal of the Geotechnical Division, vol. 102, GT9, pp. 963-973.

Kulhawy, F. and Peterson, M.S. (1979) "Behaviour of Sand-Concrete Interfaces", Proc. 6th PanAmerican Conference of Soil Mechanics and Foundation Engineering, Lima, vol. 2, pp. 225-236.

LaRochelle, P. and Lefebvre, G. (1971) "Sampling Disturbance in Champlain Clay", American Society of Testing and Materials, STP-483, pp. 143-163.

Leonards, G.K. and Rain, O.H. (1960) "Rockfill Dams: TVA Central Core Dams", Transactions, American Society of Civil Engineers, vol. 125, Part 2, pp. 201-203.

Leonards, G.A and Narain, J. (1963) "Flexibility of Clay and Cracking of Earth Dams", American Society of Civil Engineers, Journal of the Soil Mechanics and Foundation Division, vol. 89, SM2, pp. 47-98.

Löfquist, B. (1951) "Earth Pressure in a Thin Impervious Core", Proc. 4th. Int. Congress on Large Dams, New Delhi, vol. 1, pp. 99-109.

Lombardi, G. (1979) "Long Term Measurements in Underground Openings and Their Interpretation with Special Consideration to the Rheological Behaviour of the Rock", Proc. Int. Symp. Field Instr. in Rock Mec., Zurich, vol. 2, pp. 839-858.

Lambe, T.W. (1951) "Soil Testing for Engineers", John Willey and Sons, Inc. 2nd edition.

Marsal, R.J. (1959) "Earth Dams in Mexico", Proc. 1st PanAmerican Conf. Soil Mechanics and Foundation Engineering, Mexico, vol. 3, pp. 1294-1303.

Milovic, D.M. (1971) "Effect of Sampling on Some Soil Characteristics", American Society for Testing and Materials, STP-483, pp. 164-179.

Morgenstern, N.R. and Tchalenko, J.S. (1967) " Microscope Structures in Kaolin Subjected to Direct Shear", Geotechnique, vol. 17(3), pp. 309-328.

Morgenstren, N.R. and Eigenbrod, K.D. (1974) "Classification of Argillaceous Soils and Rocks", American Society of Civil Engineers, Journal of the Geotechnical Division, vol. 100, GT10, pp. 1137-1156.

Makowecki, D. (1979) "Nuclear Densometer - Information Manual for Underwood MacLellan Ltd." (unpublished)

McHenry, J.R. (1963) "Theory and Application of Neutron Scattering in the Measurement of Soil Moisture", Soil Science, vol 95,(5),pp. 294-307.

Neden, R.J. (1984) "Soil-Concrete Interface of a Test Fill", Master of Engineering Project, Department of Civil Engineering, University of Alberta, 50p.

Noonan, D.K. and Nixon, S.F. (1972) "The Determination of Young's Modulus from Shear Box Test", Canadian Geotechnical Journal, vol. 9, pp. 504-507.

Pantecorvo, B (1941) "Neutron Well Logging", Oil and Gas Journal, Setember 1941, pg. 32

Palmer, A.C. and Rice, J.R. (1973) "The Growth of Slip Surfaces in Progressive FAilure of Over-Consolidated Clays", Proc. Royal Society of London, Series A, vol. 332, pp. 527-548.

Peattie, K.R. and Sparrow, R.W. (1954) "The Fundamental Action of Earth Pressure Cells", Journal of the Mechanics of Physics and Solids, vol. 2, pp. 141-155.

Penmam A.D.M.; Charles, J.A.; Nash, J.K. and Humpheys, J.D (1975) "Performance of Culvert Under Winscar Dam", Geotechnique, 25(4), pp. 713-730.

Plantema, G. (1953) "A Soil Pressure Cell and Calibration Equipment", Proc. 3rd. International Conference of Soil Mechanics and Foundation Engineering, Zurich, vol. 1, pp. 283-288.

Poulos, H.G. and Davis, E.H. (1974) " Elastic Solutions for Soil and Rock Mechanics", John Willey and Sons, Inc., 411p.

Rankine, W.J.M. (1857) "On the Stability of Loose Earth", Phil. Trans. Royal Society of London, vol. 147.

Roa, F.R. (1981) "Some Considerations for Tunnel Design", 10th. International Conference of Soil Mechanics and Foundation Engineering, Stockholm, vol. 1, pp. 353-356.

Rouvray, A.L. and Goodman, R.E. (1972) "Finite Element Analysis of Crack Initiation in a Block Model Experiment", Rock Mechanics, vol. 4, pp. 203-223.

Rukykh, D.L. (1981) "Use of the Finite Element Method for Determining Fill Earth Pressure on Retaining Walls", Soil Mechanics and Foundation Engineering, vol. 18, No. 2, pp. 75-79.

Saha, P.K. (1982) "Finite Element Modelling and Structural Behaviour of Concrete Tunnel Linings", Ph.D. Thesis, Urbana, Illinois.

Seed, H.B. and Chan, C.K. (1959) "Structure and Strength Characteristics of Compacted Clays", American Society of Civil Engineers, Journal of the Soil Mechanics and Foundation Engineering, vol. 85, SM5, pp. 87-128.

Sharma, H.D. (1976) "Generalization of Sequential Nonlinear Analyses. A Study of Rockfill Dams With Joint Elements", Proc. 2nd International Conference of Numerical Methods in Geomechanics, Blackburg, vol. 2, pp. 662-685.

Simmons, J.V. (1981) "Shearband Yielding and Strain Softening", Ph.D. Thesis, Department of Civil Engineering, University of Alberta.

Smith, P.C., Johnson, A.I., Fisher, C.P. e Womack, L.M. (1968) "The Use of Nuclear Meters in Soil Investigation: A Summary of Worlwide Research and Practice", American Society for Testing and Materials, STP-412, Philadelphia, 1968.

Squier, L.R. (1970) "Load Transfer in Earth and Rockfill Dams", American Society of Civil Engineers, Journal of the Soil Mechanics and Foundation Engineering, vol. 96, SM1, pp. 213-233

Thomas, H.S.H. and Ward, W.H. (1969) "The Design, Construction and Performance of a Vibrating Wire Earth Pressure Cell", Geotechnique, vol. 9(1), pp. 39-51.

Thurner, H. and Sandstrom, A. (1980) "A New Device for Instant Compaction Control", International Conference on Compaction, Laboratoire Central des Ponts e Chausses, vol II, pg. 611

Tory, A.C. and Sparrow, R.W. (1967) "The Influence of Diaphragm Flexibility on the Performance of an Earth Pressure Cell", Journal of Science Instrumentation, vol. 44, pp. 781-785.

Van Dillen, D.E. and Ewing, R.D. (1981) "BMINES - A Finite Element Code for Rock Mechanics Application", 22nd U.S. Symposium on Rock Mechanics, MIT, pp. 373-378.

Vaughan, P.R. and Kennard, M.F. (1972) "Earth Pressure at a Junction Between an Embankment Dam and a Concrete Dam", European Congress of Soil Mechanics and Foundation Engineering, Madrid, pp. 215-221.

Vesic, A.S. (1970) "Test on Instrumented Piles, Ogeechee River Site", American Society of Civil Engineers, Journal of the Soil Mechanics and Foundation Engineering, vol. 96, SM2, pp. 561-584.

Wannanem, A.O. (Chairman - Task Force on Use of Neutron Meters Committee on Hydrometeorology, 1964) "Use of Neutons Meter in Soil Moisture Measurements", Proc. American Society of Civil Engineers, Journal of the Hydraulic Division, 1964, HY6, pp. 21-43

Wu, T. (1980) "Predicting Performance of Buried Conducts", Ph.D. Thesis, Department of Civil Engineering, Purdue University.

Xierum, Ge. (1981) "Nonlinear Analyses of a Joint Element and Its Application in Rock Engineering", Int. Journal for Numerical and Analytical Methods in Geomechanics, vol. 5, pp. 229-245.

Zienkiewicz, O.C.; Vallipan, S. and King, I.P. (1968) "Stress Analyses of a Rock as a No Tension Material", Ceotechnique, vol. 18(1), pp. 56-66.

Zienkiewicz, O.C.; Best, B.; Dullage, C. and Stagg, K.G. (1970) " Analysis of Nonlinear Problems in Rock Mechanics with Particular Reference to Jointed Rock Systems", Proc. 2nd International Congress on the Int. Society for Rock Mechanics, Belgrade, vol. 3, pp. 501-509.

Zienkiewicz, O.C. (1971) "The Finite Element Method in Engineering Science", McGraw Hill Book Company, New York.

APPENDIX A - NUCLEAR DENSOMETERS

Quality control of earth work construction is imperative to ensure that construction specifications are followed.

For this purpose, several methods have been developed, presenting different technology and with varying degrees of accuracy and sophistication. They vary from a simple visual inspection to equipment that inform the operator of the compaction machine of the degree of compaction achieved, during the operation (Thurner and Sandstrom, 1980)

However, the great majority of methods available furnish only the density of the material and consequently its relative density (for granular materials) or the degree of compaction (for fine grained materials). The exception to this role was presented by Hilf (1961). It is one of the few methods that permits the determination of both moisture content (the variation with respect to the optimum moisture content) and the degree of compaction for fine grained soils. Almost simultaneously a second method was presented that makes use of a radioactive source and was named the Nuclear Method (A.S.T.M., 1961).

Although the equipment for nuclear measurements was first developed for oil exploration (Pantecorvo, 1941), the technology spreaded to several different areas, including Forestry, Agriculture, Botany and Civil Engineering.

As major advantages, the Nuclear Densometers are simple to operate, require minimum mantainance, require minimum personnel (one person required), do not require a laboratory on the job site, and can produce results faster than any other method.

Although the accuracy of the method is sometimes questioned, it has been proved that a good calibration can improve the results significantly (Wannanen, 1964; Holmes, 1966) and render them completely acceptable.

The measurement of both moisture content and density makes use of rays or particles emitted from a radioactive source. In general, this source produces four types of radiation:

- alpha particles
- beta particles
- gamma rays
- neutrons

Among these four types of radiation, the first two are considered inactive from the point of view of compaction control, since they are unable to emerge from the container housing the radioactive source.

The water content determination makes use of the high energy (fast) neutrons emitted by the source. These neutrons are scattered in a randon manner by the soil and lose energy in elastic collisions with low-weight nuclei. Since neutrons and hydrogen (a fundamental component of water) have almost equal mass, the scattered neutrons lose more energy in collisions with hydrogen than with any other atom generally found in the soil. Some of the neutrons, slowed by the collisions, return to the vicinity of the source and can be counted by a thermal (low-energy or slow) neutron counter. The count obtained is an indication of the number of hydrogen atoms present. Water is the principal source of hydrogen atoms in soil and therefore, the count can provide a measure of the amount of water in the soil surrounding the source of fast neutrons

On the other hand, gamma rays emitted by the source are scattered by the electrons existing in the soil mass and lose energy in the process. The number of scattered rays returning to a detector placed near the source can also be counted.

The electron density increases proportionally with the soil density and causes greater scattering and energy loss. Thus, with increased density, the chances that scattered gamma rays will return to the detector with sufficient energy to be counted decreases and the count rate drops. In common types of soil, therefore, a low gamma ray count indicates high density and vice-versa (Waananen, 1964). More detailed description of these phenomena can be found in papers by Belcher et al (1950), Gurr (1962), Johnson (1962), McHenry (1963) and Smith et al (1968), among others.

Several different types of Nuclear Densometers are commercially available. They vary in shape, are to be used in boreholes or at ground surface (or subsurface), use different radioactive sources and so on. But in all cases, the basic principle of operation still holds.

For this research work, a Model BR-Campbell Nuclear Portaprobe was used.

It makes use of Cesium 137[4] as the radioactive source, is 35.5 cm X 23.0 cm X 20.5 cm high and weighs less than 15.0 kg (Makowecki, 1979).

The moisture content is determined at the ground surface and the density is obtained at depth (up to 30.0 cm). The same unit holds the radioactive source and the counter, and uses a rechargeable battery.

The test procedure followed the standard proposed by ASTM-2922-71 (A.S.T.M., 1971).

As mentioned in Chapter 3, four measurements of both moisture content and density were obtained after each layer was placed. At the same time, small samples were collected to determine the moisture content in the laboratory.

In Figure A.1 a correlation between the moisture content obtained by both methods (laboratory determination and nuclear densometer) is presented. As can be seen, the field results are up to 4% greater. Only a few measurement contradict this trend. At most, laboratory measurements of moisture content exceeds those taken in the field by 0.5%.

It is well known that the nuclear densometers tend to furnish higher values of moisture content, but never higher than 1% over the real value. It is believed that the remaining discrepancy between field and laboratory measurements is a consequence of the time lag between

---

[4] Other material commonly used as radioactive sources are Radium 226 and Americium 241

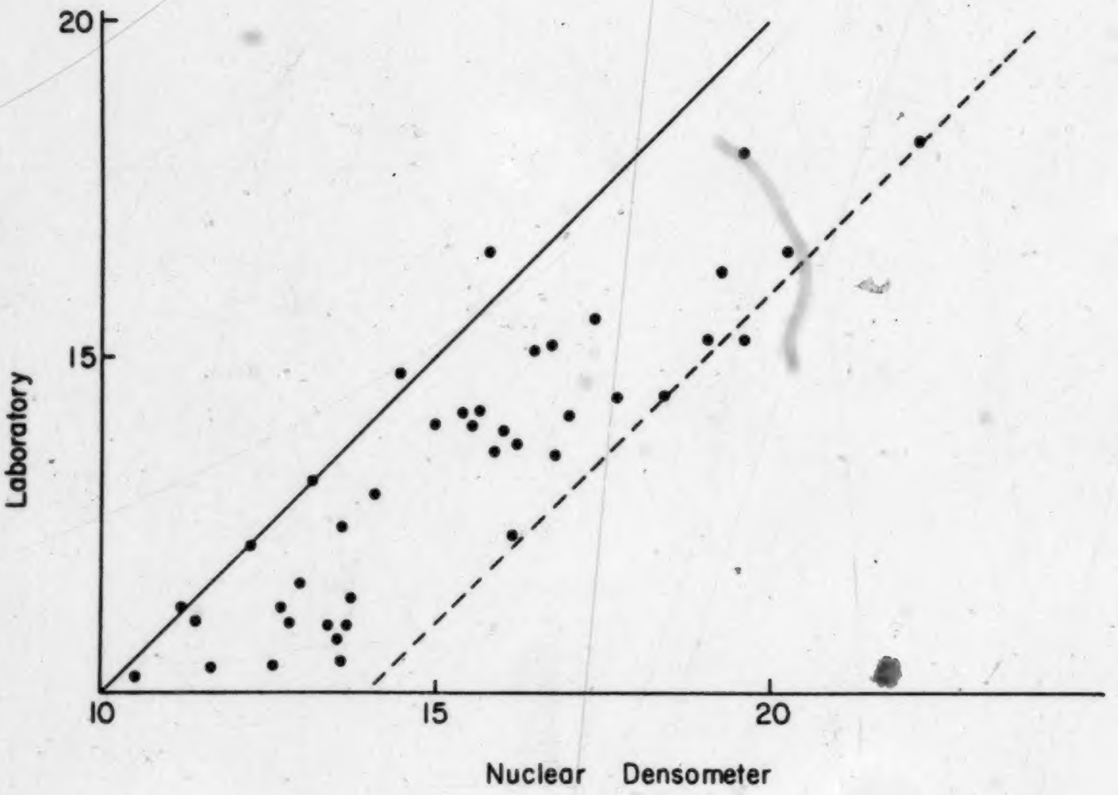

Figure A.1 Comparison Between Laboratory Nuclear Densometer

collecting the samples and taking them to the laboratory. Some samples were stored a few hours before reaching the laboratory.

In Figure A.2 the average moisture content for each layer (average of four tests) is plotted as a function of the similar average for the laboratory determination. It can be noticed that the scatter has been reduced significantly, suggesting the need for more than one test per compacted zone.

Unfortunately the density was only determined using the nuclear densometers, not allowing for a similar comparison. However, it is well known that the accuracy in determining densities, using the nuclear densometers, is higher then for moisture content determinations.

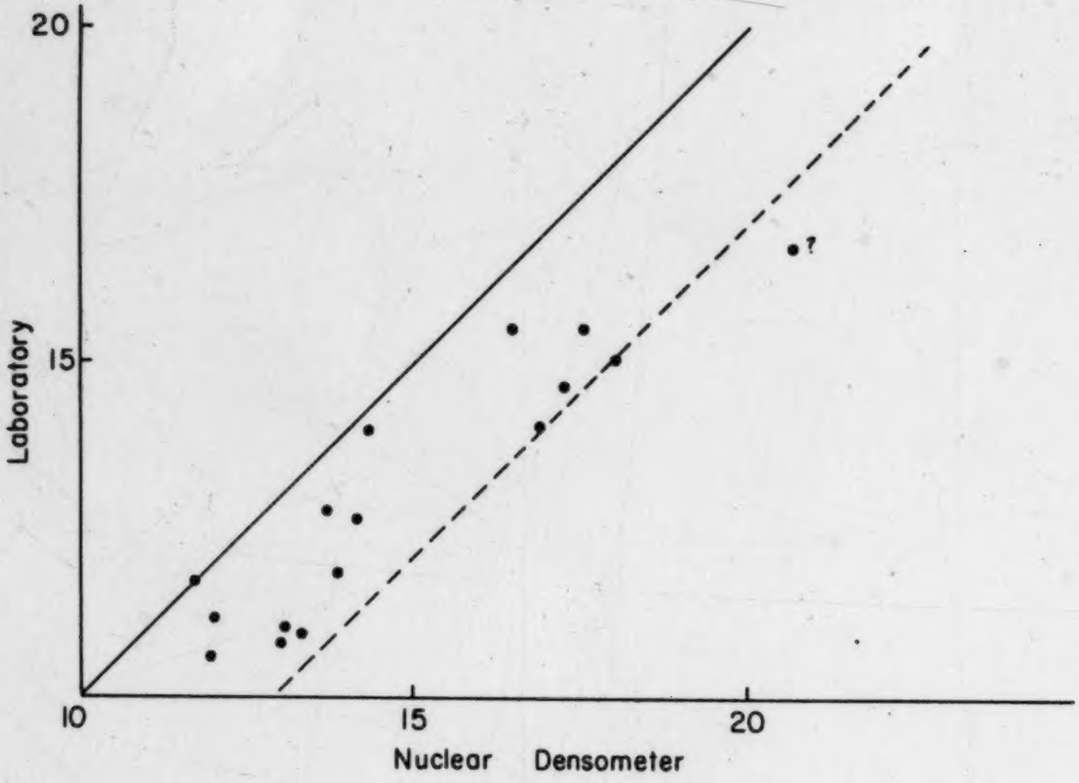

Figure A.2 Laboratory vs Nuclear Densometer - Average Results

APPENDIX B - MULTIPOINT EXTENSOMETER CURVES

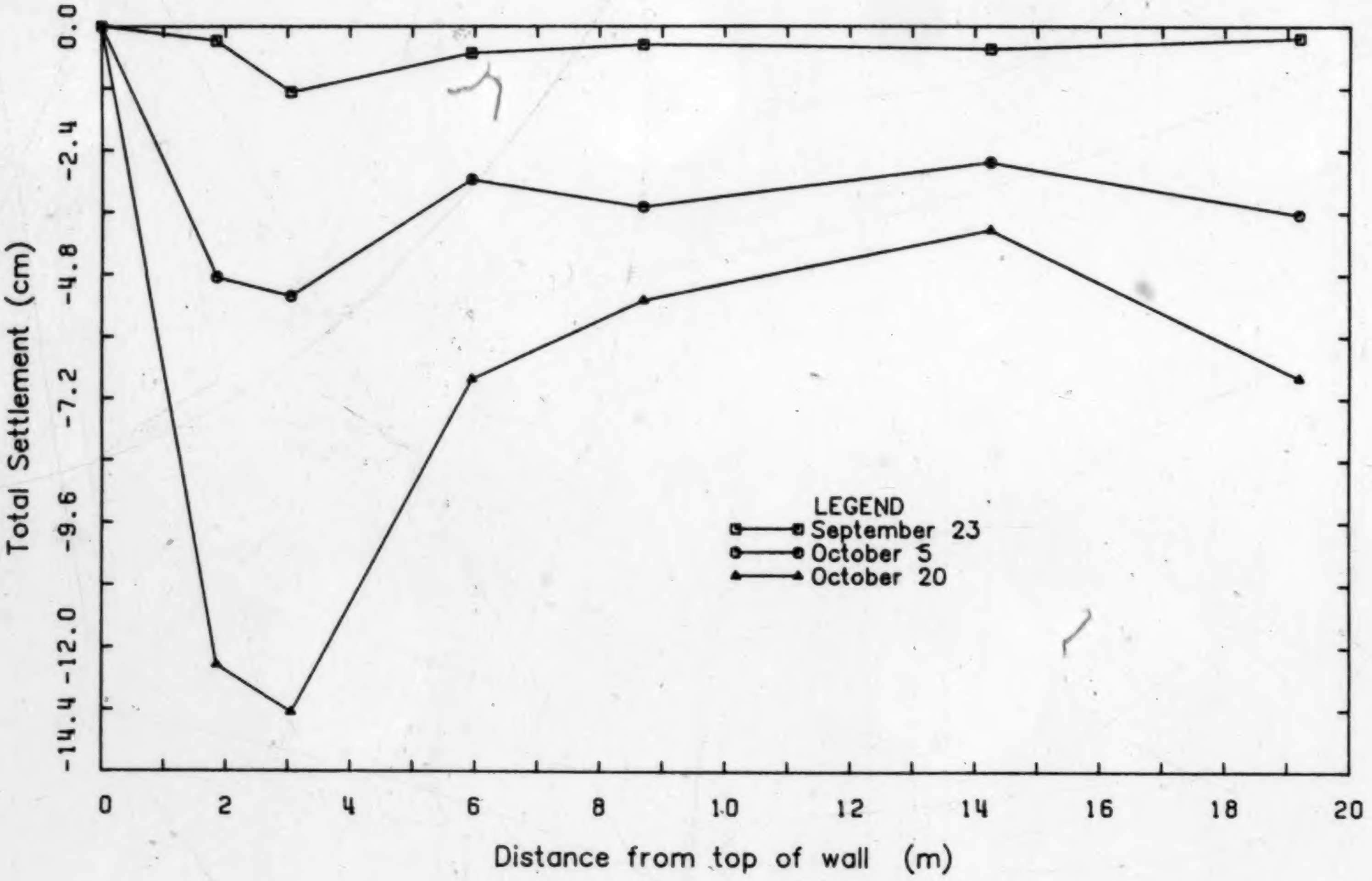

FIGURE B-1 TOTAL SETTLEMENT VS DISTANCE FROM TOP OF WALL MP#1

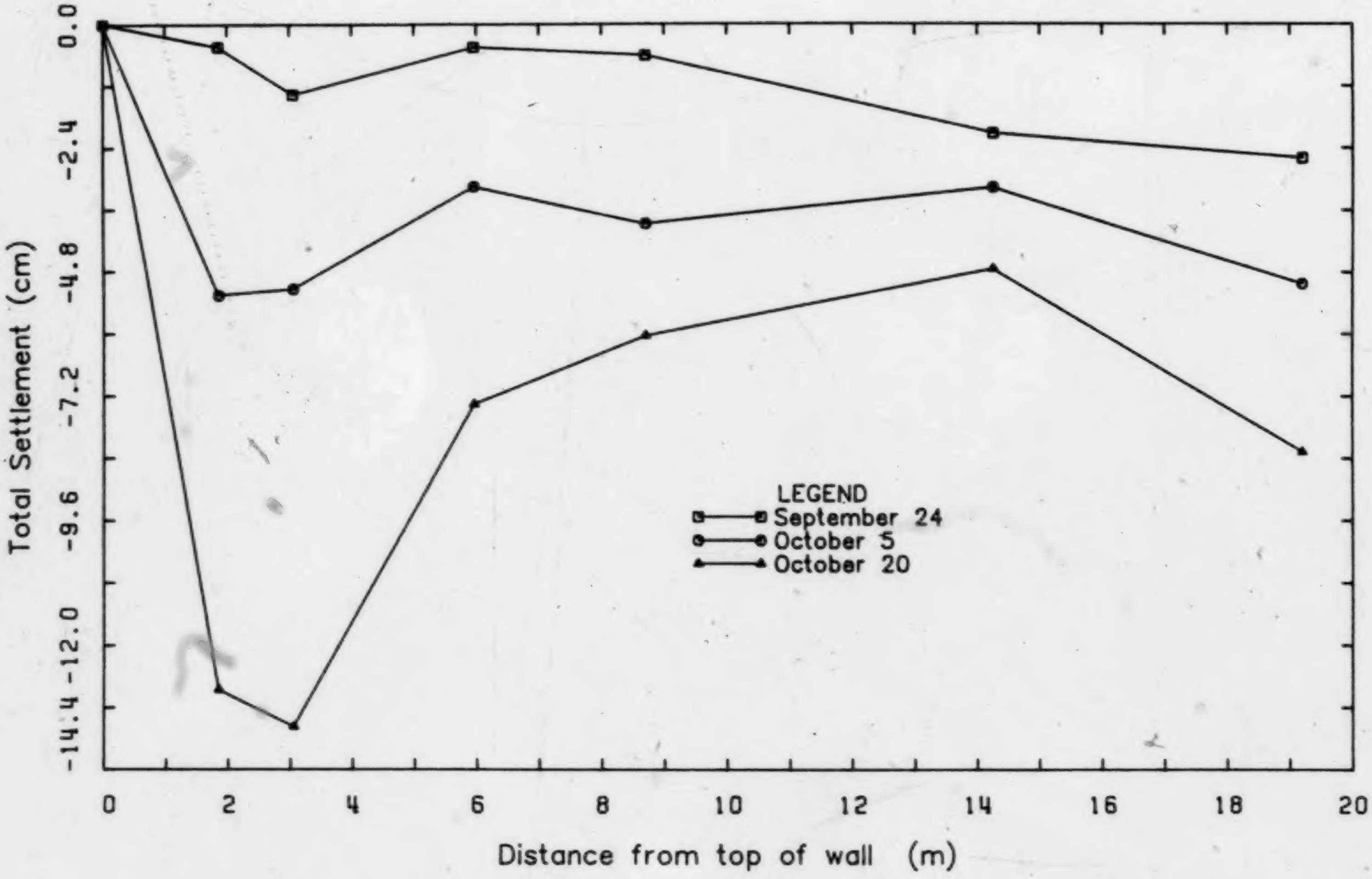

FIGURE B–2 TOTAL SETTLEMENT VS DISTANCE FROM TOP OF WALL MP#2

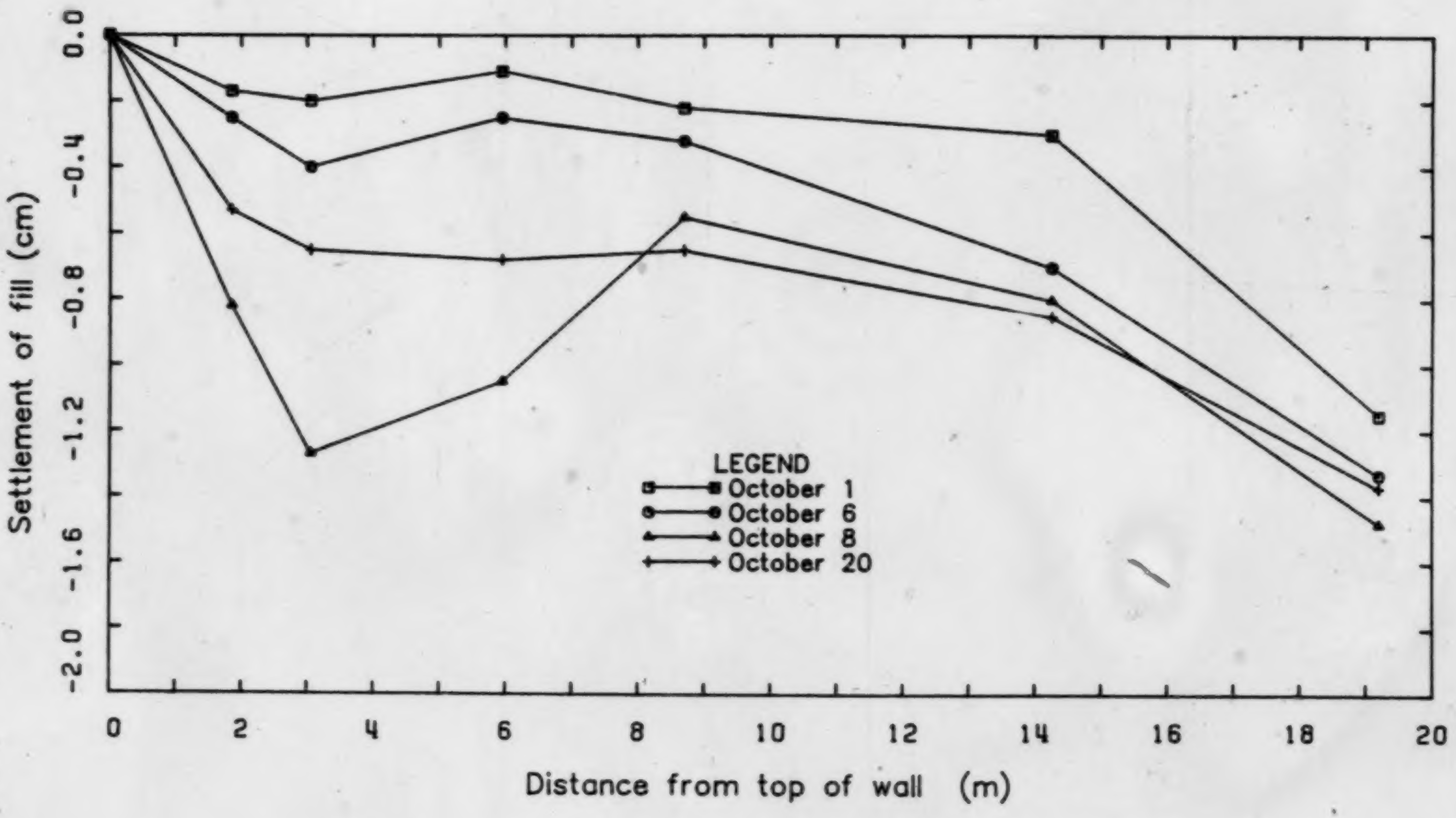

FIGURE B-3 FILL SETTLEMENT VS DISTANCE FROM TOP OF WALL MP#2

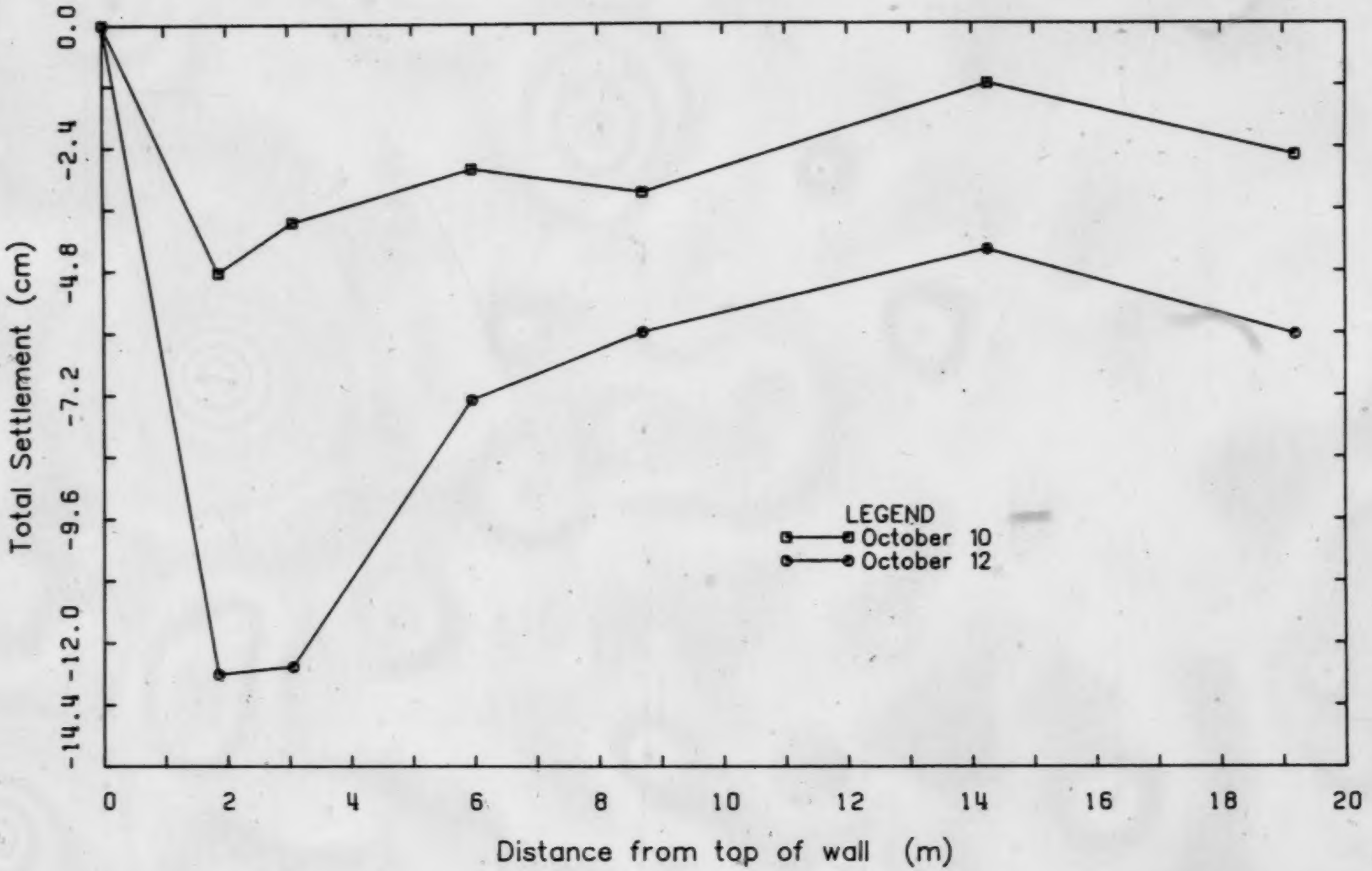

FIGURE B–4 TOTAL SETTLEMENT VS DISTANCE FROM TOP OF WALL MP#3

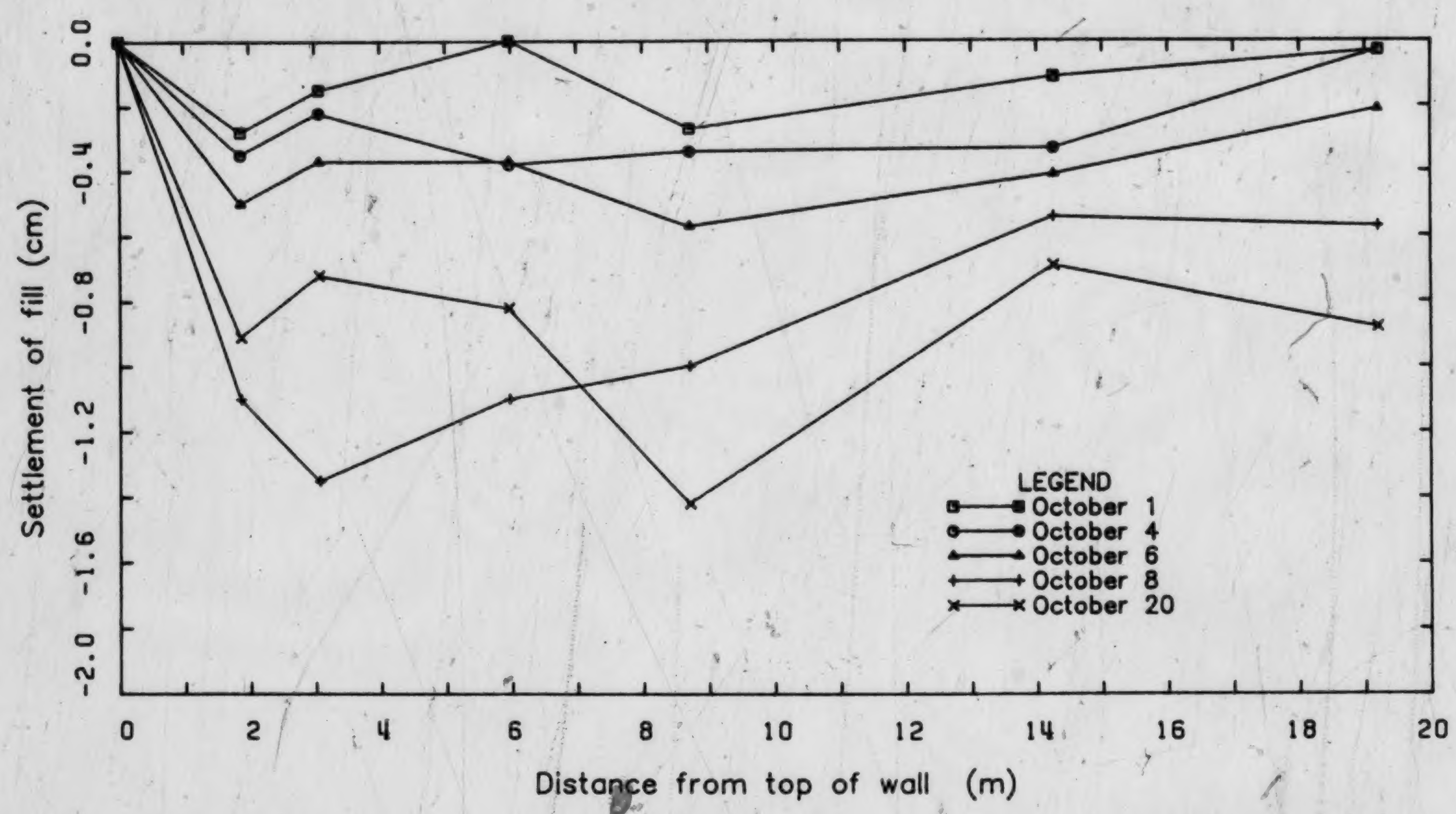

FIGURE B-5 FILL SETTLEMENT VS DISTANCE FROM TOP OF WALL MP#3

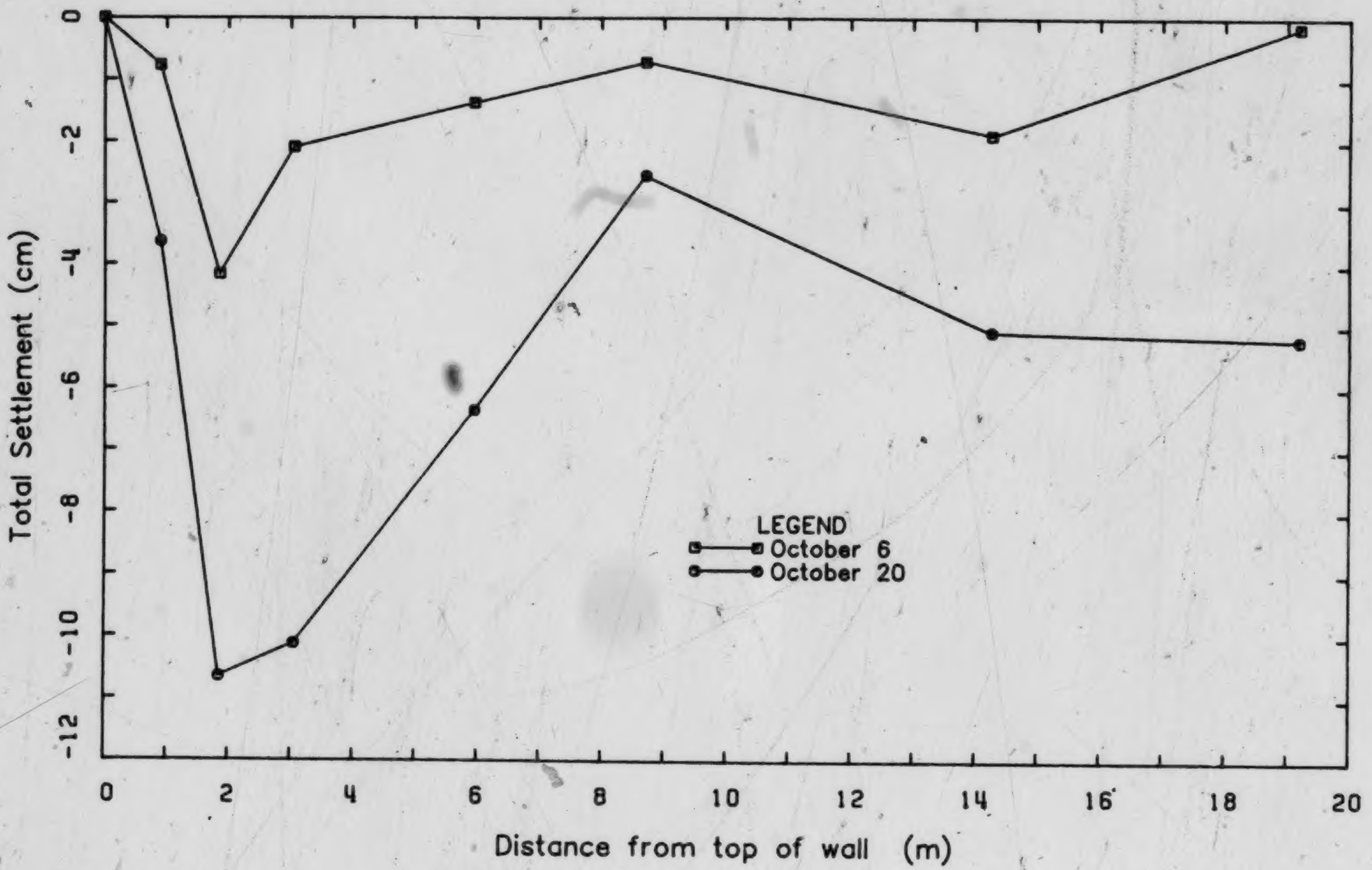

FIGURE B-6 TOTAL SETTLEMENT VS DISTANCE FROM TOP OF WALL MP#5

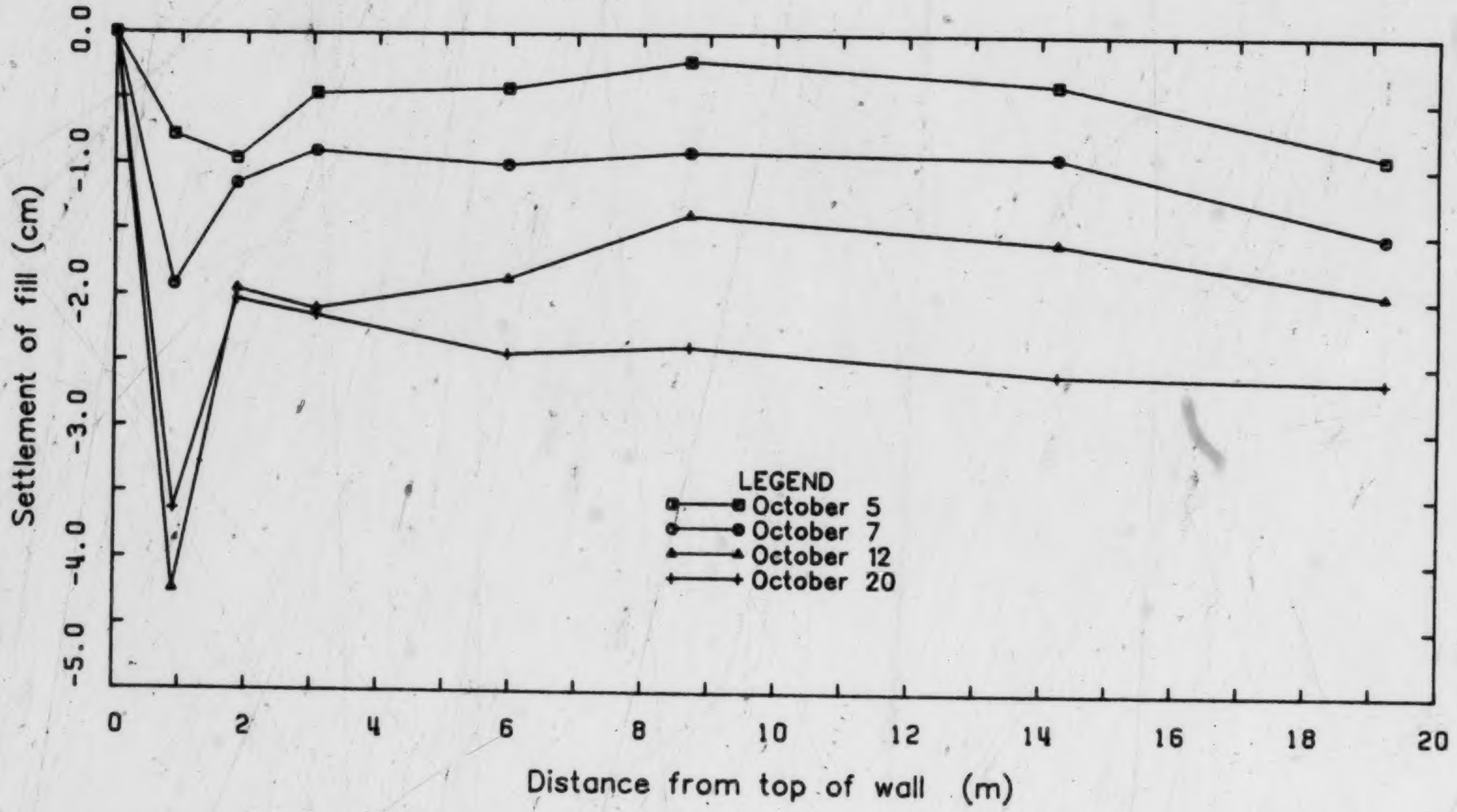

FIGURE B-7 FILL SETTLEMENT VS DISTANCE FROM TOP OF WALL MP#5

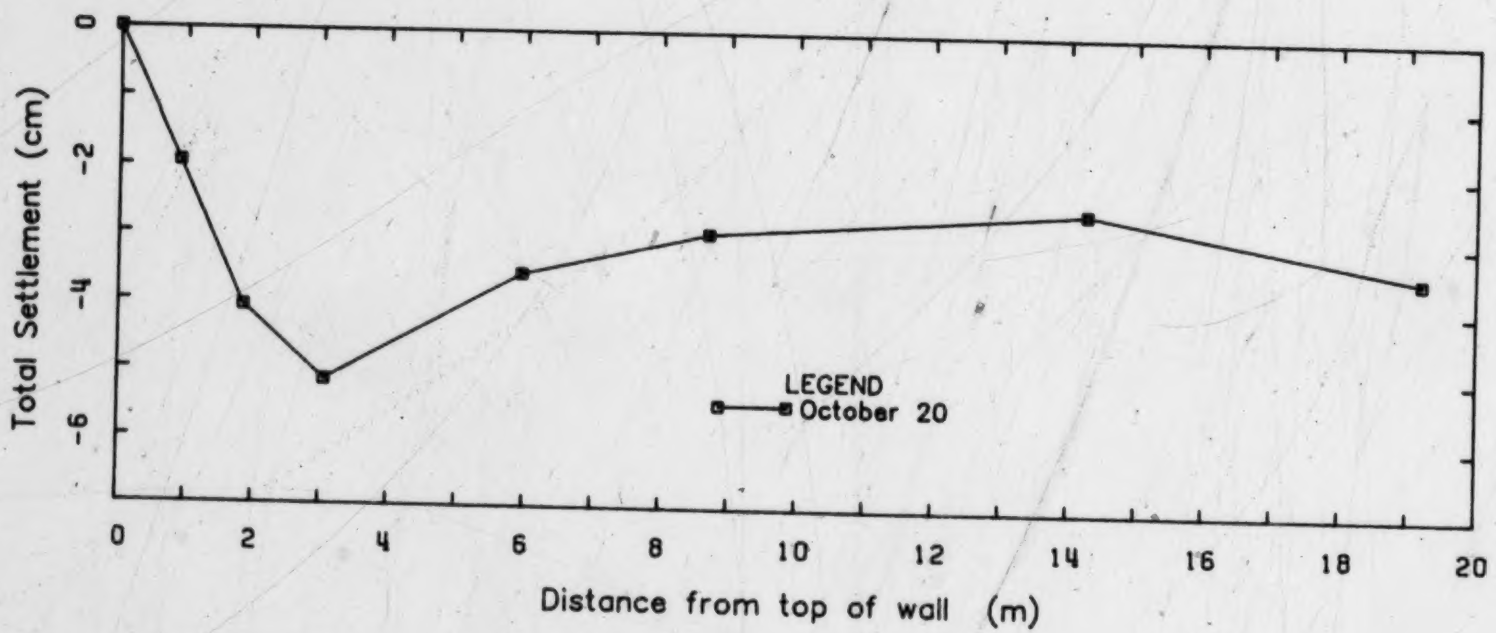

FIGURE B-8 TOTAL SETTLEMENT VS DISTANCE FROM TOP OF WALL MP#6

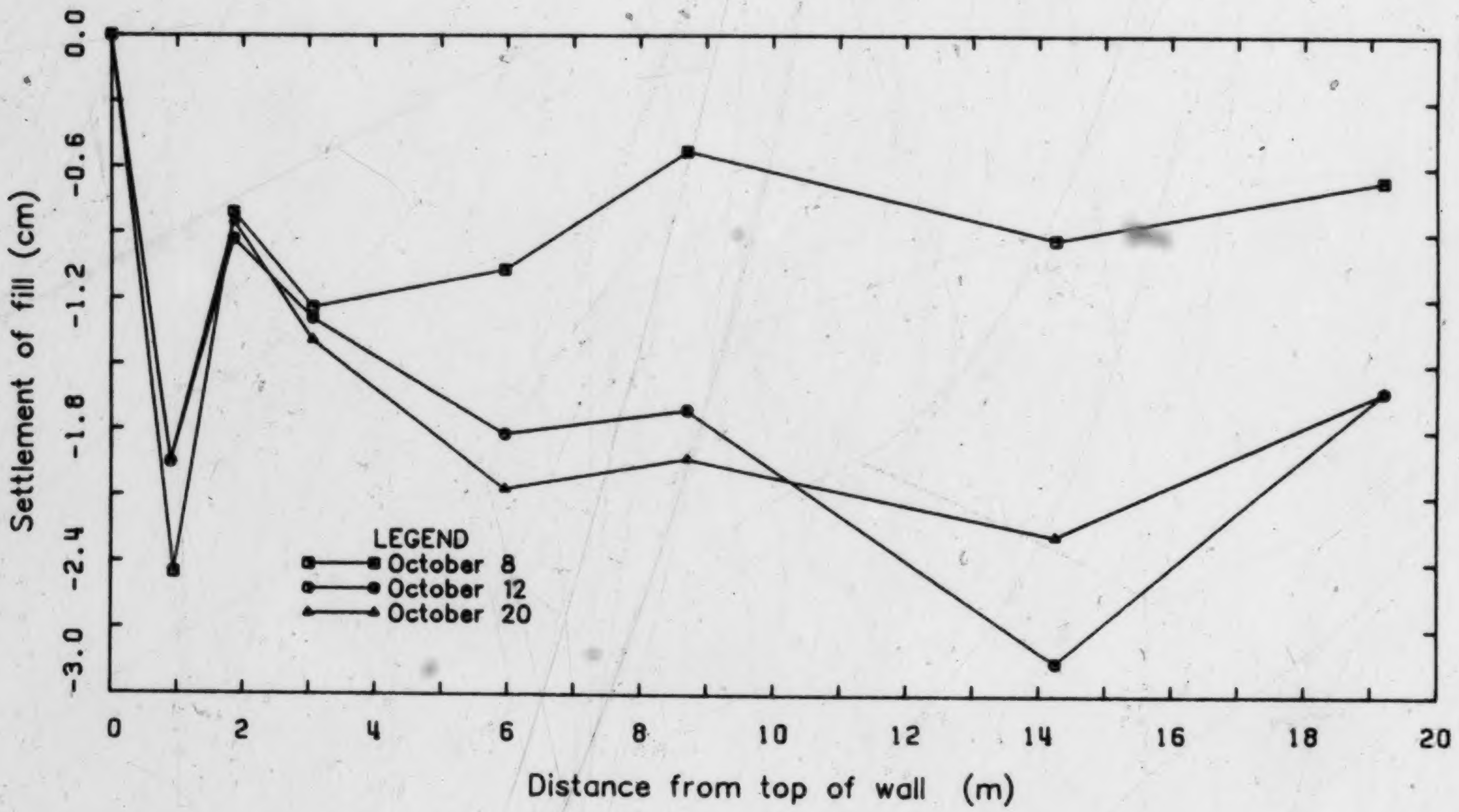

FIGURE B-9 FILL SETTLEMENT VS DISTANCE FROM TOP OF WALL MP#6

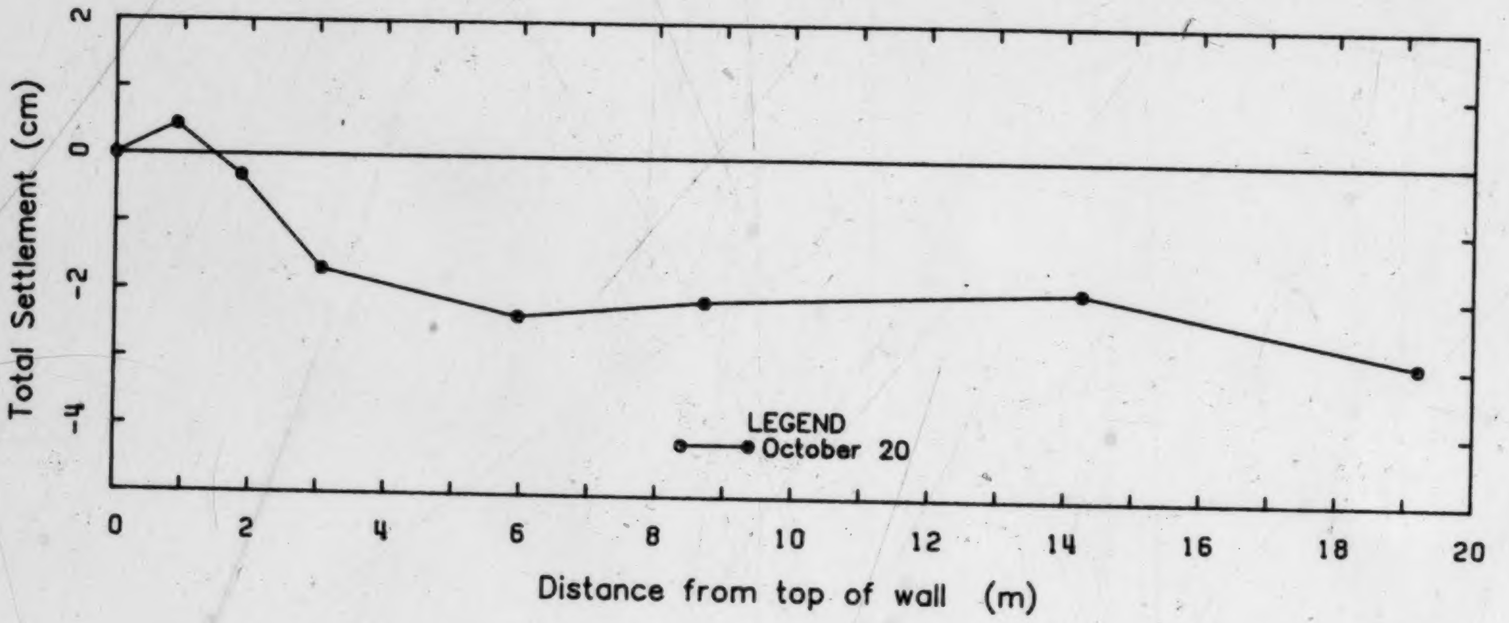

FIGURE B-10 TOTAL SETTLEMENT VS DISTANCE FROM TOP OF WALL MP#7

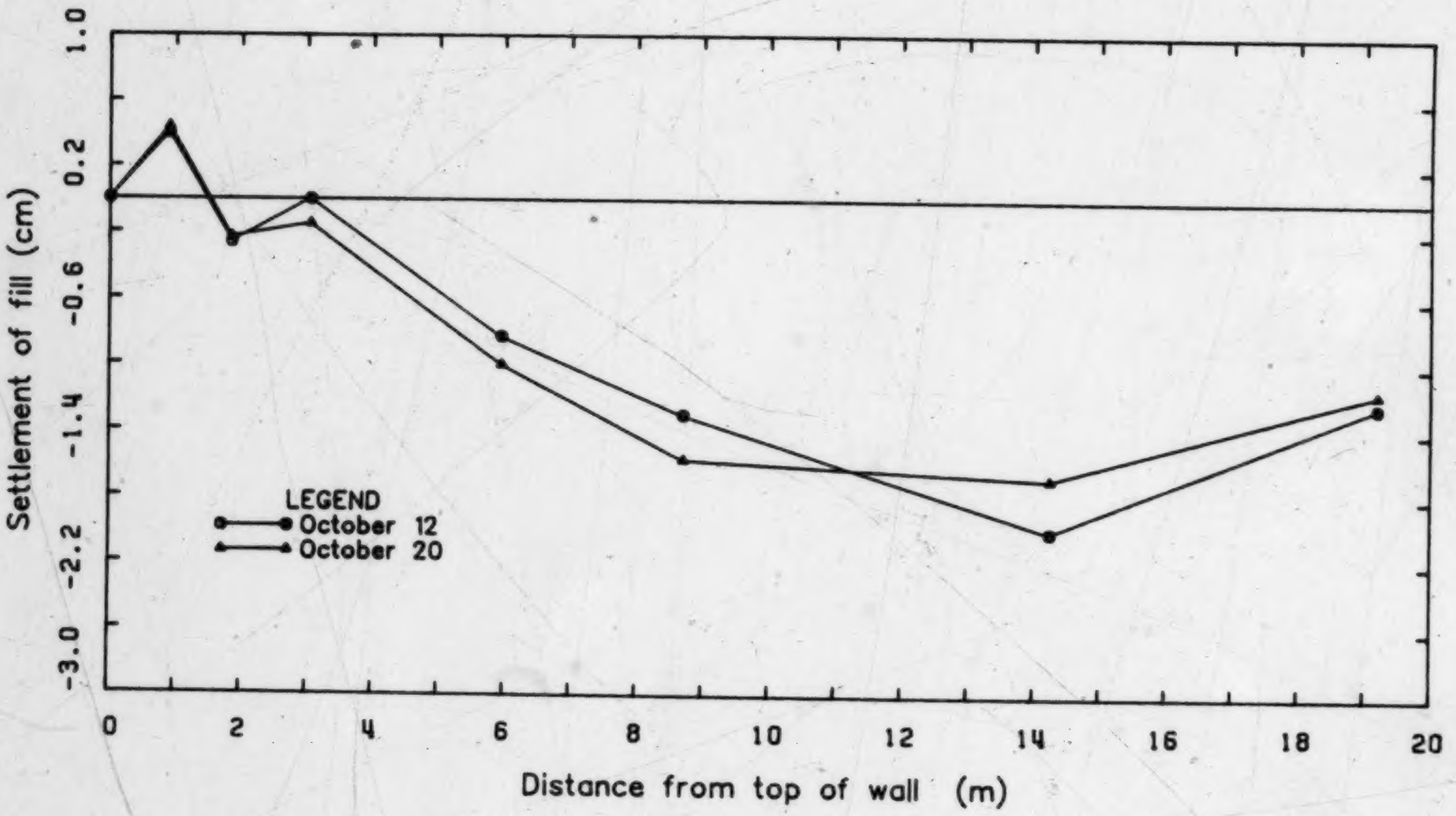

FIGURE B-11 FILL SETTLEMENT VS DISTANCE FROM TOP OF WALL MP#7

APPENDIX C - TRIAXIAL TESTS FOR FINITE ELEMENT ANALYSES

As discussed in Chapter 6, the Finite Element Program used to back analyse the results of the Test Embankment makes use of conventional triaxial compression tests to represent the behaviour of the soil mass. (Krishnayya, 1973).

Three basic items have to be provided to the subroutine, to obtain the desired elastic parameters (Bulk Modulus (K) and Shear Modulus (G)):

- An unconfined compression test
- Consolidated drained triaxial compression tests covering the range of expected stresses
- Measurement of volume change during shear.

The unconfined tests provide a lower bound for interpolation between results at different values of confining pressure. The upper bound is given by the highest confining pressure used in the tests. Linear extrapolations are automatically performed for states of stress exceeding the maximum confining pressure input.

The greater the number of curves between these two boundaries, the more accurate are the interpolations.

The volumetric strain allows the program to determine the Poisson's Ratio (ν). It is not assumed constant but varies depending on the stress level.

Of these three requirements, only the first two were mantained and a new feature was introduced into the program allowing for either variable or constant Poisson's Ratio. In the first case, volumetric changes would be input and in the latter, the value of Poisson's Ratio would be given.

The tests were run in samples 63 mm (2.5") in diameter and 126 mm (5") high. Each sample was prepared separately by compacting soil, at the optimum moisture content, inside a split ring mold. A trial method had shown that by compacting the material in three layers, and applying 11 blows per layer using a Standard Proctor Hammer (5 1/2 lb, 12" drop), densities around the maximum dry density were obtained, as shown in Table C.1. In the same table values of confining pressure, axial strain to failure and maximum shear stress are also presented.

After the sample was compacted and removed from the mold, both ends were trimmed to bring the sample to the desirable height.

All samples were first saturated using a back-pressure of 250 kPa [8] and the amount of water flowing into the sample was monitored to determine the end of volume change.

Finally, the sample was sheared using a rate of axial deformation of 0.009 mm/min. With this rate full drainage was ensured.

It is important to note that volume change was not observed during shear, primarily because the influence of constant Poisson's Ratio seems not significant.

---

[8] According to Bishop and Henkel (1962, pg 113 - second edition) a back pressure of 206kPa (30 psi) is usually sufficient to dissolve all the air.

γ_t kN/m	Wi %	σ_3 kN/m	τ kN/m	ϵ_f %
20.7	13.5	0.0	162.0	6.0
20.5	15.0	62.0	300.0	14.5
21.1	14.2	119.0	385.2	20.0
19.8	13.8	150.0	459.9	19.9

Table C.1 Summary of Triaxial Compression Tests

Figure C.1 presents the stress-strain curves for four of the tests performed during this program. From the Mohr-Coulomb envelope the measured strength parameters are,

c = 50 kPa and ϕ = 34°

For similar material from the Mica Dam, Duncan et al (1980) reported:

c = 56 kPa and ϕ = 33° to 34°

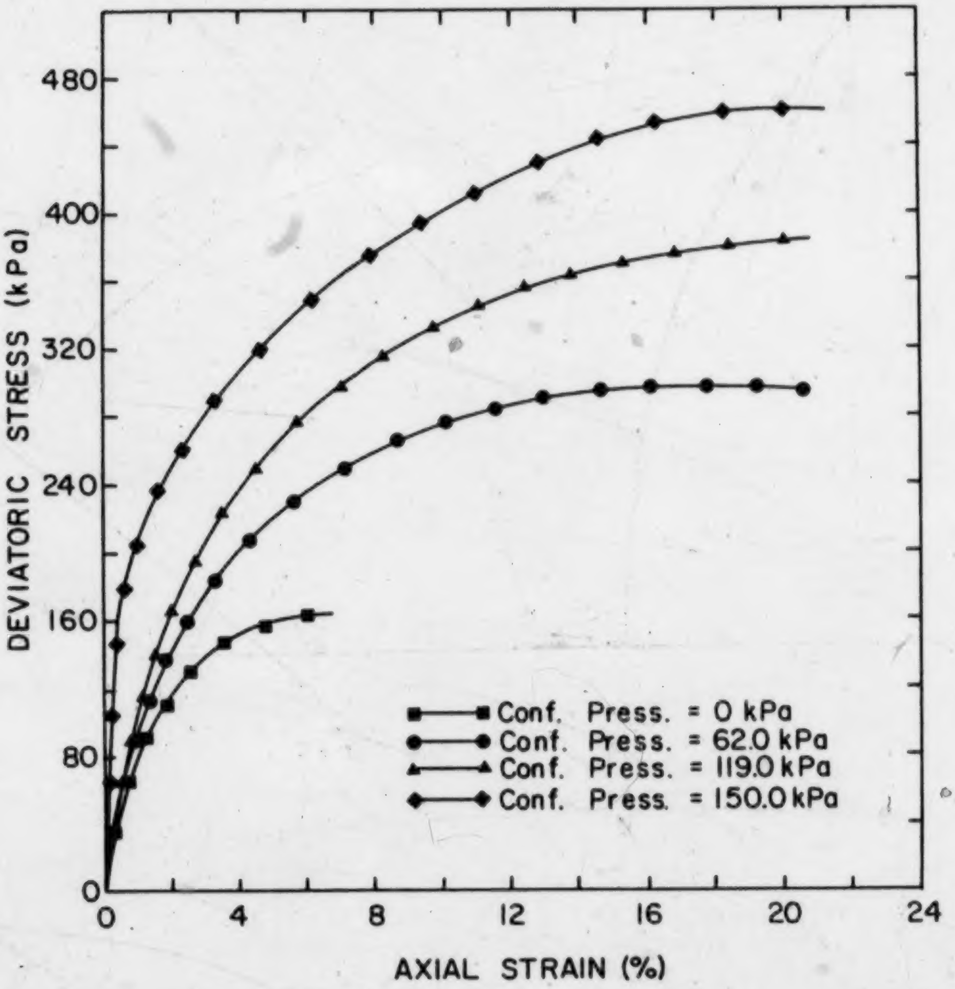

Figure C.1 Stress-Strain Curves for Triaxial Tests

APPENDIX D - DETAILS OF THE LARGE SHEAR TEST APPARATUS

This Appendix presents some design details of the large shear box apparatus described in Chapter 4. Most of the relevant dimensions are shown in the figures that follow, and a series of plates provide a general view of the equipment.

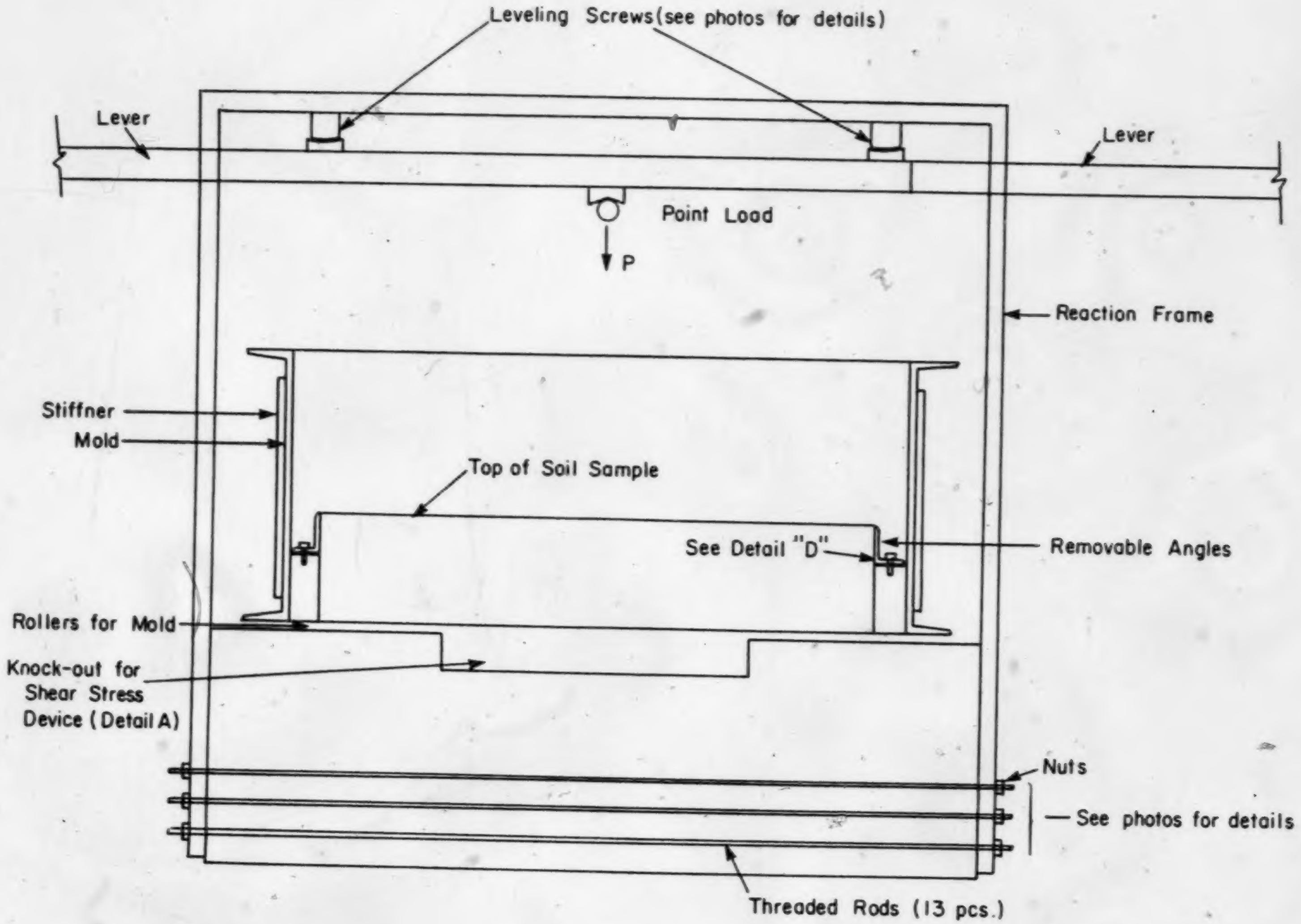
Leveling Screws(see photos for details)
Lever
Lever
Point Load
P
Reaction Frame
Stiffner
Mold
Top of Soil Sample
See Detail "D"
Removable Angles
Rollers for Mold
Knock-out for Shear Stress Device (Detail A)
Nuts
See photos for details
Threaded Rods (13 pcs.)

Figure D.1 Detailed View of Large Shear Box Test

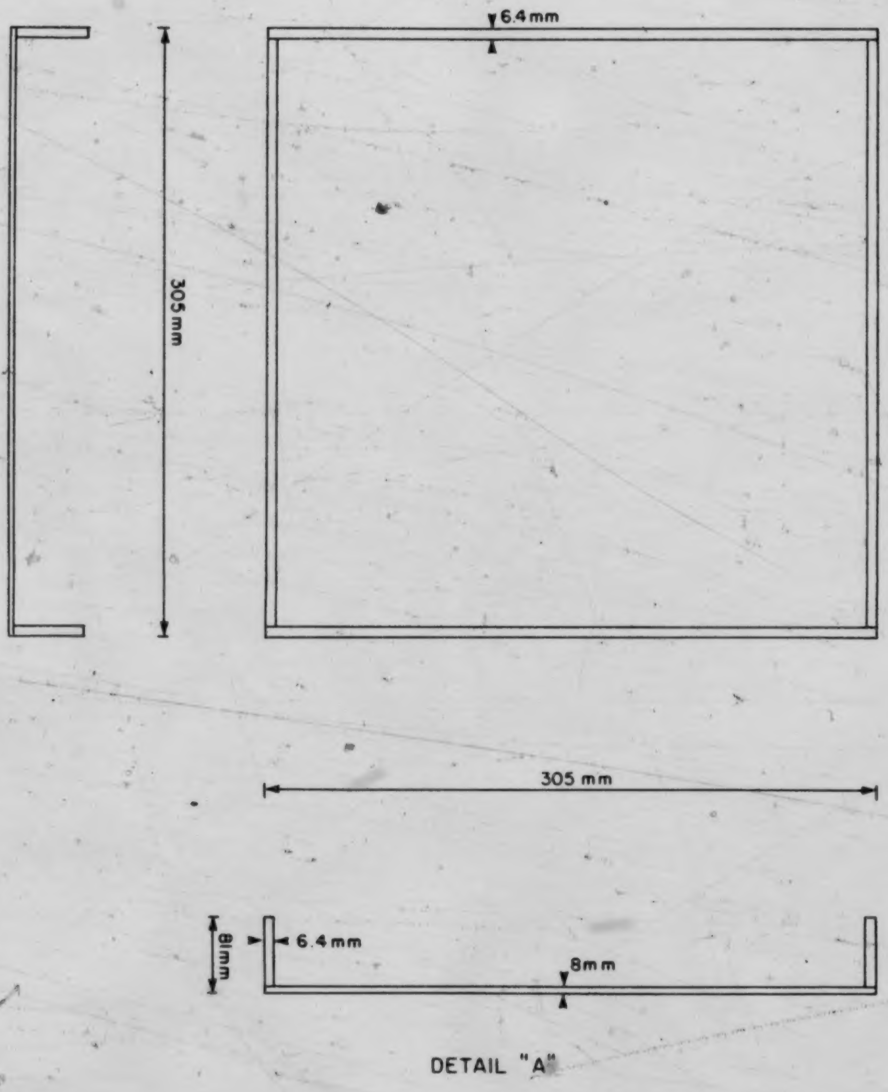
6.4mm
305 mm
305 mm
81mm
6.4mm
8mm
DETAIL "A"

Figure D.2 Detail of Recess for Shear Stress Device

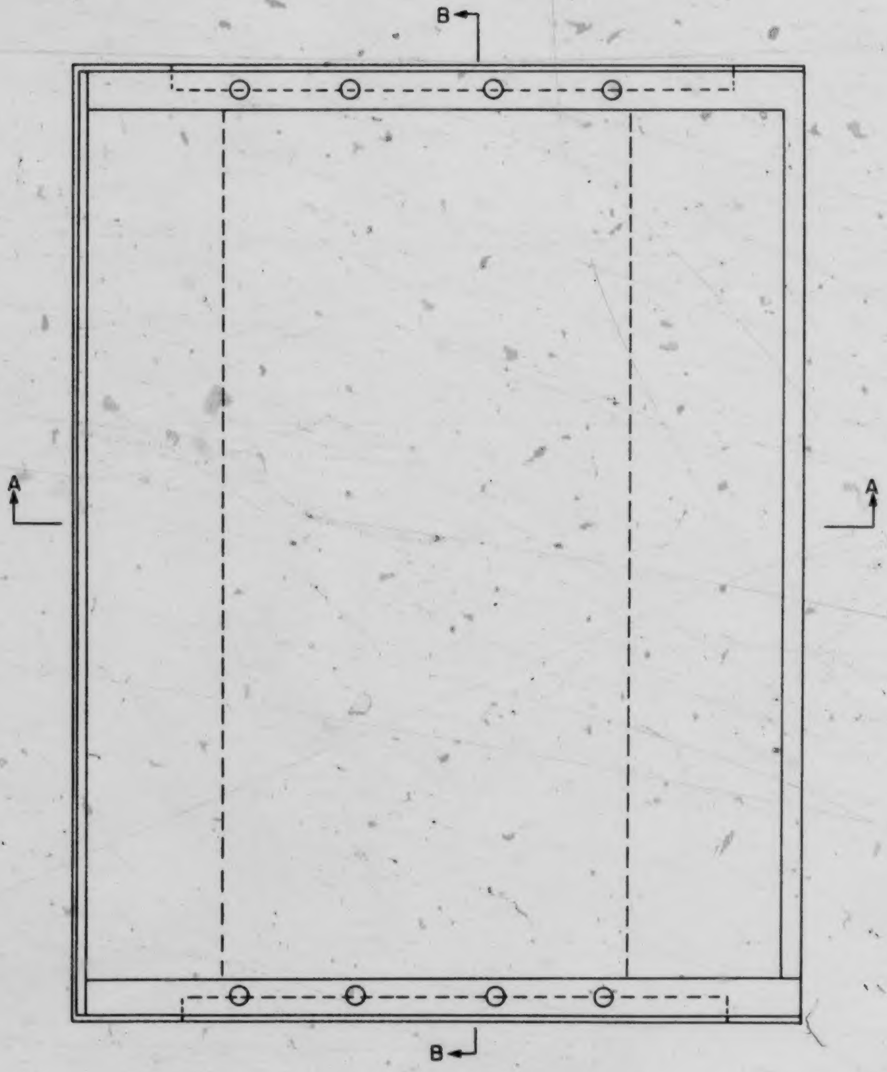

Figure D.3 View of Modified Version of Shear Stress Device

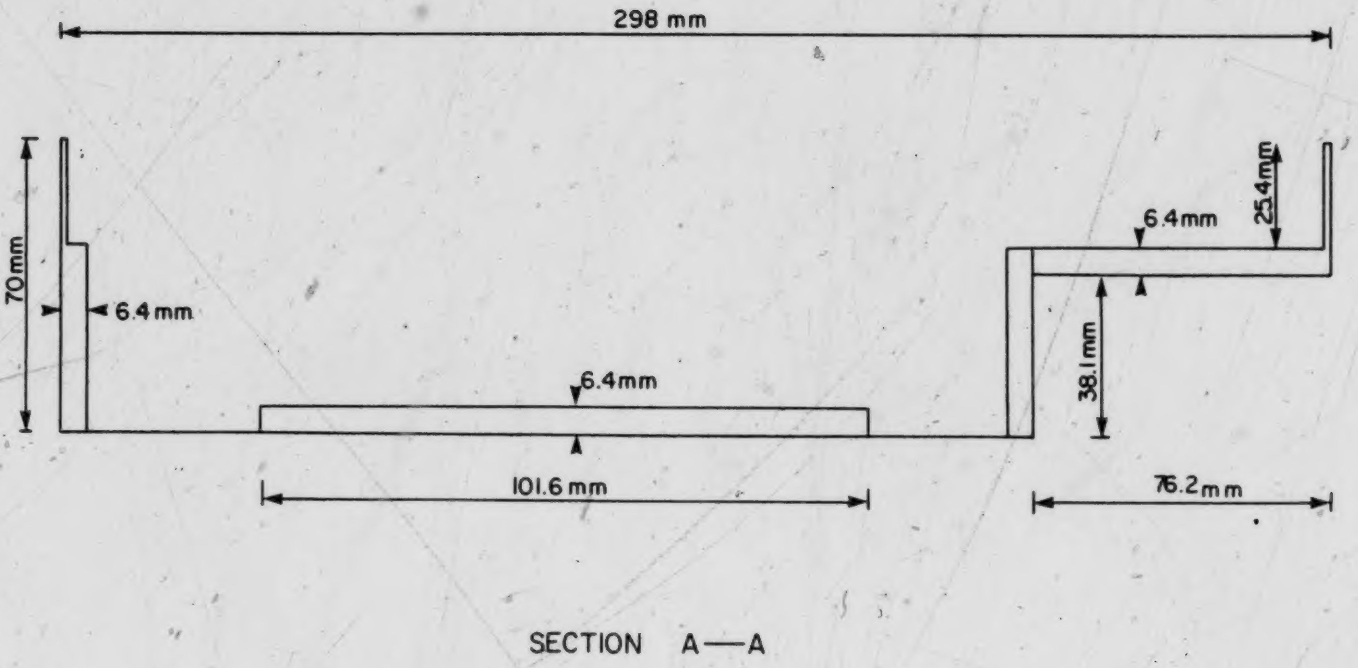
298 mm
70mm
6.4mm
6.4mm
101.6mm
6.4mm
25.4mm
38.1mm
76.2mm
SECTION A—A

Figure D.4 Detail of Outer Box for Shear Stress Devices

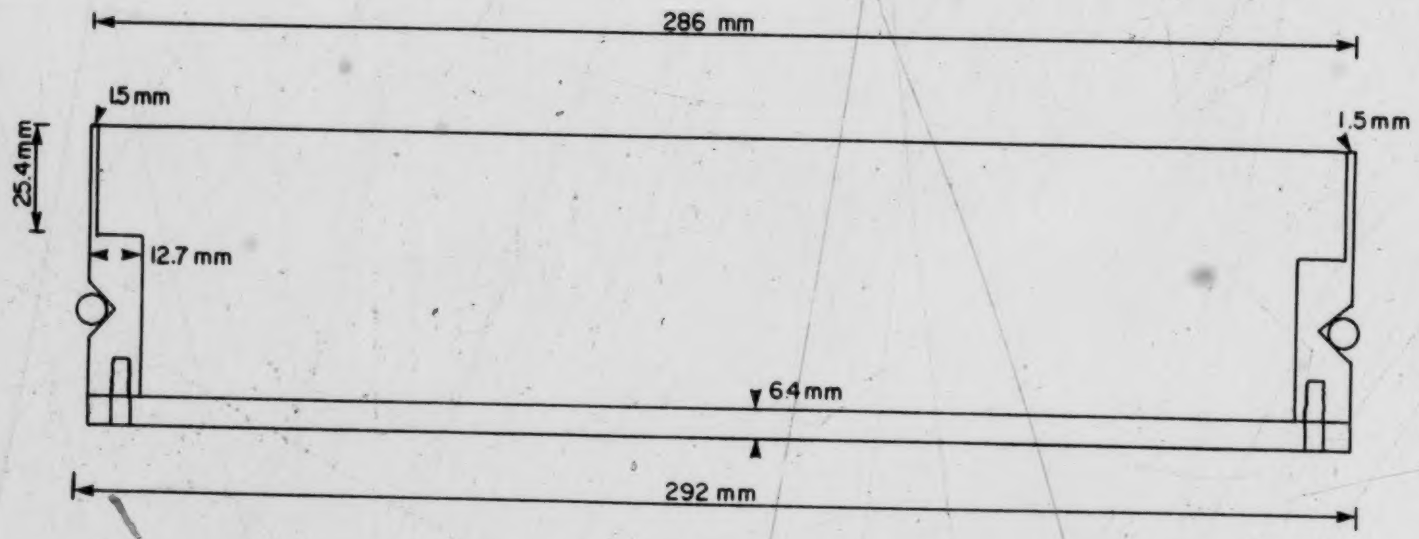
286 mm
1.5 mm
1.5 mm
25.4 mm
12.7 mm
64 mm
292 mm

Section B - B

Figure D.5 Detail of Inner Box for Shear Stress Device

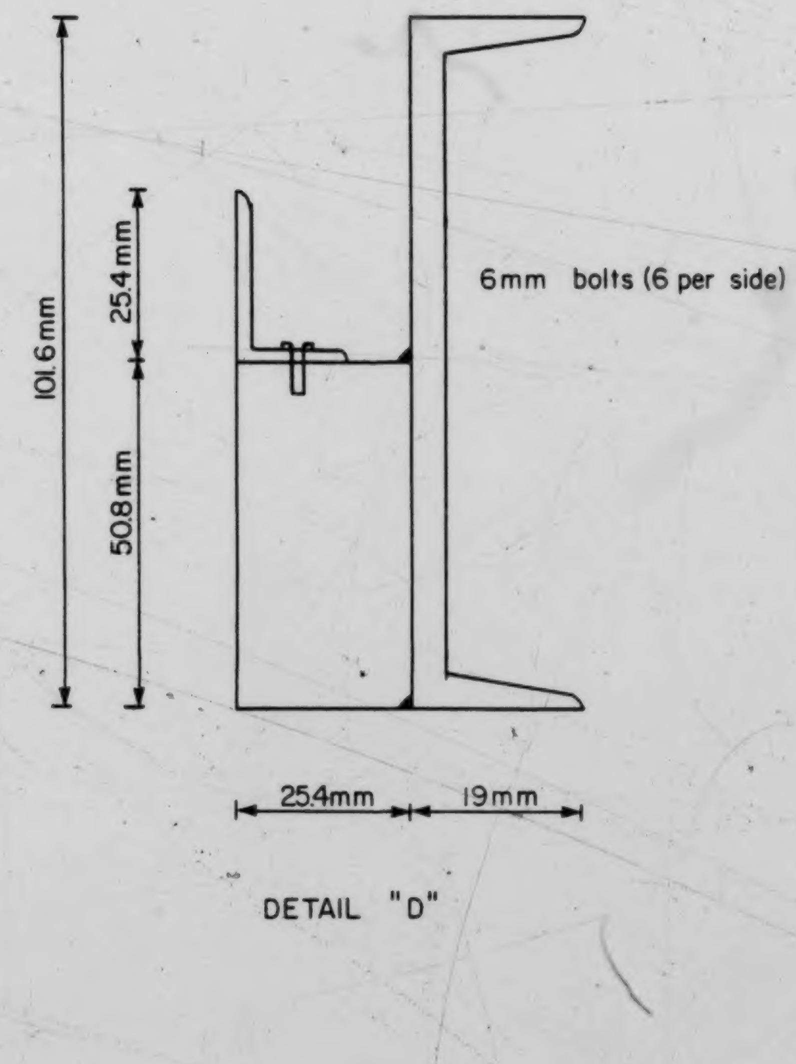
101.6 mm
25.4 mm
50.8 mm
6 mm bolts (6 per side)
25.4 mm
19 mm
DETAIL "D"

Figure D.6 Detail of Removable Angle to Reduce Sample Size

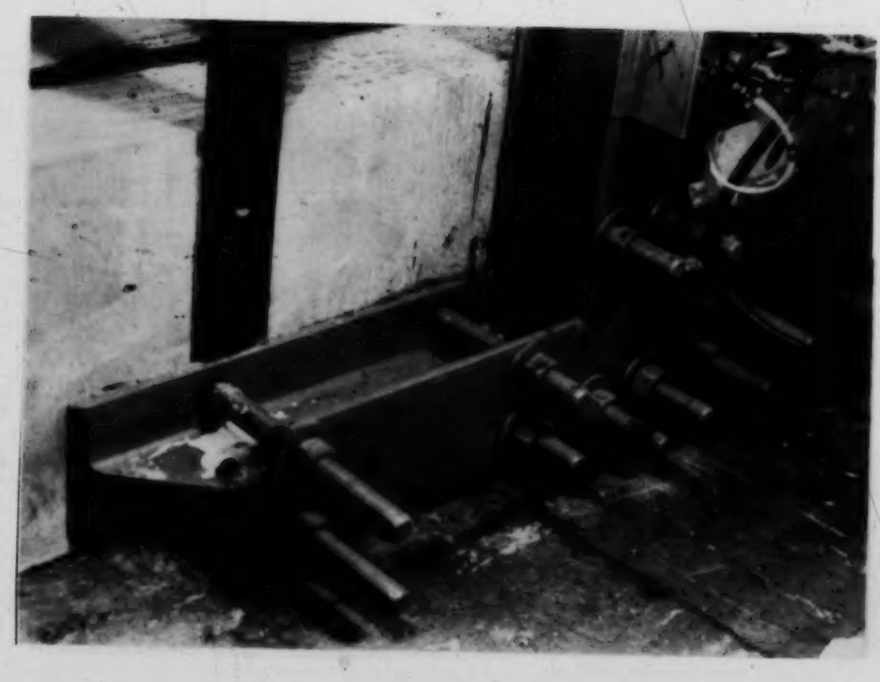

Plate D.1 Detail of Connection U-Frame - Concrete Base

APPENDIX E - VERTICAL DISPLACEMENT DURING SHEAR

In addition to the vertical displacement curve shown in Chapter 4, in this Appendix a few other curves are presented allowing for a more detailed discussion of the vertical displacements measured during shear. As mentioned in Chapter 4, the magnitude of the internal measurements of vertical displacements were, in most cases, within the accuracy of the LVDT used. Therefore, the quantitative values are not completely reliable.

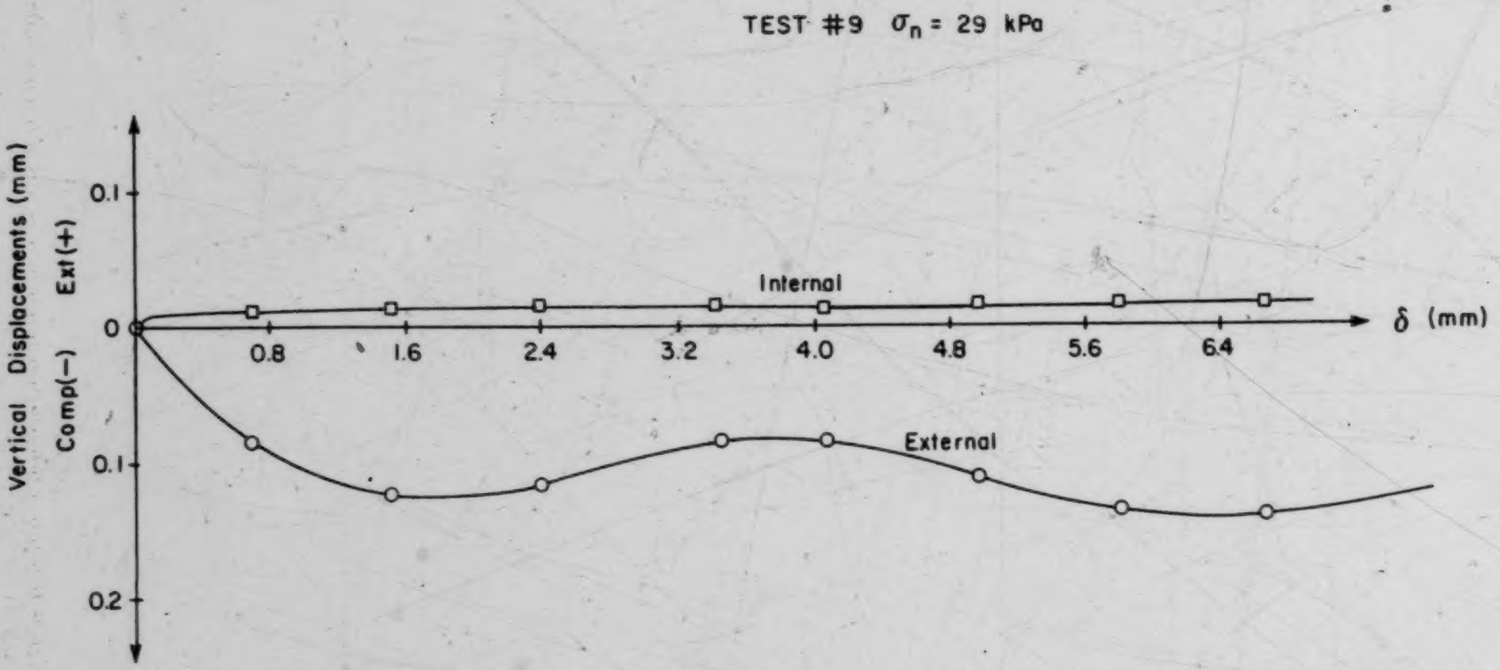

Figure E.1 Vertical Displacements During Shear - Test#9

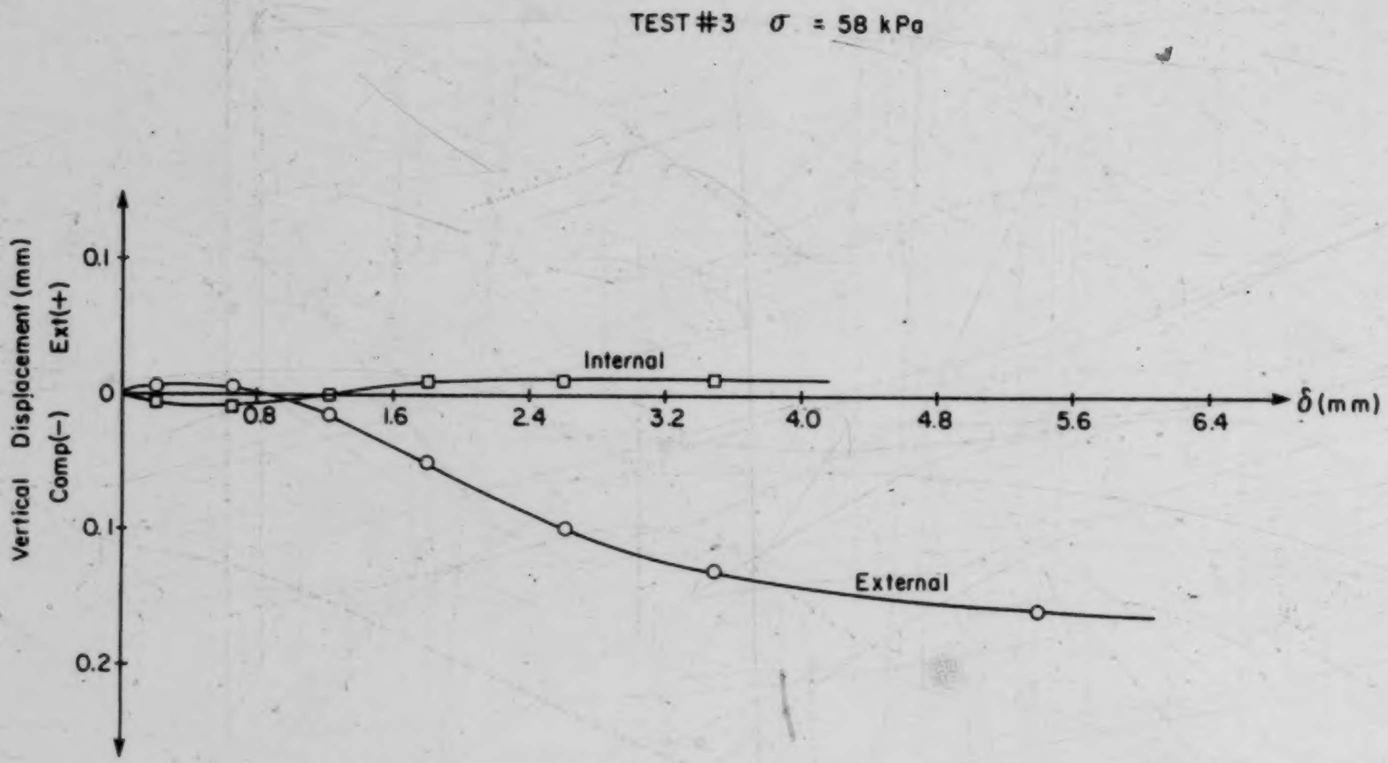

Figure E.2 Vertical Displacements During Shear - Test#3

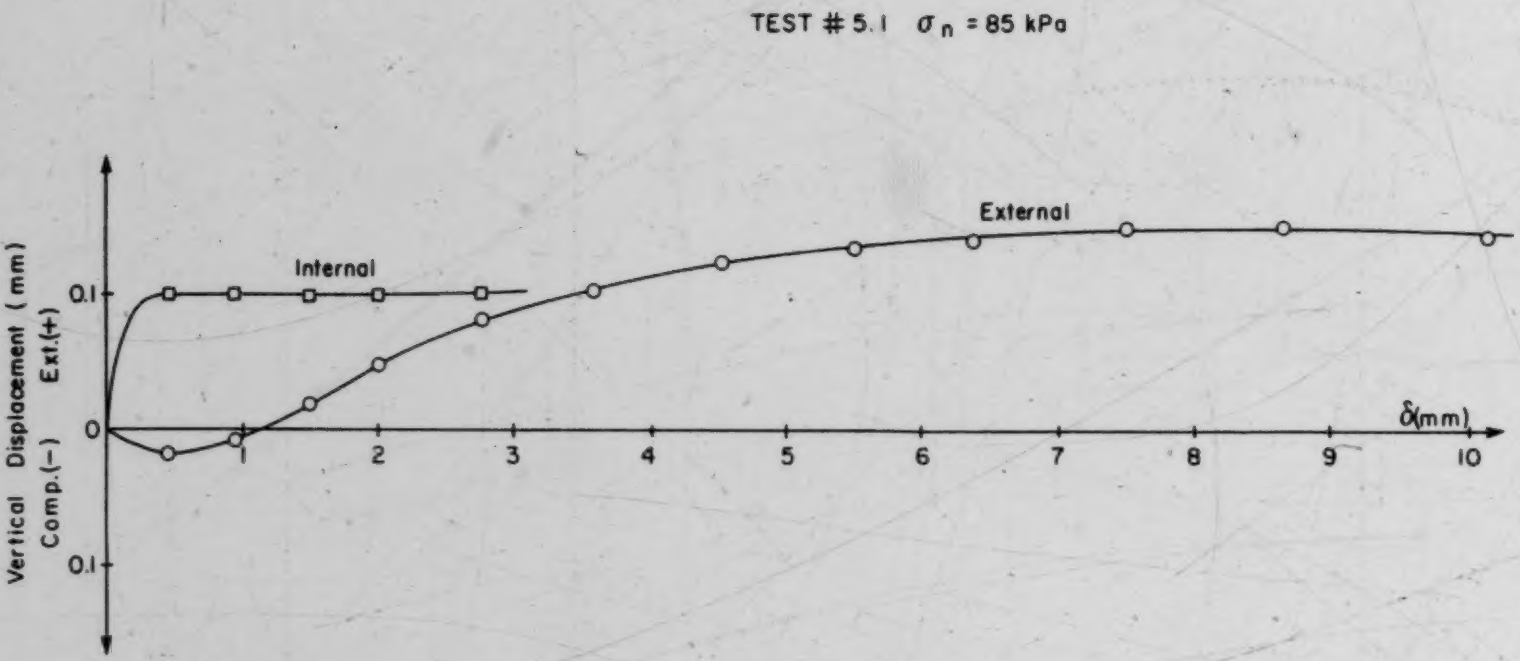

Figure E.3 Vertical Displacements During Shear - Test#5.1

APPENDIX F - FORTRAN PROGRAM FOR PHENOMENOLOGICAL MODEL

In this Appendix a listing of the computer program developed to solve the phenomenological model is presented.

The input parameters are as follow:

NBL - number of blocks composing the model
AKA - constants for even springs
AKB - constants for odd springs
FORA - incremental force to be applied to the model
NINC - number of load increments
TAU3 - maximum shear strength for units "R"
RETAU1 - residual shear strength for units "R"

The output includes:

1. Forces in all nodes
2. Displacements and shear stresses of all nodes

LISTING OF COMPUTER PROGRAM

```
C   MODEL FOR LABORATORY TESTS USING SPRINGS   C
C   THE TESTS ARE REPLACED BY A GROUP OF
C   SPRINGS AND BLOCKS OF MATERIAL THAT
C   HAVE SHEAR STRENGTH. AFTER THE MAXIMUM
C   RESISTANCE OF THIS BLOCKS IS REACHED, THE
C   PARALEL SPRING WILL HOLD ALL THE FORCE,
C   BUT THE ELEMENT CAN STILL DISPLACES
C
C          BOTH SPRINGS
C   HAVE A LINEARLY INCREASING FUNCTION TO
C   DESCRIBE THEIR BEHAVIOUR
C
C              (VERSION 84.25 - JUNE/84)
C
C
C
      DIMENSION
DELT(300),AK(200),RTAU(200),FOR(200),
     1DISP(300),CENTAU(300),EXTAU(300),CENDIS(300),

2NCO(200),DE(200),TFOR(200),RETAU(200),TAU(200),
     3F(200),ICO(200),DET(200),AKE(200),EXDIS(200),
     4FF(200)
C
C
```

```
C
C
      READ(5,201)NBL,AKA,AKB,FORA,NINC,TAU3,RETAU1
      READ(5,300) ICBL,LCBL
      READ(5,301) ANORM
      READ(5,302) KKO
  302 FORMAT(I5)
  301 FORMAT(F15.8)
  300 FORMAT(2I5)
      NSP=NBL*2
      IICB=ICBL*2
      IFCB=LCBL*2
      WRITE(6,331)
      WRITE(6,332)
      WRITE(6,332)
      WRITE(6,333)
  333 FORMAT(' *   LABORATARY BIG SHEAR BOX TEST
*')
      WRITE(6,332)
      WRITE(6,332)
      WRITE(6,331)
  332 FORMAT(' *
*')
  331 FORMAT('
****************************************')
      MI=(NSP)/2
      MAA=NSP+2
      DO 396 K=1,MAA
      FOR(K)=0.0
      DELT(K)=0.0
      ICO(K)=1
  396 NCO(K)=0
      AREA=(0.66/MI)
      FOR2=0.0
      DELTF=FORA
      NSP1=NSP-1
      DO 2 I=1,NSP1,2
C     AK(I)=AKB
      K=I+1
C     AK(K)=AKA
      AK1=AKB*1.9
      AB=I
      AC=NSP
      AA=AB/AC
      AKC=AKB*0.1
      AK(I)=AKC+((AK1-AKC)*AA)
      AK3=AKA*0.8
      AK2=AKA*1.2
      AK(K)=AK3+((AK2-AK3)*AA)
      TAU(K)=TAU3
      RETAU(K)=RETAU1
    2 CONTINUE
      DO 5000 MJ=1,NINC
      WRITE(6,199)
      WRITE(6,200)MJ
      WRITE(6,199)
      DO 3 MK=2,NSP,2
      IF(AK(MK).EQ.0.0.AND.ICO(MK).EQ.1)
     1RETAU(MK)=RTAU(MK)*0.994
      IF(ICO(MK).GT.1) RETAU(MK)=RETAU(MK)*0.995
      IF(ICO(MK).GT.1.AND.RTAU(MK).EQ.RETAU1)
     1RETAU(MK)=RETAU1
      ML=MK-1
C
C
C
      R50=0.4*TAU3
      R60=0.5*TAU3
      R65=0.60*TAU3
      R70=0.7*TAU3
      R75=0.75*TAU3
      R80=0.8*TAU3
      R85=0.85*TAU3
      R90=0.9*TAU3
      R95=0.95*TAU3
      IF(NCO(MK).LT.1.AND.RTAU(MK).GE.R50.AND.
     1RTAU(MK).LT.R60) AK(MK)=0.85*AKA
      IF(NCO(MK).LT.1.AND.RTAU(MK).GE.R60.AND.
     1RTAU(MK).LT.R65) AK(MK)=0.75*AKA
      IF(NCO(MK).LT.1.AND.RTAU(MK).GE.R65.AND.
     1RTAU(MK).LT.R70) AK(MK)=0.65*AKA
```

```
         IF(NCO(MK).LT.1.AND.RTAU(MK).GE.R70.AND.
        1RTAU(MK).LT.R75) AK(MK)=0.55*AKA
         IF(NCO(MK).LT.1.AND.RTAU(MK).GE.R75.AND.
        2RTAU(MK).LT.R80) AK(MK)=0.45*AKA
         IF(NCO(MK).LT.1.AND.RTAU(MK).GE.R80.AND.
        3RTAU(MK).LT.R85) AK(MK)=0.33*AKA
         IF(NCO(MK).LT.1.AND.RTAU(MK).GE.R85.AND.
        4RTAU(MK).LT.R90) AK(MK)=0.20*AKA
         IF(NCO(MK).LT.1.AND.RTAU(MK).GE.R90.AND.
        5RTAU(MK).LT.R95) AK(MK)=0.08*AKA
         IF(NCO(MK).LT.1.AND.RTAU(MK).GE.R95)
        1AK(MK)=0.05*AKA
C
C
C
        S1=0.25*TAU3
        S2=0.30*TAU3
        S3=0.35*TAU3
        S4=0.38*TAU3
        S5=0.40*TAU3

IF(NCO(MK).LT.1.AND.RTAU(MK).GE.S1.AND.RTAU(MK).
     6LT.S2) AK(ML)=1.25*AKB

IF(NCO(MK).LT.1.AND.RTAU(MK).GE.S2.AND.RTAU(MK).
     7LT.S3) AK(ML)=1.40*AKB
```

```
      IF(NCO(MK).LT.1.AND.RTAU(MK).GE.S3.AND.RTAU(MK).
     8LT.S4) AK(ML)=1.60*AKB

      IF(NCO(MK).LT.1.AND.RTAU(MK).GE.S4.AND.RTAU(MK).
     9LT.S5) AK(ML)=1.85*AKB

      IF(NCO(MK).LT.1.AND.RTAU(MK).GE.S4.AND.RTAU(MK).
     &LT.R95) AK(ML)=AKB*2.
       IF(NCO(MK).LT.1.AND.RTAU(MK).GE.R95)
     1AK(ML)=2.000*AKB
       IF(AK(MK).EQ.0.0) AK(ML)=AKB*2.000
C
       DE(MK)=0.0
     3 CONTINUE
C
C
C
       CALL SPRING (AK,AKE,DELT,TAU,AREA,FF,F,
     1NSP,RETAU,AKA,MJ)
C
C


       FOR1=DELTF
       NITER=0
       NNK=0
   531 FOR0=FOR0+FOR1
       ABC=FOR1
      DO 12 K=1,MAA
   12 FOR(K)=0.0
  532 WRITE(6,345) FOR0,FOR1
  345 FORMAT('  APPLIED FORCE =  ',F8.5,'
     1 INC FORCE= ',F8.5)
      NITER=NITER+1
      IF(NITER.EQ.1) WRITE(6,2323)
 2323 FORMAT( 'NODE   FORCE   NODE   FORCE
     1NODE    FORCE    NODE   FORCE')
C     WRITE(6,981)
C 981 FORMAT('  NODE     DISP.       TOT.DISP/INC')
      IF(KKO.EQ.1) FOR1=FOR1*AKE(1)
      DO 520 JJ=2,NSP,2
      IF(AK(JJ)) 520,520,521
  520 AAA=0.0
      GO TO 522
  521 CONTINUE
  522 DO 900 M=2,MAA,2
      DE1=0.0
      DE1=FOR1/AKE(M)
      IF(AK(M).EQ.0.0) DE1=0.0
      FOR6=DE1*AK(M)
      FOR1=FOR1-FOR6
      DE(M)=DE(M)+DE1
C     WRITE(6,980) M,DE1,DE(M)
C 980 FORMAT(I5,2F15.9)
      K=M+1
      FOR(M)=FOR(M)+FOR6
   20 FOR(K)=FOR(K)+FOR1
C
      TFOR(M)=TFOR(M)+FOR(M)
C1413 FORMAT(2I4,4F15.8)
C
   51 RTAU(M)=TFOR(M)/AREA
      MA=NSP
      IF(AK(MA).EQ.1.AND.M.EQ.MA.AND.RTAU(MA).
     1EQ.RETAU1) GO TO 900
      IF(AK(MA).EQ.1.AND.M.EQ.MA.AND.RTAU(MA).
     1GT.RETAU1) GO TO 667
      IF(M.EQ.MAA) GO TO 900
      TAU1=1.005*TAU(M)
      TAU2=0.995*TAU(M)
      IF(AK(M).EQ.0.0.AND.RTAU(M).GT.RETAU1)
     1GO TO 667
      IF(AK(M).EQ.0.0.AND.RTAU(M).EQ.RETAU1)
     1GO TO 900
      IF(RTAU(M)-TAU2) 900,900,466
  466 IF(RTAU(M)-TAU1) 900,900,665
C
C
C
  665 T1=1.05*TAU(M)
      T2=1.1*TAU(M)
      T3=1.2*TAU(M)
```

```
C     IF(M.EQ.NSP) GO TO 900
      FOR0=FOR0-ABC
      IF(RTAU(M).GT.TAU(M).AND.RTAU(M).LT.T1)
     1 FOR1=0.95*ABC
      IF(RTAU(M).GT.T1.AND.RTAU(M).LT.T2)
     2 FOR1=0.85*ABC
      IF(RTAU(M).GT.T2.AND.RTAU(M).LT.T3)
     3 FOR1=0.75*ABC
      IF(RTAU(M).GT.T3) FOR1=0.5*ABC
      DO 52 J=2,M,2
      TFOR(J)=TFOR(J)-FOR(J)
   52 RTAU(J)=0.0
      NCO(M)=1
      DO 23 N=1,MAA
      FOR(N)=0.0
   23 DE(N)=0.0
      GO TO 531
C
  667 TFOR(M)=FF(M)
      FOR1=FOR1+FOR6
C*****WRITE(6,1212) M
C1212 FORMAT('PASSED 667 FOR ELEMENT=',I5)
      NCO(M)=2
      ICO(M)=ICO(M)+1
      RTAU(M)=TFOR(M)/AREA
      GO TO 900
  900 IF(RTAU(M).GE.TAU2.AND.RTAU(M).LE.TAU1)
```

```
     1AK(M)=0.0
      CONTINUE
      DO 401 JH=2,MAA,2
  401 DET(JH)=0.0
      MN=NSP
      DO 5 KJ=2,MAA,2
      DET(KJ)=0.0
      DO 6 IJ=KJ,MAA,2
      DET(KJ)=DET(KJ)+DE(IJ)
    6 CONTINUE
C     IF(AK(MN).EQ.1) DET(KJ)=DET(KJ)-DE(MN)
    5 CONTINUE
  533 DO 756 K=2,NSP,2
      J=K+1
      DELT(K)=DELT(K)+DET(K)
  756 CONTINUE
C
C
      WRITE(6,1221) (J,FOR(J),J=1,NSP)
 1221 FORMAT(2(I4,F8.3,3X,I4,F8.3,3X))
      WRITE(6,99)
      WRITE(6,120)
  120 FORMAT('     SP    DISP     STRESS
     1    SP    DISP     STRESS ')
      DO 675 I=2,NSP,2
      DISP(I)=DELT(I)*1000.
  675 CONTINUE
```

```
      WRITE(6,202)(K,DISP(K),RTAU(K),K=2,NSP,2)
      WRITE(6,99)
   99 FORMAT(/)
C
C
      NKK=0
      EXDIS(MJ)=DISP(2)
      CAREA=((IFCB-IICB)*AREA)/2.
      TOTFOR=0.0
      WRITE(6,1409)
 1409 FORMAT('  INTERNAL FORCE')
      DO 21 I=IICB,IFCB,2
   21 TOTFOR=TOTFOR+TFOR(I)
      WRITE(6,1410) TOTFOR,CAREA
 1410 FORMAT(2F12.6)
      CENT=TOTFOR/CAREA
      CENTAU(MJ)=CENT
      MA=IFCB-2
      CENDIS(MJ)=DISP(MA)
 1598 FORMAT(2F15.8)
      EXFOR=0.0
      WRITE(6,1411)
 1411 FORMAT('  EXTERNAL FORCE')
      NSP2=NSP
      DO 22 J=2,NSP2,2
   22 EXFOR=EXFOR+TFOR(J)
C
```

```
C
      EXAR=AREA*(NSP/2)
      WRITE(6,1412) EXFOR,EXAR
 1412 FORMAT(2F12.6)
      EXT=EXFOR/EXAR
      EXTAU(MJ)=EXT
 1599 FORMAT(2F15.8)
 5000 CONTINUE
 5001 WRITE(6,1597)
 1597 FORMAT('   INTERNAL MEASUREMENTS')
      WRITE(6,1598)(CENDIS(I),CENTAU(I),I=1,MJ)
C     WRITE(6,1600)
C1600 FORMAT('   EXTERNAL MEASUREMENTS')
C     WRITE(6,1599)(EXDIS(I),EXTAU(I),I=1,MJ)
C
C
C       FORMAT STATMENTS
C
C
  199 FORMAT('      ******************************')
  200 FORMAT('      ***    INCREMENT #',I4,'
****')
  201 FORMAT(I4,3F18.3,I4,2F8.3)
  202 FORMAT(2(3X,I4,F10.4,F10.4))
      STOP
      END
C
```

```
C           SUBROUTINE SPRING
C
C
         SUBROUTINE SPRING (AK,AKE,DELT,TAU,AREA,
        1FF,F,NSP,RETAU,AKA,MJ)
         DIMENSION AK(1),AKE(1),DELT(1),TAU(1),
        1RETAU(1),FF(1),F(1)
         IF(MJ.EQ.1) WRITE(6,401)
     401 FORMAT(' SPR. #      CONST.
        1     SPR. #      CONST. ')
         IF(MJ.EQ.1) WRITE(6,400) (I,AK(I),I=1,NSP)
         WRITE(6,99)
      99 FORMAT(//)
     400 FORMAT(2(3X,I4,2X,F15.3))
         MA=NSP
         MAA=NSP+2
         IF(AK(MA).EQ.0.0) AK(MA)=1.0
         DO 409 I=1,MAA
     409 AKE(I)=0.0
         NSPA=NSP
         AKE(NSPA)=AK(NSPA)
         LM=NSPA-1
         MM=NSPA+1
         DO 1 J=1,LM,2
         I=J+2
         K=J+1
         A=1/(AK(NSPA-J))
      B=1/(AKE(MM-J))
      C=A+B
      AKE(NSPA-J)=1/C
   12 IF(J.EQ.LM) GO TO 1
      AKE(NSPA-K)=AK(NSPA-K)+AKE(NSPA-J)
      F(K)=TAU(K)*AREA
      FF(K)=RETAU(K)*AREA
    1 CONTINUE
      AKE(1)=AKA*0.25
      IF(MJ-1) 76,76,78
   76 AAAA=AKE(1)
   78 AKE(NSP+1)=AAAA
      AKE(NSP+2)=AAAA
      IF(AK(MA).EQ.1.) AKE(MA)=AKA*1000
      IF(MJ.EQ.1) WRITE(6,77)
   77 FORMAT('NODE      EQ.CONST
     1   NODE      EQ.CONST    ')
      IF(MJ.EQ.1) WRITE(6,300)(I,AKE(I),I=1,NSP)
      WRITE(6,99)
  300 FORMAT(2(I4,2X,F15.5,4X))
      WRITE(6,99)
      RETURN
      END
```

APPENDIX G - GOODMAN'S JOINT ELEMENT FORMULATION

This Appendix includes a brief derivation of the joint element proposed by Goodman et al (1968).

First, the element "strains" are defined as (refer to Figure G.1)

$$[\epsilon_j] = \begin{bmatrix} u_o \\ v_o \\ w_o \end{bmatrix} = \begin{bmatrix} (u_k + u_m)/2 & - & (u_i - u_j)/2 \\ (v_k + v_m)/2 & - & (v_i - v_j)/2 \\ (v_k - v_m)/t & - & (v_j - v_i)/t \end{bmatrix}$$

where:

$[\epsilon_j]$ - element "strain matrix"

u_o, v_o and w_o - displacements defined for the center of the element. These values also considered to be the in the tangential, normal and rotational strain components of the element.

Therefore, the strain-displacement relationship can be writen:

$$[\epsilon_j] = \begin{bmatrix} -1/2 & 0 & -1/2 & 0 & 1/2 & 0 & 1/2 & 0 \\ 0 & -1/2 & 0 & -1/2 & 0 & 1/2 & 0 & 1/2 \\ 0 & 1/t & 0 & -1/t & 0 & 1/t & 0 & -1/t \end{bmatrix} \begin{bmatrix} u_i \\ v_i \\ u_j \\ v_j \\ u_k \\ v_k \\ u_m \\ v_m \end{bmatrix}$$

This equation can be writen as:

$$\{\epsilon_j\} = [L_o]\,\{u_i\} \quad \ldots\ldots\ldots\ldots\ldots\ldots \quad (G.1)$$

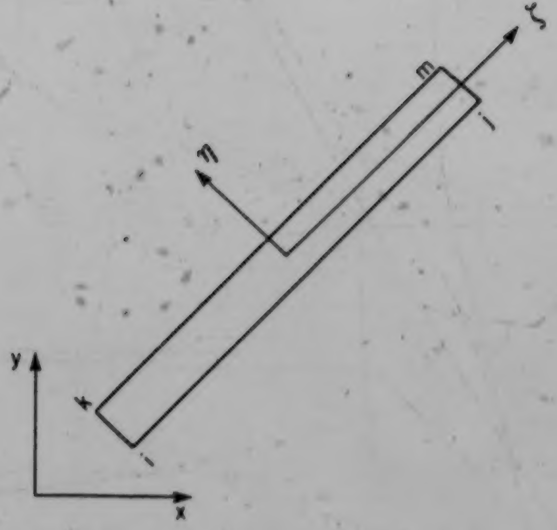

Figure G.1 Representation of Goodman's Joint Element

Note that the third line of the L_0 matrix corresponds to the rotation. Its application has no meaning in soils and therefore its calculation will be disregarded. Similarly, the calculations of moments will also be neglected and matrices $\{\epsilon_j\}$ and $[L_0]$ will have their last line eliminated.

The stresses are related to the nodal forces by the following equations:

$$\Delta\sigma_n = \frac{1}{t}\,(\Delta F_{n\,k} + \Delta F_{n\,m})$$

and

$$\Delta\tau_{ns} = \frac{1}{t}\,(\Delta F_{s\,k} + \Delta F_{s\,m})$$

where:

$\Delta\sigma_n$ - normal stress in the direction of the η axis

$\Delta\tau_{ns}$ - shear stress in the direction of the ξ axis

t - length of joint element

ΔF_{nk} - force applied to node k in the η direction

ΔF_{nm} - force applied to node m in the η direction

ΔF_{sk} - force applied to node k in the ξ direction

ΔF_{sm} - force applied to node m in the ξ direction

In general, these two equations are written, in matrix form, as:

$$\begin{bmatrix} \Delta F_{s\,i} \\ \Delta F_{n\,i} \\ \Delta F_{s\,j} \\ \Delta F_{n\,j} \\ \Delta F_{s\,k} \\ \Delta F_{n\,k} \\ \Delta F_{s\,m} \\ \Delta F_{n\,m} \end{bmatrix} = \begin{bmatrix} -t/2 & 0 \\ 0 & -t/2 \\ -t/2 & 0 \\ 0 & -t/2 \\ -t/2 & 0 \\ 0 & t/2 \\ t/2 & 0 \\ 0 & t/2 \end{bmatrix} \begin{bmatrix} \Delta\tau_{ns} \\ \Delta\sigma_n \end{bmatrix}$$

5 OF/DE 5

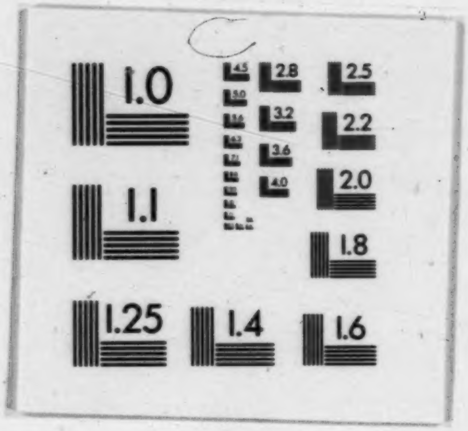
1.0
4.5
5.0
5.6
2.8
3.2
3.6
4.0
2.5
2.2
2.0
1.1
1.8
1.25
1.4
1.6

or,

$$\{\Delta F\}_{s,n} = [B]\ \{\Delta\sigma_j\}_{s,n} \quad \ldots\ldots\ldots\ldots\ldots \quad (G.2)$$

The stresses in the joint elements can be related to the "strains" using the constitutive matrix:

$$\begin{bmatrix} \Delta\tau_{s,n} \\ \Delta\sigma_n \end{bmatrix} = \begin{bmatrix} K_s & 0 \\ 0 & K_n \end{bmatrix}$$

or,

$$\{\Delta\sigma\}_{s,n} = [C_j]\{\epsilon_j\} \quad \ldots\ldots\ldots\ldots\ldots\ldots\ldots \quad (G.3)$$

where:

$[C_j]$ - constitutive matrix

By using equations (G.1), (G.2) and (G.3) the nodal displacements can be related to the nodal forces as:

$$\{\Delta F\}_{s,n} = [B][C_j][L_o]\{u\}_{s,n} \quad \ldots\ldots\ldots\ldots \quad (G.4)$$

or,

$$\{\Delta F\}_{s,n} = [K]\ \{u\}_{s,n}$$

where [K] is the stiffness matrix defined as

$$[K] = [B][C_j][L_o] \quad \ldots\ldots\ldots\ldots\ldots\ldots\ldots \quad (G.5)$$

Finally it remains to express the stiffness matrix in terms of the global coordinate system x and y. This can be conviniently done by using the "transformation matrix" as shown below:

$$\begin{bmatrix} \Delta F_s \\ \Delta F_n \end{bmatrix} = \begin{bmatrix} \cos a & \sin a \\ -\sin a & \cos a \end{bmatrix} \begin{bmatrix} F_x \\ F_y \end{bmatrix}$$

for each node. For all the nodes, in short form, it can be written:

$$\{\Delta F\}_{s,n} = [T]\,\{F\}_{x,y} \quad \ldots\ldots\ldots\ldots\ldots\ldots\ldots\ldots\ldots\ldots \quad (G.6)$$

where, the value of a can be determined from the joint element coordinates as follows:

$$a = \arctan\,[(Y_j - Y_i)/(X_j - X_i)]$$

where:

$Y_{j,i}$ - Y coordinate of nodes j and i respectively

$X_{j,i}$ - X coordinates of nodes j and i respectively

Similarly, the displacements can be transformed to the global coordinate system X and Y as:

$$\{u\}_{s,n} = [T]\,\{u\}_{x,y} \quad \ldots\ldots\ldots\ldots\ldots\ldots\ldots\ldots\ldots \quad (G.7)$$

Equations (G.6) and (G.7) can be introduced in equation (G.4) to get the nodal forces in the global coordinate system, as a function of displacements in the same system of coordinates;

$$[T]\{\Delta F\}_{x\ y} = [B][C_j][L_o][T]\{u\}_{x\ y}$$

or, using equation (G.5):

$$\{\Delta F\}_{x\ y} = [T]^{-1}[K][T]\{u\}_{x\ y} \text{ .... } (G.8)$$

It can be shown that the transformation matrix has the property that:

$$[T]^{-1} = [T]^{T}$$

Consequently, expression (G.8) can be rewritten as:

$$\{\Delta F\}_{x\ y} = [T]^{T}[K][T]\{u\}_{x\ y} \text{ .... } (G.9)$$

Expression (G.9) can be easily implemented into any Finite Element program using routine methods of assembly, storage and equation solvers, such as those mentioned in Chapter 6. Therefore, using the displacements provided by previous analyses, equations (G.1) and (G.3) provide the "strains" and stresses in the joint elements, respectively.

It is important to note that equation (G.1) was based on the assumption that the displacements of the center of the joint element equal the "average nodal displacements". These average displacements were called "element strains" in analogy to solid elements, and these strains were considered to be constant within the element. This assumption requires, for compatibility reasons, that the elements used to represent the soil mass placed adjacent to the joint element follow a similar assumption. Since the solid element used in the program INTERDAM was of a constant strain triangular type, this requirement was fulfilled.

APPENDIX H - CONSTITUTIVE MODELS IMPLEMENTED IN INTERDAM

Several constitutive models have been implemented in the program INTERDAM to study the best representation for joint elements. In this Appendix, all these models are presented, including a brief discussion of their advantages and disadvantages. An example is presented comparing the performance of the nonlinear models.

a. Linear Elastic Law

An option to assume linear elasticity for the tangential stiffness was incorporated into the program.

b. Nonlinear Elastic Laws

The tangential stiffness for a nonlinear analyses can be obtained in four different ways. All of them are based on results of laboratory tests, in most cases assumed to be a direct shear box test. The methods are described below.

b.1 - Hyperbolic Model

The hyperbolic model was developed by Clough and Duncan, (1971) and used with sucess in modelling sand - concrete interfaces in the analysis of Port Allen Lock (Duncan and Clough, 1970). The derivation of this model is identical to that used by Duncan and Chang in 1969, in the derivation of the hyperbolic model for solid elements. The major disadvantages are:

- the shape of the shear stress-shear displacement curve has to resemble a hyperbola for the method to be accurate. This is not always the case.

- The range of applicability of the method is up to 75% of the maximum shear strength (based on experiences with solid elements - Christian, 1980). Although this range is large enough for most geotechnical applications (Christian, op.cit) it seems not to be the case for interfaces, where relatively high shear stresses develope for small normal stresses. Therefore, the method seems suitable for simulations other than the "during construction" phase. An example of such application is the development of active and passive pressures due to movements of a retaining wall (presented by Clough and Duncan, 1971).

- It was proposed to represent a conventional direct shear box test and experiences with other stress-paths have not yet been reported.

The major advantages are its simplicity of application and easy of obtaining the input parameters.

b.2 - Digital Model

A model similar to that proposed by Krishnayya (1973) is suggested to obtain the tangential stiffness for the joint element.

The stress-displacement curve is input for descrete points, for several values of normal stresses. The routine to determine the value of K_{ss} involves the following steps:

a - search for the appropriate curve corresponding to the normal stress of each particular element.

b - for that level of normal stress search for the first value of shear stress input that is lower than the shear stress of the element.

c - for that level of normal stress search for the first value of shear stress input that is higher than the shear stress of the element.

d - determine the shear displacement corresponding to each value of shear stress determined in steps b and c.

e - calculate the slope of the straight line jointed by the pair of points found in b, c and d. This is the value of K_{ss} used in the subsequent step of loading.

It is important to note that interpolation between two values of inputed normal stress is allowed if the corresponding normal stress of the element does not equal one of the input curves.

Several disadvantages can be pointed out for this method:

1. The method would require a test with zero normal load to be performed (lower bound), in order to allow interpolations for low normal stresses, as occur for early stages of loading. In most cases, such a test would provide unsatisfactory stress-displacement curves and can not be imposed as a requirement. Furthermore, extrapolations from the lowest value of inputted normal stress can lead to predictions of negative normal stress values and numerical problems would arise.

To overcome this problem it is proposed that the first input curve will be used for normal stress levels below the first input normal stress. This will lead to a stiffer joint element for low normal stress levels and require tests to be performed with normal stresses as low as possible.

2. Similar to the previous model, the value of K_t is dependent upon the calculated value of normal stress. As mentioned before, this value depends upon an assumed value of the elastic parameter K_{nn}. Whether or not the calculated stress level is correct is still an open question and the normal stress can vary significantly depending upon the stiffness imposed.

In terms of advantages it can be said that:

1. There are no signs that numerical problems arise for degrees of strength mobilization greater than 75%.

2. Stress paths other than that of the conventional shear box test can be used.

b.3 - Modified Digital Method

In order to overcome the normal stress dependency, a modified digital model is proposed.

In this method, the search for the appropriate curve is not dependent upon the calculated normal stress, but on the shear displacement. The method involves the following steps:

a - search for the input displacements immediately smaller and higher than the calculated displacement.

b - for the first lower input displacement (δ_{n-1}), determine the first shear stress higher than the calculated shear stress of the element. Get the first one lower than the one searched.

c - determine over which curve this point is located (σ_n).

d - get the shear stress corresponding to the first higher inputed displacement (δ_{n+1}) over the same curve.

e - interpolate between the points obtained in b and d and determine the shear stress correspondent to the calculated shear displacement (δ_n).

f - check whether the calculated shear stress is higher or lower than the interpolated shear stress.

g - if higher, get the next higher curve and proceed as in b, d and e. If lower, get the next lower curve and proceed in similar fashion.

h - in case the interpolated shear stress is lower than the shear stress of the element and the curve searched in c is the first one inputted, extrapolation is required. Therefore the next higher curve is used.

i - determine the interpolated normal stress using the two curves chosen as explained before.

j - determine the interpolated shear stress for the two values of shear displacement δ_{n-1} and δ_n.

k - determine the slope of the curve determined in j and this is the value of K_{ss} for the next step of loading.

The advantages of the method are as described below:

1. It allows extrapolation without risk of predicting negative normal stresses.

2. The method is independent of the calculated normal stress of the element.

The major disadvantage lies in the fact that the shear stress of the element, given by:

$$\tau = K_{ss} \times \sigma_n$$

is based upon values determined from the previous values of σ_n and τ. In other words, the two values (τ and K_{ss}) are dependent on σ_n.

It is important to mention that the size of the joint element influences the average displacement calculated as proposed in Chapter 4. Therefore, any formulation based upon the calculated displacement has to be corrected for the size of the shear box test used. In other words, if a shear box test with dimensions "l" is used to represent the behaviour of a joint element with length "L", the value of the displacement to be used in the above procedure would be given by:

$$\sigma_c = \sigma_n \times l/L$$

A further disadvantage regards amount of of the input data required. If good accuracy is desired, several points should be input and the process of data entry becames very time consuming.

b.4 - Normalized Shear Stress Model (τ/σ)

As mentioned in Chapter 4, a new constitutive law was proposed based upon the test results.

It was noticed that, in most cases, if the tests were plotted with the shear stress normalized for the normal stress, a narrow band was obtained that could be represented by two straight lines.

In this method the displacement, corrected as mentioned before, is used to determine the corresponding value of the ratio τ/σ. Since the method is bilinear this value is obtained by using either of the two equations provided:

$$\tau/\sigma = \delta \tan \Phi_i \quad \text{for} \quad \delta \leq \delta_o$$

$$\tau/\sigma = (\tau/\sigma)_o + (\delta - \delta_o) \tan \Phi_t \quad \text{for } \delta > \delta_o$$

The shear stress can therefore be obtained by multiplying the ratio τ/σ obtained above by the corresponding normal stress calculated for the element. The shear stiffness was then obtained as:

$$K_{ss} = \tau/\delta \quad \text{if} \quad \delta \leq \delta_o$$

$$K_{ss} = (\tau - \tau_o) / (\delta - \delta_o) \quad \text{if} \quad \delta > \delta_o$$

As in the first digital method described herein (see b.2), the major disadvantage of this model lies in its dependency upon the normal stress. Particularly, for the first straight line, defined as:

$$\tau/\sigma_n = \delta \tan \Phi_i$$

it can be shown that the stiffness is dependent only on the normal stress, or:

$$\tau/\delta = \sigma \tan \Phi_i \quad \text{.............................} \quad \text{H.1}$$

Since:

$$K_{ss} = \tau/\delta \quad \text{..................................} \text{H.2}$$

it follows that:

$$K_{ss} = [\tau/(\sigma_n \times \delta)] = \tan \Phi_i$$

or

$$K_{ss} = \tau/\delta = \sigma_n \tan \Phi_i \text{ .... } \quad \text{H.3}$$

Since the value of σ_n is not reliable, it implies that K_{ss} can be of questionable value.

As with the hyperbolic model (see b.1), the major advantage is simplicity of parameters input.

In order to ensure that the nonlinear stress displacement models were being followed with acceptable fidelity, the subincremental procedure, described in item g of section 6.2.2 of Chapter 6, was introduced. This procedure is particularly important for the last method described, the normalized shear stress model, near the transition between the two straight lines, primarily due to the abrupt change in slope that takes place.

The accuracy of all four nonlinear methods of determining the tangential stiffness was assessed using a single example. The mesh used was the same as that used to test the joint element procedure (section 6.4.1.1, Chapter 6).

The run was performed in twelve loading steps, the first one being the application of the normal stress, equal to 90 kPa. From the second to the twelveth steps, loads were imposed at nodes 3 and 6 (see Figure 6.3, Chapter 6). The loading steps were chosen in order to apply "small increments" of load. No tests were performed to ensure that the increments were small enough to produce the best results.

The results of this test are presented in Figure H.1 . It can be seen that the digital methods (for this example either one since they provide exactly the same result) provided the closest result to both the interpolated curve (linear interpolation between the two inputted curves) as well as to a test run at a normal stress of 90 kPa. Note that if subincrements or smaller loading steps were used all curves would get closer to the "correct" result, but even then the digital would have provided the best agreement.

Therefore, the nonlinear analysis presented in subsequent sections will make use of a digital method. Furthermore, it was decided to use method b.3 (modified digital) for the reasons presented above.

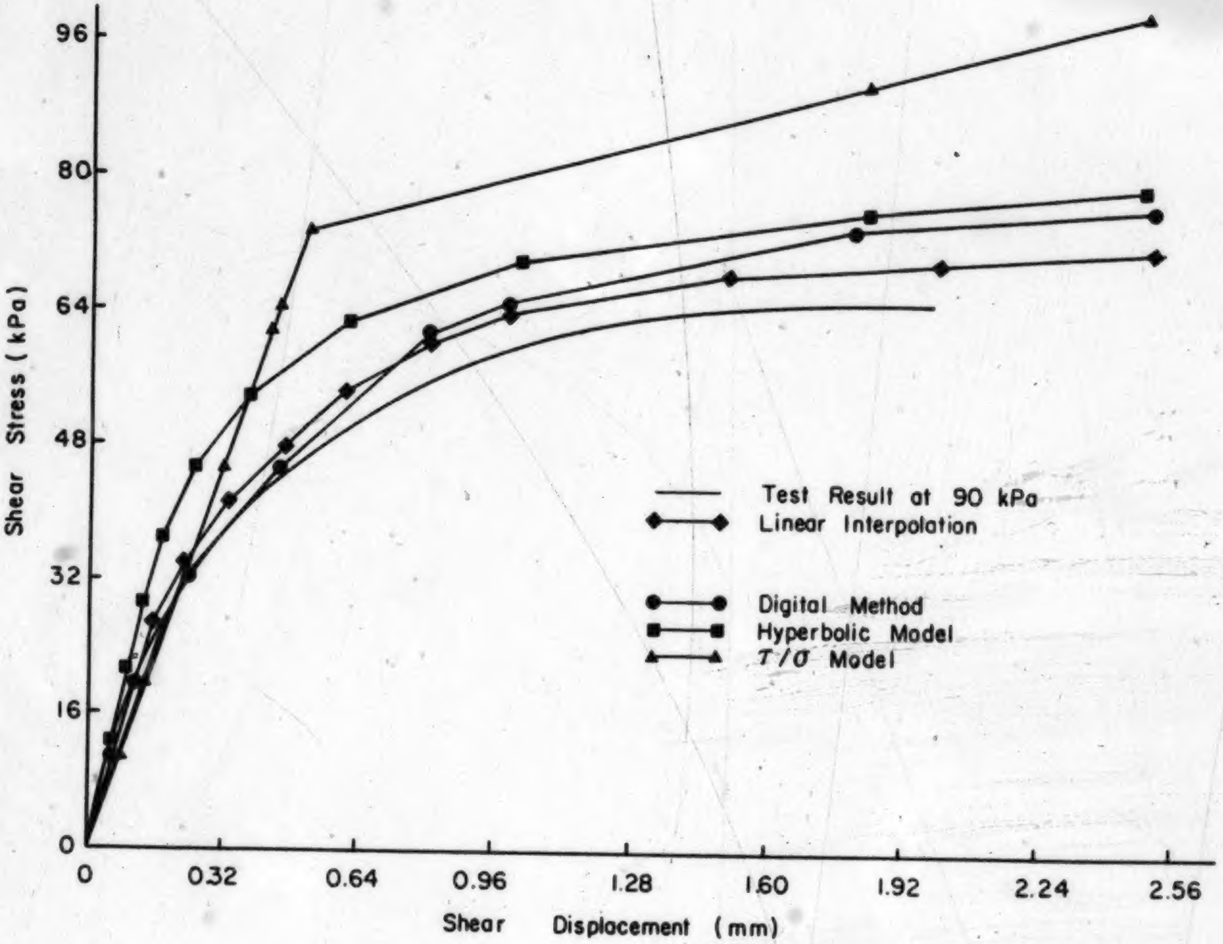

Figure H.1 Comparison for Constitutive Models